Diss. ETH No. 23731

NANOSTRUCTURED CALCIUM AND IRON COMPOUNDS AS NOVEL FOOD FORTIFICANTS: PRODUCTION, CHARACTERIZATION AND ABSORPTION IN ANIMAL MODELS

A thesis submitted to attain the degree of

DOCTOR OF SCIENCES of ETH ZURICH

(Dr. sc. ETH Zurich)

presented by

LIDIJA POSAVEC

MSc in Food Science, ETH Zurich

born on 06.01.1985

citizen of Personico TI, Switzerland

accepted on the recommendation of

Prof. Dr. med. Michael B. Zimmermann, examiner

Dr. Florentine M. Hilty-Vančura, co-examiner

Dr. Diego Moretti, co-examiner

Prof. Susan Fairweather-Tait, co-examiner

2016

to all the great people who made this achievement possible

ACKNOWLEDGMENTS

I sincerely thank Prof. Dr. med Michael Zimmermann for giving me this unique opportunity of writing a PhD thesis at the Laboratory of Human Nutrition. A special thank goes to Dr. Florentine Hilty-Vančura for supervising my work and guiding me with her valuable expertise in this research experience. I would like to thank Prof. Anne Grobler for hosting during my research at the Preclinical Drug Development Platform in Potchefstroom, South Africa. I would like to thank also Prof. Marius Smuts for hosting me at the Centre of Excellence for Nutrition in Potchefstroom, South Africa. I would like to thank Dr. Diego Moretti and Prof. Susan Fairweather-Tait from University of East Anglia for taking the task as external co-examiner.

A special thank goes to all current and previous members of the Laboratory of Human Nutrition, especially my office mate Susanne Dold who always had to listen to my stories during the last four years ☺. I would like to thank Sara Stinca for being my personal trainer in TRX and Coralie Signorell for the fun noodle-nights and chats. A special thank goes to Dr. Jesper Knijnenburg for the fruitful collaboration, fun braais and for the '*really good time*' in South Africa.

I would like to thank Christophe Zeder, Dr. Jeannine Baumgartner, Hylton Bunnting and Erna Kemp for their extremely valuable contributions during the studies. I would to thank all the people form Vivarium and all the students (Fabiola Alig, Virginie Sottas, Oezge Bas and Céline Heri) and laboratory assistants (Socrates Foschini and Juwela Lam) who greatly helped me to achieve this result.

A special thank goes to all my friends, especially Cristina, Pamela and Heike for their great friendship and all the fun we shared.

Finally, I would like to express my deepest gratitude to my parents, Ivan and Svetlana and my brother Boris for their endless support, love and for teaching me that nothing is impossible. Moreover, I would like to thank Diego for his infinite wise suggestions, love and for standing by my side during this unique journey.

Cover image (clockwise top left):

modified pictures of XRD patterns, sensory performance experiment, TEM image and powder appearance of nanocalcium phosphates

TABLE OF CONTENTS

ABBREVIATIONS I

SUMMARY III

RIASSUNTO VII

INTRODUCTION 1

LITERATURE 5

1 Physiology of calcium 5

1.1 Calcium metabolism 5

1.1.1 Absorption and excretion 6

1.1.2 Dietary factors affecting calcium absorption and balance 8

1.2 Calcium deficiency and overload 9

1.2.1 Epidemiology of calcium deficiency 10

1.3 Bone metabolism 11

1.3.1 Bone remodeling 11

1.3.2 Biomarkers for bone formation / resorption 12

1.3.3 Techniques to measure bone quality 13

1.3.3.1 DXA 14

1.3.3.2 CT 14

2 Physiology of iron 16

2.1 Iron metabolism 16

2.1.1 Absorption / excretion / storage 17

2.1.2 Dietary factors affecting iron absorption 19

2.2 Iron deficiency and overload 20

2.2.1 Epidemiology of iron deficiency 21

3 Strategies to overcome calcium and iron deficiency 22

3.1 Calcium 25

3.2 Iron 26

4 Nanostructured compounds for fortification and supplementation 28

4.1 Nanoparticles in nutrition: potential benefits in nutrition and risks for human health 28

4.2 Common methods used to produce nanostructured materials 29

4.2.1 Production of nanostructured calcium using flame (assisted) spray pyrolysis .. 30

4.2.2 Production of nano iron-β-lactoglobulin using reduction 33

4.3 Methods used to characterize nanostructured materials 34

4.3.1 Specific surface area and estimated primary particle size 34

4.3.2 Phase composition 36

5 Studying calcium and iron absorption 37

5.1 In vitro 37

5.1.1 Dissolution 37

5.1.2 In vitro digestion 40

5.1.3 Cells 40

5.2 In vivo 41

5.2.1 Calcium balance 42

5.2.2 Long-term bone mineralization 43

5.2.3 Calcium and iron appearance in serum 44

5.2.4 Hemoglobin dose-response 47

6 References 48

MANUSCRIPT 1 61

MANUSCRIPT 2 87

MANUSCRIPT 3 117

GENERAL DISCUSSION 153

CONCLUSIONS 165

ABBREVIATIONS

$1,25(OH)_2D_3$	active hormonal form of vitamin D
AI	Adequate Intake
AOAC	Association of Official Analytical Chemists
BET	Brunauer-Emnment-Teller
BMC	bone mineral content
BMD	bone mineral density
$CaCO_3$	calcium carbonate
Ca:P	calcium phosphate with defined molar ratio
CT	computed tomography
d_{BET}	BET-equivalent diameter
DCPA	dicalcium phosphate anhydrous
DCPD	dicalcium phosphate dehydrate
Dcytb	duodenal cytochrome B reductase
DMT1	divalent metal transporter 1
DXA	dual-energy X-ray absorptiometry
EAR	Estimated Average Requirements
eCaC	epithelial Ca^{2+} channel
ECF	extracellular fluid
EDX	Energy Dispersive X-ray Analysis
FASP	flame assisted spray pyrolysis
Fe-TR	transferrin bound
Fpn	ferroportin
FSP	flame spray pyrolysis
GI	gastrointestinal
H_2O_2	hydrogen peroxide
HAp	hydroxyapatite
Hb	hemoglobin
HCP	heme carrier protein / heme transporter
HO	hemoxygenase
IDA	iron deficiency anemia
IRP 1/2	iron responsive protein
MARRS	membrane-associated, rapid-response steroid-binding protein
µCT	micro-computed tomography
MRI	magnetic resonance imaging
NCX	Na^+/Ca^{2+} exchanger
OCT	octacalcium phosphate
OVX	ovariectomized
PMCA	plasma membrane Ca^{2+} ATPase

PTH	parathyroid hormone
qCT	quantitative CT
RBV	relative bioavailability
RDA	Recommended Dietary Allowance
ROI	region of interest
ROS	reactive oxygen species
SF	serum ferritin
STEM	scanning transmission electron microscopy
sTFr	transferrin receptor saturation
SSA	specific surface area
TCP	tricalcium phpsphate
TEM	transmission electron microscopy
TF	transferrin
TRPV5/6	transient receptor potential channel
TTCP	tetracalcium phosphate
VAFS	vapor-fed aerosol flame synthesis
VDR	intestinal vitamin D receptor
WHO	World Health Organization
XRD	X-ray diffraction
XPS	X-ray photoelectron spectroscopy

SUMMARY

Background Diets deficient in calcium are a risk factor for osteoporosis and fractures in the elderly, while iron deficiency primarily affects children and young women and may impair development, cognition and work capacity. The use of nanostructured calcium and iron compounds in food fortification and supplementation may increase absorption compared to currently available compounds. A decrease in particle size to the nanoscale was shown to be a potentially useful approach to increase solubility and bioavailability of minerals. However, studies investigating this 'nano' effect have largely ignored material properties such as chemical composition and crystal structure (amorphous vs. crystalline) which may also influence mineral bioavailability. In addition, rigorous characterization of nanoscale compounds tested *in vivo* is often not done, making it difficult to compare studies and compounds, and understand the determinants of absorption.

Aim and objectives The overall aim of this thesis was to investigate and understand the link between material properties and *in vivo* bioavailability of nanostructured calcium and iron compounds. This has been achieved by a) developing nanostructured calcium carbonates and phosphates using flame assisted spray pyrolysis (FASP) and understanding their properties before and after aging; b) assessing the bioavailability of nanostructured calcium compounds by specific surface area (SSA) and by chemical composition in growing rats and their performance in food systems; c) assessing bioavailability of novel iron-amyloid fibril hybrids in rats and their performance in food systems.

Experiments

Manuscript 1 – Production and characterization of nanostructured calcium carbonate and phosphate for nutrition

We produced high SSA calcium carbonate ($CaCO_3$) and calcium phosphates using FASP aerosol technology, and monitored their SSA, crystal size and composition during aging in pure and doped form. We used their solubility in 0.01 M H_3PO_4 as an indicator of *in vivo* bioavailability. The results showed that an increase in primary particle size during aging can be inhibited by doping the powders with strontium, zinc, magnesium and phosphorus, with best results for magnesium (Mg) and phosphorus (P). We also characterized the compounds with varying calcium to phosphorus molar ratios (Ca:P). While the amorphous content

increased with increasing amount of dopant, SSA remained approximately 130 m^2/g for Ca:P ratios between 1 and 2.33. Among the different Ca:P ratios, Ca:P = 1 showed to be the more promising based on its high SSA, high calcium content, low amounts of stable HAp and because it remains X-ray diffraction (XRD)-amorphous during aging.

Generally, nanosized powders released more calcium upon dissolution than the commercial micron-sized powders and Ca:P = 1 performed better than $CaCO_3$ and Mg-doped $CaCO_3$. Interestingly, there was no further increase in released calcium if SSA was increased above 23 m^2/g. Possibly, calcium phosphate nanopowders dissolved so rapidly that no difference in dissolution kinetics could be observed, while a size effect may still be visible for larger particles. For the compounds investigated, composition (Ca:P = 1 vs. $CaCO_3$) and structure (crystalline vs. amorphous), but not SSA, were the determinant factors for dissolution.

Manuscript 2 – Bioavailability of nanostructured calcium compounds in growing rats

We evaluated the bioavailability of nanostructured calcium compounds *in vivo* in growing male rats. Three $CaCO_3$ with SSAs of 3, 36 and 64 m^2/g were compared in order to investigate calcium bioavailability by SSA. In addition the bioavailability at similar SSA was studied by changing chemical composition, specifically by comparing $CaCO_3$ (64 m^2/g) to a mixture of $CaCO_3$ and HAp 50/50 wt% ($CaCO_3$:HAp 50/50, 94 m^2/g) and pure HAp (100 m^2/g). We characterized the compounds for SSA, phase composition (XRD) and crystallinity (XRD and transmission electron microscopy [TEM]). We evaluated calcium dissolution in 0.01 M H_3PO_4 and color change in sensitive food matrices as indicator for sensory performance. We quantified calcium absorption, retention and fractional retention during a 5-day metabolic balance study. Additionally, bone mineral density (BMD) in femur and L1-4 vertebra, calcium content of femur and parathyroid hormone level in serum were measured as secondary outcomes.

We found that calcium fractional retention was significantly higher for HAp 100 m^2/g when compared to $CaCO_3$ 64 m^2/g, but not when compared to $CaCO_3$:HAp 50/50. On the other hand, calcium bioavailability did not improve with increasing SSA of pure $CaCO_3$, suggesting that chemical composition might be more relevant for calcium bioavailability than SSA. Histologic examination of selected organs did not detect tissue accumulation of calcium suggesting primary compound safety. The simple linear regression between absorbed calcium and *in vitro* dissolved calcium was not significant. Of all compounds, HAp 100 m^2/g

overall showed the better *in vitro* and *in vivo* performance compared to the other tested compounds, and compared to commonly-used $CaCO_3$, may be a promising alternative for nutritional applications.

Manuscript 3 – Bioavailability of novel iron fortificants in rats

We prepared iron-amyloid fibril hybrids by denaturing beta-lactoglobulin from its globular shape into an elongated self-assembled fibrilar structure (BLG fibrils). Iron nanoparticles were then nucleated on the surface of fibrils by using a reducing agent. Iron-amyloid fibril hybrids (Fe-FibBLG) and the pure nano iron without fibrils (Fe-Nano) were characterized by colorimetry (reducing effect of BLG fibrils Fe(II)/Fe(III)), transmission electron microscopy (structure), small angle neutron scattering (phase composition), energy dispersive X-ray analysis (material-elements detection), X-ray photoelectron spectroscopy (surface chemical composition) and *in vitro* digestion (human digestion simulation of fibrils and nanoparticles separately). In rats, we assessed the relative bioavailability (RBV) compared to $FeSO_4$ of the two nano iron compounds in a hemoglobin depletion-repletion study (compounds in powder form) and in a stable iron isotope study (compounds in liquid form). In both studies, RBV of the nanocompounds was not significantly different from each other or from $FeSO_4$. The compound's primary safety was evaluated by extensive organ histology. No histological changes related to the compounds were observed. Fe-FibBLG showed good dispersability in aqueous matrices and it therefore may be more suitable as a fortificant of liquids than the pure Fe-nano and other Fe nanoparticles. However, the sensory advantage of Fe-FibBLG over $FeSO_4$ in reactive food matrices was only modest.

Conclusion The *in vivo* performance of the calcium and iron nanocompounds suggests that combining specific chemical properties with small size might be the key to design highly bioavailable minerals. For calcium compounds, an increase in SSA over 23 m^2/g did not further improve calcium dissolution, suggesting that, rather than SSA, chemical composition and crystal structure might play a key role in their *in vitro* and *in vivo* performance. Nanostructured calcium phosphates, especially HAp, might be a valid alternative to calcium supplementation and fortification, compared to $CaCO_3$. However, its long term efficacy in improving BMD and reducing risk of osteoporosis needs to be investigated. The highly bioavailable iron-amyloid fibril hybrids with their good colloidal stability are promising fortificants of liquid matrices. However, our animal results should be confirmed in

bioavailability studies in humans. For all nanocompounds, future toxicological studies must be carefully done in order to demonstrate safety. Finally, we showed how a material design approach aiming to select specific material properties may be a valid alternative to nanosizing alone. Use of a material design approach to maximize bioavailability while staying above the current regulatory limits for nanoparticles might allow the food industry to avoid the 'nano' label and likely improve consumer acceptance towards newly engineered nanomaterials for nutrition.

RIASSUNTO

Premessa Una dieta povera in calcio può portare allo sviluppo di osteoporosi, specialmente negli anziani, mentre una priva in ferro può compromettere lo sviluppo, la cognizione nei bambini e la capacità lavorativa di giovani donne. L'uso di composti di calcio e di ferro di dimensioni nanometriche come fortificanti e supplementi potrebbe migliorarne drasticamente l'assorbimento rispetto a compositi correntemente disponibili. Diminuire la dimensione di alcune particelle fino a scala nanometrica si è dimostrato essere un valido approccio per aumentare la solubilità e biodisponibilità di minerali. Tuttavia, studi che hanno valutato questo effetto 'nano' hanno spesso ignorato di considerare anche le proprietà dei materiali come ad esempio la composizione chimica e la struttura (amorfa vs. cristallina), le quali possono influenzare la biodisponibilità. Inoltre, manca spesso una caratterizzazione soddisfacente dei composti testati *in vivo*, rendendo difficile il confronto tra studi e composti.

Scopo ed obiettivi L'obiettivo generale di questa tesi è quello di indagare e capire il legame tra le proprietà dei materiali e della biodisponibilità *in vivo* di nanoparicelle di calcio e di ferro. Questo scopo è stato indagato tramite a) la produzione di composti di nanoparticelle di calcio utilizzando il metodo 'flame assisted spray pyrolysis' (FASP) e monitorandone le proprietà prima e dopo l'invecchiamento; b) la valutazione della biodisponibilità nei ratti dei composti di nanoparticelle di calcio carbonato e fosfato, prendendo in considerazione l'area della superficie (AS) e la composizione chimica, e analizzandone il comportamento in diversi alimenti; c) la valutazione della biodisponibilità di nuovi ibridi composti da fibrille-amiloide e ferro nei ratti e analizzandone il comportamento in diversi alimenti.

Ricerca

Manoscritto 1 – Produzione e caratterizzazione di nanoparticelle di calcio in forma di calcio carbonato o calcio fosfato

Nanoparticelle di calcio carbonato ($CaCO_3$) e fosfato con grandi AS sono state prodotte utilizzando la tecnologia FASP. Le AS, dimensioni cristalline e composizione chimiche delle polveri in forma pura o mista (con l'aggiunta di altri elementi), sono state monitorate durante la loro esposizione all'ambiente circostante come segno d'invecchiamento. La loro solubilità in acido è stata misurata come surrogato per la biodisponibilità. I risultati ottenuti

hanno dimostrato che l'invecchiamento del calcio carbonato può essere ritardato mediante l'incorporazione di stronzio, zinco, magnesio (Mg) e fosforo (P) nel cristallo. Fosforo e Mg hanno dato i migliori risultati nel mantenere piccolo il cristallo di $CaCO_3$. Diversi rapporti molari tra calcio e fosforo (Ca:P) sono stati prodotti e caratterizzati. È stato osservato come la quantità di parte amorfa aumenta con l'aumentare della quantità di P. L'AS tuttavia, è rimasta costante attorno a 130 m^2/g per rapporti di Ca:P tra 1 e 2.33. Tra i diversi rapporti di Ca:P sintetizzati, Ca: P = 1 è stato selezionato per la sua alta AS, l'alto contenuto di calcio, la bassa presenza di apatite (HAp) e perché rimasto amorfo (cristallografia a raggi X) durante l'invecchiamento.

In generale, è stato osservato che durante l'esperimento di solubilità in acido (0.01 M H_3PO_4), le nanoparticelle hanno rilasciato più calcio rispetto alle microparticelle commerciali e che la polvere contenente Ca:P = 1 è risultata la migliore a confronto di puro $CaCO_3$ e Mg-$CaCO_3$. È interessante notare che, la quantità di Ca sciolto durante l'esperimento non è aumentata con l'aumentare dell'AS sopra 23 m^2/g. Una possibile spiegazione è che le nanoparticelle prodotte si siano sciolte così rapidamente da non permettere di osservare alcuna differenza nella cinetica. Comunque un effetto della dimensione/AS è stato osservato per le particelle più grandi. Dai risultati si vede che la composizione (Ca:P = 1 vs. $CaCO_3$) e la struttura (cristallina vs. amorfa), ma non l'AS, sembrano essere i fattori decisivi per la dissoluzione delle nanoparticelle di calcio prodotte.

Manoscritto 2 – La biodisponibilità delle nanoparticelle di calcio nei ratti in crescita

La biodisponibilità delle nanoparticelle di calcio è stata valutata nei ratti in crescita. Tre $CaCO_3$ con AS di 3, 36 e 64 m^2/g sono stati confrontati al fine di indagare l'effetto della AS sulla biodisponibilità. Inoltre l'effetto della composizione chimica di nanoparticelle con simile AS è stato studiato confrontando il più piccolo dei $CaCO_3$ (64 m^2/g) con una miscela di $CaCO_3$ e HAp 50/50 wt% ($CaCO_3$:HAp 50/50, 94 m^2/g) e con pura HAp (100 m^2/g). I 5 composti sono stati caratterizzati tramite misurazione della AS, della composizione chimica (XRD) e della cristallinità (XRD e TEM). La loro solubilità è stata valutata in acido (0.01 M H_3PO_4) ed il cambiamento di colore e pH sono stati misurati in alcuni alimenti. Uno studio focalizzato sul bilancio del calcio nei ratti per un periodo di 5 giorni è servito a misurarne l'assorbimento, la conservazione e conservazione frazionaria. Inoltre, la densità ossea nel femore e nelle

vertebre lombari L1-4, il contenuto di calcio del femore e l'ormone paratiroide nel siero sono stati giudicati come esiti secondari.

Nella comparazione delle nanoparticelle di calcio, prendendo in considerazione soltanto il cambiamento della composizione chimica, abbiamo osservato che la conservazione frazionaria di calcio è aumentata in modo significativo per HAp 100 m^2/g se comparata con $CaCO_3$ 64 m^2/g, ma non con $CaCO_3$:HAp 50/50. D'altro canto, non è stata osservata alcuna differenza su alcuno degli esiti primari o secondari quando la SA è stata considerata per il puro $CaCO_3$. L'ampia analisi istologica di diversi organi animali non ha rivelato alcun accumulo visivo di calcio nei tessuti, suggerendo un'indicativa sicurezza nell'uso di queste nanoparticelle per scopi alimentari. La quantità di calcio assorbito non è stata correlata in modo significante con il calcio sciolto in acido. Tra tutti i composti esaminati HAp 100 m^2/g ha mostrato le migliori prestazioni *in vitro* e *in vivo*, risultando essere una potenziale alternativa al più comunemente usato $CaCO_3$.

Manoscritto 3 – La biodisponibilità nei ratti di nuovi fortificanti di ferro

Ibridi composti da fibrille-amiloide e ferro sono stati sintetizzanti mediante denaturazione della proteina beta-lattoglobulina, passando dalla forma globulare originale ad una struttura allungata (fibrilla). Dopodiché, nanoparticelle di ferro sono state aggiunte alla superficie delle fibrille mediante riduzione. Gli ibridi composti da fibrille-amiloide e ferro (Fe-FibBLG) e singole nanoparticelle di ferro senza fibrille (Fe-Nano) sono stati caratterizzati attraverso test colorimetrico (contenuto di Fe (II)/Fe (III)), TEM (struttura), dispersione di neutroni a piccolo angolo (composizione chimica), EDX (composizione del materiale), XPS (composizione chimica di superficie) e dalla digestione (simulazione della digestione umana di fibrille e nanoparticelle separatamente). La biodisponibilità relativa (RBV) di questi due nuovi composti rispetto a $FeSO_4$ è stata misurata nei ratti mediante uno studio di svuotamento-rifornimento dell'emoglobina (composti in polvere) e uno studio con isotopi stabili (composti in forma liquida). I risultati ottenuti mostrano che per entrambi gli studi le RBV misurate non erano differenti in modo significante né da $FeSO_4$ né tra i compositi stessi. Una sicurezza primaria nell'uso dei compositi per scopi alimentari è stata data da un'ampia analisi istologica su diversi organi, dove non sono stati riscontrati depositi di ferro o anomalie dovute ai composti. Fe-FibBLG ha mostrato essere disperdibile e quindi adatto alla fortificazione di alimenti liquidi, cosa che invece non è possibile per il Fe-Nano a causa

dell'assenza delle fibrille. Tuttavia, il vantaggio di Fe-FibBLG rispetto a $FeSO_4$, come fortificante per alimenti a rischio di cambiamenti di colore, è stato solo parziale.

Conclusione Le buone prestazioni delle nanoparticelle di calcio e ferro prodotte hanno dimostrato che combinare le proprietà chimiche con la riduzione della dimensione a livello 'nano' potrebbe essere la chiave per la futura progettazione di minerali altamente biodisponibili. Per le nanoparticelle contenenti calcio, un aumento dell'AS oltre i 23 m^2/g non ha ulteriormente migliorato la dissoluzione di calcio, suggerendo che, piuttosto che mirare ad ottenere una AS più grande possibile, si dovrebbe lavorare sulla composizione chimica e sulla struttura amorfa. Questi elementi potrebbero essere la chiave per ottimizzare le prestazioni *in vitro* ed *in vivo* delle nanoparticelle di calcio. I fosfati di calcio con dimensioni nanometriche, in particolare HAp, potrebbero essere una valida alternativa al $CaCO_3$ per la supplementazione e la fortificazione di alimenti. Tuttavia, un'efficacia a lungo termine per migliorare la densità ossea e ridurre il rischio di osteoporosi data da una prolungata assunzione di HAp, deve essere ulteriormente indagata. Gli ibridi composti da fibrille-amiloide e ferro si sono dimostrati altamente biodisponibili e, grazie alla loro stabilità colloidale, hanno mostrato risultati promettenti come fortificanti di alimenti liquidi. Tuttavia, per entrambi i minerali, i risultati ottenuti con gli studi sugli animali devono ancora essere confermati con studi di biodisponibilità negli esseri umani. Prima di poter fare ciò, successivi studi tossicologici dovranno essere eseguiti al fine di dimostrare la sicurezza di queste nanoparticelle. Infine, abbiamo dimostrato come il mirare alla progettazione di materiali con l'obiettivo di selezionare specifiche proprietà può essere una valida scelta alla sola riduzione delle dimensioni a livello 'nano'. Infine, l'approccio di progettare il materiale in modo specifico per evitare l'etichetta 'nano' data dall'industria alimentare ma mantenendone le proprietà desiderate, potrebbe sicuramente essere un modo per migliorare la percezione e l'accettazione da parte del consumatore di questi materiali di nuova generazione.

INTRODUCTION

Calcium deficiency affects negatively elderly population (especially post-menopausal women) and if not treated can lead to impaired bone quality, osteoporosis and increased risk of fractures (Hernlund *et al.*, 2013). Iron deficiency affects children and women and if not overcome, can lead to impaired growth and cognitive development in children and lower work capacity in adults (Zimmermann and Hurrell, 2007). The most effective strategies to overcome deficiency and anemia are oral supplementation and fortification (Hurrell, 2002). However, several food components together with aging of the intestinal tract (Coudray *et al.*, 2006) can lead to suboptimal mineral absorption. Rapid and increased mineral dissolution from nanostructured powders may allow them to be absorbed more efficiently in humans.

The increase in specific surface area (SSA) has been proposed as an effective strategy to improve mineral bioavailability. Specifically for iron, $FePO_4$ produced by flame spray pyrolysis (FSP) (Rohner *et al.*, 2007) and mixed iron-zinc phosphates were as bioavailable as the 'gold standard' FeSO4 in rats (Hilty *et al.*, 2010). Iron-zinc phosphates also showed markedly reduced color changes in solid matrices such as yogurt, however, they might precipitate with time in liquid ones.

Usually nanosized calcium is commonly produced by grinding or precipitation and only few attempts to synthesize calcium oxide (Knijnenburg *et al.*, 2013) and phosphate (Loher *et al.* (2005) nanocompounds with FSP technology were made in the past. However, aging of CaO at ambient conditions resulted in changes in composition and SSA (Knijnenburg *et al.*, 2013). Although size reduction has shown positive effect on calcium concentration in serum and an increase in bone mineral density in several studies (Chen *et al.*, 2008; Gao *et al.*, 2008; Huang *et al.*, 2009; Meiron *et al.*, 2011), no common agreement has been reached yet on the efficacy of this approach. Moreover, no agreement has been found on whether *in vitro* calcium solubility can predict *in vivo* absorption as in case of iron (Swain *et al.*, 2003). Recently, a dissolution method proposed by Meiron *et al.* (2011) suggests to use the time to reach half of final pH as indication for *in vivo* bioavailability. The authors could find good agreement between their *in vitro* and *in vivo* data for a synthetically produced amorphous $CaCO_3$.

The aim of this thesis is to evaluate the *in vivo* bioavailability of novel nanostructured calcium and iron materials synthesized using a material-design approach in order to investigate the link between material properties and their *in vivo* bioavailability. This investigation will be discussed in four main parts. In the first part, the thesis summarizes what is currently known about the bioavailability of nanostructured calcium and iron compounds in a Literature chapter. Secondly, the research carried out to understand material properties with respective *in vivo* bioavailability is summarized in the manuscript section. Specifically, the original research manuscripts describe the 'dissolution and storage stability of nanostructured calcium carbonates and phosphates for nutrition' (*Manuscript 1*), 'the effect of specific surface area and chemical composition of nanostructured calcium carbonates and phosphates on *in vitro* solubility and calcium retention in growing rats' (*Manuscript 2*) and the 'amyloid fibrils reduce, stabilize and deliver bioavailable nanosized iron' (*Manuscript 3*). Lastly, a critical consideration of the current research with an overview on the open questions is given in the general discussion and conclusion part.

Chen H. S., Chang J. H., and Wu J. S. B., 2008, Calcium bioavailability of nanonized pearl powder for adults: Journal of Food Science, v. 73, no. 9, p. 246-251.

Coudray C., Feillet-Coudray C., Rambeau M., Tressol J. C., Gueux E., Mazur A., and Rayssiguier Y., 2006, The effect of aging on intestinal absorption and status of calcium, magnesium, zinc, and copper in rats: A stable isotope study: Journal of Trace Elements in Medicine and Biology, v. 20, no. 2, p. 73-81.

Gao H. Y., Chen H. I., Chen W. X., Tao F., Zheng Y. H., Jiang Y. M., and Ruan H. J., 2008, Effect of nanometer pearl powder on calcium absorption and utilization in rats: Food Chemistry, v. 109, no. 3, p. 493-498.

Hernlund E., Svedbom A., Ivergard M., Compston J., Cooper C., Stenmark J., McCloskey E. V., Jonsson B., and Kanis J. A., 2013, Osteoporosis in the european union: Medical management, epidemiology and economic burden. A report prepared in collaboration with the international osteoporosis foundation (iof) and the european federation of pharmaceutical industry associations (efpia): Archives of Osteoporosis, v. 8, p. 136.

Hilty F. M., Arnold M., Hilbe M., Teleki A., Knijnenburg J. T. N., Ehrensperger F., Hurrell R. F., Pratsinis S. E., Langhans W., and Zimmermann M. B., 2010, Iron from nanocompounds containing iron and zinc is highly bioavailable in rats without tissue accumulation: Nature Nanotechnology, v. 5, no. 5, p. 374-380.

Huang S., Chen J. C., Hsu C. W., and Chang W. H., 2009, Effects of nano calcium carbonate and nano calcium citrate on toxicity in icr mice and on bone mineral density in an ovariectomized mice model: Nanotechnology, v. 20, no. 37, p. 1-7.

Hurrell R. F., 2002, Fortification: Overcoming technical and practical barriers: The Journal of Nutrition, v. 132, no. 4, p. 806-812.

Knijnenburg J. T. N., Hilty F. M., Krumeich F., Zimmermann M. B., and Pratsinis S. E., 2013, Multimineral nutritional supplements in a nano-cao matrix: Journal of Materials Research, v. 28, no. 8, p. 1129-1138.

Loher S., Stark W. J., Maciejewski M., Baiker A., Pratsinis S. E., Reichardt D., Maspero F., Krumeich F., and Gunther D., 2005, Fluoro-apatite and calcium phosphate nanoparticles by flame synthesis: Chemistry of Materials, v. 17, no. 1, p. 36-42.

Meiron O. E., Bar-David E., Aflalo E. D., Shechter A., Stepensky D., Berman A., and Sagi A., 2011, Solubility and bioavailability of stabilized amorphous calcium carbonate: Journal of Bone and Mineral Research, v. 26, no. 2, p. 364-372.

Rohner F., Ernst F. O., Arnold M., Hibe M., Biebinger R., Ehrensperger F., Pratsinis S. E., Langhans W., Hurrell R. F., and Zimmermann M. B., 2007, Synthesis, characterization, and bioavailability in rats of ferric phosphate nanoparticles: The Journal of Nutrition, v. 137, no. 3, p. 614-619.

Swain J. H., Newman S. M., and Hunt J. R., 2003, Bioavailability of elemental iron powders to rats is less than bakery-grade ferrous sulfate and predicted by iron solubility and particle surface area: The Journal of Nutrition, v. 133, no. 11, p. 3546-3552.

Zimmermann M. B., and Hurrell R. F., 2007, Nutritional iron deficiency: Lancet, v. 370, no. 9586, p. 511-520.

LITERATURE

1 Physiology of calcium

1.1 Calcium metabolism

Calcium has an atomic weight of 40 g/mol and occurs as a divalent cation Ca^{2+}. In nature, it constitutes part of seashells, bones and teeth, occurring in the form of limestone ($CaCO_3$), hydroxyapatite (HAp, $Ca_{10}(PO_4)_6(OH)_2$) (Dorozhkin, 2007), gypsum ($CaSO_4 \cdot H_2O$) (Becker *et al.*, 2005) and several others. In the human body, calcium plays an essential role in mediating major processes such as muscle contraction, hormone synthesis and most importantly is essential in the bone remodeling process (Institute of Medicine, 2011).

Calcium accounts for 1-2% of the total body weight, 99% of which is found as HAp in mineralized tissues such as bones and teeth. Bone, besides giving structure to the body in form of a skeleton, and protection to the internal organs, serves as the main calcium store (Cashman, 2002). The remaining 1% of calcium can be also found in soft tissues, plasma and extracellular fluid (ECF) (Kiela *et al.*, 2012). An adult human body contains approximately 1000 mg calcium (DiMeglio *et al.*, 2014).

Once dietary calcium is ingested (600-1200 mg/day), it can be actively or passively (DiMeglio *et al.* (2014), see chapter 1.1.1) absorbed along the whole gastrointestinal tract but absorption efficiency varies depending on gastrointestinal pH and transit time (Bronner, 2003b). Absorbed calcium enters the common blood pool and circulates in the ECF while the unabsorbed part of it is excreted in feces. Circulating calcium serves as mediator for vascular contraction and vasodilation, muscle contraction, nerve transmission and glandular secretion (Institute of Medicine, 2011). Body Ca^{2+} pool in the plasma ranges from 2.12 to 2.62 mmol/L (8.5-10.5 mg/dL) (Institute of Medicine, 2011) and it is tightly regulated by parathyroid gland, as shown in **Figure 1**. Calcium concentration in plasma is maintained constant by calcitropic hormones such as parathyroid hormone (PTH), 1,25 dihydroxycholecalciferol ($1,25(OH)_2D_3$) and calcitonin, that specifically target kidney, bone and intestinal organs in order to modulate its entry into the extracellular space (Institute of Medicine, 2011). Low body calcium pool triggers the release of PTH from the thyroid gland

which increases calcium absorption by the gastrointestinal (GI) tract, retention by the kidneys and resorption by the bones (Kiela *et al.*, 2012).

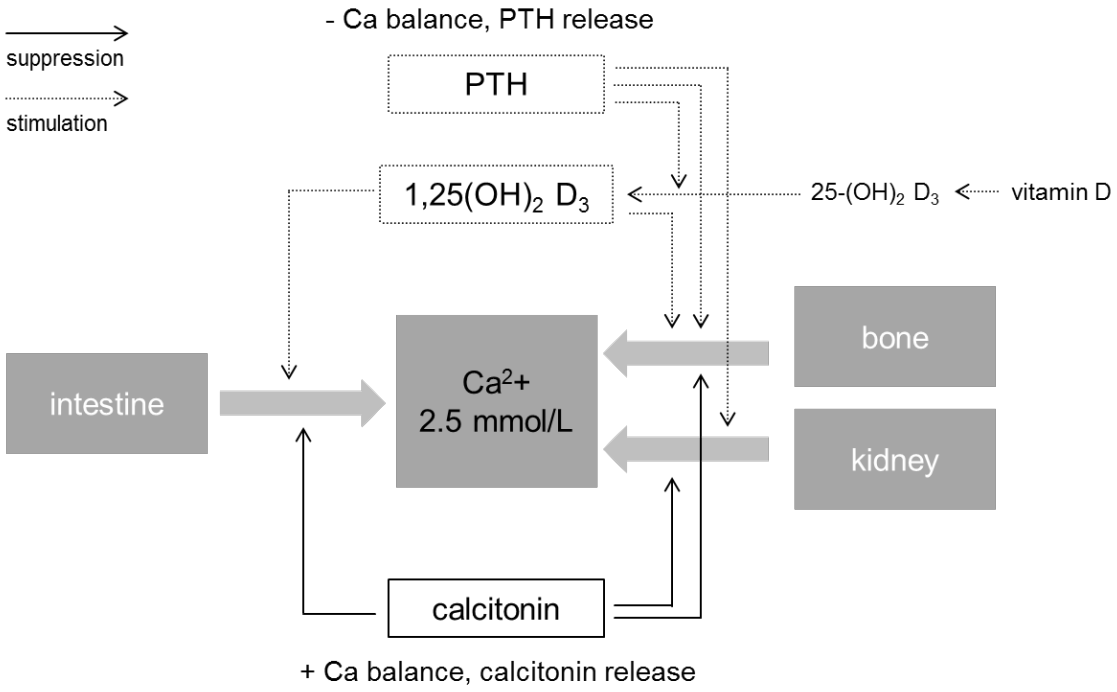

Figure 1: Body calcium homeostasis adapted from Kiela *et al.* (2012). Abbreviations: PTH – parathyroid hormone.

Excess calcium is stored in bones and it is mobilized when needed in order to maintain constant levels of serum calcium. Low Ca^{2+} concentration in the ECF is sensed by the parathyroid gland, which responds by releasing PTH and increases the production of calcitriol (active hormonal form of vitamin D, $1,25(OH)_2D_3$). PTH and $1,25(OH)_2D_3$ together increase calcium resorption in the kidneys and mobilize it from bones in order to increase the amount of circulating calcium. Moreover, $1,25(OH)_2D_3$ acts on the intestine to increase calcium absorption (DeLuca, 2004). On the other hand, high Ca^{2+} in the ECF triggers the release of calcitonin by the c-cells of the thyroid gland, discontinuing bone resorption and suppressing PTH release (Institute of Medicine, 2011).

1.1.1 Absorption and excretion

Calcium is absorbed through the whole GI tract either by active transport (transcellular, saturable) or by passive diffusion (paracellular, insaturable) across the enterocytes. The transport of calcium across the enterocytes is either active or passive and the mechanisms are schematically shown in **Figure 2**. The active transport is regulated by calcitriol and by vitamin D acting on the intestinal vitamin D receptor (VDR) and the membrane-associated,

rapid-response steroid-binding protein (MARRS), while the passive transport occurs depending on the luminal:serosal electrochemical gradient (**Figure 2**) (Fleet and Schoch, 2010). Three different models have been proposed to describe the active transport of calcium (DiMeglio *et al.*, 2014). The first type, also called facilitated diffusion, is modulated by $1,25(OH)_2D_3$. In this case, Ca^{2+} enters the enterocyte via the apical membrane channel TRPV5/6 (Hoenderop *et al.*, 2003) (previously identified as epithelial Ca^{2+} channel, eCaC (Hoenderop *et al.*, 2002)), binds to calbindin-D_{9K} which functions as transporter in the cytosol (Bronner *et al.*, 1986) and buffers Ca^{2+} excretion (Cui *et al.*, 2012), and it is released in the blood by the ATP-dependent plasma membrane calcium ATpase (PMCA1b) or the Na^+/Ca^{2+} exchanger (NCX1) (Khanal and Nemere, 2008). The second one, called vescicular transport, allows the entrance and exit of Ca^{2+} in lysosomes by endo- and exocytosis. The third one is called transcaltachia and is stimulated by $1,25(OH)_2D_3$ but no gene transcription is involved in this process (DiMeglio *et al.*, 2014). On the other hand, passive transport consists of the paracellular transport of Ca^{2+} between the tight junctions and vitamin D dependent receptors Claudin 2 and 12 and it is modulated by the concentration gradient and depends on the permeability of the GI tract (DiMeglio *et al.*, 2014).

Intestinal calcium absorption accounts, on average, for 25% of the ingested amount in an adult subject (Hunt and Johnson, 2007) and the absorption efficiency declines with increasing age (Coudray *et al.*, 2006; Heaney *et al.*, 1989). However, fractional calcium absorption was shown to be inversely correlated with the logarithm of the ingested amount in healthy female subjects, ranging from 28.6 to 64.0% for 500 and 15 mg, respectively (Heaney *et al.*, 1990b). Whether calcium will be absorbed by either active or passive transport depends on the quantity ingested and on the location in the GI tract (Bronner, 2003a). For instance, active transport occurs mainly in the duodenum and to a limited extent in the jejunum and colon; and from a normal calcium load of 400-600 mg per meal, this can account up to 60% of absorbed calcium (DiMeglio *et al.*, 2014). On the other hand, passive transport can occur throughout the whole GI tract, and the absorption is proportional to the amount of mineral available in the gut lumen (Duflos *et al.*, 1995).

Unabsorbed calcium is excreted through feces. In addition, endogenous losses from the GI in the form of digestive secretion and shed mucosal cells can account for up to a daily loss of 2.1 mg/kg body weight for an adult subject (Abrams *et al.*, 1991). Phosphorus intake was

found to be the major contributor (22%) to the total variance (29%) in endogenous losses together with body size and protein intake (Davies *et al.*, 2004). When blood is filtered in the kidneys, calcium is either reabsorbed or excreted in the urine. This reabsorption process is tightly regulated depending on the calcium levels in the blood but its efficiency declines with aging (Heaney and Recker, 1994).

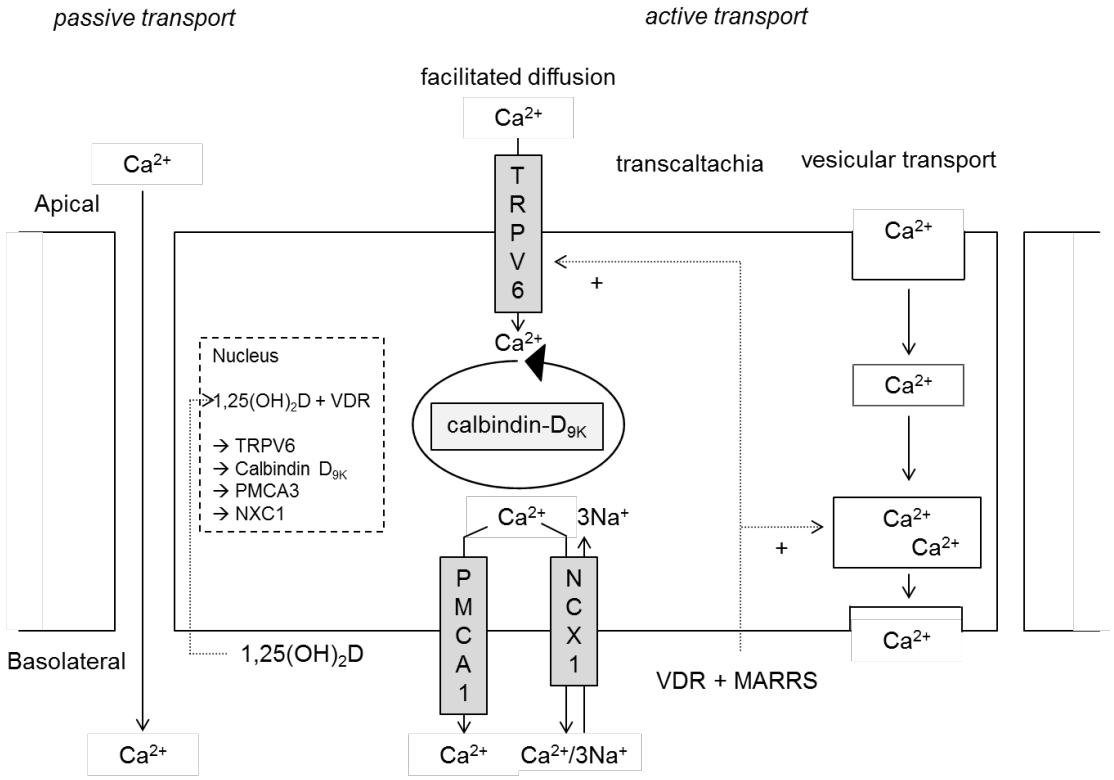

Figure 2: Schematic of the intestinal Ca^{2+} absorption showing active and passive transport across the enterocytes. Figure adapted from DiMeglio *et al.* (2014). Abbreviations: TRPV – transient receptor potential channel, PMCA – plasma membrane Ca^{2+} ATPase, NCX – Na^{+}/Ca^{2+} exchanger, VDR – intestinal vitamin D receptor, MARRS – membrane-associated, rapid-response steroid-binding protein.

1.1.2 Dietary factors affecting calcium absorption and balance

Dairy products (cheese, milk and yogurt), certain roots and legumes, as well as some vegetables are major food sources of bioavailable calcium (Weaver and Plawecki, 1994), while all the others only contribute in a small part to the requirements. Several food components can either increase or decrease calcium absorption. Food components that could alter calcium balance include nutrients such as protein, phosphorus, fat, sodium, and vitamin D or non-nutrients such as oxalates, phytates, and fiber (Weaver and Plawecki, 1994).

Negative calcium balance can be caused by food components that can either directly inhibit the absorption of dietary calcium or increase its urinary excretion. In both cases, the final outcome is a reduction in the total calcium balance, which increases calcium mobilization from bones. If this condition of negative balance is prolonged over time, it can ultimately result in the development of osteoporosis. Food components such as oxalate (present in spinach, kale and legumes (Franceschi and Horner, 1980)), phytic acid (major storage form of phosphorus in cereals and legumes, present in fiber containing whole grain products) and fibers can form unabsorbable complexes with calcium in the intestine reducing its absorption. Phytic acid can bind to calcium at gastric pH 2 (Graf, 1983) and its affinity increases with rising pH, and effectiveness also depends on the matrix (Dendougui and Schwedt, 2004). In rats, the addition of fructo-oligosaccharides to the diet reduced the inhibitory effect of phytic acid, supposedly by stimulating microbial activity to produce organic acids that lower the pH in the colon and increase calcium solubility (Lopez *et al.*, 2000). Sodium, alcohol, caffeine (tea and coffee) and excess protein (Darling *et al.*, 2009) were proposed as factors contributing to increased calcium excretion in the urine, therefore possibly resulting in a long term bone loss (Institute of Medicine, 2011).

On the other hand, lactose (Favus and Angeidbackman, 1984), proteins and phosphopeptides have been proposed as possible enhancers of calcium absorption by keeping it in solution and hence available for absorption (Gueguen and Pointillart, 2000). Specifically, urinary retention of calcium was improved by phosphorus, potassium bicarbonate (Sebastian and Morris, 1994) or potassium citrate (Moseley *et al.*, 2013). But, in the case of potassium bicarbonate it has been not fully clarified whether this effect is due to potassium or bicarbonate, as shown by Dawson-Hughes *et al.* (2009). Additionally, whey acidic proteins have been shown to reduce bone loss in rats (Kruger *et al.*, 2005) and dietary prebiotics (such as fructo-oligosaccharides) have a positive effect on absorption, bone structure and density (Scholz-Ahrens *et al.*, 2001); specifically, inulin demonstrated the most significant effect on improving calcium bioavailability in rats (Kruger *et al.*, 2003a) and also in young adolescents (Abrams *et al.*, 2005).

1.2 Calcium deficiency and overload

Calcium deficiency can be caused by inadequate intake, decreased absorption that may be related to either physiological conditions (such as aging, or vitamin D deficiency (DeLuca,

2004)) or dietary inhibitors, and increased excretion. All these factors lead to a negative calcium balance (excretion > absorption), and calcium is mobilized from the bones in order to increase its concentration in the blood and maintain calcium balance. Prolonged mobilization of calcium from the bones results in decreased bone mineral density (BMD), osteopenia and ultimately in osteoporosis (Institute of Medicine, 2011).

Normal bone mineral density is defined as 1 standard deviation of a normal adult reference mean, while a cut-off of 1-2.5 standard deviations and a cut-off > 2.5 standard deviations are categorized as osteopenia (low bone mass) and osteoporosis, respectively (Riggs and Melton, 1995; WHO, 1994). Osteoporosis is characterized by deterioration of bone mass and architecture with increasing risk of fractures (Christiansen, 1991). Fractures in the vertebra, hip, wrist-forearm, humeral and femoral in subjects older than 50 years, have been directly related to osteoporosis (Johnell and Kanis, 2005).

The safe upper level of calcium intake is 2500 mg. Excess intake can cause adverse effects such as hypercalcemia, hypercalciuria, vascular and soft tissue calcification, kidney stones, prostate cancer, interactions with iron and zinc and constipation (Institute of Medicine, 2011).

1.2.1 Epidemiology of calcium deficiency

Even though the risk of calcium deficiency has decreased over the past two decades, in 2011, 3.5 billion people worldwide were estimated to be at risk of calcium deficiency, especially in southern-hemisphere countries such as Africa, India and Indonesia (Kumssa *et al.*, 2015). Even though most of the northern-hemisphere countries, together with Australia, were at low risk of calcium deficiency, the risk of developing osteoporosis remained high (Kumssa *et al.*, 2015) as a possible consequence of vitamin D deficiency. Among 27 European countries, 22 million women and 5.5 million men were estimated to have osteoporosis, causing mostly fragility fractures to the hip, forearm and vertebra (Hernlund *et al.*, 2013). It was estimated that about 45% of women over 50 years of age in the United States have osteoporosis at one or more sites of risk of fracture (Melton *et al.*, 1992). The projections showed a drastic increase of fragility hip fractures from 1990 to 2050, projecting that the risk of hip fracture would affect up to 6.26 million people in 2050 (Cooper *et al.*, 1992). Annual costs caused by osteoporosis have been estimated to be up to £ 1.7 billion and $ 17.9 billion in the United Kingdom and the United States, respectively (Holroyd *et al.*, 2008).

1.3 Bone metabolism

1.3.1 Bone remodeling

The bone is comprised of 65% minerals (mainly HAp), 20-25% of organic matrix (mostly type I collagen, and cell protein and extracellular components in a minor amount) and 10% of water (Burr and Akkus, 2014). The bone is arranged in different layers and comprises a porous (trabecular, within the marrow cavity) and a more dense (cortical, outside shell) part; both parts serve as long term calcium storage sites. The bone gives stiffness, structure and protection to the body, and it is also a very dynamic tissue that is constantly formed by osteoblasts to store calcium or reabsorbed by osteoclasts to release it, forming the bone modeling cycle. This dynamic process is necessary to constantly create a structurally complete bone, to heal micro fractures and to ensure constant calcium concentration in blood. The remodeling cycle (**Figure 3**) is composed of 5 different stages and takes about 4-6 months to be completed (Allen and Burr, 2014). In the first stage the osteoclasts are activated (activation phase), then they initiate the mineral dissolution at the remodeling site, releasing collagen fragments (resorption phase). Bone resorption is either stopped by the osteoclast-osteoblast interaction or by the activation of osteoblasts activity during bone resorption phase (Sims and Gooi, 2008). Once the loose collagen fragments are removed, osteoblasts take over and start the formation process (reversal phase). Osteoblasts then form osteoids (type I collagen) and mineralize them with calcium and phosphorus (P) to build new bone (formation phase). At last, the mineralized matrix grows in to HAp crystals and further stabilizes (quiescence phase) (Allen and Burr, 2014).

In pre- and postmenopausal women from Denmark, high bone turnover measured with biochemical markers was directly associated with low bone mass in the spine, proximal femur and distal forearm (Ravn *et al.*, 1996). Pre- and early menopausal women had increased bone turnover (Ravn *et al.*, 1996). Especially in women during and after the menopause, bone loss is drastically increased up to 10 times greater than in the pre-menopausal period (Gallagher *et al.*, 1987). This loss is caused by the decrease in estrogen (hormone responsible for blocking remodeling), with a subsequent increase in osteoclasts activity. As well as hormonal changes, immobilization or reduced physical activity are associated with bone loss (Sievanen, 2010).

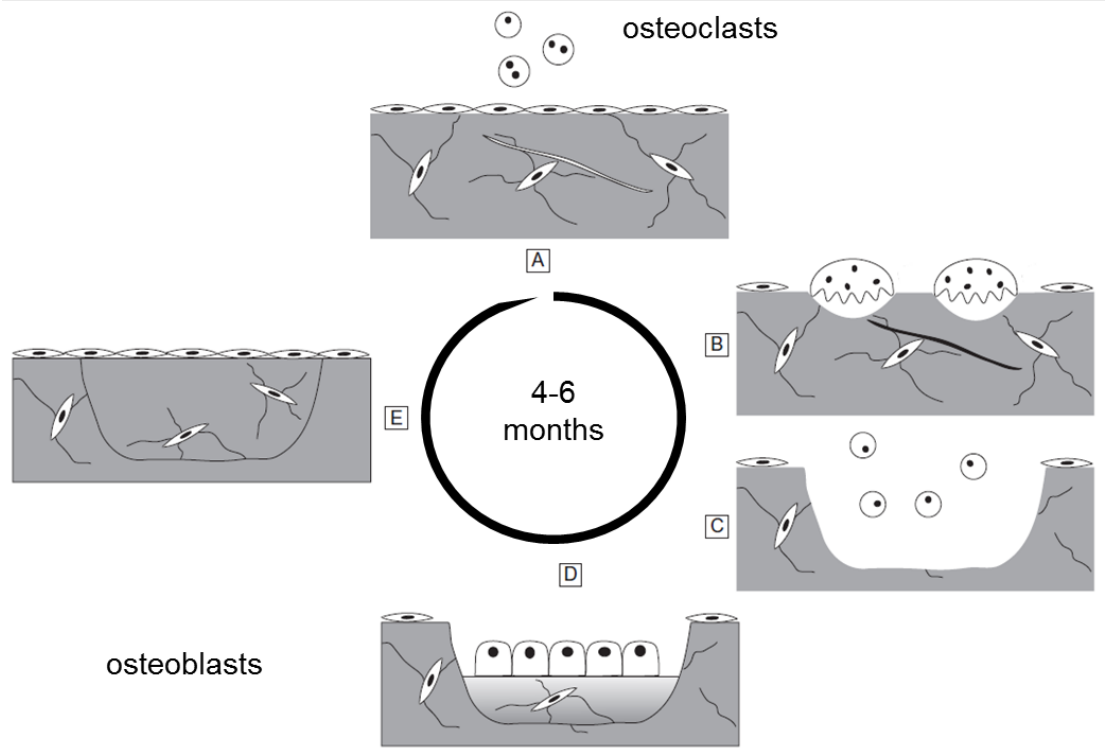

Figure 3: Schematic showing of the bone remodeling cycle (Allen and Burr, 2014) including A) activation, B) resorption, C) reversal, D) formation and E) quiescence.

In rats, high impact exercise alone was as efficient as dietary calcium supplementation coupled with exercise in increasing BMD (Welch *et al.*, 2008). Also soy (protein), specifically isoflavones, have been associated with a decreased risk of fracture in Asian female population (Zafar *et al.*, 2004), but this positive effect on suppressing of bone resorption was not confirmed in post-menopausal women by Cheong *et al.* (2007). Besides the significant role vitamin D plays in calcium absorption and BMD, also vitamin K was proposed to have a beneficial effect on bone mineralization, due to its role in the synthesis of osteocalcin and bone γ-carboxyglutamic acid (Reid and Macdonald, 2001). Low vitamin K intakes were associated with increased risk of hip fracture (Booth *et al.*, 2000) but not on BMD or bone turnover (Kruger *et al.*, 2006).

1.3.2 Biomarkers for bone formation / resorption

Measurement of biomarkers involved in the remodeling process is a very fast and inexpensive tool to provide an insight into the individual calcium status and, together with BMD, is a good indicator for risk of fractures. Biomarkers of bone resorption, such as collagen fragments (N-telopeptide or C-telopeptide) and cross-links (pyridinoline and deoxypyridinoline), are released during the resorption phase and are measured in serum and urine, whilst formation biomarkers such as alkaline phosphatase, osteocalcin and

procollagen type I N propeptide can be measured in serum (Allen and Burr, 2014). Even though biomarkers are a very useful tool to measure bone loss at the whole body level and hence predict the risk of fracture, they vary greatly within individuals and between assays (up to 15% inter- and intra assay variations) or can be subject to diurnal/nocturnal (osteocalcin and urinary crosslinks) and seasonal variations caused by different production of vitamin D (Woitge *et al.*, 1998). For instance, C-telopeptide is subject to circadian rhythm especially when the subjects are non-fasting, and age-related variations are observed in growing children. Reference values are available for pre-menopausal women but less information is available for the other population groups (Chubb, 2012). Recently, a metabolomics approach was used to assess metabolic changes associated with calcium deficiency in order to identify new urinary biomarkers possibly be associated with calcium deficiency (Wang *et al.*, 2013). The authors reported significant correlations between calcium intake and two biomarkers, pseudouridine and citrate, in post-menopausal women, however the function of these biomarkers in calcium metabolism still needs to be clarified (Wang *et al.*, 2013).

1.3.3 Techniques to measure bone quality

Bones serve as a calcium reservoir. Bone mass acquisition is at its highest during infancy and puberty and varies depending on skeletal site. Peak bone mass is achieved during the third decade of life (18-20 years (Baxter-Jones *et al.*, 2011)) where total calcium stores are around 900 mg for adult females and 1200 mg for males (Institute of Medicine, 2011), but these values can vary depending on total calcium intake, genetic background, physical activity and hormonal status (Bonjour *et al.*, 1994; Institute of Medicine, 2011). Bone mass is estimated by BMD which corresponds to a measure for bone strength and it was shown to be inversely correlated with the risk of fractures (Gardsell *et al.*, 1991). In an old model estimating the fracture risk in US women, Ross *et al.* (1988) projected that if not treated, 1.44 million fractures due to osteoporosis would occur (Ross *et al.*, 1988). Therefore improving BMD by having an adequate calcium intake would be the best strategy to reduce the risk of fractures and treatment-related costs.

Bone quality is measured not only as a diagnostic tool for osteoporosis, but also for results of experimental manipulations in the laboratory. Bone quality is measured using dual-energy X-ray absorptiometry (DXA), computed tomography (CT), magnetic resonance imaging (MRI),

ultrasound or radionuclide imaging, depending on the desired information. In the following section, emphasis will be given to the first two methods since they are the most practical for laboratory experiments.

1.3.3.1 DXA

DXA quantifies lean tissue mass, fat mass, total body mass and it is the most widely used technique to measure bone mineral content and BMD in human subjects in a non-invasive manner (Adams, 1997). Due to its fast scanning times and low radiation exposures it is also very useful in experimental measures. Databases to determine osteopenia and osteoporosis have been developed in comparison to healthy 30 years old subjects, which allows for a fast assessment of BMD quality (Allen and Krohn, 2014). BMD is calculated by dividing BMC by the area of a certain region, also defined as region of interest (ROI) (Formica *et al.*, 1995).

DXA differentiates bone from soft tissue and it is a 2 dimensional technique which only gives information about the areal density (g/cm^2) and no information about volume (g/cm^3), bone geometry or bone type (cortical or cancellous) is given. Another limitation is that, because the obtained value is an areal density, it changes depending on bone size. Even though scan interpretation is usually operator dependent (Lentle and Prior, 2003), the obtained values are reliable indicators for bone quality and risk of osteoporosis (Katikaneni *et al.*, 2009). When considering laboratory research models, DXA is a very useful and fast tool where BMD can be assessed either *in-* or *ex-vivo* and the most accessible parts are femur, lumbar vertebra L1-4 and full body (Stone and Turner, 2012).

1.3.3.2 CT

The generally called CT imaging can be divided into quantitative CT (qCT) and micro-CT. Both CT imaging techniques have shown to be a valid alternative to DXA (Bagi *et al.*, 2006). The novel approach of CT is that 3D scans can be obtained and therefore, in addition to bone mineral content (BMC) and BMD, also information about bone geometry and structure (volumetric bone mineral density) is provided (Day *et al.*, 2000). CT, as well as DXA is a non-invasive technique, however requires higher radiation exposure (almost 15 times larger than a classic X-ray for a typical central CT scan), which depends on the resolution and slice number (Allen and Krohn, 2014). CT has higher resolution when compared to DXA, therefore even if two objects are very close to each other, they can still be differentiated and

specifically, it can give information about the microarchitecture, distinguishing between cortical and trabecular regions (van der Linden *et al.*, 2006).

2 Physiology of iron

2.1 Iron metabolism

Iron has an atomic weight of 55.8 g/mol and its oxidation state ranges from Fe^{-2} to Fe^{6+} with ferrous (Fe^{2+}, water soluble) and ferric (Fe^{3+}, not water soluble) oxidative forms being the most biologically relevant ones. In nature, it is the second most abundant metal by weight that constitutes the earth's crust and of the most frequent forms are hematite (Fe_2O_3) and magnetite (Fe_3O_4) (Lide, 2015; Papanikolaou and Pantopoulos, 2005). The reduced form of iron, Fe^{2+}, is well absorbed, however, in contact with oxygen, it oxidizes to Fe^{3+}, becoming poorly bioavailable (Papanikolaou and Pantopoulos, 2005). A high fraction of cellular iron is associated with proteins in the form of heme (composed by protoporphyrin IX and a Fe(II) ion). The most abundant forms of hemoproteins serve as oxygen carriers in the erythroid (hemoglobin) and muscle (myoglobin) tissues (Paoli *et al.*, 2002). On the other hand, non-heme iron exists as iron-sulfur clusters and serve as electron transfer, transcriptional regulation, structural stabilization and catalysis (Papanikolaou and Pantopoulos, 2005).

The human body contains 3.5-5 g of Fe, most of which can be found in hemoglobin (3-3.5 g) and myoglobin (0.4-0.5 g). Lower amounts are present in ferritin and hemosiderin (1 g), heme and non-heme enzymes (0.1 g), intracellular or iron transit pool (7 mg) and transferrin (3 mg) (Aggett, 2012). Because iron is recycled and not excreted, basal (1-1.5 mg/d) (Green *et al.*, 1968) and menstrual losses are regulated by increasing intestinal absorption (Finch, 1994), and only 1-2 mg of iron need to be replaced daily (Aggett, 2012). **Figure 4** shows the main body sites where iron can be found and how homeostasis is maintained. Extracellular iron concentration is kept very tight, around 3 mg, and circulates in blood bound to transferrin (Fe-Tr). Daily, 20-25 mg iron are passed to the bone marrow for erythropoiesis (Hentze *et al.*, 2004), while iron coming from old erythrocytes is recycled by macrophages. Excess iron is stored in the hepatocytes of the liver and tissue macrophages from where it can be readily mobilized if required (Hentze *et al.*, 2004).

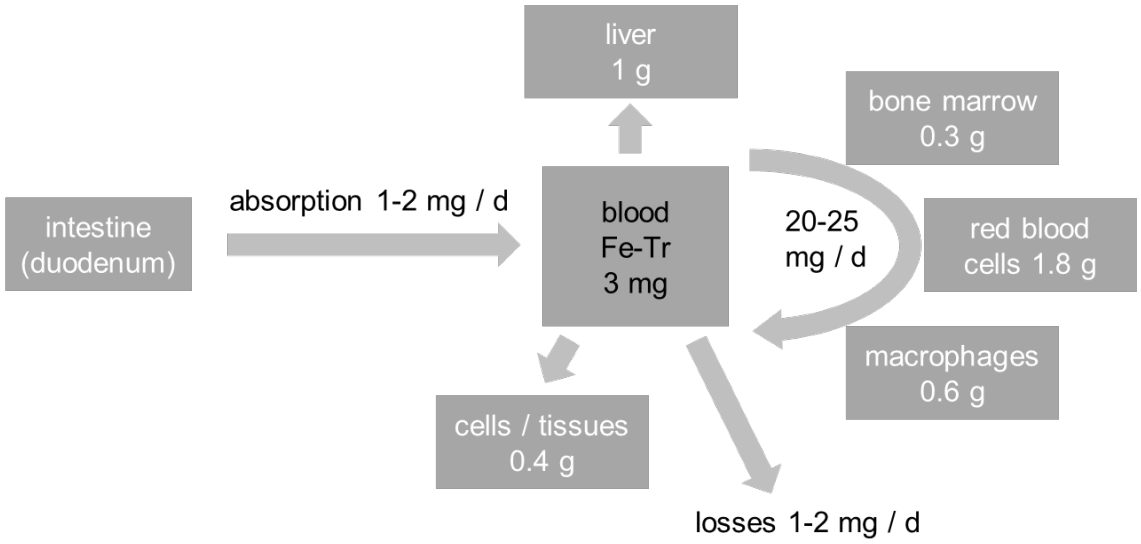

Figure 4: Body iron homeostasis adapted from Papanikolaou and Pantopoulos (2005). Abbreviations: Tf – transferrin.

2.1.1 Absorption / excretion / storage

Bioavailability of iron from the diet varies greatly depending on whether the ingested source is composed of heme (hemoglobin and myoglobin coming from meat) or non-heme iron (vegetables, fruits, cereals and animal non-heme sources). Depending on the body iron stores, heme and non-heme iron usually contribute to 15-35% and 2-20% of total absorbed iron, respectively (Carpenter and Mahoney, 1992).

Once ingested, iron is absorbed across the enterocytes of the duodenum and proximal jejunum (Frazer and Anderson, 2005). As shown in **Figure 5**, the uptake mechanism changes depending on whether it is in form of heme or non-heme. Non-heme iron (Fe^{3+}) is first reduced to the Fe^{2+} form by the duodenal cytochrome B reductase (Dcytb) (McKie *et al.*, 2001) and then transported by the divalent metal transporter (DMT 1) (Gunshin *et al.*, 1997) into the cytosol. It was suggested that heme iron is translocated intact though the duodenal enterocytes across the heme transporter (HCP 1) (Shayeghi *et al.*, 2005). However, HCP 1 has later been characterized as a folate/proton symporter in rats, showing its role in intestinal folate absorption (Inoue *et al.*, 2008; West and Oates, 2008) and until now, no specific transporter has been identified for intestinal heme uptake (West and Oates, 2008). Once in the cytosol, heme is degraded by entrocytic hemoxygenase (HO) (Raffin *et al.*, 1974) and joins the non-heme common Fe^{2+} transit pool (Jacobs, 1977). It can be then either stored as ferritin (Harrison and Arosio, 1996) and hemosiderin, or released into the blood stream via ferroportin (Fpn) (Abboud and Haile, 2000; Donovan *et al.*, 2000), oxidized back to Fe^{3+} and

bound to the iron transport protein transferrin (Tf). One molecule of Tf can reversibly bind 2 atoms of Fe^{3+} (Aisen *et al.*, 1978) with stronger affinity in the extracellular fluid and weaker affinity in the endosome, allowing Fe^{3+} to stay in solution under physiological conditions and dissociate in the endosome (Gkouvatsos *et al.*, 2012).

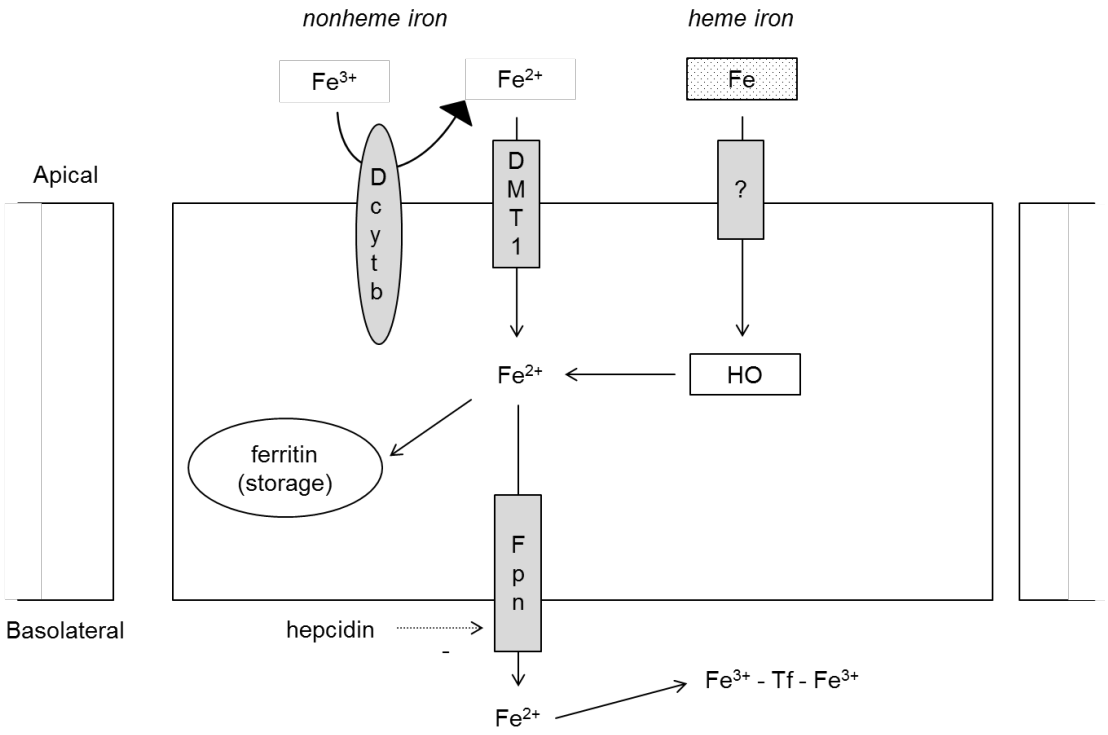

Figure 5: Schematic showing the intestinal iron absorption showing heme and non-heme transport across the enterocytes. Figure adapted from De Domenico *et al.* (2008) and Aggett (2012). Abbreviations: Dcytb - duodenal cytochrome B reductase, DMT 1 – divalent metal transporter, ? – unidentified heme transporter, HO – hemoxygenase, Fpn – ferroportin.

Homeostasis of cellular iron is regulated post-transcriptionally by two iron responsive proteins (IRP1 and IRP2) that can bind to iron responsive elements present on ferritin and Tf mRNA (Aggett, 2012; Rouault, 2006). In case of low iron concentration in the cell, IRP binds to ferritin mRNA inhibiting its translation and at the same time stabilize Tf mRNA protecting it from nuclease degradation. When iron concentration is high, IRPs are degraded and cannot bind to mRNA, allowing ferritin synthesis and degradation of Tr mRNA (Rouault, 2006). Hepcidin, a hormone primarily secreted by the liver (Park *et al.*, 2001), plays a central role in regulating systemic iron homeostasis (Pigeon *et al.*, 2001; Roetto *et al.*, 2003). Hepcidin reduces the amount of circulating Fe-Tr, by downregulating Fpn and DMT 1 and therefore, respectively decreasing iron release and increasing iron uptake from the enterocytes and macrophages. However, whether its mode of action includes the direct binding to Fpn or a general decrease in the expression components of the export-factor

components, still remains unexplained (Hentze *et al.*, 2004). In case of acute or chronic infections and inflammation, the immune system secretes inflammatory cytokines which upregulate hepcidin. This leads to a mild to moderate anemia (Cartwright *et al.*, 1946) and hemoglobin falls to 80-95 g /L, caused by a sequestration of circulating iron and increased retention and decreased export of iron (Weiss and Goodnough, 2005).

2.1.2 Dietary factors affecting iron absorption

The efficiency and the amount of iron taken up by the enterocytes can be modulated by the individual iron status (iron homeostasis, Chapter 2.1), individual inflammation status (hepcidin, Chapter 2.1.1), type of dietary iron (heme vs. non-heme) and by the dietary source. While principal dietary sources of non-heme iron are plants and animals, heme iron comes exclusively from animal sources (Hurrell and Egli, 2010) and could contribute up to 40% of total absorbed iron of a meat eating population (Monsen *et al.*, 1978). The absorption of non-heme iron, on the other hand, varies depending on the presence of food components that could potentially inhibit its absorption (Hurrell and Egli, 2010), such as milk proteins (casein, whey and egg white) (Cook and Monsen, 1976), polyphenols (especially tannic and gallic acid rich black tea and coffee) (Hurrell *et al.*, 1999) and phytates (cereals, legumes, nuts and seeds). The latter is known to have a dose-dependent inhibitory effect that starts already at a low concentration of 2-10 mg/meal (Hallberg *et al.*, 1989). Also calcium was shown to reduce iron absorption in humans (Cook *et al.*, 1991; Hallberg *et al.*, 1991), but no negative long term health effects causes by iron-calcium interaction were proposed (Minihane and Fairweather-Tait, 1998). The inhibitory effect of calcium is supposedly related to the possible internalization of DMT1 in the presence of Ca^{2+} as observed in Caco-2 cell models (Thompson *et al.*, 2010) and in downregulation of DMT1 expression in animal models (Shawki and Mackenzie, 2010). Additionally, Shawki and Mackenzie (2010) observed how the downregulation of DMT1 was also caused by alkaline-earth metal ions Ba^{2+}, Sr^{2+}, and Mg^{2+}.

On the other hand, food components that can enhance iron uptake are ascorbic acid (Cook and Monsen, 1977; Cook and Reddy, 2001; Lynch and Cook, 1980; Reddy and Cook, 1991), citric, malic and lactic acids (Aggett, 2012). Ascorbic acid functions as a reductant of ferric to ferrous iron and as a potential iron chelator, but is very sensitive to food processing, cooking and storage (Hurrell and Egli, 2010; Teucher *et al.*, 2004). Muscle tissue has shown

enhancing properties for non-heme iron absorption in adults (Hurrell *et al.*, 1988) and infants (Engelmann *et al.*, 1998). This 'meat effect' was then related to the reducing and chelating properties of the amino acids cysteine and histidine (Layrisse *et al.*, 1984; Vattem *et al.*, 2001). Recently it was shown how *in vitro* pepsin digestion can result in a multitude of iron-binding peptides. However, the ones containing glutamic and aspartamic acid were isolated and proposed as low molecular weight iron-binding proteins that can protect iron from complexing and helping iron to remain absorbable also at higher intestinal pH (Storcksdieck Genannt Bonsmann and Hurrell, 2007).

2.2 Iron deficiency and overload

Iron deficiency (ID) is caused by a long term negative iron balance that ultimately results in impaired erythropoiesis. The World Health Organization (WHO) defines ID as 'a condition in which there are no mobilizable iron stores (hemosiderin and ferritin) and in which signs of a compromised supply of iron to tissues, including the erythron, are noted' (WHO, 2001). Low iron intake or intake of poorly bioavailable iron eventually depletes body iron stores and, if not replenished, can lead to iron deficiency anemia (IDA). IDA is characterized by a decline in the size of red blood cells and a decrease in hemoglobin levels below 2 SD compared to a normal population value of the same gender/age (WHO, 2001). Indicators such as hemoglobin, mean cell volume, serum ferritin (SF), transferrin receptor saturation (sTFr), sTfR-to-SF ratio, body iron stores, and zinc protoporphyrin, with respective proposed cutoffs, are commonly used indicators of iron status (WHO and CDC, 2007; Zimmermann and Hurrell, 2007).

IDA can adversely affect children's mental and physical development (Grantham-McGregor and Ani, 2001) while adults can present a decreased reduced work capacity and cognitive performance (Sachdev *et al.*, 2005) and also be more vulnerable towards developing infections (Dunne *et al.*, 2002). Pregnant women have increased iron needs and therefore also a higher risk of developing IDA (Zimmermann and Hurrell, 2007), which can then cause preterm delivery, low birth weight and possibly inferior neonatal health (Allen, 2000).

Iron overload can be caused by inherited overload syndromes (hemochromatosis) (Pietrangelo, 2004) or by increased iron intake (Aggett, 2012). Independent of the origin, chronic iron overload has been linked to increased cancer incidence, cardiovascular disease, neurological disease, arthropathies, and diabetes mellitus (Aggett, 2012). Iron toxicity is

caused under anaerobic conditions where Fe^{2+} reacts with hydrogen peroxide (H_2O_2) in the Fenton and Haber-Weiss reaction, producing reactive oxygen species (ROS), also known as free radicals (Papanikolaou and Pantopoulos, 2005). Free radicals are particularly dangerous because they can oxidize and therefore damage proteins and cell membrane (Papanikolaou and Pantopoulos, 2005).

2.2.1 Epidemiology of iron deficiency

In 2002, micronutrient deficiency was classified as one of the main contributors to loss of healthy life (Ezzati *et al.*, 2002), and latest reports have estimated that IDA was responsible for 50% of all cases of anemia (WHO, 2008) and was the cause of death of 800'000 individuals worldwide (Stoltzfus, 2003). In 2010, anemia was estimated to account for 8.8% of the total disability, with pre-school children (< 5 years), pregnant and non-pregnant women being the population groups with the highest burden (Kassebaum *et al.*, 2014). According to the latest reports by WHO, Africa and South-East Asia have the highest anemia prevalence (WHO, 2008). Specifically, in Africa, anemia prevalence was estimated to be of 67.6%, 57.1% and 47.5% in pre-school children, pregnant women and non-pregnant women, respectively, in the investigated WHO regions. While in South-East Asia, the prevalence corresponded to 65.5%, 48.2% and 45.7% for the same population groups. In Europe, the prevalence was much lower but still present, corresponding to 21.7%, 25.1% and 19.0%. In total, anemia affects about 170, 315 and 54.5 million people in Africa, South-East Asia and Europe, respectively.

3 Strategies to overcome calcium and iron deficiency

Micronutrient deficiency and malnutrition play a central role in the impaired underdevelopment of an individual and are the primary causes of reduced work capacity, illness and disability, especially in unprivileged groups. Therefore, WHO has identified micronutrient and malnutrition as major causes for an inadequate national socio-economic development (Allen *et al.*, 2006). Micronutrient deficiency is usually caused by suboptimal dietary intakes associated with monotonous diet (Zimmermann *et al.*, 2005). Calcium and iron requirements vary depending on gender (especially for iron) and life stage, as shown in **Table 1**. The values reflecting the dietary reference intakes for the US population are reported from the Institute of Medicine and as estimated average requirement (EAR) and as adequate intake (AI), while the ones for the European populations are reported from the European Commission and indicated as population reference intakes (PRI).

In order to overcome micronutrient and mineral deficiency, the approaches used are seen as complementary to each other and they are comprised of dietary diversification, nutritional education, public health and food safety measures, food fortification and supplementation (Allen *et al.*, 2006). Food diversification is the most often recommended approach. However, it involves long term change in lifestyle and requires the consumption of foods rich in calcium (milk and dairy products) and iron (meat). Unfortunately, this approach is not always achievable especially for low income countries or individuals with specific dietary restrictions as lactose intolerant and vegetarians. Supplementation is often seen as the fastest option to overcome deficiency, while fortification, although having a wider and sustainable effect, is not that immediate (Allen *et al.*, 2006). In **Table 2** the major compounds used for food fortification and supplementation are summarized and ranked according to their element content.

Table 1: Dietary reference intake (DRI), 1) Estimated Average Requirements (EAR), 2) Recommended Dietary Allowance (RDA) and Adequate Intake (AI) (Institute of Medicine, 2011) and *population reference intake (PRI)* (EFSA Panel, 2015a, b). Abbreviations: m = months, y = years.

	Ca (mg/d)			Fe (mg/d)		
Life stage/group	EAR	**RDA** and AI*	*PRI*	EAR	**RDA** and AI*	*PRI*
Infants						
0-6 m	-	200*		-	0.27*	
6-12 m	-	260*		6.9	**11**	
4-12 m			*330*			*8*
Children						
1-3 y	500	700		3.0	**7**	
4-8 y	800	1000		4.1	**10**	
1-4 y			*600*			*8*
4-7 y			*750*			*8*
7-10 y			*900*			*10*
Males						
9-13 y	1100	**1300**		5.9	**8**	
10-13 y			*1100*			*12*
14-18 y	1100	**1300**		7.7	**11**	
13-19 y			*1200*			*12*
19-70 y	800	**1000**	*1000*	6	**8**	*10*
> 70 y	1000	**1200**	*1000*	6	**8**	*10*
Females						
9-13 y	1100	**1300**		5.7	**8**	
10-13 y			*1100*			*15*
14-18 y	1100	**1300**		7.9	**15**	
13-19 y			*1200*			*15*
19-50 y	800	**1000**	*1000*	8.1	**18**	*15*
51-70 y	800	**1200**	*1000*	5	**8**	*10*
> 70 y	1000	**1200**	*1000*	5	**8**	*10*
Pregnancy						
14-18 y	1000	**1300**		23	**27**	
19-50 y	800	**1000**		22	**27**	
all ages			*1000*			*30*
Lactation						
14-18 y	1000	**1300**		7	**10**	
19-50 y	800	**1000**		6.5	**9**	
all ages			*1000*			*20*

Dietary supplements are not intended as conventional food or as the sole item of a meal and can occur in form of tablet, pill, capsule or liquid (Halsted, 2003). The Center for Disease Control and Prevention estimated that 40% of the supplements consumed by adults are multivitamins and multiminerals and that supplement consumption has increased from 40 to 50% from 1988 to 2006 (Gahche *et al.*, 2011). Between 2005 and 2006 in the United States, Qato *et al.* (2008) estimated that nearly half of the older adults (aged 57-85 years) that participated in the study regularly consumed at least 1 dietary supplement (Qato *et al.*, 2008) and 61% of women over 60 years were regularly consuming supplemental calcium (Gahche *et al.*, 2011). In Europe, a study conducted in Lausanne (Switzerland), reported that

16.8% of the investigated subjects consumed general vitamin and mineral supplements, 6% calcium and 1.8% iron supplements (Marques-Vidal *et al.*, 2009). Calcium supplements are especially consumed by postmenopausal women to reduce the risk of developing osteoporosis (Fairweather-Tait and Teucher, 2002a), while iron supplements are very suitable to overcome deficiency in women (Fairweather-Tait and Teucher, 2002b) and pregnant women with increased iron requirements (Baltussen *et al.*, 2004). On the other hand, fortification consists of adding the micronutrients directly to staple or processed food (Allen *et al.*, 2006) and this approach is seen as a more sustainable and cost-effective option (Zimmermann and Hurrell, 2007), especially in developing countries since it has the advantage of reaching all population groups, including children (Baltussen *et al.*, 2004; Fairweather-Tait and Teucher, 2002b). Requirements such as high consumption of the fortified food by the target population and the use of well absorbed fortificants that do not cause sensory changes of target foods are necessary in order to have a successful outcome (Allen *et al.*, 2006). Additionally, the interested individuals are not required to change their food habits. Types of fortification consist of mass fortification of goods that reach the general population (salt, four, rice), of targeted fortification of foods designed for specific population subgroups (complementary foods for toddlers) and of market-driven fortification driven by food industries (ready-to-eat products) (Allen *et al.*, 2006).

When choosing the right supplement/fortificant, several factors come into play such as costs, element bioavailability, target population and target food (in the case of fortification). It is very challenging to find the perfect compound that covers all these aspects in the most effective way.

Table 2: Major calcium and iron sources (with their approximate element content calculated from the chemical formula) approved as fortificants and supplement by the Food and Drug Administration and by the European Parliament and Council Food Supplements. Table adapted from Fairweather-Tait and Teucher (2002b).

	Calcium			Iron	
	g Ca/100 g	chemical formula *(molar mass g/mol)*		g Fe/100 g	chemical formula *(molar mass g/mol)*
Compound			Compound		
Calcium oxide	71	CaO *56*	Elemental iron (electrolytic)	100	Fe *56*
Calcium hydroxide	54	$Ca(OH)_2$ *74*	Ferrous carbonate	48	$FeCO_3$ *116*
Calcium carbonate	40	$CaCO_3$ *100*	Ferrous fumarate	33	$C_4H_2FeO_4$ *170*
Calcium phosphates Ca:P molar ratio 1-1.67	24-40	1 Ca – *172* 5 Ca – *502*	Ferrous sulfate	33	$FeSO_4.H_2O$ *170*
Calcium chloride	36	$CaCl_2$ *111*	Ferric pyrophosphate	30	$Fe_4(P_2O_7)_3$ *745*
Calcium citrate	21	$Ca_3(C_6H_5O_7)_2$ *570*	Ferric phosphate	30	$FePO_4 \cdot 2H_2O$ *187*
Calcium glycerolphosphate	19	$C_3H_7CaO_6P$ *210*	Ferrous lactate	24	$C_6H_{10}FeO_6$ *234*
Calcium lactate	18	$C_6H_{10}CaO_6$ *218*	Ferrous citrate	23	$C_6H_6FeO_7$ *246*
Calcium gluconate	9	$C_{12}H_{22}CaO_{14}$ *430*	Ferric sodium pyrophosphate	22	$FeNaO_7P_2$ *253*
			Ferric saccharate	15	$C_{18}H_{24}Fe_2O_{24}$ *736*
			Sodium iron EDTA	13	$C_{10}H_{12}FeN_2NaO_8 \cdot 3H_2O$ *421*
			Ferrous gluconate	12	$C_{12}H_{26}FeO_{16}$ *482*

3.1 Calcium

In the US, calcium supplements contain around 1000 mg calcium (Slesinski *et al.*, 1996), while the fortification level is set at 120 mg/serving beverage (Russell *et al.*, 2010) and 300 mg/150 g (Heaney *et al.*, 2000). Because of their high calcium content and low price, $CaCO_3$ and calcium phosphates are widely used as calcium sources, but they both have poor solubility at neutral pH (Levenson and Bockman, 1994) and therefore are subject to sedimentation when added to beverages and, in the absence of gastric acid secretion, are poorly soluble (Pak and Avioli, 1988). The advantage of calcium phosphate is the concurrent supply of calcium and phosphorus, both essential elements in bone structure. Calcium phosphates consist of calcium and phosphate atoms, but their crystal structure, calcium

content and solubility changes with varying Ca:P molar ratio (Dorozhkin, 2007). Nutritionally relevant calcium phosphates are dicalcium phosphate ($HCaPO_4$, Ca:P = 1), tricalcium phosphate (Ca_3PO_4, Ca:P = 1.5) and hydroxyapatite (HAp, $Ca_5(PO_4)_3(OH)$, Ca:P = 1.67) (Levenson and Bockman, 1994; Lide, 2015). Although $CaCO_3$ is the most used calcium source, studies have shown how calcium phosphates such as tricalcium phosphate (Heaney *et al.*, 2010) or HAp (Kruger *et al.*, 2003b) would result to be just as bioavailable. On the other hand, calcium sources such as citrate, lactate or gluconate contain less calcium but their solubility does not depend on pH (Levenson and Bockman, 1994) and therefore might be preferred for achlorhydric patients (Recker, 1985) or more in general in elderly with impaired gastric acid output (Coudray *et al.*, 2006). In a randomized control trial, calcium lactate-citrate and calcium lactate-malate have shown the same bioavailability as calcium carbonate and calcium gluconate (Kressel, 2010).

Food fortification with calcium is very challenging because of pH changes caused by the release of Ca^{2+} ions, high requirements of calcium and the risk of resulting in a chalky texture and feel (Tobelmann, 2001). Calcium fortified foods consist of foods that do not normally contain high calcium amounts such as fruit juices, other beverages, breakfast cereals, bread and bread products (Rafferty *et al.*, 2007). Zhao *et al.* (2005) showed that calcium absorption from soy milk fortified with $CaCO_3$ and from cow's milk at similar calcium loads do not differ. On the other hand, tricalcium phosphate (Ca:P = 1.5) showed significantly lower absorption of calcium (Nickel *et al.*, 1996). In an animal balance study, HAp (Ca:P = 1.67) was as well absorbed as carbonate when added to milk (Kruger *et al.*, 2003b).

3.2 Iron

In order to overcome IDA during pregnancy, iron supplements are given at a dose of 60 mg iron/d for at least 6 months (Stoltzfus and Dreyfuss, 1998) while the fortification level is typically set to 2 mg iron/100 g food (Hurrell *et al.*, 1991). Iron containing compounds can either be soluble in water (such as ferrous sulfate or gluconate), in dilute acid (ferrous fumarate) or insoluble in water/dilute acid (such as elemental iron, ferric pyrophosphate and ferric phosphate). Water soluble compounds, besides being the most bioavailable, cause undesirable color and taste changes (Hilty *et al.*, 2010; Hilty *et al.*, 2011) and protein precipitation in the specific case of ferrous sulfate (Hurrell, 2007). Low matrix pH and high polyphenol content are both determinants of matrix reactivity to the iron fortificant.

Specifically, low pH increases iron solubility which than can easily react with hydroxyl groups of polyphenols, resulting in iron-polyphenols complexes and hence undesirable color changes (Hilty *et al.*, 2011; Perron and Brumaghim, 2009). On the other hand, water insoluble compounds, such as electrolytic iron (recommended for cereal flour) (Hurrell, 2007) and ferric pyrophosphate are less likely to cause color changes in food but at the same time are poorly bioavailable (Allen *et al.*, 2006). Therefore it is recommended that these compounds are added at twice the level of ferrous sulfate (Hurrell, 2007). Finally, iron chelators such as sodium iron EDTA and ferrous bisglycinate have the advantage of protecting iron from the inhibitory effect of phytic acid, but because it is very soluble in water or dilute acid, sensory changes can still easily occur. Sodium iron EDTA is therefore recommended as an iron fortificant in high-phytate cereals and in low-phytate fish sauce and soy sauce to half and same level of ferrous sulfate, respectively (Hurrell, 2007).

4 Nanostructured compounds for fortification and supplementation

Nano-structuring was originally used in drug research to improve the efficacy of pharmaceuticals (Muller *et al.*, 2001). In nutrition, size reduction of poorly absorbable calcium and iron compounds has been proposed as a promising approach to significantly increase their bioavailability while keeping their sensory changes to the minimum. The definition of nanostructured-materials or nanomaterials is a consideration of both particle size and specific surface area (SSA, m^2/g). Specifically, The European Commission (2011) stated in the articles nr. 2 and 5 that nanomaterials are '*natural, incidental or manufactured material containing particles, in an unbound state or as an aggregate or as an agglomerate and where, for 50% or more of the particles in the number size distribution, one or more external dimensions is in the size range 1 nm–100 nm*'. In addition, article nr. 5 says that '*materials with SSA ≥ 60 m^2/cm^3 or having SSA ≤ 60 m^2/cm^3 but presenting a number size distribution complying with the mentioned definition, would be defined as nanomaterials*'. However, article nr. 5 only applies together with nr. 2. For instance, a porous material that has an SSA > 60 but no more than 50% of the powder has particles size of 1-100 nm will not be classified as nanoparticle.

4.1 Nanoparticles in nutrition: potential benefits in nutrition and risks for human health

Crystal engineering has shown to be a valid approach to improve the bioavailability of poorly soluble pharmaceutical drugs (Blagden *et al.*, 2007), and the same approach can be applied in nutrition. For instance, the reduction in particle size increases the surface-to-volume ratio, and a smaller particle size, increases the percentage of material that is on the surface (Nel *et al.*, 2006). This results in an increased instability and therefore reactivity (Hornyak *et al.*, 2009b), faster dissolution and increased dissolution rate (Hilty and Zimmermann, 2014a). The high SSA together with small particle size makes nanoparticles very attractive for nutritional application and the nanosizing-approach has shown promising results in increasing the bioavailability of several micronutrients such as iron, calcium, magnesium, zinc, selenium and copper (Hilty and Zimmermann, 2014b). Specifically for iron, Wegmuller *et al.* (2004), Rohner *et al.* (2007) and Hilty *et al.* (2010) showed that iron pyro- and ortho-phosphate (both water insoluble and poorly soluble in diluted acid (Hurrell, 2002)) can become as bioavailable as the 'gold standard' $FeSO_4$ (water soluble) once reduced in size.

But also size reduction of $CaCO_3$ has mainly shown increased calcium bioavailability (Erfanian *et al.*, 2014; Gao *et al.*, 2008; Huang *et al.*, 2009; Meiron *et al.*, 2011), but not always (Shahnazari *et al.*, 2009).

An increase in SSA, and also amorphous structuring might have an advantage in increasing the bioavailability of a compound. Crystalline materials are defined as '*substance consisting of atoms arranged in a pattern that repeats periodically in three dimensions*', while the amorphous (or non-crystalline) state is defined as materials that '*when characterized by X-ray crystallography, do not exhibit the sharp reflections associated with crystalline materials, but instead, exhibit a few broad halos*' (Bagley *et al.*, 1974). Amorphous materials, together with nano-crystalline materials, can be seen as isotropic, that means they possess the same properties and function equally well in all spatial directions (Weiner *et al.*, 2000). They can therefore be shaped easily and present potentially increased solubility compared to their crystalline form (Weiner *et al.*, 2003). For instance, amorphous pharmaceuticals are considered to be more soluble than their crystalline form (Hancock and Parks, 2000) and amorphous CaCO3 was observed in nature as transient precursor phases for the crystalline and stable aragonite and calcite (Addadi *et al.*, 2003). It was previously shown that amorphous structuring can increase the dissolution of iron-zinc nanoparticles, independent of the SSA and that a high SSA is more relevant in case of crystalline compounds (Hilty *et al.*, 2009). Other compounds such as amorphous $CaCO_3$ or phosphate, have been of interest especially for their increased calcium bioavailability (Meiron *et al.*, 2011) or as biomaterials (drug-delivery systems (Ginebra *et al.*, 2006) and cements in orthopedic and dental applications (Combes and Rey, 2010; Gras *et al.*, 2013)).

4.2 Common methods used to produce nanostructured materials

Nanostructured materials can be produced in a top-down or a bottom-up manner or in a hybrid fabrication technology that includes both methods (Hornyak *et al.*, 2009c). In the top-down process, a solid bulk material is reduced into solid nanoparticles, using mechanical (such as milling or grinding), physical or chemical processes. Milling results in size reduction by applying mechanical force and attrition that deform a bulk, resulting in broken particles with grain size < 5 nm (Hornyak *et al.*, 2009c). The final product can be, however, highly polydisperse and contaminated (Hornyak *et al.*, 2009c). Nanometer pearl powder with an average diameter of 40–80 nm were, for example, produced by grinding natural pearls (Gao

et al., 2008). In a bottom-up process, atoms and molecules that are usually in liquid form are transformed into solid nanoparticles using methods such as wet precipitation, spray drying or aerosol synthesis. Production via precipitation method consists of adding a precipitation agent to the dissolved precursor. Particle size can be controlled by varying precursor's concentration or solution's pH (Jolivet *et al.*, 2008). Also spray drying can be successfully used to produce nanoscale materials (Carne-Sanchez *et al.*, 2013). For instance, calcium phosphate nanoparticles were produced by the spray drying method, resulting however in a quite small SSA of 12-50 m^2/g (Sun *et al.*, 2010), while HAp was synthesized with an average size of 20 nm (Luo and Nieh, 1995).

In the following section the bottom-up synthesis will be discussed. Specifically, the production of nanostructured calcium by flame (assisted) spray pyrolysis (main research focus of the Particle Technology Laboratory, ETH Zurich) and of nanostructured iron by precipitation on protein fibrils (main research focus of the Laboratory of Soft Materials, ETH Zurich) will be covered.

4.2.1 Production of nanostructured calcium using flame (assisted) spray pyrolysis

Aerosol synthesis of nano-materials can be carried out using flame assisted spray pyrolysis (FASP, low enthalpy precursor solution), flame spray pyrolysis (FSP, high enthalpy precursor solution) and vapor-fed aerosol flame synthesis (VAFS, vapor precursor) (Teoh *et al.*, 2010). FSP and FASP allow the synthesis of tailor-made products where composition and particle size can be specifically controlled with changing precursors composition and solvents. Any combination of elements can be dissolved in the precursor, and as long as the element is not removed in the flame, multimineral compounds can be produced (Hilty *et al.*, 2010; Knijnenburg *et al.*, 2013; Teoh *et al.*, 2010). The main advantages of aerosol processes are the absence of liquid by-products, low cost precursors, easy and inexpensive particle collection method, high purity products and fewer production steps. On the other hand, disadvantages such as formation of unbreakable hard agglomerates, porous, hollow or inhomogeneous particles, and polydisperse particle size distributions can occur (Buesser and Pratsinis, 2012; Strobel and Pratsinis, 2007).

In FSP synthesis (**Figure 6** left), a liquid precursor containing the desired elements is constantly fed though a nozzle, dispersed by oxygen resulting in fine spray and together with the methane/oxygen gases, the liquid phase evaporates and forms precursor vapor.

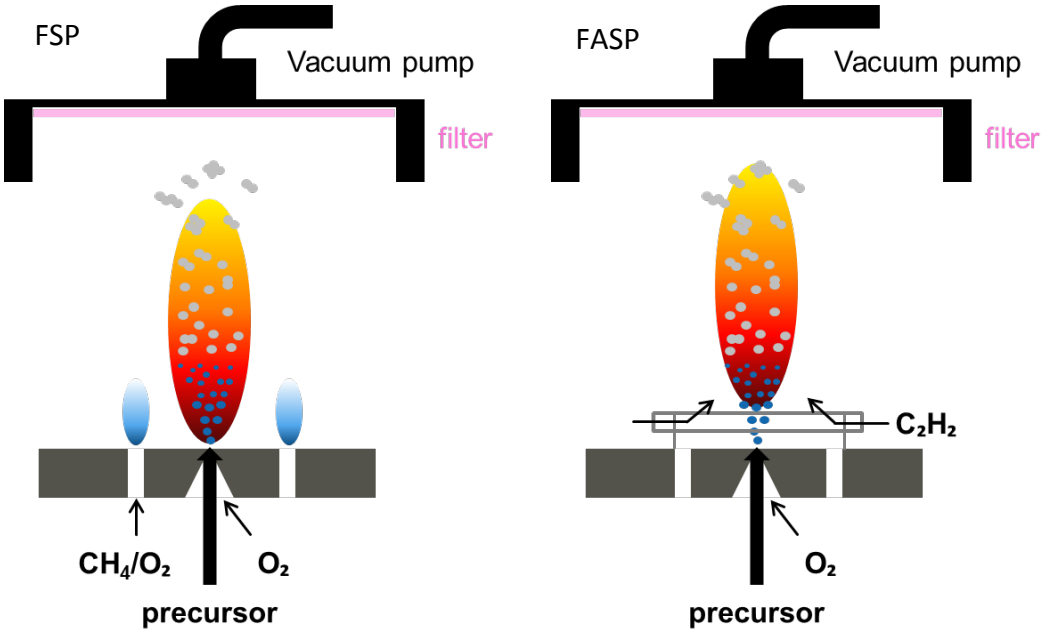

Figure 6: Schematic showing of the flame spray pyrolysis (FSP, left) and flame assisted spray pyrolysis (FASP, right) setups, adapted from Rudin and Pratsinis (2012).

Particle formation is shown in **Figure 7** and occurs in the flame by nucleation due to supersaturation of the vapor. Particle growth is then ensured by coalescence, sintering, aggregation and agglomeration (Pratsinis, 1998). Ideally, the entire solvent should evaporate (gas-to-particle conversion), resulting in homogeneous nanoparticles. FSP produced nanomaterials are usually non-porous particles with a narrow size distribution (Pratsinis and Vemury, 1996). Fast cooling rates (corresponding to shorter residence times in the flame) directly influence formation of hard agglomerates and decrease particle size (Strobel and Pratsinis, 2007). Size can also be systematically varied using precursor concentration and composition (the higher the concentration, the bigger the particle size (Strobel and Pratsinis, 2007)), precursor flow rate (higher flow rate correspond to lower SSA due to increased residence times at higher temperatures (Maedler and Pratsinis, 2002)) and flow rate of the dispersion gas (higher flow rates lead to lower flame temperature, resulting in smaller particles (Maedler *et al.*, 2002a)).

When the solvent does not evaporate completely (droplet-to-particle conversion), larger particles are additionally formed, resulting in an undesired bimodal and inhomogeneous size distribution of the particles (Maedler *et al.*, 2002b). The droplet-to-particle conversion could be eliminated by increasing the burning enthalpy of the precursor/gas system, specifically by substituting methane with acetylene such as in case of FASP.

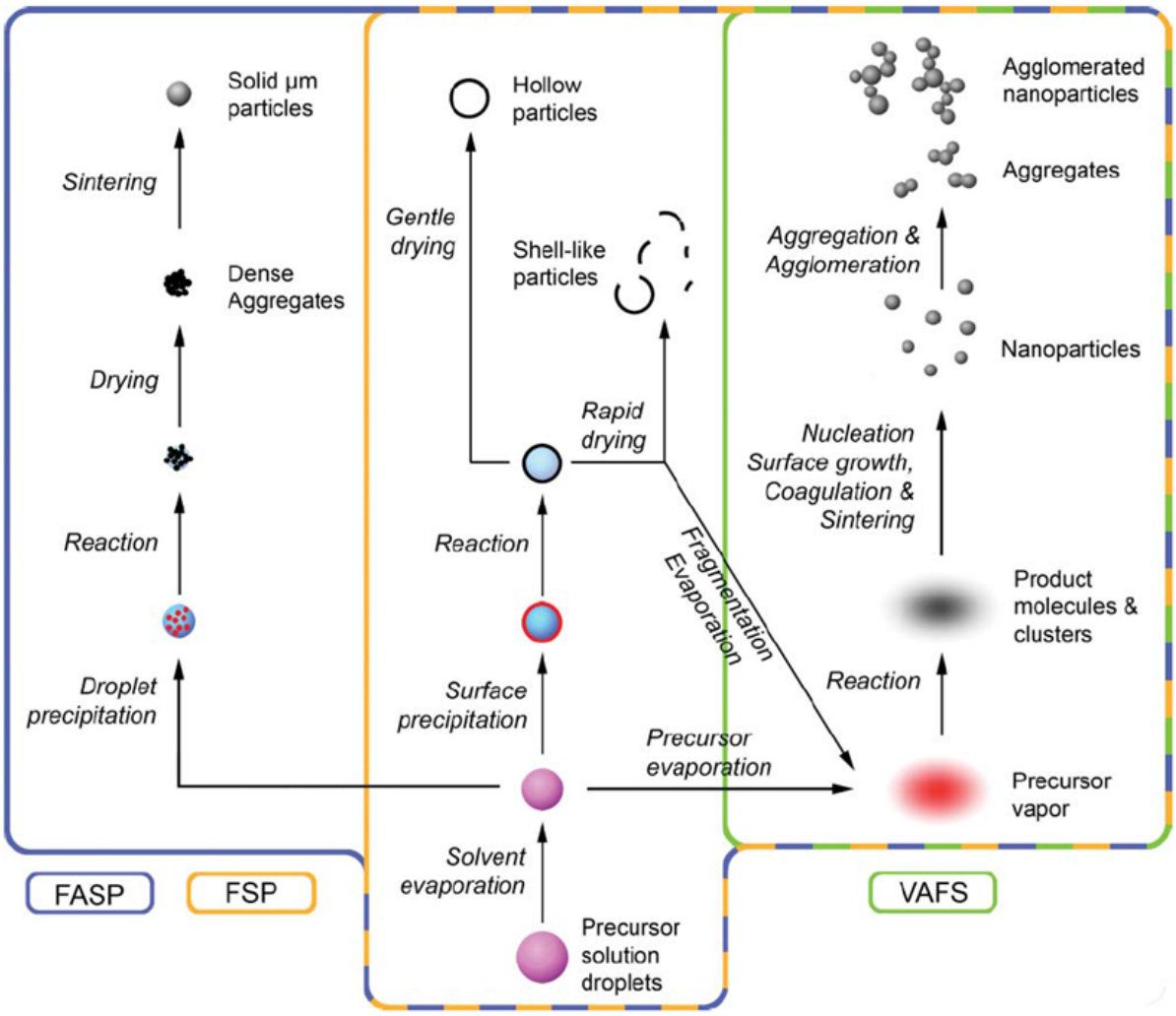

Figure 7: Schematic showing of particle formation in the FASP, FSP and VASP process (Strobel and Pratsinis, 2007).

FASP (**Figure 6** right) works on the same principle as FSP, but in this case the burning enthalpy is given by acetylene (C_2H_2) and the gas is sprayed through a circular ring positioned 1 cm above the nozzle (Rudin *et al.*, 2011). The higher burning enthalpy has shown to increase the homogeneity of $FePO_4$ and to remove the poorly dissolvable iron oxide that was formed during FSP synthesis (Rudin and Pratsinis, 2012).

Previously, Loher *et al.* (2005) successfully produced and characterized FSP-made calcium phosphates with calcium to phosphorus molar ratio from 1.43 to 1.63. Using calcium carboxylate and tributyl-phosphate as precursors, the authors showed how a molar ratio < 1.5 increased the formation of $Ca_2P_2O_7$ phase. Also $CaCO_3$ nanoparticles with varying structure and size (20-50 nm) were produced using aerosol synthesis by Huber *et al.* (2005).

4.2.2 Production of nano iron-β-lactoglobulin using reduction

Amyloid proteins (such as insulin, serum albumins, ovalbumin, lysozyme, α-lactalbumin and β-lactoglobulin (Lara *et al.*, 2011)) have the unique property of acting as gelling and foaming agents, being therefore particularly relevant for food, cosmetic, and pharmaceutical applications (Mezzenga *et al.*, 2005). Amyloids consist of protein and peptides that can self-assemble into fibrillary nanostructured shapes (also called fibrils) (Cherny and Gazit, 2008). They are considered suitable for nanotechnological bio-application because of their unique properties and bio-compatibility (Knowles and Buehler, 2011). Fibrils are usually produced by unfolding a native monomer at different temperature (37-70°C) and pH conditions from 1.6 to 3 and after few hours of incubation, the unfolded proteins self-rearrange into fibrils composed by the typical β-strands (Cherny and Gazit, 2008; Lara *et al.*, 2011) with a typical diameter of 7-10 nm (Shirahama and Cohen, 1967), as shown in **Figure 8**.

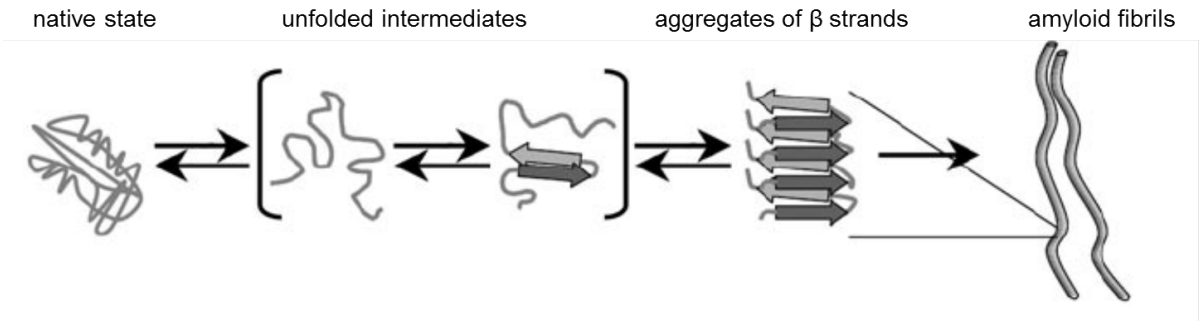

Figure 8: Unfolding and assembling design of amyloid fibrils (Cherny and Gazit, 2008).

The amyloid fibrilized-structures, specifically β-lactoglobulin, have been proposed as carriers for nanostructured particles such as gold (Bolisetty *et al.*, 2011), titania (Bolisetty *et al.*, 2012) and iron (Amar-Yuli *et al.*, 2011). In the synthesis of iron-decorated-fibrils, ß-lactoglobulin (BLG) can be isolated from whey (by-product in cheese manufacturing) is composed by 162 amino acid residues and has a molar mass of 18.3 kDa (Fox and McSweeney, 1998). With temperatures > 70°C, depending on the starting pH and ionic strength, the protein unfolds and aggregates forming of hydrogen and disulfide bonds and a β-sheet structure. By varying the pH, structural aggregates in form of fibrils, spherical micelles and 'worm-like' aggregates can be formed (Jung *et al.*, 2008). When keeping the solution at pH 2 with low ionic strength, and heating it up to 80°C, formation of long, semi flexible, linear fibrils occurs. Additionally, their reduction effect could be used to attach gold nanoparticles to the fibrils surface via an in-situ reducing (Bolisetty *et al.*, 2011) and this reaction could be used also for iron. Such obtained fibril-iron nanoparticle structure has the

potential of being stable as colloidal dispersions since the fibrils build a 3D network (Bolisetty *et al.*, 2013), therefore being applicable in the food industry as carriers for iron and ultimately as fortificants of liquid matrices. The formation of small peptides during the digestion process would ideally protect the iron from building non-bioavailable complexes (e.g. phytate) (see chapter 2.1.2) in the stomach and being available for absorption once in the duodenum.

4.3 Methods used to characterize nanostructured materials

Several methods investigating SSA (N_2-absorption), crystallinity and crystal size (X-ray diffraction (XRD), transmission electron microscopy), hydrodynamic diameter (dynamic light scattering), phase composition (XRD, Raman spectroscopy, thermogravimetric analysis) can be used depending on the desired outcome (Lin *et al.*, 2014). In the following section, only the analytical methods used to characterize calcium nanoparticles will be described.

4.3.1 Specific surface area and estimated primary particle size

The SSA (m^2/g) can be measured using the very popular and useful Brunauer-Emmet-Teller (BET) method (Brunauer *et al.*, 1938). Specifically, the adsorption of N_2 on the powders' surface is measured after degassing and drying the sample. In addition to the SSA, pore size and pore size distribution of a material, BET also gives the possibility of determine the estimated average BET-equivalent diameter (d_{BET}, **Equation 1**) (Hornyak *et al.*, 2009a).

Equation 1:

$$d_{BET} = \frac{6}{SSA * \delta_P} \qquad where\ \delta_P = compounds' density$$

The extrapolation of d_{BET} gives an accurate result only when assuming monodisperse, dense and spherical particles (Maedler *et al.*, 2002b). Therefore it can become less accurate for compounds without a clear density such as compounds without a defined chemical composition, the use of SSA alone might be more appropriate.

Particle size is therefore better measured using dynamic light scattering (DLS) (Hornyak *et al.*, 2009a). The method gives information about hydrodynamic size, shape, structure and aggregation state of a stable dispersion by measuring the random motion of the particles with the scattered light intensity fluctuation of a laser light beam (Brar and Verma, 2011).

Inaccuracies can be produced by the assumption of spherical particles (Hornyak *et al.*, 2009a), and sample preparation must be optimized to achieve the best results.

High resolution images can be obtained by scanning (SEM) and transmission (TEM) electron microscopy. Both methods are often used to reveal shape, heterogeneity and degrees of aggregation of nanomaterials. Results in size and size distribution measurement of nano particle are comparable to DLS (Bootz *et al.*, 2004). Advantages and disadvantages of the characterization methods are summarized in **Table 3**.

Table 3: Advantages and disadvantages of DLS, SEM and TEM for the determination of particle size. Adapted from Lin *et al.* (2014).

Method	physicochemical characteristic analyzed	Strength	Limitations
Dynamic light scattering (DLS)	Hydrodynamic size distribution	Non-destructive/invasive manner Rapid and more reproducible measurement Measures in any liquid media, solvent of interest Hydrodynamic sizes accurately determined for monodisperse samples Modest cost of apparatus	Insensitive correlation of size fractions with a specific composition Influence of small numbers of large particles Limit in polydisperse sample measures Limited size resolution Assumption of spherical shape samples
Scanning electron microscopy (SEM)	Size and size distribution Shape Aggregation Dispersion	Direct measurement of the size/size distribution and shape of nanomaterials High resolution (down to sub-nanometer) Images of biomolecules in natural state provided using ESEM	Conducting sample or coating conductive materials required Dry samples required Sample analysis in non-physiological conditions (except ESEM) Biased statistics of size distribution in heterogeneous samples Expensive equipment Cryogenic method required for most NP-bioconjugates Reduced resolution in ESEM
Transmission electron microscopy (TEM)	Size and size distribution Shape heterogeneity Aggregation Dispersion	Direct measurement of the size/size distribution and shape of nanomaterials with higher spatial resolution than SEM Several analytical methods coupled with TEM for investigation of electronic structure and chemical composition of nanomaterials	Ultrathin samples in required Samples in non-physiological condition Sample damage/alternation Poor sampling Expensive equipment

4.3.2 Phase composition

Phase composition and crystal structure can easily be determined by XRD. In this method, when an X-ray beam hits the atoms of a compound, the beam is diffracted with changes in intensity and angle, and this change are compound specific and give information about spacing between planes of atoms and consequently crystal structure and type (Hornyak *et al.*, 2009a). A crystalline pattern is composed by characteristic 'peaks' that can be fitted to one or more corresponding structures. The presence of the different phases and the corresponding crystal size can be further quantified using the software Diffrac Topas (Bruker). However, in the case of amorphous materials, the pattern results in a broad hump and no information can be obtained. Also vibrational spectroscopy (such as Raman spectroscopy) is a useful tool to determine phase composition, especially in the case of amorphous materials. In Raman spectroscopy, vibrational frequencies are directly linked to the energy difference between the scattered and the incident light. Only molecules with symmetric vibrational (polarization) nodes and transitions are 'raman-active' (Hornyak *et al.*, 2009a). For example, calcium phosphates and $CaCO_3$ are raman-active, but not CaO. Specific vibrations can be detected for different bonds, such as P-O or P-O-P vibrations and calcium phosphate having more complicated crystal conformation than $CaCO_3$ (Tao and James, 2013). This method is however only qualitative. Lastly, phase composition can be determined by TEM, which can be coupled with chemical analyses and give information about size, size distribution and shape of nanostructured materials.

5 Studying calcium and iron absorption

There are several methods used to measure calcium and iron bioavailability which include both *in vitro* and *in vivo* studies. *In vitro* tests, such as solubility in acidic medium, dialysis or digestion in media mimicking parts of the gastrointestinal mucosa or cell layers (such as Caco-2 cells) are good options to estimate compound's absorption, but unfortunately they do not allow the inclusion of possible nutritional, psychological and ecological factors that might influence the bioavailability (Gueguen and Pointillart, 2000). There are several *in vitro* models mimicking *in vivo* absorption and despite the fact that the more complex models try to copy *in vivo* systems as closely as possible, their biggest limitations remain the lack of host response factors, no continuous emptying patterns (static model), absence of microbial general ecosystems and lack of *in vitro-in vivo* correlations (Guerra *et al.*, 2012). Therefore, when possible, *in vivo* experiments, such as animal models or human studies are preferred. Even though, *in vitro* results are often used to predict *in vivo* absorption, especially for iron (Swain *et al.*, 2003), this is unfortunately not always true for calcium (Gueguen and Pointillart, 2000).

In the following section, the most common *in vitro* and *in vivo* methods used to estimate absorption and bioavailability with their positive and negative characteristics will be discussed.

5.1 In vitro

5.1.1 Dissolution

Dissolution is the process by which a solute dissolves in a solvent and gives information about how fast a certain solubility limit (equilibrium) is reached (Cornell and Schwertmann, 2003a). Solubility is a thermodynamic value defined as the maximum concentration of a material (solute) in a solution that is in a thermodynamic equilibrium with a solid phase at a specified temperature and pressure (Lide, 2015). Dissolution kinetics determine how fast the solubility limit (equilibrium) is reached, however no general relationship is given between the dissolution rate and solubility of the same compound (Cornell and Schwertmann, 2003b). Solubility isotherm figures are commonly used to show how the concentration of an ion changes with respect to pH at constant temperature. They give information about the stability of salts at a given pH. For instance, **Figure 9** shows how Ca^{2+} concentration increases with decreasing pH, suggesting that the specific compound becomes more soluble.

Consequently, HAp is the less soluble compound, while for pH < 8.5 or pH > 8.5, the more soluble compounds are tetracalcium phosphate (TTCP) and dicalcium phosphate dehydrate (DCPD), respectively (Fernandez *et al.*, 1999).

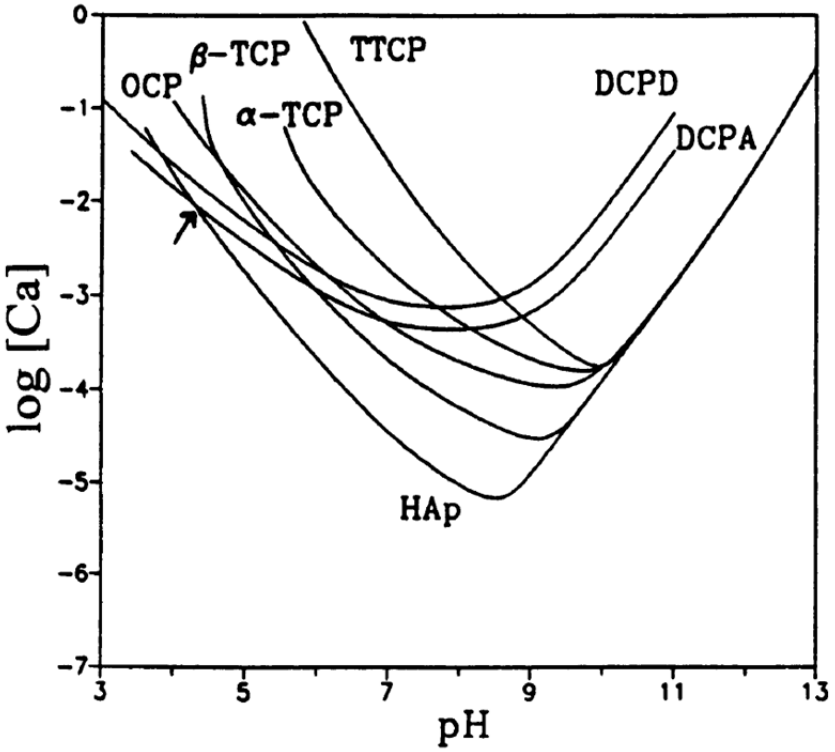

Figure 9: Log Ca^{2+} vs pH Solubility isotherms of different calcium phosphate salts in equilibrium with their solutions for the ternary system $Ca(OH_2)$ – H_3PO_4 – H_2O (37°C) (Tung, 1998). Abbreviations: DCPD – dicalcium phosphate dehydrate ($CaHPO_4.2H_2O$, Ca:P = 1.0, DCPA – dicalcium phosphate anhydrous ($CaHPO_4$, Ca:P = 1), OCT – octacalcium phosphate ($Ca_8H_2(PO_4)6{\cdot}5H_2O$, Ca:P = 1.33, α- and β-TCP – tricalcium phpsphate (α- or β-$Ca_3(PO_4)_2$, Ca:P = 1.5), HAp – hydroxyapatite ($Ca_5(PO_4)_3OH$, Ca:P = 1.67), TTCP – tetracalcium phosphate ($Ca_4(PO_4)_2O$, Ca:P = 2.0).

Dissolution rate can be influenced by several factors including the properties of overall system (temperature, pressure, UV light), the properties of the solution phase (pH, redox potential, acid concentration, complexing agents and reductants) and the properties of the solute (crystal lattice energy, SSA, amorphous or crystalline structuring, chemical composition) (Cornell and Schwertmann, 2003a). Crystal lattice energy corresponds to the heat needed to dissociate one mole of solid into its components in gas form (Hornyak *et al.*, 2009b). Therefore, high lattice energy usually corresponds to lower solubility and the values are: 2'804 for $CaCO_3$ (Lide, 2015), 10'602 for TCP (Lide, 2015) and 32'997 KJ/mol for HAp (Zhang and Tamilselvan, 2007). Clearly HAp has a higher lattice energy which relates very well with the low solubility values. Dissolution of calcium compounds such as $CaCO_3$ and calcium phosphates is pH dependent and dissolution stops when saturation is reached and

no more calcium can be readily dissolved. The lattice energy of a crystal can be increased or lowered (Hilty *et al.*, 2011; Knijnenburg *et al.*, 2013) by introducing an external ion (doping) therefore the dopant must be carefully considered. For instance, lattice energy of Fe_2O_3 (14'309 kJ/mol) and ZnO (4'142 kJ/mol) can be decreased by adding calcium to the system which results in lower system lattice energy ($CaCO_3$ = 2'804 kJ/mol, $Ca_2Fe_2O_5$ = 7'046 kJ/mol, CaO = 3'414 kJ/mol) (Knijnenburg *et al.*, 2013). Similarly, iron solubility was increased by doping of Fe_2O_3 with magnesium and calcium (Hilty *et al.*, 2011), P (for PO_3^{-4}:Fe ratio < 0.3) and Zn, however, the concomitant doping of Zn/P did not improve dissolution any further (Hilty *et al.*, 2009).

It has been suggested that calcium absorption could be predicted by *in vitro* dissolution and several attempts have been made to find a link between the two (Lee *et al.*, 2015; Pak and Avioli, 1988). For instance, Kressel (2010) tested dissolution in 100 ml water and apple juice and bioavailability of four calcium compounds, however the authors did not statistically correlate the results of the two experiments. Brennan *et al.* (1991) determined the dissolution of 27 $CaCO_3$ supplements available on the US market after stirring at 75 rpm individual $CaCO_3$ tablets into 900 ml of 0.1 N HCl at 37°C for 90 minutes. Dissolved calcium was measured at 30, 60 and 90 min after filtering the sample through a 0.45 µm cellulose acetate membrane. They showed how only 5 preparations dissolved more than 75% in the first 30 min and that dissolution correlated negatively with the amount of filler used. However, this approach has also been criticized. For instance, Heaney *et al.* (1990a) did not find any detectable effect of solubility on absorption when correlating the dissolution in water (pH 7) and the fractional absorption in adult women (Hansen *et al.*, 1996). Calcium dissolution is a very challenging topic and despite there were several attempts to correlate absorption with *in vitro* solubility, so far no standardized method is available. Additionally, not only how much calcium can be delivered (solubility) but also how fast the dissolution occurs might be an indication of *in vivo* bioavailability. Indeed, more recently, Meiron *et al.* (2011) focused on determining how long it would take for a calcium compound to reach half of final pH (t_{pH50}) after dissolving 40 mg calcium in 50 ml 0.1 M H_3PO_4. In this case, t_{pH50} showed good agreement with the *in vivo* fractional absorption of ^{45}Ca.

Iron dissolution, on the other hand, is very well documented and an *in vitro* method used to predict *in vivo* bioavailability has been established. The method consists of dissolving the

iron compound in 0.1 M HCl (pH 1) and measuring dissolved iron after incubating at 37°C for 30 min (Forbes *et al.*, 1989). The results of the dissolution assay were linked to in vivo relative bioavailability data in rats with good agreements between the two (R^2 = 0.82, P < 0.05 (Swain *et al.*, 2003), R^2 = 0.76, P < 0.05 (Hilty *et al.*, 2010)), even though the direct correlation was not always statistically proven (Rohner *et al.*, 2007; Shah *et al.*, 1977).

5.1.2 In vitro digestion

The *in vitro* digestion model is not a one-step model as in case of dissolution, but it is composed of several steps where enzymes (pepsin, pancreatin, α-amylase, etc.) and pH are changed mimicking gastrointestinal digestion. This method is preferred for complex food matrices (plant based and meat) where other food components are expected to interact with the target micronutrient. A good summary of studies that applied *in vitro* digestion is given by Hur *et al.* (2011), but the authors point out how *in vitro* digestion models often vary in methodology, increasing the difficulty in comparing different studies. In addition, their results still need to be confirmed by *in vivo* studies. Bosscher *et al.* (2001) used an *in vitro* method composed by a simulated gastric and intestinal digestion and found good agreement for the *in vivo* absorption of calcium and iron from infant formula.

5.1.3 Cells

In vitro bioavailability assays have been improved by combining the dissolution/dialysis steps with the uptake process in cells (Au and Reddy, 2000; Bering *et al.*, 2006; Fairweather-Tait *et al.*, 2007; Glahn *et al.*, 1998). Specifically, a human colon carcinoma cell line, Caco-2, has been implemented for the purpose (Alvarez-Hernandez *et al.*, 1991; Hidalgo *et al.*, 1989). This cell line is derived from colon carcinoma cells and shows many of the functional and morphological properties of mature human enterocytes such as growth in monolayer, cylindrical polarized morphology, microvilli and tight junctions (Sambuy *et al.*, 2005), and although compared to mucosal cells *in vivo*, the mucin layer is missing, they still have a higher transepithelial resistance (Jovani *et al.*, 2001) and express small intestinal enzyme activities (Sambuy *et al.*, 2005).

Cell models can be used to measure mineral uptake and transport over a given period of time. For that purpose, the cell layer is grown on a permeable membrane that allows the cell to take the ions up from the apical part and to excrete it through the basolateral part. This allows for measuring ion uptake and transport by subtracting the concentration in the

basolateral membrane from the apical one and the retention by measuring ion concentration in the cells. Recently, a triple co-culture *in vitro* cell models has been developed consisting of Caco-2, HT29 (mucus producing cells) (Behrens *et al.*, 2001) and Raji B (immune function) to study drug absorption in a more complex and complete way (Antunes *et al.*, 2013).

Cell studies are also particularly important for studying uptake mechanisms and evaluating nanomaterial's toxicity, especially for insoluble materials such as silica (Schrurs and Lison, 2012), silver nanoparticles (Zhang *et al.*, 2014), carbon nanotubes, gold nanoparticles, super-paramagnetic iron oxide nanoparticles and quantum dots (Lewinski *et al.*, 2008; Mailander and Landfester, 2009). Pereira *et al.* (2013) suggested an endocytosis pathway for the uptake of Fe^{3+}, having demonstrated no cell accumulation of a newly developed organic acid-modified Fe(III) oxo-hydroxide. Later on, the primary safety of Fe(III) oxo-hydroxide was suggested by the absence of iron accumulation in the intestinal mucosa and by the promotion of beneficial microbiota (Pereira *et al.*, 2014). The exposure route can either be oral or aerobic and therefore the cell type must be carefully selected.

5.2 In vivo

In vivo studies reflect closely all the micronutrient-food components-gastrointestinal tract interactions. Human experiments are the ultimate necessary experiment, but for ethical, material and financial reasons, it is still preferable to carry out experiments using animal models (Gueguen and Pointillart, 2000). Animal models are most of the time used as surrogate for human experiments and allow the use of otherwise considered unethical procedures such as metabolic cages, repeated blood collection and the use of radiotracers and sample collection and extensive histological investigations to be carried out (Festing and Altman, 2002; Gueguen and Pointillart, 2000). Ultimately, because the selected animal species can be standardized by strain, age, gender, Hb value, ovariectomy, etc., this reduces variation between individuals and it increases the statistical power of the experiment.

One of the biggest challenges in animal studies is to select the most appropriate animal species for the purpose. For instance, rats present high phytase activity (Iqbal *et al.*, 1994) and have a grain based diet, but they are still preferred compared to the omnivore pigs because smaller and therefore less caging space is required. In addition, while in human subjects a calcium imbalance can be measured by an increase in calcium excretion in urine,

in rats and pigs, this excretion is very poor. The rat model is still a useful model to rank the bioavailability of iron compounds relative to $FeSO_4$ (Cunniff, 1997).

5.2.1 Calcium balance

Balance studies are often used to determine calcium absorption from a source in a short period of time and they allow for source comparison. The model gives information about the apparent absorption (intake – excretion [fecal]) and retention (intake – excretion [fecal + urine]). Therefore, complete food intake monitoring and collection of feces and urine is necessary. Balance studies are very difficult to perform on humans because they require metabolic units, standardized meals and constant subject monitoring for several days (Matkovic and Heaney, 1992). Such studies are easier to perform on animals using specially designed metabolic cages (**Figure 10**) that enables for separate collection of feces, urine and spilt food. For this type of study, growing rats are usually preferred because they represent periods of major skeletal growth (infancy and adolescence, corresponding to 4-8 weeks old rats (Kruger *et al.*, 2003b)) when more calcium is absorbed and stored (Matkovic, 1991). Disadvantages include the presence of a grid floor and forced single caging which can both have negative consequences for the animal wellbeing. Classical balance studies do not consider the net absorption (intake – (fecal excretion + endogenous losses), resulting in an underestimation of true calcium absorption.

Because urinary calcium excretion in humans is higher than in animals, a simplified version of the balance study can be used to compare different calcium sources. This method consists of measuring calcium urinary excretion after a single oral calcium dose to a fasting subject as a measure of acute absorption (Gueguen and Pointillart, 2000). Because the urinary response to ingested calcium can be obtained over a few hours post administration, this test is usually very fast and simple (Pak *et al.*, 1975).

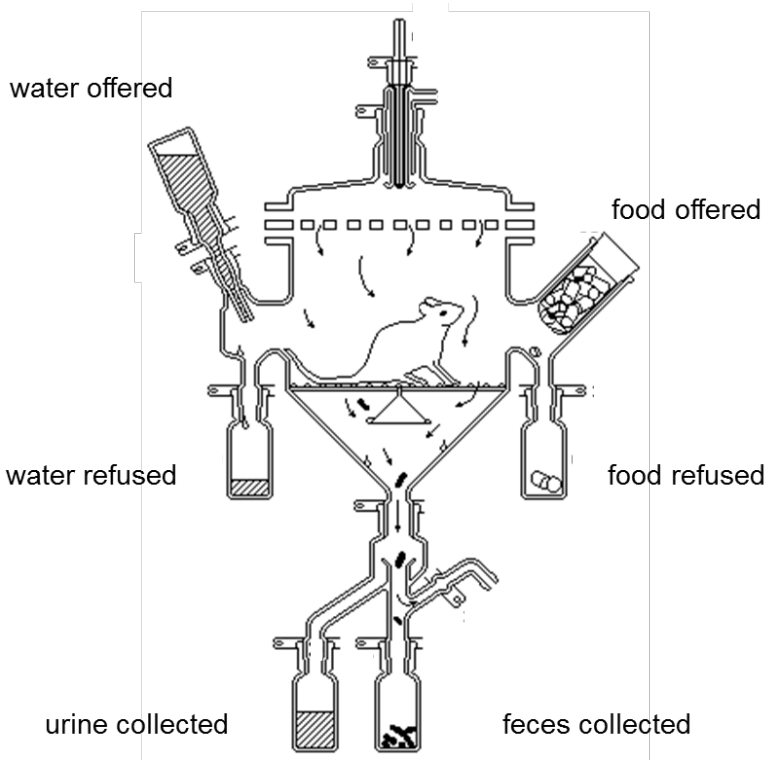

Figure 10: Schematic showing of a metabolic age for rats (www.inchem.org).

5.2.2 Long-term bone mineralization

The evaluation of bone parameters (such as BMD (Park *et al.*, 2010), bone breaking strength (Leppanen *et al.*, 2006) and morphometric parameters) after long term calcium feeding remains the most reliable way of estimating the long term-effects of different calcium concentrations and sources (Gueguen and Pointillart, 2000). For this purpose, the ovariectomized (OVX) rat model is currently used as a preclinical animal model for studying postmenopausal induced bone loss (Kalu, 1991) and osteoporosis (Lelovas *et al.*, 2008) since it correctly emulates the important clinical feature of the estrogen depleted human skeleton (Jee and Yao, 2001). The Food and Drug Administration (Thompson *et al.*, 1995) introduced the rat as the preferred animal to be used as OVX model, but more recently, also mice (Ohman *et al.*, 2011) have been used for the purpose.

The model for studying osteoporosis can be implemented in skeletally immature or mature (10 month of age) rats. Immature rats have the advantage of reaching a lower peak bone mass, which resembles closely the human primary risk of developing osteoporosis, while mature rats are more appropriate for OVX or immobilization osteoporosis. The OVX model is used to study postmenopausal osteoporosis and after ovariectomy, bone loss can be detected in different skeletal regions: femoral neck after 30 days, proximal tibial metaphysis

after 14 days and lumbar vertebra after 60 days (Lelovas *et al.*, 2008). The immobilization model reduces drastically the normal movement of the animal and can be induced either surgically (nerve, tendon or spinal cord resection) or in conservative way (limb bandaging, limb casting and tail suspension). The earlier detection of bone loss can be seen in: femoral diaphysis after 21 days, proximal and distal tibial metaphysis after 14-30 days and tibial diaphysis 42 days (Lelovas *et al.*, 2008).

5.2.3 Calcium and iron appearance in serum

Serum appearance methods consist of a single calcium dose administration, with a subsequent monitoring of calcium appearance in serum/plasma from hours to days (distribution and storage) and can be used to compare different calcium sources (Gueguen and Pointillart, 2000). The increase of calcium in plasma corresponds to the area under the curve above fasting level and resembles the curves used in pharmacokinetic experiments. For this purpose, stable and radio tracers are widely preferred to non-labeled techniques because they require lower rise in serum calcium to be measured, avoiding changes in calcium homeostasis (Heaney, 2001). Any element can be found in form of stable or radio isotope. The atomic mass of the 'normal calcium' of 40.078 is an average of all the stable forms. Stable isotopes are all part of 'normal calcium' just in other relative quantities. The most common radio- or stable isotopes used in the research of calcium absorption are summarized in **Table 4**. Both radio and stable isotopes allow for determining the distribution, retention or incorporation of calcium. Radioisotopes can be easily detected and measured in the desired compartment, such as blood, urine, feces (Griffin and Abrams, 2005) and bones (Koo *et al.*, 1993)), by scintillation counting or in the whole body (Dainty, 2001). However the scintillation detection method does not work accurately for two or more simultaneously administered radiotracers. The limiting factor in the choice of the radioisotope is the energy emitted during decay (β-emitter), the emitted energy and the half-life. Longer half-life (^{41}Ca) allow for studies looking at calcium incorporation in the skeleton (Fairweather-Tait and Teucher, 2002a).

Table 4: Commonly used radio and **stable isotopes** in the research of calcium absorption (Lide, 2015). Abbreviations: $t_{1/2}$ = half-life, d = days, m = months, y = years.

Element or Isotope	Natural abundance (atom %)	Atomic mass	$t_{1/2}$
Ca	-	40.078	-
^{40}Ca	96.941	39.9625909	5.29×10^{21} y
^{41}Ca	-	40.962278	9.9×10^{4} y
^{42}Ca	0.647	41.958618	-
^{43}Ca	0.135	42.958766	-
^{44}Ca	2.086	43.9555486	-
^{45}Ca	-	44.95619	162.7 d
^{46}Ca	0.004	45.95369	$< 0.4 \times 10^{16}$ y
^{47}Ca	-	46.95454	4.536 d
^{48}Ca	0.187	47.95253	4.4×10^{19} y
^{49}Ca	-	48.95566	8.72 m

However, stable isotopes do not emit radiations caused by decay. They are therefore considered harmless and preferred in human studies and are especially suitable for studies involving children or pregnant women (Abrams, 1999; Kastenmayer *et al.*, 1994). The choice of the right stable isotope is usually a compromise between natural abundance (very low natural abundance is preferred), price (the higher the abundance, the lower the price) and detection limit (the lower the abundance, the more difficult the detection), therefore ^{42}Ca, ^{43}Ca and ^{48}Ca are the preferred ones. Stable isotope ratios are measured using mass spectrometry (Walczyk, 2001). The same principles apply to iron (atomic mass of 55.845) and the most commonly used radioactive and stable isotopes for studying bioavailability are summarized in **Table 5**.

Table 5: Commonly used radio and **stable isotopes** in the research of iron absorption (Lide, 2015). Abbreviations: $t_{1/2}$ = half-life, d = days, m = months, y = years.

Element or Isotope	Natural abundance (atom %)	Atomic mass	$t_{1/2}$
Fe	-	55.845	-
^{52}Fe	-	51.94811	8.28 h
^{53}Fe	-	52.94531	8.51 m
^{54}Fe	5.845	53.93961	$> 3.1 \times 10^{22}$ y
^{55}Fe	-	54.938292	2.75 y
^{56}Fe	91.754	55.934936	-
^{57}Fe	2.119	56.935393	-
^{58}Fe	0.282	57.933274	-
^{59}Fe	-	58.934874	44.51 d

The labeling of the calcium source can occur either intrinsically or extrinsically. For the intrinsic labeling, the label is endogenously or biosynthetically incorporated into the animal or plant by normal metabolic processes (Nickel *et al.*, 1996), and the isotope is incorporated

in its natural form in the edible part of an animal or plant and becomes part of the native mineral (Weaver, 1985). For instance, an animal such as a cow, can be labeled by injecting the isotope in its system and the isotope can then be measured in the produced milk (Nickel *et al.*, 1996), while a plant can either be grown using labeled fertilizer or the label can be incorporated by foliar application (Weaver, 1985). Extrinsic labeling is cheaper and faster than the intrinsic approach and it consists of the addition of the label immediately before food ingestion in the form of a meal or beverage. It is assumed that once ingested, the label enters the common mineral pool and is absorbed in the same way as native mineral (Nickel *et al.*, 1996). Several studies compared extrinsic against intrinsic labeling, finding good agreement between the two for calcium solutions (Marshall and Nordin, 1981), dairy products (Buchowski *et al.*, 1989; Nickel *et al.*, 1996), wheat flour (Weaver *et al.*, 1992). But not for products containing insoluble calcium salts such as oxalate and phytates (Weaver and Heaney, 1991), where extrinsic labeling resulted in an overestimation of absorbed calcium. This was probably caused by an incomplete exchange of added label and native calcium bound to oxalate (Weaver and Heaney, 1991). Extrinsic labeling alone of soy and cow milk was found not to be an appropriate approach to evaluate calcium bioavailability because of the non uniform distribution of the label (Heaney *et al.*, 2000).

Iron absorption and bioavailability is often evaluated using an extrinsic iron tag (radio- or stable isotopes) technique for single meals (Benito and Miller, 1998). In the case of radio isotopes, ‘whole body counting’ is used to measure retention of iron over time in animals up to 14 days after administration (Benito and Miller, 1998). The other method is called ‘red cell incorporation’ and consists of measuring iron incorporation in the red blood cells 14 days post administration of a single meal dose (Benito and Miller, 1998). However, also in this case, the amount of absorbed iron can be overestimated. A study with stable isotopes, compared intrinsic against extrinsic labeling of yeasts that were fed to rats, and concluded that extrinsic labeling was suitable for copper, selenium and inorganic iron but not zinc (Boza *et al.*, 1995). However, extrinsic labeling overestimated absorption by 10 to 20% for complex matrices such as corn, soy beans, soy flour, wheat, maize and rice in both human and animal studies (Weaver, 1985).

5.2.4 Hemoglobin dose-response

The dose-response method is an official method of the Association of Official Analytical Chemists (AOAC) that is used to compare bioavailability of iron between different sources (Cunniff, 1997). Forbes *et al.* (1989) concluded that the results obtained with the AOAC method could reliably predict iron bioavailability in human subjects. However, since rats are known to produce high amounts of phytase as a digestion enzyme, therefore this model is not useful to investigate food components that enhance or inhibit iron absorption (such as chelators) in humans, but only appropriate when iron bioavailability depends on solubility in the stomach (Reddy and Cook).

The method compares the increase in hemoglobin after a period of iron repletion (14 days) between the desired iron sources compared to the gold standard $FeSO_4$ as a measure for relative bioavailability (RBV). In order to increase their iron absorption, rats are fed an iron deficient diet for 24 days reaching a final hemoglobin value of 30-50 g/l. After the depletion period, the animals are fed an iron sufficient diet of either 10 or 20 mg Fe/kg diet for 13-15 days. These two concentrations are used to extrapolate a linear pattern between hemoglobin increase and iron intake (Cunniff, 1997).

6 References

Abboud S., and Haile D. J., 2000, A novel mammalian iron-regulated protein involved in intracellular iron metabolism: Journal of Biological Chemistry, v. 275, no. 26, p. 19906-19912.

Abrams S. A., 1999, Using stable isotopes to assess mineral absorption and utilization by children: American Journal of Clinical Nutrition, v. 70, no. 6, p. 955-964.

Abrams S. A., Griffin I. J., Hawthorne K. M., Liang L., Gunn S. K., Darlington G., and Ellis K. J., 2005, A combination of prebiotic short- and long-chain inulin-type fructans enhances calcium absorption and bone mineralization in young adolescents: American Journal of Clinical Nutrition, v. 82, no. 2, p. 471-476.

Abrams S. A., Sidbury J. B., Muenzer J., Esteban N. V., Vieira N. E., and Yergey A. L., 1991, Stable isotopic measurement of endogenous fecal calcium excretion in children: Journal of Pediatric Gastroenterology and Nutrition, v. 12, no. 4, p. 469-473.

Adams J. E., 1997, Single and dual energy x-ray absorptiometry: European Radiology, v. 7, p. 20-31.

Addadi L., Raz S., and Weiner S., 2003, Taking advantage of disorder: Amorphous calcium carbonate and its roles in biomineralization: Advanced Materials, v. 15, no. 12, p. 959-970.

Aggett P. J., 2012, Iron, Present knowledge in nutrition, Wiley-Blackwell, p. 506-520.

Aisen P., Leibman A., and Zweier J., 1978, Stoichiometric and site characteristics of the binding of iron to human transferrin: The Journal of Biological Chemistry, v. 253, no. 6, p. 1930-1937.

Allen L., de Benoist B., Dary O., and Hurrell R., 2006, Guidelines on food fortification with micronutrients, Geneva: World Health Organization.

Allen L. H., 2000, Anemia and iron deficiency: Effects on pregnancy outcome: American Journal of Clinical Nutrition, v. 71, no. 5, p. 1280-1284.

Allen M. R., and Burr D. B., 2014, Chapter 4 - bone modeling and remodeling, *in* Burr, D. B., and Allen, M. R., eds., Basic and applied bone biology: San Diego, Elsevier Science, p. 75-90.

Allen M. R., and Krohn K., 2014, Chapter 5 - skeletal imaging, *in* Burr, D. B., and Allen, M. R., eds., Basic and applied bone biology: San Diego, Elsevier Science, p. 93-113.

Alvarez-Hernandez X., Nichols G. M., and Glass J., 1991, Caco-2 cell-line - a system for studying intestinal iron transport across epithelial-cell monolayers: Biochimica Et Biophysica Acta, v. 1070, no. 1, p. 205-208.

Amar-Yuli I., Adamcik J., Lara C., Bolisetty S., Vallooran J. J., and Mezzenga R., 2011, Templating effects of lyotropic liquid crystals in the encapsulation of amyloid fibrils and their stimuli-responsive magnetic behavior: Soft Matter, v. 7, no. 7, p. 3348-3357.

Antunes F., Andrade F., Araujo F., Ferreira D., and Sarmento B., 2013, Establishment of a triple co-culture in vitro cell models to study intestinal absorption of peptide drugs: European Journal of Pharmaceutics and Biopharmaceutics, v. 83, no. 3, p. 427-435.

Au A. P., and Reddy M. B., 2000, Caco-2 cells can be used to assess human iron bioavailability from a semipurified meal: The Journal of Nutrition, v. 130, no. 5, p. 1329-1334.

Bagi C. M., Hanson N., Andresen C., Pero R., Lariviere R., Turner C. H., and Laib A., 2006, The use of micro-ct to evaluate cortical bone geometry and strength in nude rats: Correlation with mechanical testing, pqct and dxa: Bone, v. 38, no. 1, p. 136-144.

Bagley B. G., Cohen M. H., Economou E. N., Enderby J. E., Freed K. F., Fritzsche H., Grigorovici R., Kirkpatrick E. S., and Tauc J., 1974, Amorphous and liquid semiconductors, Springer, p. 441.

Baltussen R., Knai C., and Sharan M., 2004, Iron fortification and iron supplementation are cost-effective interventions to reduce iron deficiency in four subregions of the world: The Journal of Nutrition, v. 134, no. 10, p. 2678-2684.

Baxter-Jones A. D., Faulkner R. A., Forwood M. R., Mirwald R. L., and Bailey D. A., 2011, Bone mineral accrual from 8 to 30 years of age: An estimation of peak bone mass: Journal of Bone and Mineral Research, v. 26, no. 8, p. 1729-1739.

Becker A., Sotje I., Paulmann C., Beckmann F., Donath T., Boese R., Prymak O., Tiemann H., and Epple M., 2005, Calcium sulfate hemihydrate is the inorganic mineral in statoliths of scyphozoan medusae (cnidaria): Dalton Transactions, no. 8, p. 1545-1550.

Behrens I., Stenberg P., Artursson P., and Kissel T., 2001, Transport of lipophilic drug molecules in a new mucus-secreting cell culture model based on ht29-mtx cells: Pharmaceutical Research, v. 18, no. 8, p. 1138-1145.

Benito P., and Miller D., 1998, Iron absorption and bioavailability: An updated review: Nutrition Research, v. 18, no. 3, p. 581-603.

Bering S., Bukhave K., Henriksen M., Sandstrom B., Pariagh S., Fairweather-Tait S. J., and Lund E. K., 2006, Development of a three-tier in vitro system, using caco-2 cells, to assess the effects of lactate on iron uptake and transport from rye bread following in vitro digestion: Journal of the Science of Food and Agriculture, v. 86, no. 14, p. 2438-2444.

Blagden N., de Matas M., Gavan P. T., and York P., 2007, Crystal engineering of active pharmaceutical ingredients to improve solubility and dissolution rates: Advanced Drug Delivery Reviews, v. 59, no. 7, p. 617-630.

Bolisetty S., Adamcik J., Heier J., and Mezzenga R., 2012, Amyloid directed synthesis of titanium dioxide nanowires and their applications in hybrid photovoltaic devices: Advanced Functional Materials, v. 22, no. 16, p. 3424-3428.

Bolisetty S., Vallooran J. J., Adamcik J., Handschin S., Gramm F., and Mezzenga R., 2011, Amyloid-mediated synthesis of giant, fluorescent, gold single crystals and their hybrid sandwiched composites driven by liquid crystalline interactions: Journal of Colloid and Interface Science, v. 361, no. 1, p. 90-96.

Bolisetty S., Vallooran J. J., Adamcik J., and Mezzenga R., 2013, Magnetic-responsive hybrids of fe3o4 nanoparticles with beta-lactoglobulin amyloid fibrils and nanoclusters: ACS Nano, v. 7, no. 7, p. 6146-6155.

Bonjour J. P., Theintz G., Law F., Slosman D., and Rizzoli R., 1994, Peak bone mass: Osteoporosis International, v. 4 Suppl 1, p. 7-13.

Booth S. L., Tucker K. L., Chen H., Hannan M. T., Gagnon D. R., Cupples L. A., Wilson P. W., Ordovas J., Schaefer E. J., Dawson-Hughes B., and Kiel D. P., 2000, Dietary vitamin k intakes are associated with hip fracture but not with bone mineral density in elderly men and women: American Journal of Clinical Nutrition, v. 71, no. 5, p. 1201-1208.

Bootz A., Vogel V., Schubert D., and Kreuter J., 2004, Comparison of scanning electron microscopy, dynamic light scattering and analytical ultracentrifugation for the sizing of poly(butyl cyanoacrylate) nanoparticles: European Journal of Pharmaceutics and Biopharmaceutics, v. 57, no. 2, p. 369-375.

Bosscher D., Van Caillie-Bertrand M., Robberecht H., Van Dyck K., Van Cauwenbergh R., and Deelstra H., 2001, In vitro availability of calcium, iron, and zinc from first-age infant formulae and human milk: Journal of Pediatric Gastroenterology and Nutrition, v. 32, no. 1, p. 54-58.

Boza J. J., Fox T. E., Eagles J., Wilson P. D. G., and Fairweathertait S. J., 1995, The validity of extrinsic stable isotopic labeling for mineral absorption studies in rats: The Journal of Nutrition, v. 125, no. 6, p. 1611-1616.

Brar S. K., and Verma M., 2011, Measurement of nanoparticles by light-scattering techniques: Trends in Analytical Chemistry, v. 30, no. 1, p. 4-17.

Brennan M. J., Duncan W. E., Wartofsky L., Butler V. M., and Wray H. L., 1991, In vitro dissolution of calcium carbonate preparations: Calcified Tissue International, v. 49, no. 5, p. 308-312.

Bronner F., 2003a, Mechanisms and functional aspects of intestinal calcium absorption: Journal of Experimental Zoology Part A - Comparative Experimental Biology, v. 300a, no. 1, p. 47-52.

Bronner F., 2003b, Mechanisms of intestinal calcium absorption: Journal of Cellular Biochemistry, v. 88, no. 2, p. 387-393.

Bronner F., Pansu D., and Stein W. D., 1986, An analysis of intestinal calcium-transport across the rat intestine: American Journal of Physiology, v. 250, no. 5, p. 561-569.

Brunauer S., Emmett P. H., and Teller E., 1938, Adsorption of gases in multimolecular layers: Journal of the American Chemical Society, v. 60, p. 309-319.

Buchowski M. S., Sowizral K. C., Lengemann F. W., Van Campen D., and Miller D. D., 1989, A comparison of intrinsic and extrinsic tracer methods for estimating calcium bioavailability to rats from dairy foods: The Journal of Nutrition, v. 119, no. 2, p. 228-234.

Buesser B., and Pratsinis S. E., 2012, Design of nanomaterial synthesis by aerosol processes: Annual Review of Chemical and Biomolecular Engineering, v. 3, p. 103-127.

Burr D. B., and Akkus O., 2014, Chapter 1 - bone morphology and organization, *in* Burr, D. B., and Allen, M. R., eds., Basic and applied bone biology: San Diego, Elsevier Science, p. 3-25.

Carne-Sanchez A., Imaz I., Cano-Sarabia M., and Maspoch D., 2013, A spray-drying strategy for synthesis of nanoscale metal-organic frameworks and their assembly into hollow superstructures: Nature Chemistry, v. 5, no. 3, p. 203-211.

Carpenter C. E., and Mahoney A. W., 1992, Contributions of heme and nonheme iron to human-nutrition: Critical Reviews in Food Science and Nutrition, v. 31, no. 4, p. 333-367.

Cartwright G. E., Lauritsen M. A., Jones P. J., Merrill I. M., and Wintrobe M. M., 1946, The anemia of infection .1. Hypoferremia, hypercupremia, and alterations in porphyrin metabolism in patients: Journal of Clinical Investigation, v. 25, no. 1, p. 65-80.

Cashman K. D., 2002, Calcium intake, calcium bioavailability and bone health: British Journal of Nutrition, v. 87, p. 169-177.

Cheong J. M. K., Martin B. R., Jackson G. S., Elmore D., McCabe G. P., Nolan J. R., Barnes S., Peacock M., and Weaver C. M., 2007, Soy isoflavones do not affect bone resorption in postmenopausal women: A dose-response study using a novel approach with ca-41: Journal of Clinical Endocrinology & Metabolism, v. 92, no. 2, p. 577-582.

Cherny I., and Gazit E., 2008, Amyloids: Not only pathological agents but also ordered nanomaterials: Angewandte Chemie International Edition, v. 47, no. 22, p. 4062-4069.

Christiansen C., 1991, Consensus development conference - prophylaxis and treatment of osteoporosis: American Journal of Medicine, v. 90, no. 1, p. 107-110.

Chubb S. A., 2012, Measurement of c-terminal telopeptide of type i collagen (ctx) in serum: Clinical Biochemistry, v. 45, no. 12, p. 928-935.

Combes C., and Rey C., 2010, Amorphous calcium phosphates: Synthesis, properties and uses in biomaterials: Acta Biomaterialia, v. 6, no. 9, p. 3362-3378.

Cook J. D., Dassenko S. A., and Whittaker P., 1991, Calcium supplementation - effect on iron-absorption: American Journal of Clinical Nutrition, v. 53, no. 1, p. 106-111.

Cook J. D., and Monsen E. R., 1976, Food iron absorption in human subjects. Iii. Comparison of the effect of animal proteins on nonheme iron absorption: American Journal of Clinical Nutrition, v. 29, no. 8, p. 859-867.

Cook J. D., and Monsen E. R., 1977, Vitamin c, the common cold, and iron absorption: American Journal of Clinical Nutrition, v. 30, no. 2, p. 235-241.

Cook J. D., and Reddy M. B., 2001, Effect of ascorbic acid intake on nonheme-iron absorption from a complete diet: American Journal of Clinical Nutrition, v. 73, no. 1, p. 93-98.

Cooper C., Campion G., and Melton L. J., 1992, Hip-fractures in the elderly - a worldwide projection: Osteoporosis International, v. 2, no. 6, p. 285-289.

Cornell R. M., and Schwertmann U., 2003a, Dissolution, The iron oxides, Wiley-VCH Verlag GmbH & Co. KGaA, p. 297-344.

Cornell R. M., and Schwertmann U., 2003b, Solubility, The iron oxides, Wiley-VCH Verlag GmbH & Co. KGaA, p. 201-220.

Coudray C., Feillet-Coudray C., Rambeau M., Tressol J. C., Gueux E., Mazur A., and Rayssiguier Y., 2006, The effect of aging on intestinal absorption and status of calcium, magnesium, zinc, and copper in rats: A stable isotope study: Journal of Trace Elements in Medicine and Biology, v. 20, no. 2, p. 73-81.

Cui M., Li Q., Johnson R., and Fleet J. C., 2012, Villin promoter-mediated transgenic expression of transient receptor potential cation channel, subfamily v, member 6 (trpv6) increases intestinal calcium absorption in wild-type and vitamin d receptor knockout mice: Journal of Bone and Mineral Research, v. 27, no. 10, p. 2097-2107.

Cunniff P., 1997, Aoac official method 9743.1: Bioavailability of iron: Rat hemoglobin repletion bioassay., Official methods of analysis of aoac international: Gaitherburg, AOAC International, p. 62-63.

Dainty J. R., 2001, Use of stable isotopes and mathematical modelling to investigate human mineral metabolism: Nutrition Research Reviews, v. 14, no. 2, p. 295-315.

Darling A. L., Millward D. J., Torgerson D. J., Hewitt C. E., and Lanham-New S. A., 2009, Dietary protein and bone health: A systematic review and meta-analysis: American Journal of Clinical Nutrition, v. 90, no. 6, p. 1674-1692.

Davies K. M., Rafferty K., and Heaney R. P., 2004, Determinants of endogenous calcium entry into the gut: American Journal of Clinical Nutrition, v. 80, no. 4, p. 919-923.

Dawson-Hughes B., Harris S. S., Palermo N. J., Castaneda-Sceppa C., Rasmussen H. M., and Dallal G. E., 2009, Treatment with potassium bicarbonate lowers calcium excretion and bone resorption in older men and women: Journal of Clinical Endocrinology & Metabolism, v. 94, no. 1, p. 96-102.

Day J. S., Ding M., Odgaard A., Sumner D. R., Hvid I., and Weinans H., 2000, Parallel plate model for trabecular bone exhibits volume fraction-dependent bias: Bone, v. 27, no. 5, p. 715-720.

De Domenico I., McVey Ward D., and Kaplan J., 2008, Regulation of iron acquisition and storage: Consequences for iron-linked disorders: Nature Reviews - Molecular Cell Biology, v. 9, no. 1, p. 72-81.

DeLuca H. F., 2004, Overview of general physiologic features and functions of vitamin d: American Journal of Clinical Nutrition, v. 80, no. 6 Suppl, p. 1689-1696.

Dendougui F., and Schwedt G., 2004, In vitro analysis of binding capacities of calcium to phytic acid in different food samples: European Food Research and Technology, v. 219, no. 4, p. 409-415.

DiMeglio L. A., Imel E. A., Burr D. B., and Allen M. R., 2014, Chapter 13 - calcium and phosphate: Hormonal regulation and metabolism, *in* Burr, D. B., and Allen, M. R., eds., Basic and applied bone biology: San Diego, Elsevier Science, p. 261-282.

Donovan A., Brownlie A., Zhou Y., Shepard J., Pratt S. J., Moynihan J., Paw B. H., Drejer A., Barut B., Zapata A., Law T. C., Brugnara C., Lux S. E., Pinkus G. S., Pinkus J. L., Kingsley P. D., Palis J., Fleming M. D., Andrews N. C., and Zon L. I., 2000, Positional cloning of zebrafish ferroportin1 identifies a conserved vertebrate iron exporter: Nature, v. 403, no. 6771, p. 776-781.

Dorozhkin S. V., 2007, Calcium orthophosphates: Journal of Materials Science, v. 42, no. 4, p. 1061-1095.

Duflos C., Bellaton C., Pansu D., and Bronner F., 1995, Calcium solubility, intestinal sojourn time and paracellular permeability codetermine passive calcium-absorption in rats: The Journal of Nutrition, v. 125, no. 9, p. 2348-2355.

Dunne J. R., Malone D., Tracy J. K., Gannon C., and Napolitano L. M., 2002, Perioperative anemia: An independent risk factor for infection, mortality, and resource utilization in surgery: Journal of Surgical Research, v. 102, no. 2, p. 237-244.

EFSA Panel, 2015a, Scientific opinion on dietary reference values for calcium: EFSA Journal, v. 13, no. 5, p. 82.

EFSA Panel, 2015b, Scientific opinion on dietary reference values for iron: EFSA Journal, v. 13, no. 10, p. 115.

Engelmann M. D. M., Davidsson L., Sandstrom B., Walczyk T., Hurrell R. F., and Michaelsen K. F., 1998, The influence of meat on nonheme iron absorption in infants: Pediatric Research, v. 43, no. 6, p. 768-773.

Erfanian A., Mirhosseini H., Abd Manap M. Y., Rasti B., and Bejo M. H., 2014, Influence of nano-size reduction on absorption and bioavailability of calcium from fortified milk powder in rats: Food Research International, v. 66, p. 1-11.

Ezzati M., Lopez A. D., Rodgers A., Vander Hoorn S., Murray C. J. L., and Coll C. R. A., 2002, Selected major risk factors and global and regional burden of disease: Lancet, v. 360, no. 9343, p. 1347-1360.

Fairweather-Tait S., Phillips I., Wortley G., Harvey L., and Glahn R., 2007, The use of solubility, dialyzability, and caco-2 cell methods to predict iron bioavailability: International Journal for Vitamin and Nutrition Research, v. 77, no. 3, p. 158-165.

Fairweather-Tait S. J., and Teucher B., 2002a, Calcium bioavailability in relation to bone health: International Journal for Vitamin and Nutrition Research, v. 72, no. 1, p. 13-18.

Fairweather-Tait S. J., and Teucher B., 2002b, Iron and calcium bioavailability of fortified foods and dietary supplements: Nutrition Reviews, v. 60, no. 11, p. 360-367.

Favus M. J., and Angeidbackman E., 1984, Effects of lactose on calcium-absorption and secretion by rat ileum: American Journal of Physiology, v. 246, no. 3, p. 281-285.

Fernandez E., Gil F. J., Ginebra M. P., Driessens F. C. M., Planell J. A., and Best S. M., 1999, Calcium phosphate bone cements for clinical applications - part i: Solution chemistry: Journal of Materials Science - Materials in Medicine, v. 10, no. 3, p. 169-176.

Festing M. F. W., and Altman D. G., 2002, Guidelines for the design and statistical analysis of experiments using laboratory animals: ILAR Journal, v. 43, no. 4, p. 244-258.

Finch C., 1994, Regulators of iron balance in humans: Blood, v. 84, no. 6, p. 1697-1702.

Fleet J. C., and Schoch R. D., 2010, Molecular mechanisms for regulation of intestinal calcium absorption by vitamin d and other factors: Critical Reviews in Clinical Laboratory Sciences, v. 47, no. 4, p. 181-195.

Forbes A. L., Arnaud M. J., Chichester C. O., Cook J. D., Harrison B. N., Hurrell R. F., Kahn S. G., Morris E. R., Tanner J. T., and Whittaker P., 1989, Comparison of in vitro, animal, and clinical determinations of iron bioavailability: International nutritional anemia consultative group task force report on iron bioavailability: American Journal of Clinical Nutrition, v. 49, no. 2, p. 225-238.

Formica C., Loro M. L., Gilsanz V., and Seeman E., 1995, Inhomogeneity in body-fat distribution may result in inaccuracy in the measurement of vertebral bone mass: Journal of Bone and Mineral Research, v. 10, no. 10, p. 1504-1511.

Fox P. F., and McSweeney P. L. H., 1998, Dairy chemistry and biochemistry, Springer Science & Business Media.

Franceschi V. R., and Horner H. T., 1980, Calcium-oxalate crystals in plants: Botanical Review, v. 46, no. 4, p. 361-427.

Frazer D. M., and Anderson G. J., 2005, Iron imports. I. Intestinal iron absorption and its regulation: American Journal of Physiology - Gastrointestinal and Liver Physiology, v. 289, no. 4, p. 631-635.

Gahche J., Bailey R., Burt V., Hughes J., Yetley E., Dwyer J., Picciano M. F., McDowell M., and Sempos S., 2011, Dietary supplement use among u.S. Adults has increased since nhanes iii (1988-1994): National Center for Health Statistics, NCHS data brief, no 61.

Gallagher J. C., Goldgar D., and Moy A., 1987, Total bone calcium in normal women: Effect of age and menopause status: Journal of Bone and Mineral Research, v. 2, no. 6, p. 491-496.

Gao H. Y., Chen H. I., Chen W. X., Tao F., Zheng Y. H., Jiang Y. M., and Ruan H. J., 2008, Effect of nanometer pearl powder on calcium absorption and utilization in rats: Food Chemistry, v. 109, no. 3, p. 493-498.

Gardsell P., Johnell O., and Nilsson B. E., 1991, The predictive value of bone loss for fragility fractures in women: A longitudinal study over 15 years: Calcified Tissue International, v. 49, no. 2, p. 90-94.

Ginebra M. P., Traykova T., and Planell J. A., 2006, Calcium phosphate cements as bone drug delivery systems: A review: Journal of Controlled Release, v. 113, no. 2, p. 102-110.

Gkouvatsos K., Papanikolaou G., and Pantopoulos K., 2012, Regulation of iron transport and the role of transferrin: Biochimica Et Biophysica Acta, v. 1820, no. 3, p. 188-202.

Glahn R. P., Lai C., Hsu J., Thompson J. F., Guo M. R., and Van Campen D. R., 1998, Decreased citrate improves iron availability from infant formula: Application of an in vitro digestion caco-2 cell culture model: The Journal of Nutrition, v. 128, no. 2, p. 257-264.

Graf E., 1983, Calcium-binding to phytic acid: Journal of Agricultural and Food Chemistry, v. 31, no. 4, p. 851-855.

Grantham-McGregor S., and Ani C., 2001, A review of studies on the effect of iron deficiency on cognitive development in children: The Journal of Nutrition, v. 131, no. 2, p. 649-666.

Gras P., Rey C., Marsan O., Sarda S., and Combes C., 2013, Synthesis and characterisation of hydrated calcium pyrophosphate phases of biological interest: European Journal of Inorganic Chemistry, p. 1-11.

Green R., Charlton R., Seftel H., Bothwell T., Mayet F., Adams B., Finch C., and Layrisse M., 1968, Body iron excretion in man: A collaborative study: The American Journal of Medicine, v. 45, no. 3, p. 336-353.

Griffin I. J., and Abrams S. A., 2005, Methodological considerations in measuring human calcium absorption: Relevance to study the effects of inulin-type fructans: British Journal of Nutrition, v. 93, p. 105-110.

Gueguen L., and Pointillart A., 2000, The bioavailability of dietary calcium: Journal of the American College of Nutrition, v. 19, no. 2, p. 119-136.

Guerra A., Etienne-Mesmin L., Livrelli V., Denis S., Blanquet-Diot S., and Alric M., 2012, Relevance and challenges in modeling human gastric and small intestinal digestion: Trends in Biotechnology, v. 30, no. 11, p. 591-600.

Gunshin H., Mackenzie B., Berger U. V., Gunshin Y., Romero M. F., Boron W. F., Nussberger S., Gollan J. L., and Hediger M. A., 1997, Cloning and characterization of a mammalian proton-coupled metal-ion transporter: Nature, v. 388, no. 6641, p. 482-488.

Hallberg L., Brune M., Erlandsson M., Sandberg A. S., and Rossanderhulten L., 1991, Calcium - effect of different amounts on nonheme-iron and heme-iron absorption in humans: American Journal of Clinical Nutrition, v. 53, no. 1, p. 112-119.

Hallberg L., Brune M., and Rossander L., 1989, Iron-absorption in man - ascorbic-acid and dose-dependent inhibition by phytate: American Journal of Clinical Nutrition, v. 49, no. 1, p. 140-144.

Halsted C. H., 2003, Dietary supplements and functional foods: 2 sides of a coin?: American Journal of Clinical Nutrition, v. 77, no. 4, p. 1001-1007.

Hancock B. C., and Parks M., 2000, What is the true solubility advantage for amorphous pharmaceuticals?: Pharmaceutical Research, v. 17, no. 4, p. 397-404.

Hansen C., Werner E., Erbes H. J., Larrat V., and Kaltwasser J. P., 1996, Intestinal calcium absorption from different calcium preparations: Influence of anion and solubility: Osteoporosis International, v. 6, no. 5, p. 386-393.

Harrison P. M., and Arosio P., 1996, The ferritins: Molecular properties, iron storage function and cellular regulation: Biochimica Et Biophysica Acta, v. 1275, no. 3, p. 161-203.

Heaney R. P., 2001, Factors influencing the measurement of bioavailability, taking calcium as a model: The Journal of Nutrition, v. 131, p. 1344-1348.

Heaney R. P., Dowell M. S., Rafferty K., and Bierman J., 2000, Bioavailability of the calcium in fortified soy imitation milk, with some observations on method: American Journal of Clinical Nutrition, v. 71, no. 5, p. 1166-1169.

Heaney R. P., and Recker R. R., 1994, Determinants of endogenous fecal calcium in healthy women: Journal of Bone and Mineral Research, v. 9, no. 10, p. 1621-1627.

Heaney R. P., Recker R. R., Stegman M. R., and Moy A. J., 1989, Calcium-absorption in women - relationships to calcium intake, estrogen status, and age: Journal of Bone and Mineral Research, v. 4, no. 4, p. 469-475.

Heaney R. P., Recker R. R., Watson P., and Lappe J. M., 2010, Phosphate and carbonate salts of calcium support robust bone building in osteoporosis: American Journal of Clinical Nutrition, v. 92, no. 1, p. 101-105.

Heaney R. P., Recker R. R., and Weaver C. M., 1990a, Absorbability of calcium sources - the limited role of solubility: Calcified Tissue International, v. 46, no. 5, p. 300-304.

Heaney R. P., Weaver C. M., and Fitzsimmons M. L., 1990b, Influence of calcium load on absorption fraction: Journal of Bone and Mineral Research, v. 5, no. 11, p. 1135-1138.

Hentze M. W., Muckenthaler M. U., and Andrews N. C., 2004, Balancing acts: Molecular control of mammalian iron metabolism: Cell, v. 117, no. 3, p. 285-297.

Hernlund E., Svedbom A., Ivergard M., Compston J., Cooper C., Stenmark J., McCloskey E. V., Jonsson B., and Kanis J. A., 2013, Osteoporosis in the european union: Medical management, epidemiology and economic burden. A report prepared in collaboration with the international osteoporosis foundation (iof) and the european federation of pharmaceutical industry associations (efpia): Archives of Osteoporosis, v. 8, p. 136.

Hidalgo I. J., Raub T. J., and Borchardt R. T., 1989, Characterization of the human-colon carcinoma cell-line (caco-2) as a model system for intestinal epithelial permeability: Gastroenterology, v. 96, no. 3, p. 736-749.

Hilty F. M., Arnold M., Hilbe M., Teleki A., Knijnenburg J. T. N., Ehrensperger F., Hurrell R. F., Pratsinis S. E., Langhans W., and Zimmermann M. B., 2010, Iron from nanocompounds containing iron and zinc is highly bioavailable in rats without tissue accumulation: Nature Nanotechnology, v. 5, no. 5, p. 374-380.

Hilty F. M., Knijnenburg J. T. N., Teleki A., Krumeich F., Hurrell R. F., Pratsinis S. E., and Zimmermann M. B., 2011, Incorporation of mg and ca into nanostructured fe2o3 improves fe solubility in dilute acid and sensory characteristics in foods: Journal of Food Science, v. 76, no. 1, p. 2-10.

Hilty F. M., Teleki A., Krumeich F., Buchel R., Hurrell R. F., Pratsinis S. E., and Zimmermann M. B., 2009, Development and optimization of iron- and zinc-containing nanostructured powders for nutritional applications: Nanotechnology, v. 20, no. 47.

Hilty F. M., and Zimmermann M. B., 2014a, Nano- structured minerals and trace elements for food and nutrition applications: Nano- and Microencapsulation for Foods, p. 199-222.

Hilty F. M., and Zimmermann M. B., 2014b, Nano-structured minerals and trace elements, *in* Kwak, H.-S., ed., Nano- and microencapsulation for foods, John Wiley & Sons, Ltd., p. 199-222.

Hoenderop J. G. J., Nilius B., and Bindels R. J. M., 2002, Molecular mechanism of active ca2+ reabsorption in the distal nephron: Annual Review of Physiology, v. 64, p. 529-549.

Hoenderop J. G. J., Voets T., Hoefs S., Weidema F., Prenen J., Nilius B., and Bindels R. J. M., 2003, Homo- and heterotetrameric architecture of the epithelial ca2+ channels trpv5 and trpv6: EMBO Journal, v. 22, no. 4, p. 776-785.

Holroyd C., Cooper C., and Dennison E., 2008, Epidemiology of osteoporosis: Best Practice & Research Clinical Endocrinology & Metabolism, v. 22, no. 5, p. 671-685.

Hornyak G. L., Tibbals H. F., Dutta J., and Moore J. J., 2009a, Characterization metods, Introduction to nanoscience and nanotechnology, CRC Press, p. 167-171.

Hornyak G. L., Tibbals H. F., Dutta J., and Moore J. J., 2009b, Chemical interactions at the nanoscale, Introduction to nanoscience and nanotechnology, CRC Press, p. 488-542.

Hornyak G. L., Tibbals H. F., Dutta J., and Moore J. J., 2009c, Fabrication methods, Introduction to nanoscience and nanotechnology, p. 177-236.

Huang S., Chen J. C., Hsu C. W., and Chang W. H., 2009, Effects of nano calcium carbonate and nano calcium citrate on toxicity in icr mice and on bone mineral density in an ovariectomized mice model: Nanotechnology, v. 20, no. 37, p. 1-7.

Huber M., Stark W. J., Loher S., Maciejewski M., Krumeich F., and Baiker A., 2005, Flame synthesis of calcium carbonate nanoparticles: Chemical Communications, no. 5, p. 648-650.

Hunt C. D., and Johnson L. K., 2007, Calcium requirements: New estimations for men and women by cross-sectional statistical analyses of calcium balance data from metabolic studies: American Journal of Clinical Nutrition, v. 86, no. 4, p. 1054-1063.

Hur S. J., Lim B. O., Decker E. A., and McClements D. J., 2011, In vitro human digestion models for food applications: Food Chemistry, v. 125, no. 1, p. 1-12.

Hurrell R., 2002, How to ensure adequate iron absorption from iron-fortified food: Nutrition Reviews, v. 60, no. 7, p. 7-15.

Hurrell R., 2007, Linking the bioavailability of iron compounds to the efficacy of iron-fortified foods: International Journal for Vitamin and Nutrition Research, v. 77, no. 3, p. 166-173.

Hurrell R., and Egli I., 2010, Iron bioavailability and dietary reference values: American Journal of Clinical Nutrition, v. 91, no. 5, p. 1461-1467.

Hurrell R. F., Lynch S. R., Trinidad T. P., Dassenko S. A., and Cook J. D., 1988, Iron-absorption in humans - bovine serum-albumin compared with beef muscle and egg-white: American Journal of Clinical Nutrition, v. 47, no. 1, p. 102-107.

Hurrell R. F., Reddy M., and Cook J. D., 1999, Inhibition of non-haem iron absorption in man by polyphenolic-containing beverages: British Journal of Nutrition, v. 81, no. 4, p. 289-295.

Hurrell R. F., Reddy M. B., Dassenko S. A., Cook J. D., and Shepherd D., 1991, Ferrous fumarate fortification of a chocolate drink powder: British Journal of Nutrition, v. 65, no. 2, p. 271-283.

Inoue K., Nakai Y., Ueda S., Kamigaso S., Ohta K. Y., Hatakeyama M., Hayashi Y., Otagiri M., and Yuasa H., 2008, Functional characterization of pcft/hcp1 as the molecular entity of the carrier-mediated intestinal folate transport system in the rat model: American Journal of Physiology - Gastrointestinal and Liver Physiology, v. 294, no. 3, p. 660-668.

Institute of Medicine, 2011, Dietary reference intakes: Calcium, vitamin d, Washington, D.C., The National Academies Press, Choice: Current reviews for academic libraries, p. 1115.

Iqbal T. H., Lewis K. O., and Cooper B. T., 1994, Phytase activity in the human and rat small-intestine: Gut, v. 35, no. 9, p. 1233-1236.

Jacobs A., 1977, Low molecular weight intracellular iron transport compounds: Blood, v. 50, no. 3, p. 433-439.

Jee W. S., and Yao W., 2001, Overview: Animal models of osteopenia and osteoporosis: Journal of Musculoskeletal & Neuronal Interactions, v. 1, no. 3, p. 193-207.

Johnell O., and Kanis J., 2005, Epidemiology of osteoporotic fractures: Osteoporosis International, v. 16, p. 3-7.

Jolivet J. P., Cassaignon S., Chaneac C., Chiche D., and Tronc E., 2008, Design of oxide nanoparticles by aqueous chemistry: Journal of Sol-Gel Science and Technology, v. 46, no. 3, p. 299-305.

Jovani M., Barbera R., Farre R., and de Aguilera E. M., 2001, Calcium, iron, and zinc uptake from digests of infant formulas by caco-2 cells: Journal of Agricultural and Food Chemistry, v. 49, no. 7, p. 3480-3485.

Jung J. M., Savin G., Pouzot M., Schmitt C., and Mezzenga R., 2008, Structure of heat-induced beta-lactoglobulin aggregates and their complexes with sodium-dodecyl sulfate: Biomacromolecules, v. 9, no. 9, p. 2477-2486.

Kalu D. N., 1991, The ovariectomized rat model of postmenopausal bone loss: Bone and Mineral, v. 15, no. 3, p. 175-191.

Kassebaum N. J., Jasrasaria R., Naghavi M., Wulf S. K., Johns N., Lozano R., Regan M., Weatherall D., Chou D. P., Eisele T. P., Flaxman S. R., Pullan R. L., Brooker S. J., and Murray C. J. L., 2014, A systematic analysis of global anemia burden from 1990 to 2010: Blood, v. 123, no. 5, p. 615-624.

Kastenmayer P., Davidsson L., Galan P., Cherouvrier F., Hercberg S., and Hurrell R. F., 1994, A double stable-isotope technique for measuring iron-absorption in infants: British Journal of Nutrition, v. 71, no. 3, p. 411-424.

Katikaneni R., Ponnapakkam A., Miller E., Ponnapakkam T., and Gensure R. C., 2009, A new technique for precisely and accurately measuring lumbar spine bone mineral density in mice using clinical dual energy x-ray absorptiometry (dxa): Toxicology Mechanisms and Methods, v. 19, no. 3, p. 225-231.

Khanal R. C., and Nemere I., 2008, Regulation of intestinal calcium transport: Annual Review of Nutrition, v. 28, p. 179-196.

Kiela P. R., Collins J. F., and Ghishan F. K., 2012, Physiology of the gastrointestinal tract, Amsterdam, Elsevier, p. 2197.

Knijnenburg J. T. N., Hilty F. M., Krumeich F., Zimmermann M. B., and Pratsinis S. E., 2013, Multimineral nutritional supplements in a nano-cao matrix: Journal of Materials Research, v. 28, no. 8, p. 1129-1138.

Knowles T. P. J., and Buehler M. J., 2011, Nanomechanics of functional and pathological amyloid materials: Nature Nanotechnology, v. 6, no. 8, p. 469-479.

Koo J., Weaver C. M., Neylan M. J., and Miller G. D., 1993, Isotopic tracer techniques for assessing calcium-absorption in rats: Journal of Nutritional Biochemistry, v. 4, no. 2, p. 72-76.

Kressel G., 2010, Bioavailability and solubility of different calcium-salts as a basis for calcium enrichment of beverages: Food and Nutrition Sciences, v. 1, no. 2, p. 53-58.

Kruger M. C., Booth C. L., Coad J., Schollum L. M., Kuhn-Sherlock B., and Shearer M. J., 2006, Effect of calcium fortified milk supplementation with or without vitamin k on biochemical markers of bone turnover in premenopausal women: Nutrition, v. 22, no. 11-12, p. 1120-1128.

Kruger M. C., Brown K. E., Collett G., Layton L., and Schollum L. M., 2003a, The effect of fructooligosaccharides with various degrees of polymerization on calcium bioavailability in the growing rat: Experimental Biology and Medicine, v. 228, no. 6, p. 683-688.

Kruger M. C., Gallaher B. W., and Schollum L. M., 2003b, Bioavailability of calcium is equivalent from milk fortified with either calcium carbonate or milk calcium in growing male rats: Nutrition Research, v. 23, no. 9, p. 1229-1237.

Kruger M. C., Plimmer G. G., Schollum L. M., Haggarty N., Ram S., and Palmano K., 2005, The effect of whey acidic protein fractions on bone loss in the ovariectomised rat: British Journal of Nutrition, v. 94, no. 2, p. 244-252.

Kumssa D. B., Joy E. J. M., Ander E. L., Watts M. J., Young S. D., Walker S., and Broadley M. R., 2015, Dietary calcium and zinc deficiency risks are decreasing but remain prevalent: Scientific Reports, v. 5, no. 10974.

Lara C., Adamcik J., Jordens S., and Mezzenga R., 2011, General self-assembly mechanism converting hydrolyzed globular proteins into giant multistranded amyloid ribbons: Biomacromolecules, v. 12, no. 5, p. 1868-1875.

Layrisse M., Martineztorres C., Leets I., Taylor P., and Ramirez J., 1984, Effect of histidine, cysteine, glutathione or beef on iron-absorption in humans: The Journal of Nutrition, v. 114, no. 1, p. 217-223.

Lee J. A., Kim M. K., Kim H. M., Lee J. K., Jeong J., Kim Y. R., Oh J. M., and Choi S. J., 2015, The fate of calcium carbonate nanoparticles administered by oral route: Absorption and their interaction with biological matrices: International Journal of Nanomedicine, v. 10, p. 2273-2293.

Lelovas P. P., Xanthos T. T., Thoma S. E., Lyritis G. P., and Dontasi I. A., 2008, The laboratory rat as an animal model for osteoporosis research: Comparative Medicine, v. 58, no. 5, p. 424-430.

Lentle B. C., and Prior J. C., 2003, Osteoporosis: What a clinician expects to learn from a patient's bone density examination: Radiology, v. 228, no. 3, p. 620-628.

Leppanen O., Sievanen H., Jokihaara J., Pajamaki I., and Jarvinen T. L. N., 2006, Three-point bending of rat femur in the mediolateral direction: Introduction and validation of a novel biomechanical testing protocol: Journal of Bone and Mineral Research, v. 21, no. 8, p. 1231-1237.

Levenson D. I., and Bockman R. S., 1994, A review of calcium preparations: Nutrition Reviews, v. 52, no. 7, p. 221-232.

Lewinski N., Colvin V., and Drezek R., 2008, Cytotoxicity of nanoparticles: Small, v. 4, no. 1, p. 26-49.

Lide D. R., 2015, Crc handbook of chemistry and physics, 96th edition, internet version 2015-2016, CRC Press.

Lin P. C., Lin S., Wang P. C., and Sridhar R., 2014, Techniques for physicochemical characterization of nanomaterials: Biotechnology Advances, v. 32, no. 4, p. 711-726.

Loher S., Stark W. J., Maciejewski M., Baiker A., Pratsinis S. E., Reichardt D., Maspero F., Krumeich F., and Gunther D., 2005, Fluoro-apatite and calcium phosphate nanoparticles by flame synthesis: Chemistry of Materials, v. 17, no. 1, p. 36-42.

Lopez H. W., Coudray C., Levrat-Verny M. A., Feillet-Coudray C., Demigne C., and Remesy C., 2000, Fructooligosaccharides enhance mineral apparent absorption and counteract the deleterious effects of phytic acid on mineral homeostasis in rats: Journal of Nutritional Biochemistry, v. 11, no. 10, p. 500-508.

Luo P., and Nieh T. G., 1995, Synthesis of ultrafine hydroxyapatite particles by a spray dry method: Materials Science & Engineering C - Biomimetic Materials Sensors and Systems, v. 3, no. 2, p. 75-78.

Lynch S. R., and Cook J. D., 1980, Interaction of vitamin c and iron: Annals of the New York Academy of Sciences, v. 355, p. 32-44.

Maedler L., Kammler H. K., Mueller R., and Pratsinis S. E., 2002a, Controlled synthesis of nanostructured particles by flame spray pyrolysis: Journal of Aerosol Science, no. 33, p. 369–389.

Maedler L., and Pratsinis S. E., 2002, Bismuth oxide nanoparticles by flame spray pyrolysis: Journal of the American Ceramic Society, v. 85, no. 7, p. 1713-1718.

Maedler L., Stark W. J., and Pratsinis S. E., 2002b, Flame-made ceria nanoparticles: Journal of Materials Research, v. 17, no. 6, p. 1356-1362.

Mailander V., and Landfester K., 2009, Interaction of nanoparticles with cells: Biomacromolecules, v. 10, no. 9, p. 2379-2400.

Marques-Vidal P., Pecoud A., Hayoz D., Paccaud F., Mooser V., Waeber G., and Vollenweider P., 2009, Prevalence and characteristics of vitamin or dietary supplement users in lausanne, switzerland: The colaus study: European Journal of Clinical Nutrition, v. 63, no. 2, p. 273-281.

Marshall D. H., and Nordin B. E. C., 1981, A comparison of radioactive calcium-absorption tests with net calcium-absorption: Clinical Science, v. 61, no. 4, p. 477-481.

Matkovic V., 1991, Calcium metabolism and calcium requirements during skeletal modeling and consolidation of bone mass: American Journal of Clinical Nutrition, v. 54, no. 1 Suppl, p. 245-260.

Matkovic V., and Heaney R. P., 1992, Calcium balance during human growth - evidence for threshold behavior: American Journal of Clinical Nutrition, v. 55, no. 5, p. 992-996.

McKie A. T., Barrow D., Latunde-Dada G. O., Rolfs A., Sager G., Mudaly E., Mudaly M., Richardson C., Barlow D., Bomford A., Peters T. J., Raja K. B., Shirali S., Hediger M. A., Farzaneh F., and Simpson R. J., 2001, An iron-regulated ferric reductase associated with the absorption of dietary iron: Science, v. 291, no. 5509, p. 1755-1759.

Meiron O. E., Bar-David E., Aflalo E. D., Shechter A., Stepensky D., Berman A., and Sagi A., 2011, Solubility and bioavailability of stabilized amorphous calcium carbonate: Journal of Bone and Mineral Research, v. 26, no. 2, p. 364-372.

Melton L. J., Chrischilles E. A., Cooper C., Lane A. W., and Riggs B. L., 1992, How many women have osteoporosis: Journal of Bone and Mineral Research, v. 7, no. 9, p. 1005-1010.

Mezzenga R., Schurtenberger P., Burbidge A., and Michel M., 2005, Understanding foods as soft materials: Nature Materials, v. 4, no. 10, p. 729-740.

Minihane A. M., and Fairweather-Tait S. J., 1998, Effect of calcium supplementation on daily nonheme-iron absorption and long-term iron status: American Journal of Clinical Nutrition, v. 68, no. 1, p. 96-102.

Monsen E. R., Hallberg L., Layrisse M., Hegsted D. M., Cook J. D., Mertz W., and Finch C. A., 1978, Estimation of available dietary iron: American Journal of Clinical Nutrition, v. 31, no. 1, p. 134-141.

Moseley K. F., Weaver C. M., Appel L., Sebastian A., and Sellmeyer D. E., 2013, Potassium citrate supplementation results in sustained improvement in calcium balance in older men and women: Journal of Bone and Mineral Research, v. 28, no. 3, p. 497-504.

Muller R. H., Jacobs C., and Kayser O., 2001, Nanosuspensions as particulate drug formulations in therapy rationale for development and what we can expect for the future: Advanced Drug Delivery Reviews, v. 47, no. 1, p. 3-19.

Nel A., Xia T., Madler L., and Li N., 2006, Toxic potential of materials at the nanolevel: Science, v. 311, no. 5761, p. 622-627.

Nickel K. P., Martin B. R., Smith D. L., Smith J. B., Miller G. D., and Weaver C. M., 1996, Calcium bioavailability from bovine milk and dairy products in premenopausal women using intrinsic and extrinsic labeling techniques: The Journal of Nutrition, v. 126, no. 5, p. 1406-1411.

Ohman C., Montesi M., Lambers F. M., Salsedo E., Beraudi A., Kuhn G. A., Baleani M., Stea S., Muller R., and Viceconti M., 2011, The ovariectomized mouse is an effective model to study osteoporosis as assessed by morphometry, histology, protein expression and mechanical testing: Bone, v. 48, p. 204-212.

Pak C. Y., Kaplan R., Bone H., Townsend J., and Waters O., 1975, A simple test for the diagnosis of absorptive, resorptive and renal hypercalciurias: The New England Journal of Medicine, v. 292, no. 10, p. 497-500.

Pak C. Y. C., and Avioli L. V., 1988, Factors affecting absorbability of calcium from calcium salts and food: Calcified Tissue International, v. 43, no. 2, p. 55-60.

Paoli M., Marles-Wright J., and Smith A., 2002, Structure-function relationships in heme-proteins: DNA and Cell Biology, v. 21, no. 4, p. 271-280.

Papanikolaou G., and Pantopoulos K., 2005, Iron metabolism and toxicity: Toxicology and Applied Pharmacology, v. 202, no. 2, p. 199-211.

Park C. H., Valore E. V., Waring A. J., and Ganz T., 2001, Hepcidin, a urinary antimicrobial peptide synthesized in the liver: Journal of Biological Chemistry, v. 276, no. 11, p. 7806-7810.

Park S. B., Lee Y. J., and Chung C. K., 2010, Bone mineral density changes after ovariectomy in rats as an osteopenic model : Stepwise description of double dorso-lateral approach: Journal of Korean Neurosurgical Society, v. 48, no. 4, p. 309-312.

Pereira D. I. A., Bruggraber S. F. A., Faria N., Poots L. K., Tagmount M. A., Aslam M. F., Frazer D. M., Vulpe C. D., Anderson G. J., and Powell J. J., 2014, Nanoparticulate iron(iii) oxo-hydroxide delivers safe iron that is well absorbed and utilised in humans: Nanomedicine-Nanotechnology Biology and Medicine, v. 10, no. 8, p. 1877-1886.

Pereira D. I. A., Mergler B. I., Faria N., Bruggraber S. F. A., Aslam M. F., Poots L. K., Prassmayer L., Lonnerdal B., Brown A. P., and Powell J. J., 2013, Caco-2 cell acquisition of dietary iron(iii) invokes a nanoparticulate endocytic pathway: PloS One, v. 8, no. 11.

Perron N. R., and Brumaghim J. L., 2009, A review of the antioxidant mechanisms of polyphenol compounds related to iron binding: Cell Biochemistry and Biophysics, v. 53, no. 2, p. 75-100.

Pietrangelo A., 2004, Medical progress - hereditary hemochromatosis - a new look at an old disease: New England Journal of Medicine, v. 350, no. 23, p. 2383-2397.

Pigeon C., Ilyin G., Courselaud B., Leroyer P., Turlin B., Brissot P., and Loreal O., 2001, A new mouse liver-specific gene, encoding a protein homologous to human antimicrobial peptide hepcidin, is overexpressed during iron overload: Journal of Biological Chemistry, v. 276, no. 11, p. 7811-7819.

Pratsinis S. E., 1998, Flame aerosol synthesis of ceramic powders: Progress in Energy and Combustion Science, v. 24, no. 3, p. 197-219.

Pratsinis S. E., and Vemury S., 1996, Particle formation in gases: A review: Powder Technology, v. 88, no. 3, p. 267-273.

Qato D. M., Alexander G. C., Conti R. M., Johnson M., Schumm P., and Lindau S. T., 2008, Use of prescription and over-the-counter medications and dietary supplements among older adults in the united states: Journal of the American Medical Association, v. 300, no. 24, p. 2867-2878.

Rafferty K., Walters G., and Heaney R. P., 2007, Calcium fortificants: Overview and strategies for improving calcium nutriture of the us population: Journal of Food Science, v. 72, no. 9, p. 152-158.

Raffin S. B., Woo C. H., Roost K. T., Price D. C., and Schmid R., 1974, Intestinal-absorption of hemoglobin iron-heme cleavage by mucosal heme oxygenase: Journal of Clinical Investigation, v. 54, no. 6, p. 1344-1352.

Ravn P., Fledelius C., Rosenquist C., Overgaard K., and Christiansen C., 1996, High bone turnover is associated with low bone mass in both pre- and postmenopausal women: Bone, v. 19, no. 3, p. 291-298.

Recker R. R., 1985, Calcium absorption and achlorhydria: The New England Journal of Medicine, v. 313, no. 2, p. 70-73.

Reddy M. B., and Cook J. D., 1991, Assessment of dietary determinants of nonheme-iron absorption in humans and rats: American Journal of Clinical Nutrition, v. 54, no. 4, p. 723-728.

Reid D. M., and Macdonald H. M., 2001, Nutrition and bone: Is there more to it than just calcium and vitamin d?: QJM: An International Journal of Medicine, v. 94, no. 2, p. 53-56.

Riggs B. L., and Melton L. J., 1995, The worldwide problem of osteoporosis - insights afforded by epidemiology: Bone, v. 17, no. 5, p. 505-511.

Roetto A., Papanikolaou G., Politou M., Alberti F., Girelli D., Christakis J., Loukopoulos D., and Camaschella C., 2003, Mutant antimicrobial peptide hepcidin is associated with severe juvenile hemochromatosis: Nature Genetics, v. 33, no. 1, p. 21-22.

Rohner F., Ernst F. O., Arnold M., Hibe M., Biebinger R., Ehrensperger F., Pratsinis S. E., Langhans W., Hurrell R. F., and Zimmermann M. B., 2007, Synthesis, characterization, and bioavailability in rats of ferric phosphate nanoparticles: The Journal of Nutrition, v. 137, no. 3, p. 614-619.

Ross P. D., Wasnich R. D., Maclean C. J., Hagino R., and Vogel J. M., 1988, A model for estimating the potential costs and savings of osteoporosis prevention strategies: Bone, v. 9, no. 6, p. 337-347.

Rouault T. A., 2006, The role of iron regulatory proteins in mammalian iron homeostasis and disease: Nature Chemical Biology, v. 2, no. 8, p. 406-414.

Rudin T., and Pratsinis S. E., 2012, Homogeneous iron phosphate nanoparticles by combustion of sprays: Industrial & Engineering Chemistry Research, v. 51, no. 23, p. 7891-7900.

Rudin T., Wegner K., and Pratsinis S. E., 2011, Uniform nanoparticles by flame-assisted spray pyrolysis (fasp) of low cost precursors: Journal of Nanoparticle Research, v. 13, no. 7, p. 2715-2725.

Russell L. F., Sanford K. A., Gaul S. O., Haskett J., Johnston E. M., McRae K. B., and Stark R., 2010, Effect of calcium salts on fortified apple juice: British Food Journal, v. 112, no. 6-7, p. 751-762.

Sachdev H. P. S., Gera T., and Nestel P., 2005, Effect of iron supplementation on mental and motor development in children: Systematic review of randomised controlled trials: Public Health Nutrition, v. 8, no. 2, p. 117-132.

Sambuy Y., Angelis I., Ranaldi G., Scarino M. L., Stammati A., and Zucco F., 2005, The caco-2 cell line as a model of the intestinal barrier: Influence of cell and culture-related factors on caco-2 cell functional characteristics: Cell Biology and Toxicology, v. 21, no. 1, p. 1-26.

Scholz-Ahrens K. E., Schaafsma G., van den Heuvel E. G. H. M., and Schrezenmeir J., 2001, Effects of prebiotics on mineral metabolism: American Journal of Clinical Nutrition, v. 73, no. 2, p. 459-464.

Schrurs F., and Lison D., 2012, Focusing the research efforts: Nature Nanotechnology, v. 7, p. 546-548.

Sebastian A., and Morris R. C., 1994, Improved mineral balance and skeletal metabolism in postmenopausal women treated with potassium bicarbonate: New England Journal of Medicine, v. 331, no. 4, p. 279-279.

Shah B. G., Giroux A., and Belonje B., 1977, Specifications for reduced iron as a food additive: Journal of Agricultural and Food Chemistry, v. 25, no. 3, p. 592-594.

Shahnazari M., Martin B. R., Legette L. L., Lachcik P. J., Welch J., and Weaver C. M., 2009, Diet calcium level but not calcium supplement particle size affects bone density and mechanical properties in ovariectomized rats.: The Journal of Nutrition, v. 139, no. 10, p. 1308-1315.

Shawki A., and Mackenzie B., 2010, Interaction of calcium with the human divalent metal-ion transporter-1: Biochemical and Biophysical Research Communications, v. 393, no. 3, p. 471-475.

Shayeghi M., Latunde-Dada G. O., Oakhill J. S., Laftah A. H., Takeuchi K., Halliday N., Khan Y., Warley A., McCann F. E., Hider R. C., Frazer D. M., Anderson G. J., Vulpe C. D., Simpson R. J., and McKie A. T., 2005, Identification of an intestinal heme transporter: Cell, v. 122, no. 5, p. 789-801.

Shirahama T., and Cohen A. S., 1967, High-resolution electron microscopic analysis of the amyloid fibril: The Journal of Cell Biology, v. 33, no. 3, p. 679-708.

Sievanen H., 2010, Immobilization and bone structure in humans: Archives of Biochemistry and Biophysics, v. 503, no. 1, p. 146-152.

Sims N. A., and Gooi J. H., 2008, Bone remodeling: Multiple cellular interactions required for coupling of bone formation and resorption: Seminars in Cell & Developmental Biology, v. 19, no. 5, p. 444-451.

Slesinski M. J., Subar A. F., and Kahle L. L., 1996, Dietary intake of fat, fiber and other nutrients is related to the use of vitamin and mineral supplements in the united states: The 1992 national health interview survey: The Journal of Nutrition, v. 126, no. 12, p. 3001-3008.

Stoltzfus R. J., 2003, Iron deficiency: Global prevalence and consequences: Food and Nutrition Bulletin, v. 24, no. 4 Suppl, p. 99-103.

Stoltzfus R. J., and Dreyfuss M. L., 1998, Guidelines for the use of iron supplements to prevent and treat iron deficiency anemia, Washington, D. C., ILSI PRESS.

Stone M. D., and Turner A. J., 2012, Use of dual-energy x-ray absorptiometry (dxa) with non-human vertebrates: Application, challenges, and practical considerations for research and clinical practice, Bird's-eye view of veterinary medicine, InTech, p. 626.

Storcksdieck Genannt Bonsmann S., and Hurrell R. F., 2007, Iron-binding properties, amino acid composition, and structure of muscle tissue peptides from in vitro digestion of different meat sources: Journal of Food Science, v. 72, no. 1, p. 19-29.

Strobel R., and Pratsinis S. E., 2007, Flame aerosol synthesis of smart nanostructured materials: Journal of Materials Chemistry, v. 17, no. 45, p. 4743-4756.

Sun L. M., Chow L. C., Frukhtbeyn S. A., and Bonevich J. E., 2010, Preparation and properties of nanoparticles of calcium phosphates with various ca/p ratios: Journal of Research of the National Institute of Standards and Technology, v. 115, no. 4, p. 243-255.

Swain J. H., Newman S. M., and Hunt J. R., 2003, Bioavailability of elemental iron powders to rats is less than bakery-grade ferrous sulfate and predicted by iron solubility and particle surface area: The Journal of Nutrition, v. 133, no. 11, p. 3546-3552.

Tao J., and James J. D. Y., 2013, Chapter twenty-two - ftir and raman studies of structure and bonding in mineral and organic–mineral composites, Methods in enzymology, Volume 532, Academic Press, p. 533-556.

Teoh W. Y., Amal R., and Madler L., 2010, Flame spray pyrolysis: An enabling technology for nanoparticles design and fabrication: Nanoscale, v. 2, no. 8, p. 1324-1347.

Teucher B., Olivares M., and Cori H., 2004, Enhancers of iron absorption: Ascorbic acid and other organic acids: International Journal for Vitamin and Nutrition Research, v. 74, no. 6, p. 403-419.

The European Commission, 2011, Commission recommendation of 18 october 2011 on the definition of nanomaterial (text with eea relevance): Official Journal of the European Union.

Thompson B. A., Sharp P. A., Elliott R., and Fairweather-Tait S. J., 2010, Inhibitory effect of calcium on non-heme iron absorption may be related to translocation of dmt-1 at the apical membrane of enterocytes: Journal of Agricultural and Food Chemistry, v. 58, no. 14, p. 8414-8417.

Thompson D. D., Simmons H. A., Pirie C. M., and Ke H. Z., 1995, Fda guidelines and animal-models for osteoporosis: Bone, v. 17, no. 4, p. 125-133.

Tobelmann R., 2001, Implementing calcium fortification: An industry case study: Journal of Food Composition and Analysis, v. 14, no. 3, p. 241-244.

Tung M. S., 1998, Calcium phosphates: Structure, composition, solubility and stability, *in* Anjad, Z., ed., Calcium phospahtes in biological and industrial systems, Springer Science & Business Media, LCC.

van der Linden J. C., Waarsing J. H., and Weinans H., 2006, The use of micro-ct to study bone architecture dynamics noninvasively: Drug Discov Today Technol, v. 3, no. 2, p. 213-219.

Vattem D. A., Seth A., and Mahoney R. R., 2001, Chelation and reduction of iron by chicken muscle protein digests: The role of sulphhydryl groups: Journal of the Science of Food and Agriculture, v. 81, no. 15, p. 1476-1480.

Walczyk T., 2001, The potential of inorganic mass spectrometry in mineral and trace element nutrition research: Fresenius Journal of Analytical Chemistry, v. 370, no. 5, p. 444-453.

Wang M. Q., Yang X., Wang F., Li R., Ning H., Na L. X., Huang Y. F., Song Y., Liu L. Y., Pan H. Z., Zhang Q. J., Fan L. J., Li Y., and Sun C. H., 2013, Calcium-deficiency assessment and biomarker identification by an integrated urinary metabonomics analysis: Bmc Medicine, v. 11.

Weaver C. M., 1985, Intrinsic mineral labeling of edible plants - methods and uses: CRC Critical Reviews in Food Science and Nutrition, v. 23, no. 1, p. 75-101.

Weaver C. M., and Heaney R. P., 1991, Isotopic exchange of ingested calcium between labeled sources. Evidence that ingested calcium does not form a common absorptive pool: Calcified Tissue International, v. 49, no. 4, p. 244-247.

Weaver C. M., Heaney R. P., Martin B. R., and Fitzsimmons M. L., 1992, Extrinsic vs intrinsic labeling of the calcium in whole-wheat flour: American Journal of Clinical Nutrition, v. 55, no. 2, p. 452-454.

Weaver C. M., and Plawecki K. L., 1994, Dietary calcium - adequacy of a vegetarian diet: American Journal of Clinical Nutrition, v. 59, no. 5, p. 1238-1241.

Wegmuller R., Zimmermann M. B., Moretti D., Arnold M., Langhans W., and Hurrell R. F., 2004, Particle size reduction and encapsulation affect the bioavailability of ferric pyrophosphate in rats: The Journal of Nutrition, v. 134, no. 12, p. 3301-3304.

Weiner S., Addadi L., and Wagner H. D., 2000, Materials design in biology: Materials Science & Engineering C - Biomimetic and Supramolecular Systems, v. 11, no. 1, p. 1-8.

Weiner S., Levi-Kalisman Y., Raz S., and Addadi L., 2003, Biologically formed amorphous calcium carbonate: Connective Tissue Research, v. 44 Suppl 1, p. 214-218.

Weiss G., and Goodnough L. T., 2005, Medical progress: Anemia of chronic disease: New England Journal of Medicine, v. 352, no. 10, p. 1011-1023.

Welch J. M., Tumer C. H., Devareddy L., Arjmandi B. H., and Weaver C. M., 2008, High impact exercise is more beneficial than dietary calcium for building bone strength in the growing rat skeleton: Bone, v. 42, no. 4, p. 660-668.

West A. R., and Oates P. S., 2008, Mechanisms of heme iron absorption: Current questions and controversies: World Journal of Gastroenterology, v. 14, no. 26, p. 4101-4110.

WHO, 1994, Assessment of fracture risk and its application to screening for postmenopausal osteoporosis : Report of a who study group [meeting held in rome from 22 to 25 june 1992],

WHO, 2001, Iron deficiency anaemia : Assessment, prevention and control : A guide for programme managers, Geneva, Switzerland, World Health Organization.

WHO, 2008, Worldwide prevalence of anaemia 1993–2005: Who global database on anaemia: Public Health Nutrition, v. 12, no. 4, p. 444-454.

WHO, and CDC, 2007, Assessing the iron status of populations : Including literature reviews : Report of a joint world health organization/centers for disease control and prevention technical consultation on the assessment of iron status at the population level, Geneva, Switzerland.

Woitge H. W., Scheidt-Nave C., Kissling C., Leidig-Bruckner G., Meyer K., Grauer A., Scharla S. H., Ziegler R., and Seibel M. J., 1998, Seasonal variation of biochemical indexes of bone turnover: Results of a population-based study: Journal of Clinical Endocrinology & Metabolism, v. 83, no. 1, p. 68-75.

Zafar T. A., Weaver C. M., Jones K., Moore D. R., and Barnes S., 2004, Inulin effects on bioavailability of soy isoflavones and their calcium absorption enhancing ability: Journal of Agricultural and Food Chemistry, v. 52, no. 10, p. 2827-2831.

Zhang D. J., and Tamilselvan A., 2007, Lattice energy and mechanical stiffness of hydroxyapatite: Journal of Materials Science - Materials in Medicine, v. 18, no. 1, p. 79-87.

Zhang T. L., Wang L. M., Chen Q., and Chen C. Y., 2014, Cytotoxic potential of silver nanoparticles: Yonsei Medical Journal, v. 55, no. 2, p. 283-291.

Zhao Y. D., Martin B. R., and Weaver C. M., 2005, Calcium bioavailability of calcium carbonate fortified soymilk is equivalent to cow's milk in young women: The Journal of Nutrition, v. 135, no. 10, p. 2379-2382.

Zimmermann M. B., Chaouki N., and Hurrell R. F., 2005, Iron deficiency due to consumption of a habitual diet low in bioavailable iron: A longitudinal cohort study in moroccan children: American Journal of Clinical Nutrition, v. 81, no. 1, p. 115-121.

Zimmermann M. B., and Hurrell R. F., 2007, Nutritional iron deficiency: Lancet, v. 370, no. 9586, p. 511-520.

MANUSCRIPT 1

Dissolution and storage stability of nanostructured calcium carbonates and phosphates for nutrition

Lidija Posavec[1§], Jesper T.N. Knijnenburg[1§], Florentine M. Hilty[1], Frank Krumeich[2], Sotiris E. Pratsinis[2], Michael B. Zimmermann[1]

[1] Laboratory of Human Nutrition, Institute of Food, Nutrition and Health, Department of Health Sciences and Technology, ETH Zurich, Switzerland

[2] Particle Technology Laboratory, Institute of Process Engineering, Department of Mechanical and Process Engineering, ETH Zurich, Switzerland

[§] these authors contributed equally to this work

Journal of Nanoparticle Research (2016) 18:310

This work was supported by ETH Research Grant ETH-06 10-1 and the Swiss South African Joint Research Programme (project number IZLSZ3_149090).

Abstract

Rapid calcium (Ca) dissolution from nanostructured Ca phosphate and carbonate ($CaCO_3$) powders may allow them to be absorbed in much higher fraction in humans. Nanosized Ca phosphate and $CaCO_3$ made by flame-assisted spray pyrolysis (FASP) were characterized by nitrogen adsorption, X-ray diffraction (XRD), Raman spectroscopy, and transmission electron microscopy (TEM). As-prepared nanopowders contained both $CaCO_3$ and CaO but storing them under ambient conditions over 130 days resulted in a complete transformation into $CaCO_3$, with an increase in both crystal and particle sizes. The small particle size could be stabilized against such aging by cation (Mg, Zn, Sr) and anion (P) doping, with P and Mg being most effective. Calcium phosphate nanopowders made at Ca:P ≤ 1.5 were XRD-amorphous and contained γ-$Ca_2P_2O_7$ with increasing hydroxyapatite content at higher Ca:P. Aging of powders with Ca:P = 1.0 and 1.5 for over 500 days gradually increased particle size (but less than for $CaCO_3$) without a change in phase composition or crystallinity. In 0.01 M H_3PO_4 calcium phosphate nanopowders dissolved ≈4 times more Ca than micron-sized compounds and about twice more Ca than $CaCO_3$ nanopowders, confirming that nanosizing and/or amorphous structuring sharply increases Ca powder dissolution. Because higher Ca solubility *in vitro* generally leads to greater absorption *in vivo*, these novel FASP-made Ca nanostructured compounds may prove useful for nutrition applications, including supplementation and/or food fortification.

KEYWORDS: Flame assisted spray pyrolysis (FASP), calcium carbonate, calcium phosphate, doping, aging, dissolution

Abbreviations: **AAS**, atomic absorption spectroscopy; **AI**, adequate intake; **FASP**, flame-assisted spray pyrolysis; **FSP**, flame spray pyrolysis; **HAp**, hydroxyapatite; **ICDD**, International Centre for Diffraction Data; **RH**, relative humidity; **SAED**, selected area electron diffraction; **SSA**, specific surface area; **TEM**, transmission electron microscopy; **TGA**, thermogravimetric analysis; **XRD**, X-ray diffraction.

1. Introduction

Inadequate dietary calcium (Ca) intake is a risk factor for osteoporosis and bone fractures (Nordin, 1997; Weaver and Gallant, 2014). In many European countries, dietary Ca intake remains below recommended levels (European Commission, 1998). Consumption of Ca-rich products (such as mineral water and dairy products) can increase Ca intake (Sipponen and Harkonen, 2010), but for many individuals it remains difficult to reach the adequate intake (AI) of 1.0–1.2 g Ca/day (Institute of Medicine, 1997). Ca absorption from food sources typically ranges from 23–37% (Gueguen and Pointillart, 2000), and may be lower in at-risk groups such as hypochlorhydric patients (Recker, 1985), the elderly, and post-menopausal women (Imel *et al.*, 2014). To ensure sufficient dietary intake, Ca supplements and Ca-fortified foods may be necessary.

Nanostructuring of Ca compounds can increase Ca dissolution and bioavailability and these compounds may be promising as supplements and/or fortificants. Huang *et al.* (2009) showed that nanosizing of Ca carbonate ($CaCO_3$) and citrate could significantly improve the bone mineral density in ovariectomized mice when compared to the corresponding micron-sized compounds. Similarly, Chen *et al.* (2008) showed a significantly higher Ca absorption and retention from nanosized compared to micronsized pearl powder in humans. A combined approach of amorphous structuring and nanosizing of $CaCO_3$ significantly increased fractional Ca absorption in a rat model (Meiron *et al.*, 2011) and also in a clinical trial in post-menopausal women (Vaisman *et al.*, 2014).

Flame spray pyrolysis (FSP) (Madler *et al.*, 2002) and flame assisted spray pyrolysis (FASP) (Rudin *et al.*, 2011) are two aerosol-based processes for one-step synthesis of tailor-made high purity nanoparticles without any liquid byproducts (Strobel and Pratsinis, 2007). The FSP has been previously applied for synthesis of Fe-containing nanoparticles as food fortificants with high iron bioavailability in rats (Hilty *et al.*, 2010; Rohner *et al.*, 2007), and also for Ca-containing nanoparticles such as $CaCO_3$ (Huber *et al.*, 2005), Ca phosphates (Loher *et al.*, 2005), and Fe- and Zn-doped CaO (Knijnenburg *et al.*, 2013). However, FSP-made Ca nanoparticles produced from inexpensive nitrate precursors (Knijnenburg *et al.*, 2013) resulted in powders with a bimodal size distribution (Hilty *et al.*, 2011; Jossen *et al.*, 2005), which can be avoided using FASP (Rudin and Pratsinis, 2012). A more homogeneous

powder can significantly improve product performance as shown for nano-$FePO_4$ (Rudin and Pratsinis, 2012).

Thus, size reduction from the micron- to the nanoscale combined with amorphous (non-crystalline) structuring of FASP-made $CaCO_3$ and Ca phosphate could increase Ca dissolution and bioavailability as with Fe (Hilty *et al.*, 2010). If fractional absorption of nanostructured Ca compounds proves to be high, their use could reduce the bulkiness of Ca supplements and fortificants and potentially increase ease-of-use and AI compliance.

Nanomaterials, however, like ZnO (Ali and Winterer, 2010), CaO (Knijnenburg *et al.*, 2013), and even carbon nanotubes (Yang *et al.*, 2009) can undergo compositional and/or structural changes during their storage. This aging process may negatively influence the performance of such powders, yet there has been little systematic investigation of the stability of nanomaterials, including nanosized Ca compounds, during long-term storage.

Here, homogeneous Ca carbonates and phosphates were made by FASP (Rudin *et al.*, 2011) and their particle and crystal size and composition were investigated as function of process parameters and storage time at ambient conditions. The effect of nutritionally relevant dopants (Zn, Mg, Sr, and P) on the storage stability of $CaCO_3$ was also studied as such dopants can drastically alter nanoparticle characteristics (Knijnenburg *et al.*, 2013). Finally, the dissolution behavior of the most promising FASP-produced Ca nanocompounds was investigated, using a previously described method (Meiron *et al.*, 2011) as a potential predictor of *in vivo* bioavailability.

2. Materials and methods

2.1 Powder synthesis

Nanostructured $CaCO_3$ and Ca phosphates with and without dopant Mg, Zn and Sr were prepared by FASP (Rudin *et al.*, 2011). Their precursors were mixtures of calcium (II) nitrate tetrahydrate (puriss p.a., ACS reagent, 99-103%, Sigma Aldrich, USA), magnesium (II) nitrate tetrahydrate (puriss. p.a., Sigma Aldrich), zinc (II) nitrate hexahydrate (purum. p.a., ≥ 99%, Fluka, USA), strontium (II) nitrate (puriss., ≥98%, Sigma Aldrich) and/or tributylphosphate (97%, Sigma Aldrich), dissolved in ethanol (abs. denat. 2% 2-butanone, Alcosuisse A15-A, Alcosuisse, Switzerland). The doped powders were produced substituting Ca with the other

element (given as dopant at%), keeping the total element concentration in solution constant at 0.4 M.

The precursor solution was fed at a constant flow rate (mL/min) into the water-cooled FASP nozzle using a syringe pump (Lambda Vit-Fit, Lambda Laboratory Instruments, Switzerland), and dispersed by 3–6 L/min O_2 (≥ 99.5%, PanGas, Switzerland) while maintaining a pressure drop of 1.6–1.8 bar at the nozzle. The spray was ignited by 5–7 L/min C_2H_2 (dissolved, ≥ 99.5%, PanGas) fed through a cylindrical ring at 1 cm above the nozzle, using a stainless steel tube (inner diameter 1.6 cm) to limit air entrainment (Rudin *et al.*, 2011). Additionally, 5 L/min sheath O_2 (≥ 99.5, PanGas) was supplied around the nozzle to ensure complete C_2H_2 and precursor combustion. The particles were collected on a water-cooled glass microfiber filter (257 mm diameter, Albet-Hahnemuehle, Germany) placed at least 70 cm above the nozzle using a vacuum pump (Mink MM1202 AV, Busch, Germany). Production parameters are indicated by x/y, where x is the precursor solution feed rate (mL/min) and y is the dispersion O_2 feed rate (L/min).

2.2 Powder characterization

The specific surface area (SSA) was measured by nitrogen adsorption at 77 K in the relative pressure range p/p_0 = 0.05–0.25 (Micromeritics Tristar 3000 or Tristar II plus, Micrometritics Instruments Corp, USA) after degasing with dry N_2 for at least 1 hour at 150 °C. X-ray diffraction (XRD, Bruker AXS D8 Advance diffractometer, Bruker Instruments, USA) patterns were measured directly after production ('as prepared') and after selected storage times. The diffraction peaks were screened for phase composition by EVA software (version 10.0 rev 1, Bruker AXS) using the following ICDD card numbers: CaO 82-1690; $Ca(OH)_2$ 04-0733; $CaCO_3$ (calcite) 85-1108; $Ca_{8.8}(PO_4)_6(OH)_{1.92}$ (hydroxyapatite) 86-1201; ZnO 79-2205; and $SrCO_3$ 71-2393. Crystal sizes (d_{XRD}) and crystalline $CaCO_3$ content were obtained by Rietveld refinement with TOPAS software (version 4.2, Bruker AXS) using the fundamental parameters approach (Cheary and Coelho, 1992).

Raman spectra were measured from 100 to 3200 cm^{-1} using a Renishaw inVia Raman Microscope (Renishaw, UK) equipped with a 785 nm laser (5 mW power, 10 s exposure, 5 accumulations). The particles were deposited on a carbon foil supported on a copper grid for transmission electron microscopy (TEM) analysis which was performed on a Tecnai F30 microscope (FEI, The Netherlands; field emission gun, 300 kV) (Knijnenburg *et al.*, 2013).

The total Ca content of the powders was measured in triplicate (Hilty *et al.*, 2009) by flame atomic absorption spectroscopy (AAS, SpectrAA-240FS, Agilent Technologies, USA) using external calibration after dissolving the powders in 5 M HCl. Each sample for AAS measurement (total Ca and dissolution) contained 5000 ppm La (lanthanum nitrate hexahydrate III, puriss. p.a. ≥ 99.0%, Fluka) to eliminate P interference.

The dissolution experiments were performed in triplicate following Meiron *et al.* (2011). For each powder, 40 mg Ca was dissolved into 50 mL 0.01 M H_3PO_4. The solution was stirred at 625 rpm with a magnetic stirrer and the solution pH was recorded every 1 s for 500 s using a continuous pH meter (Seven excellence, Mettler Toledo, Switzerland). The time to reach half of final pH (tpH50) was used as a measure of powder dissolution (Meiron *et al.*, 2011). At the end of the dissolution experiment (here defined as "steady state"), an aliquot of 2 mL was filtered through a 0.1 µm filter (nylon membrane, Infochroma, Switzerland) and the filtrate was further diluted in 0.1 M HCl (prepared from concentrated HCl, puriss. p.a. ≥ 32%, Sigma-Aldrich) for AAS analysis. For the dissolution experiments, three commercial powders were used for comparison: calcium carbonate (light, Ph.Eur., Burgerstein Vitamins, Switzerland), calcium phosphate nano amorphous ($Ca_2P_2O_7 \cdot x\ H_2O$, Ca:P ≈ 1.0, SSA > 12 m^2/g (typical), Sigma Aldrich), and calcium pyrophosphate ($Ca_2P_2O_7$, ≥ 99.9% trace metal basis, Sigma Aldrich). Correlations between dissolution outcomes and parameters were tested (SPSS Statistics 20, IBM, USA) applying a linear regression model after assuming normal distribution of the data. The significance level was set at $p \leq 0.05$.

The storage stability of the nanopowders was investigated under ambient conditions. The as-prepared particles were stored in an acclimatized laboratory in open glass vials to allow air exchange. Temperature and relative humidity (RH) were recorded every 30 min with a data logger (Onset, HOBO data Logger temp/RH, USA). The average temperature was 21.6 ± 0.5 °C (19.7–22.8 °C), while the RH varied between 21.7 and 71.3%.

3. Results and discussion

3.1 Calcium carbonates

3.1.1 Undoped $CaCO_3$: production and aging stability

In flame synthesis of nanosized $CaCO_3$, the Ca-containing precursor solution is combusted and CaO is formed at high temperature. The CaO aerosol is then converted to $CaCO_3$ by

reacting with CO_2 that is produced in the combustion process (Lu *et al.*, 2009). An increase in precursor flow rate produced a visibly larger flame (Mueller *et al.*, 2003) with higher particle concentration and longer residence time (Camenzind *et al.*, 2005) at high temperature (typically above 2000 K (Rudin and Pratsinis, 2012)) that resulted in more coagulation, sintering and particle growth. The particle size was thus increased and the SSA decreased (Knijnenburg *et al.*, 2013) from 99 to 37 m^2/g for our as-prepared $CaCO_3$ powders (**Figure 1**). Increasing precursor flow rate also decreased the $CaCO_3$ content of the particles. At low precursor flow rates the particles consisted of almost pure $CaCO_3$, and this content decreased to approximately 50% (the rest was crystalline CaO) at a precursor flow rate of 15 mL/min. At low precursor flow rates, the initially formed CaO particles were small and reacted completely with CO_2 to form $CaCO_3$. Larger CaO particles were formed at higher precursor flow rates, and the diffusion of CO_2 into CaO was too slow for complete carbonate formation (Silaban and Harrison, 1995).

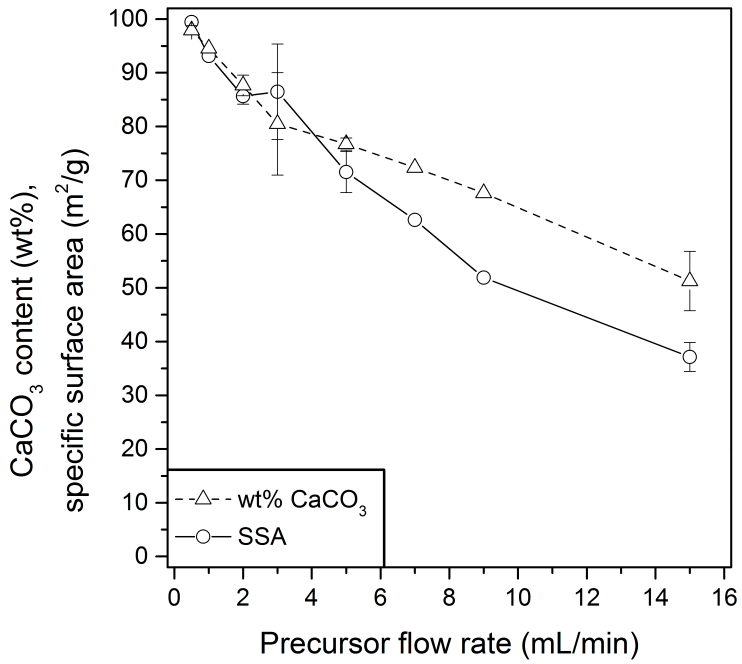

Figure 1: Specific surface area (SSA, circles) and calcium carbonate content (triangles) of as-prepared $CaCO_3$-containing powders as function of precursor flow rate to the FASP reactor. The powders were produced using 6 L/min O_2 dispersion gas.

High amounts of $CaCO_3$ are desirable because the alkaline character of CaO and $Ca(OH)_2$ causes a strong increase in pH when coming into contact with water. The alkalinity of $CaCO_3$

is less because of the buffering properties of the bicarbonate ion in acidic media (Stumm and Morgan, 1996). The $CaCO_3$ content in the FASP-made powders is higher than FSP-made Fe-doped CaO powders (Knijnenburg *et al.*, 2013). This could be attributed to the fraction of large CaO particles formed by droplet-to-particle conversion during FSP (Knijnenburg *et al.*, 2013), and probably due to the higher CO_2 partial pressure in the FASP set-up originating from combusting 7 L/min C_2H_2 compared to 1 L/min CH_4 in FSP (Knijnenburg *et al.*, 2013). The $CaCO_3$ content, however, is comparable to that of Lu *et al.* (2009) but lower than that of Huber *et al.* (2005); quite likely storage over time increased the carbonate content in their powders (Knijnenburg *et al.*, 2013), as discussed below.

Figure 2a shows the XRD patterns of a typical as-prepared Ca-containing nanopowder (produced with a 3/6 flame) after selected days of storage at ambient conditions. The CaO is unstable at room temperature in the presence of humidity (Dheilly *et al.*, 1998) and absorbs moisture to form $Ca(OH)_2$. By reaction with CO_2, $Ca(OH)_2$ is then converted to calcite $CaCO_3$ via dissolution of CO_2 in a water layer around $Ca(OH)_2$ (Shih *et al.*, 1999). This phase transformation coexisted with an increase in $CaCO_3$ crystal size (**Figure 2**a): the as-prepared $CaCO_3$ crystal size was 16 nm but after complete transformation to $CaCO_3$ in 7 days it increased to 30 nm. Even after phase transformation was complete, the crystal size kept increasing to 45 nm after > 130 days of aging. Concomitantly the SSA also decreased over time: the as-prepared powder had a SSA 89 m^2/g, and after > 130 days of aging it decreased to 40 m^2/g (relative SSA reduction of 55 %).

The change into a more defined crystal structure is also apparent from TEM images of the as-prepared and aged powders (**Figure 2**b, c). The as-prepared $CaCO_3$-containing powder consisted of agglomerated particles with not well-defined shapes that were transformed into individual cube-like crystals after aging. During aging, a clear recrystallization took place, as also evidenced by the inset SAED pattern that shows the presence of bright spots indicative of larger crystallites than the as-prepared powders.

It is likely that these nanoparticles sintered together at room temperature due to humidity (similar to growth of nano-ZnO (Ali and Winterer, 2010)) as restructuring of $CaCO_3$ takes place under humid atmosphere (Hausner *et al.*, 2007). Also, $CaCO_3$ nanoparticles grow in the presence of water vapor: a suspension of $Ca(OH)_2$ in isopropanol exposed to low (33 and

54%) (Chen *et al.*, 2006) and high (75 and 90%) (Gomez-Villalba *et al.*, 2011) RH at room temperature resulted in a RH-dependent calcite crystal size increase.

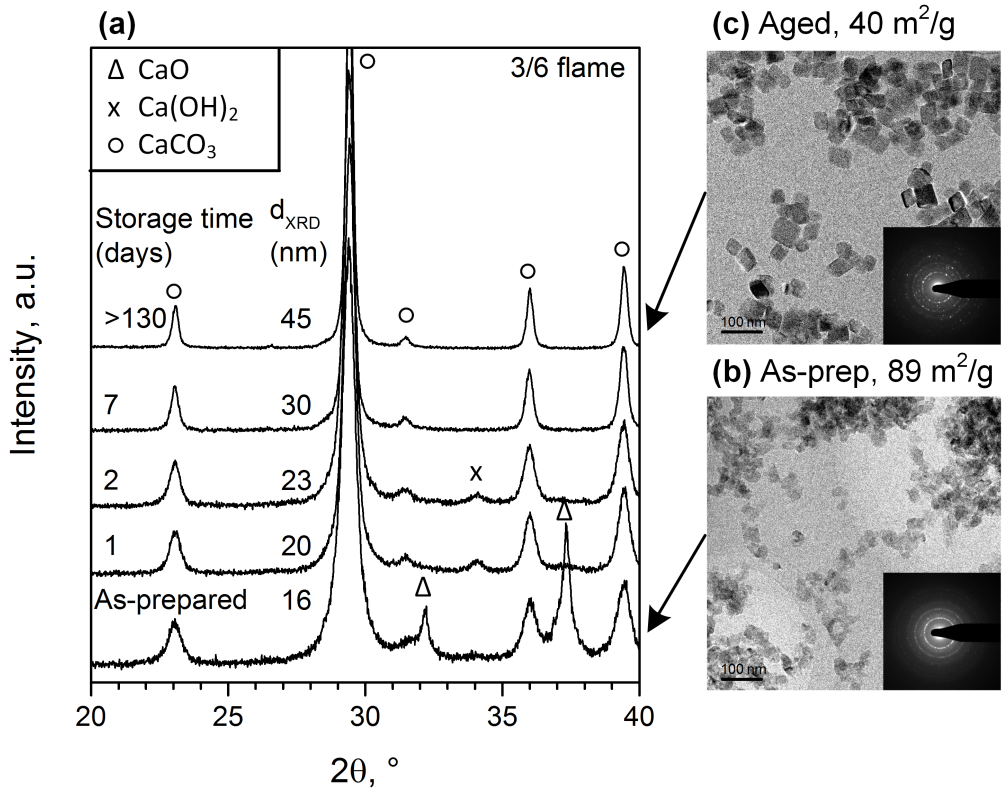

Figure 2: a. XRD patterns of as-prepared $CaCO_3$-containing powders (using a 3/6 flame) after aging for different times at ambient conditions. The patterns were normalized by the highest peak intensity. Typical TEM images of **b.** as-prepared and **c**. aged $CaCO_3$ for over 130 days.

3.1.2 Doping of $CaCO_3$: aging stability

Because this growth in crystal size would reduce surface area and thereby likely reduce *in vivo* Ca dissolution and absorption, different dopants were tested to stabilize $CaCO_3$ during storage. Zinc (Zn), magnesium (Mg), phosphorus (P), and strontium (Sr) were tested as dopants. The Zn, Mg and P were used for their nutritional relevance. The Sr and Mg were added both because of their potential benefits on bone health (Marie *et al.*, 2001; Orchard *et al.*, 2014) and their position in the periodic table in the same group as Ca.

Compared to undoped $CaCO_3$, all dopants had an inhibiting effect on crystal growth as the d_{XRD} remained smaller, with higher dopant contents being more effective (**Figure 3**). The strongest crystal growth inhibition was in the order Mg > Sr > P > Zn, with Mg being the most effective at stabilizing small crystal sizes. Independent of dopant composition, aging stopped after 25–30 days, and only for 5 at% P it continued. The best overall performance was for 30

at% Mg that seems to completely stabilize small $CaCO_3$ crystals: even after > 130 days the crystal size (16 nm) was practically the same as that of the as-prepared powder (14 nm). For each as-prepared compound (except 30 at% P), the XRD pattern showed some CaO at 37.4° (the relative amounts differ for the dopants), that had disappeared after aging, and a relatively broad peak of calcite $CaCO_3$ was visible at 29.5° (**Figure S1** in Supporting Information). At 5 at% dopant content, no dopant-specific phase was detected, likely because the dopant amounts were too low and might have formed a solid solution.

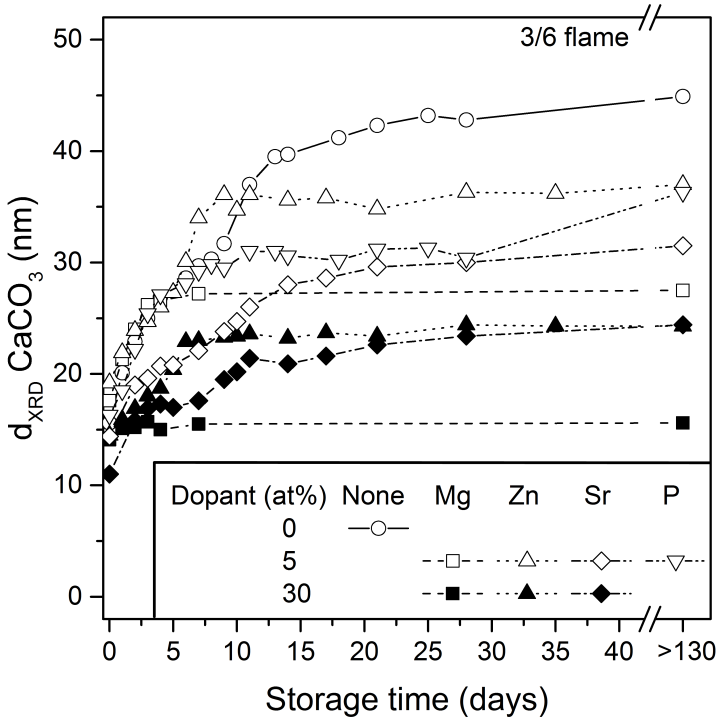

Figure 3: Average crystal size (d_{XRD}) of $CaCO_3$ as function of aging time under ambient conditions for pure and doped $CaCO_3$. The powders were produced using a 3/6 flame. The sample containing 30 at% P is not shown here because it was dominantly amorphous.

From TEM analysis, the 5 at% Mg-containing powder consisted of small primary particles sinter-necked in the form of chain-like aggregates (**Figure S2** in Supporting Information). These particles were slightly larger and more crystalline after aging, but smaller than for the undoped ones (**Figure 2**c). Increasing the Mg content to 30 at% resulted in more aggregated and agglomerated particles, but their size and crystallinity (as confirmed by their SAED patterns) was not changed after aging (**Figure S2** in Supporting Information). The XRD patterns of this powder showed no diffraction peaks for Mg phases (**Figure S1** in Supporting Information), so the Mg was likely amorphous and/or dissolved in the CaO or $CaCO_3$ (Doman

et al., 1963; Goldsmith and Heard, 1961). Raman analysis of the Mg-containing powders was not conclusive and only showed a very small peak shift (< 5 cm^{-1}) relative to $CaCO_3$ (not shown). Thus, increasing the Mg-content in $CaCO_3$ nanopowders inhibited crystal growth during aging. It was shown that Mg^{2+} inhibits $CaCO_3$ growth in aqueous solution (Davis *et al.*, 2000) and also high Mg contents stabilize amorphous $CaCO_3$ during precipitation in solution (Loste *et al.*, 2003).

The as-prepared powder with 30 at% Zn contained some crystalline ZnO. Its intensity increased by aging (**Figure S1** in Supporting Information) revealing that ZnO grew over time (Ali and Winterer, 2010) even in the presence of Ca. While still performing better than the undoped material, Zn may be not as effective as the other dopants because nano-ZnO also grows in the presence of humidity (Ali and Winterer, 2010).

Compared to the other dopants, Sr-doped $CaCO_3$ aged more slowly. With 30 at% Sr, $SrCO_3$ was formed during storage and separated out from $CaCO_3$ (**Figure S1** in Supporting Information). Due to its large ionic radius, Sr^{2+} would induce considerable lattice strain when incorporated into calcite and is thus more likely to be found outside (de Leeuw, 2002). Here, Sr did not show any benefits since Sr-doping enhanced particle growth, likely because of the hygroscopicity of $SrCO_3$ (Mao *et al.*, 2000).

P-doping of $CaCO_3$ both reduced carbonate crystal size, and increased and stabilized the powder's high SSA (**Figure S1** in Supporting Information). However, P is an anionic dopant (as a phosphate replaces the carbonate group in $CaCO_3$ rather than the Ca^{2+}), while Zn^{2+}, Sr^{2+} and Mg^{2+} are isovalent dopants for Ca^{2+}. Depending on the Ca:P ratio, a different Ca phosphate phase is formed. The FASP-synthesis of Ca phosphate nanopowders will be discussed in more detail in the next section.

Thus, at constant (3/6 flame) synthesis parameters, higher dopant contents resulted in a smaller d_{XRD} increase and SSA decrease (except for Sr-doped powders). The most promising dopants to stabilize the small $CaCO_3$ particles were Mg and P, in particular at 30 at%, because such powders consisted of the smallest $CaCO_3$ crystals and/or particles after aging, due to their higher stability towards restructuring during storage.

3.2 Calcium phosphates

3.2.1 Calcium phosphates: crystallinity and phase composition

Calcium phosphate can have a different phase composition depending on the Ca:P molar ratio that usually varies from 0.5 to 2.0 (Dorozhkin, 2007). By increasing the Ca:P ratio at constant synthesis conditions (3/6 flame) there is a gradual transformation from amorphous to crystalline powders (**Figure 4**). More specifically, Ca phosphate made at Ca:P = 0.75 and 1 were XRD-amorphous as indicated by the broad hump (2θ = 25–31°) and the absence of any diffraction peaks. Increasing Ca:P to 1.5 and 1.67 shows the formation of poorly crystalline hydroxyapatite (HAp) as indicated by the diffraction peaks that become even more visible at Ca:P = 2.33.

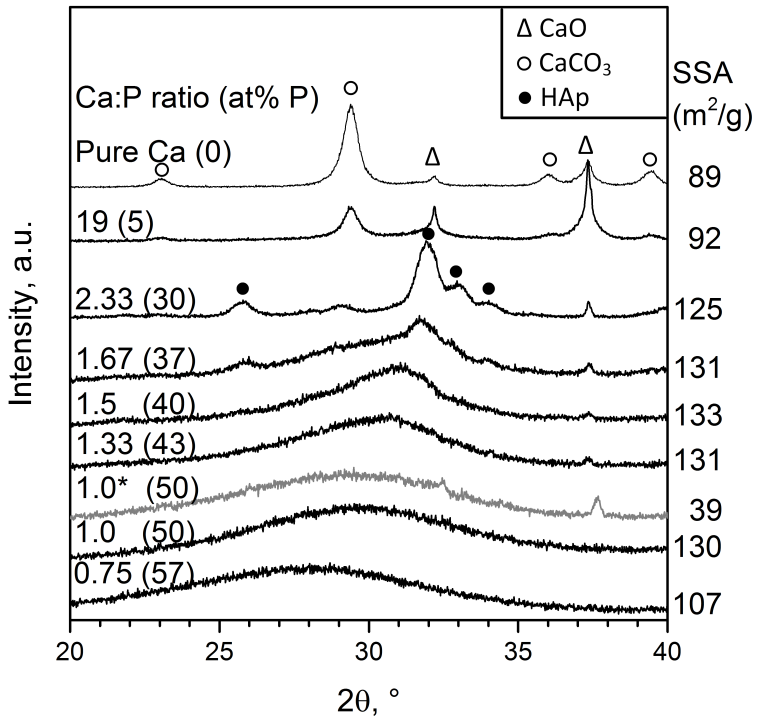

Figure 4: XRD patterns and SSA of as-prepared Ca/P-containing powders with different Ca:P ratios. The patterns were normalized by the highest peak intensity. The at% P is shown in parenthesis for comparison to the cationic dopants. The powder with the asterisk (*) was produced with a 9/3 flame instead of a 3/6 flame as for the other powders.

Loher *et al.* (2005) produced Ca phosphates at Ca:P = 1.43–1.67 and their as-prepared powders were XRD-amorphous with SSA 90 m^2/g because of the rapid cooling that did not allow the powder to crystallize. Amorphous structuring was also obtained by Sun *et al.* (2010) when producing Ca:P = 1.0–1.6 by spray drying, but their SSA did not exceed 50 m^2/g.

The highest SSA here is found for Ca:P = 1.0 to 1.67 and either decreasing or increasing the Ca:P ratio decreased the SSA (**Figure 4**). A sample containing Ca:P = 0.5 was produced as well but could not be collected from the filter, suggesting that a too low Ca:P ratio could potentially result in a more hydrated powder, probably related to the hygroscopic properties of P_2O_5 (Frear *et al.*, 1944). In contrast, the SSA of FSP-made amorphous iron phosphates was independent of composition for Fe:P ≥ 0.5 (Hilty *et al.*, 2009). For Ca:P = 1.0, increasing the precursor to dispersion flow rate ratio from 3/6 to 9/3 and essentially increasing high temperature residence time, it resulted in a larger fraction of CaO and also thrice lower SSA (**Figure 4**, gray pattern), but there was no crystalline phosphate at this composition. Further increasing the Ca:P ratio to 19 showed the formation of a mixture of $CaCO_3$ and CaO. For most materials some CaO impurity was present even for the P-rich powders, likely due to flame inhomogeneity. The CaO content increased for higher Ca:P ratios due to the reduction of the precursor P content, which allowed Ca to bind directly to oxygen. Since the powders with Ca:P = 1.0–1.5 were amorphous and had high SSA, they may be attractive for nutritional applications.

Raman analysis showed that for Ca:P = 0.75 mostly γ-$Ca_2P_2O_7$ (Ca pyrophosphate) was formed with a small amount of HAp (**Figure 5**). Increasing the Ca-content resulted in the formation of more HAp and relatively less γ-$Ca_2P_2O_7$ that was even absent for Ca:P = 1.67. This increase in γ-$Ca_2P_2O_7$ formation with decreasing Ca:P ratio was also seen in FSP-made (Loher *et al.*, 2005) and spray-dried nanosized Ca phosphate (Sun *et al.*, 2010). By changing the precursor to dispersion flow rate ratio from 3/6 to 9/3 as above, an increase in HAp content relative to γ-$Ca_2P_2O_7$ was observed (gray pattern). Also here, as for the $CaCO_3$, the larger flame and thus longer particle residence time at high temperature (Camenzind *et al.*, 2005) favored the formation of the thermodynamically more stable HAp. Some of the powders contained some $HCaPO_4$ as evidenced by the peak at 589 cm^{-1}.

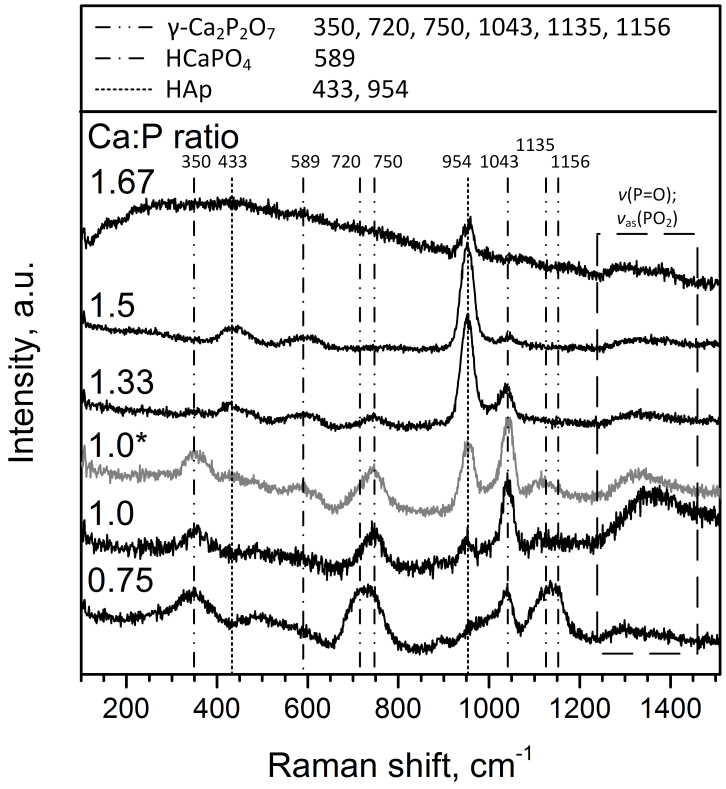

Figure 5: Raman spectra of nanopowders containing Ca:P molar ratio from 0.75 to 1.67 which showed a predominant amorphous pattern in XRD analysis. The powder with the asterisk (*) was produced with a 9/3 flame instead of a 3/6 flame as for the other powders. The following references were used for peak identification: Wopenka and Pasteris (2005), Pemberton *et al.* (1991), and Meyer (1998).

3.2.2 Calcium phosphates: aging stability

By aging the $CaCO_3$ powders initially had the strongest reduction in SSA that became constant after approximately 25 days (**Figure 6**). On the other hand, the Ca phosphate powders aged more gradually, having a slower decrease in SSA than $CaCO_3$. The powder with Ca:P = 1.5 aged slower than with Ca:P = 1.0, likely due to the higher fraction of stable HAp present in the former powder. It was anticipated that after aging, a restructuring towards a more stable structure would have taken place (Puech *et al.*, 1982), so the XRD pattern and Raman spectra were measured after aging. After 500 days aging, however, no difference in XRD patterns (not shown) and Raman spectra (**Figure 7**) were visible compared to the as-prepared powders, suggesting that aging affected particle size but did not change powder composition and crystallinity.

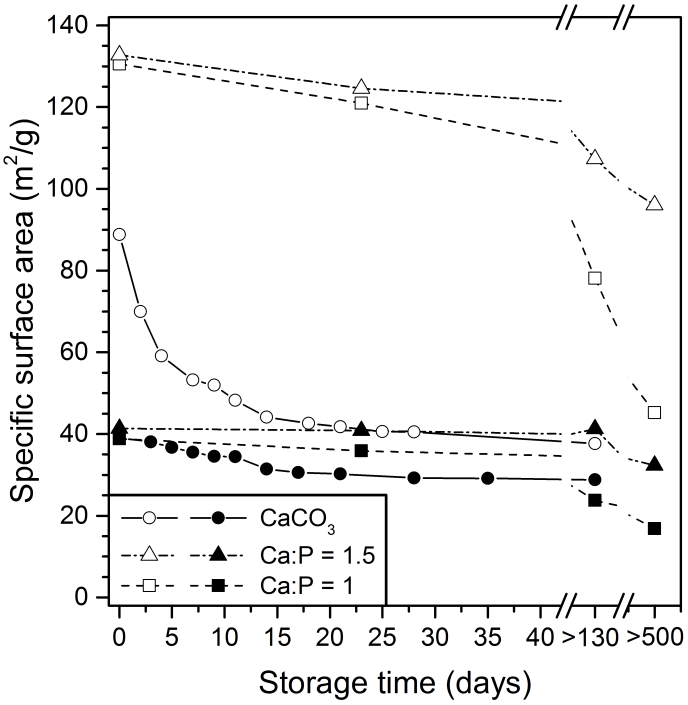

Figure 6: SSA over time during aging under ambient conditions of selected powders (Ca:P = 1.0, Ca:P = 1.5, $CaCO_3$) produced with high (3/6 flame, open symbols) and low SSA (9/3 flame for Ca:P = 1 and 15/6 flame for $CaCO_3$, filled symbols).

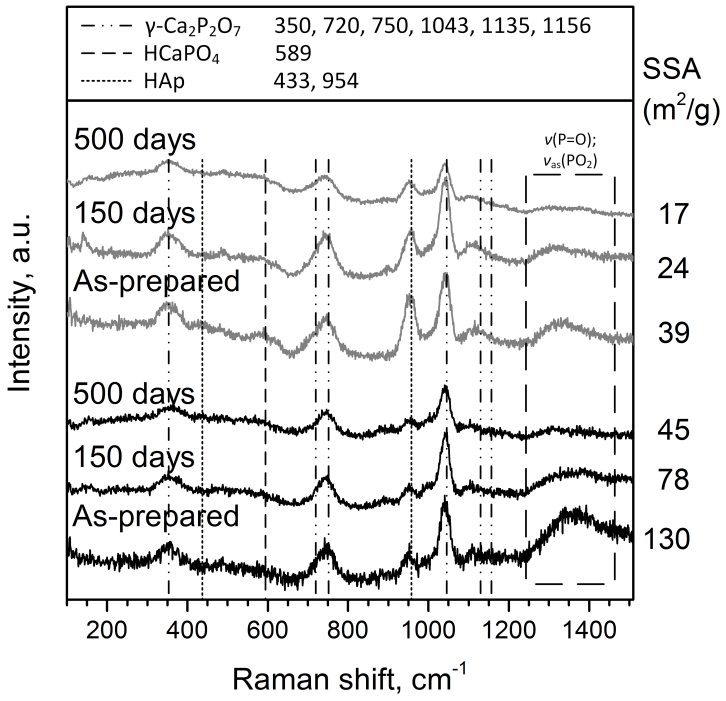

Figure 7: Raman spectra of powders with Ca:P = 1.0, as-prepared and aged for 150 and 500 days, produced with a 3/6 flame (high SSA, black) and a 9/3 flame (low SSA, gray). The following references were used for peak identification: Wopenka and Pasteris (2005), Pemberton *et al.* (1991), and Meyer (1998).

Figure 8 shows TEM images of Ca:P = 1.0 as-prepared chain-like aggregates (a) with SSA of 130 m^2/g (3/6 flame) that grew after 130 days (**Figure 8**b). For more than 500 days of aging (**Figure 8**c), the necks increased in size, but the amorphous structure was retained (see inset SAED patterns). The larger as-prepared particles (9/3 flame) with an SSA of initially 39 m^2/g, **Figure 8**d) were initially large polydisperse spheres with bridging sinter-necks between them that increased in size after aging but were still amorphous (**Figure 8**e, f). The particle growth can be related to the reduction in SSA from 130 to 45 m^2/g (-34%) and from 39 to 17 m^2/g (-43%) for the two different flame synthesis conditions after > 500 days aging. Our finding is in contrast to Puech *et al.* (1982) who observed a gradual morphological transformation from spherules to needle-shaped particles (typical of HAp) after exposing the amorphous Ca phosphate powder to water vapor. Most likely the aging conditions of our powders were not as strong as those used by Puech *et al.* (1982).

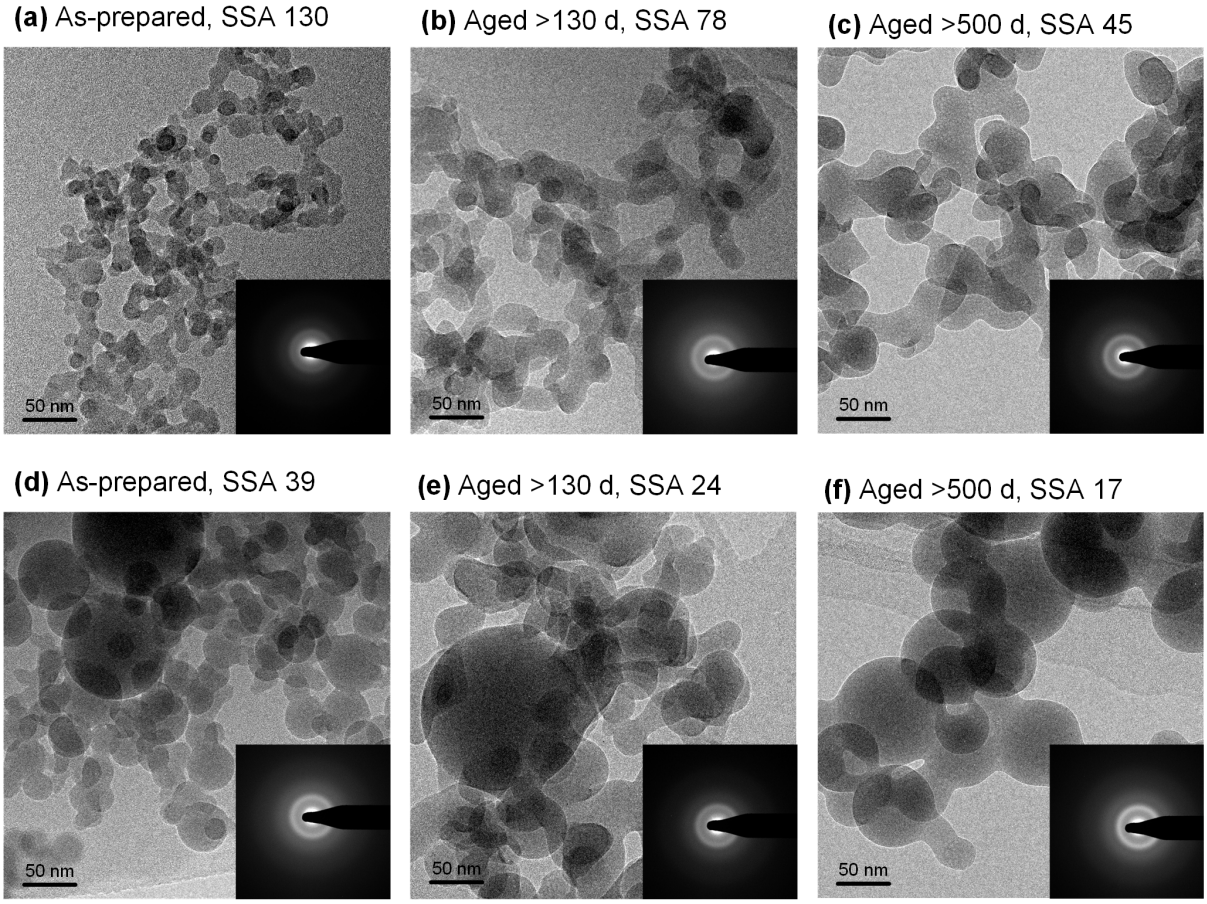

Figure 8: TEM images of Ca:P = 1.0 with two different average sizes produced with a 3/6 flame (**a-c**) and a 9/3 flame (**d-f**), right after production (**a, d**), aged for > 130 days (**b, e**), and aged > 500 days (**c, f**).

3.3 Calcium dissolution

The dissolution of the $CaCO_3$ and Ca phosphate nanopowders was measured in 0.01 M H_3PO_4 (pH = 2.2 ± 0.1). During dissolution of $CaCO_3$ and Ca phosphate in an aqueous environment the pH increases. The final pH was approximately 5.8–6.5 for the carbonates and approximately 4.2–4.7 for the Ca phosphates (except for the micron-sized crystalline Ca phosphate, which dissolved very poorly). Although the final pH was different for $CaCO_3$ and Ca phosphate, this method normalizes the amount of Ca added to the acid, eliminating any differences in dissolution performance by differences in Ca content of the powders (see **Table S1** in Supporting Information). The time to reach 50% of the final pH (t_{pH50}) and the dissolved Ca at steady state were measured.

The commercial micronsized Ca pyrophosphate had a very low SSA and delivered only 106 mg Ca/L (~13%) at steady state (**Figure 9**a). In contrast, dissolution of the Ca phosphate nanopowders (with substantially higher SSA) resulted in a fourfold increase in dissolved Ca (370–460 mg/L), confirming that nanosizing and/or amorphous state strongly improves powder dissolution. However, this strong increase in dissolved Ca was already reached with an SSA of 23 m^2/g (commercial nano-Ca phosphate), and a further increase in SSA did not further improve Ca dissolution. Despite reduction in SSA, no difference in amount of Ca delivered could be observed between the as-prepared (open orange squares) and the aged Ca phosphate (open blue squares) nanopowders.

All the FASP-made carbonates had an SSA of 50-60 m^2/g after aging—this is 25 times higher than the commercial $CaCO_3$—and there was an increase in Ca dissolved for undoped and 5 at% Mg-doped $CaCO_3$. However, increasing the Mg content to 30 at% reduced the dissolved Ca. This lower Ca release could be due to the formation of a mixed Ca-Mg carbonate during aging. Since $MgCO_3$ (3'138 kJ/mol) has a higher lattice energy than calcite $CaCO_3$ (2'804 kJ/mol) (Haynes, 2015-2016), the substitution of Ca for Mg in the $CaCO_3$ thus increases the crystal lattice energy. So even though incorporation of Mg into $CaCO_3$ increases Ca solubility at steady state (Morse *et al.*, 2007), it decreases the Ca dissolution rate (Chou *et al.*, 1989). There was, however, no indication for the formation of crystalline Ca/Mg carbonate or any other Mg-containing phase in the XRD patterns (**Figure S1** in Supporting Information) and Raman spectra (not shown).

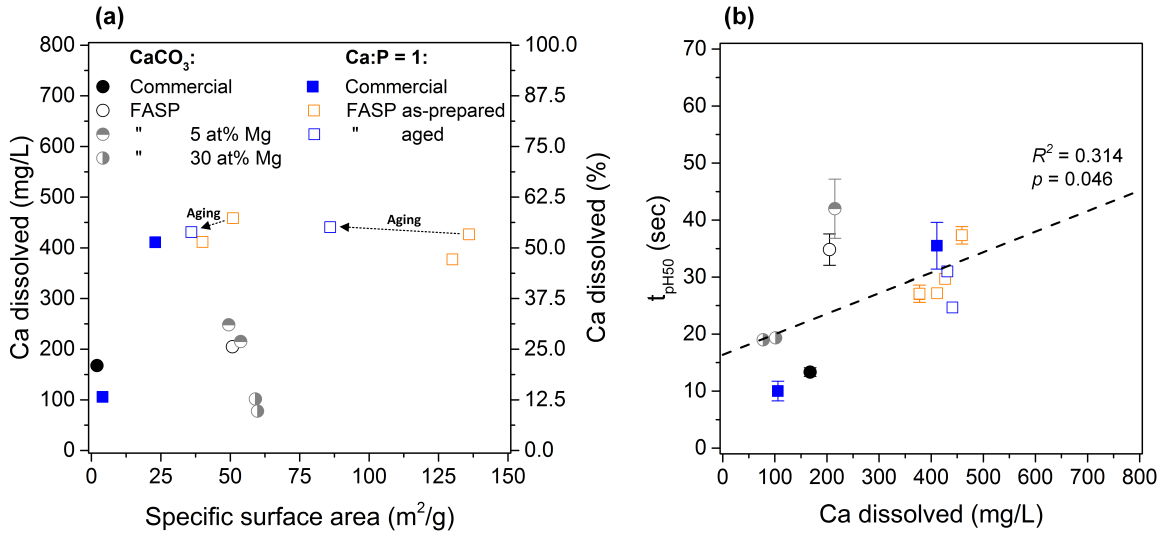

Figure 9: a. Ca dissolved (in mg/L and % of powder) as function of particle SSA after dissolution of 40 mg Ca in 50 mL 0.01 M H_3PO_4 over 500 sec. **b**. Time to reach 50% of the final pH (t_{pH50}) as function of dissolved Ca. The dashed line is a linear fit showing the correlation between the two variables. The values are displayed as an average of 3 replicates ± standard deviation. Error bars are not shown when the standard deviations are smaller than the symbol. Arrows indicate which as-prepared and aged powders were taken from the same batch. Flame synthesis parameters of the tested powders are summarized in Table S1.

There was no significant correlation between t_{pH50} and particle SSA (R^2 = 0.071, p = 0.377) after removing the outlier (one sample of $CaCO_3$ with 30 at% Mg, t_{pH50} > 100 sec) (**Figure S3** in Supporting Information). A small but significant positive correlation (R^2 = 0.314, p = 0.046) was found between t_{pH50} and the amount of dissolved Ca (**Figure 9**b). Dissolution of the commercial micron-sized $CaCO_3$ and Ca pyrophosphate showed that the two compounds were the fastest to reach pH_{50}, but released the smallest amount of Ca when compared with the FASP-made materials. Meiron *et al.* (2011) observed that amorphous state could significantly reduce t_{pH50} when changing from crystalline to amorphous $CaCO_3$ (40–100 nm particles). The commercial $CaCO_3$ used in our set of experiments performed better than the one used in that study in terms of reaching a higher final pH of 6 and reaching pH_{50} in less than 15 sec, which might be due to differences in running methods and material properties (e.g., no SSA was given).

From the dissolution results it can be seen that at steady state the Ca phosphate powders had twice as much Ca dissolved compared to the carbonates, likely because of the smaller increase in final pH (**Table S1** in Supporting Information) which allowed the dissolution of more Ca. Dissolved Ca increased for both the carbonates and phosphates when moving from micron- to nanoscale, but no additional effect was observed for SSA above 23 m^2/g.

It appears the Ca phosphate nanopowders dissolve so rapidly that no difference in dissolution kinetics could be observed. Because these compounds were amorphous even after aging, the amorphous structuring may have had a greater influence on dissolution than SSA. This may also explain the poor dissolution of crystalline micronsized commercial $Ca_2P_2O_7$, and why there was only a minor influence of SSA on $CaCO_3$ dissolution. FSP-made Fe/Zn phosphate nanopowders with amorphous structure showed no influence of SSA (86-143 m^2/g) on Fe dissolution (Hilty *et al.*, 2009). Crystallinity is a determinant of dissolution of $FePO_4$ (Willis and Allen, 1999), and amorphous content of $FePO_4$ was a better predictor of solubility and bioavailability than SSA (Dickmann *et al.*, 2016). At the end of our experiments, perhaps the nanopowders were at (or close to) their solubility limit, causing powder dissolution to slow down (Margolis and Moreno, 1992) and resulting in comparable dissolved Ca values.

Thus, for the powders investigated here, composition (Ca:P = 1 vs. $CaCO_3$) and structure (crystalline vs. amorphous) appear to be determinant factors for dissolution rather than SSA, as already observed for FSP-made Fe/Zn containing nanoparticles (Hilty *et al.*, 2009) and Ca/Fe oxides (Knijnenburg *et al.*, 2014). A size effect, however, may still be visible for larger particles, (e.g., in the micron size range for $CaCO_3$ (Economou *et al.*, 1996)).

Our findings suggest it is not possible to use t_{pH50} as a predictor for dissolution of Ca compounds because the powders that reached pH_{50} the fastest were also the ones to dissolve least Ca in the end. Furthermore, whether in vitro Ca dissolution can be related to *in vivo* Ca bioavailability remains uncertain (Hansen *et al.*, 1996; Heaney *et al.*, 1999; Heaney *et al.*, 1990; Pak and Avioli, 1988; Pak *et al.*, 1989; Tsugawa *et al.*, 1999). Various in vitro systems have been proposed (Brennan *et al.*, 1991; Meiron *et al.*, 2011; Sun *et al.*, 2010), but to date no dissolution assay has been described as the most reliable method to predict *in vivo* Ca absorption. Thus, the nutritional value of these compounds has to be confirmed in an *in vivo* analysis.

4. Conclusions

We successfully produced size-controlled nanostructured $CaCO_3$ and Ca phosphate powders using the one-step flame assisted spray pyrolysis (FASP) technology. During storage at ambient conditions (aging), the $CaCO_3$-containing particles sharply increased in size leading

to a marked reduction in SSA. Thus different dopants (Mg, Zn, Sr, and P) were tested and Mg and phosphate were found to be the most effective stabilizers of high $CaCO_3$ SSA. Nanostructured Ca phosphate powders were XRD-amorphous with HAp and γ-$Ca_2P_2O_7$ as prominent phases, and the highest SSA was obtained for Ca:P = 1.0–1.67. Storage for over 500 days reduced the SSA of these compounds, but this occurred less rapidly than for $CaCO_3$ and without any change in composition or crystallinity. Although the particle size increased as function of storage time, this did not influence Ca dissolution. Nanosizing of the Ca phosphate and $CaCO_3$ powders improved Ca dissolution, but no additional improvement occurred if the SSA was above 23 m^2/g, suggesting that amorphous structuring might be more important than SSA in Ca dissolution. The Ca phosphate powders dissolved twice as much Ca as the carbonates at steady state.

These FASP-made $CaCO_3$ and Ca phosphate nanostructured compounds may prove useful for food and nutrition applications, because they may release higher amounts of Ca *in vivo* compared to Ca compounds currently used in supplements and food fortification. Their potential for increased absorption and bioavailability need to be studied *in vivo*. If their bioavailability is high, these compounds could provide a novel source of well-absorbed Ca to improve Ca intakes in older individuals at risk for osteoporosis and related bone fractures.

Acknowledgements

The authors would like to thank Seline Staub for her assistance with production and analysis of the carbonate-containing powders. Also, the authors would like to thank Burgerstein Vitamins, Switzerland, for donating Ca compounds used in these studies. TEM measurements were performed at ScopeM (ETH Zurich). This work was financially supported by ETH Research Grant ETH-06 10-1 and the Swiss South African Joint Research Programme (project number IZLSZ3_149090).

References

Ali M., and Winterer M., 2010, Zno nanocrystals: Surprisingly 'alive': Chemistry of Materials, v. 22, no. 1, p. 85-91.

Brennan M. J., Duncan W. E., Wartofsky L., Butler V. M., and Wray H. L., 1991, In vitro dissolution of calcium carbonate preparations: Calcified Tissue International, v. 49, no. 5, p. 308-312.

Camenzind A., Strobel R., and Pratsinis S. E., 2005, Cubic or monoclinic y2o3 : Eu3+ nanoparticles by one step flame spray pyrolysis: Chemical Physics Letters, v. 415, no. 4-6, p. 193-197.

Cheary R. W., and Coelho A., 1992, A fundamental parameters approach to x-ray line profile fitting: Journal of Applied Crystallography, v. 25, p. 109-121.

Chen H. S., Chang J. H., and Wu J. S. B., 2008, Calcium bioavailability of nanonized pearl powder for adults: Journal of Food Science, v. 73, no. 9, p. H246-H251.

Chen S. F., Yu S. H., Jiang J., Li F. Q., and Liu Y. K., 2006, Polymorph discrimination of caco3 mineral in an ethanol/water solution: Formation of complex vaterite superstructures and aragonite rods: Chemistry of Materials, v. 18, no. 1, p. 115-122.

Chou L., Garrels R. M., and Wollast R., 1989, Comparative study of the kinetics and mechanisms of dissolution of carbonate minerals: Chemical Geology, v. 78, no. 3-4, p. 269-282.

Davis K. J., Dove P. M., and de Yoreo J. J., 2000, The role of mg2+ as an impurity in calcite growth: Science, v. 290, no. 5494, p. 1134-1137.

de Leeuw N. H., 2002, Molecular dynamics simulations of the growth inhibiting effect of fe2+, mg2+, cd2+, and sr2+ on calcite crystal growth: Journal of Physical Chemistry B, v. 106, no. 20, p. 5241-5249.

Dheilly R. M., Tudo J., and Queneudec M., 1998, Influence of climatic conditions on the carbonation of quicklime: Journal of Materials Engineering and Performance, v. 7, no. 6, p. 789-795.

Dickmann R. S., Strasburg G. M., Romsos D. R., Wilson L. A., Lai G. H., and Huang H., 2016, Particle size, surface area, and amorphous content as predictors of solubility and bioavailability for five commercial sources of ferric orthophosphate in ready-to-eat cereal: Nutrients, v. 8, no. 3, p. 14 pp.

Doman R. C., Barr J. B., McNally R. N., and Alper A. M., 1963, Phase equilibria in the system cao-mgo: Journal of the American Ceramic Society, v. 46, no. 7, p. 313-316.

Dorozhkin S. V., 2007, Calcium orthophosphates: Journal of Materials Science, v. 42, no. 4, p. 1061-1095.

Economou E. D., Evmiridis N. P., and Vlessidis A. G., 1996, Dissolution kinetics of caco3 in powder form and influence of particle size and pretreatment on the course of dissolution: Industrial & Engineering Chemistry Research, v. 35, no. 2, p. 465-474.

European Commission, 1998, Report on osteoporosis in the european community: Action for prevention: Office for Official Publications for the European Commission,

Frear G. L., Deese E. F., and Lefforge J. W., 1944, Calcium metaphosphate – effect of impurities on fusibility, citrate solubility, and hygroscopicity: Industrial and Engineering Chemistry, v. 36, p. 835-840.

Goldsmith J. R., and Heard H. C., 1961, Subsolidus phase relations in the system caco3-mgco3: The Journal of Geology, v. 69, no. 1, p. 45-74.

Gomez-Villalba L. S., Lopez-Arce P., Alvarez de Buergo M., and Fort R., 2011, Structural stability of a colloidal solution of ca(oh)2 nanocrystals exposed to high relative humidity conditions: Applied Physics a-Materials Science & Processing, v. 104, no. 4, p. 1249-1254.

Gueguen L., and Pointillart A., 2000, The bioavailability of dietary calcium: Journal of the American College of Nutrition, v. 19, no. 2, p. 119-136.

Hansen C., Werner E., Erbes H. J., Larrat V., and Kaltwasser J. P., 1996, Intestinal calcium absorption from different calcium preparations: Influence of anion and solubility: Osteoporosis International, v. 6, no. 5, p. 386-393.

Hausner D. B., Reeder R. J., and Strongin D. R., 2007, Humidity-induced restructuring of the calcite surface and the effect of divalent heavy metals: Journal of Colloid and Interface Science, v. 305, no. 1, p. 101-110.

Haynes W. M., 2015-2016, Crc handbook of chemistry and physics.

Heaney R. P., Dowell M. S., and Barger-Lux M. J., 1999, Absorption of calcium as the carbonate and citrate salts, with some observations on method: Osteoporosis International, v. 9, no. 1, p. 19-23.

Heaney R. P., Recker R. R., and Weaver C. M., 1990, Absorbability of calcium sources - the limited role of solubility: Calcified Tissue International, v. 46, no. 5, p. 300-304.

Hilty F. M., Arnold M., Hilbe M., Teleki A., Knijnenburg J. T. N., Ehrensperger F., Hurrell R. F., Pratsinis S. E., Langhans W., and Zimmermann M. B., 2010, Iron from nanocompounds containing iron and zinc is highly bioavailable in rats without tissue accumulation: Nature Nanotechnology, v. 5, no. 5, p. 374-380.

Hilty F. M., Knijnenburg J. T. N., Teleki A., Krumeich F., Hurrell R. F., Pratsinis S. E., and Zimmermann M. B., 2011, Incorporation of mg and ca into nanostructured fe2o3 improves fe solubility in dilute acid and sensory characteristics in foods: Journal of Food Science, v. 76, no. 1, p. 2-10.

Hilty F. M., Teleki A., Krumeich F., Buchel R., Hurrell R. F., Pratsinis S. E., and Zimmermann M. B., 2009, Development and optimization of iron- and zinc-containing nanostructured powders for nutritional applications: Nanotechnology, v. 20, no. 47, p. 475101.

Huang S., Chen J. C., Hsu C. W., and Chang W. H., 2009, Effects of nano calcium carbonate and nano calcium citrate on toxicity in icr mice and on bone mineral density in an ovariectomized mice model: Nanotechnology, v. 20, no. 37, p. 375102.

Huber M., Stark W. J., Loher S., Maciejewski M., Krumeich F., and Baiker A., 2005, Flame synthesis of calcium carbonate nanoparticles: Chemical Communications, no. 5, p. 648-650.

Imel E. A., DiMeglio L. A., and Burr D. B., 2014, Chapter 16 - metabolic bone diseases, *in* Burr, D. B., and Allen, M. R., eds., Basic and applied bone biology: San Diego, Elsevier Science, p. 317-344.

Institute of Medicine, 1997, Dietary reference intake for calcium, phosphorus, magnesium, vitamin d and fluoride, http://fnic.nal.usda.gov/dietary-guidance/dietary-reference-intakes/dri-tables, USDA.

Jossen R., Pratsinis S. E., Stark W. J., and Madler L., 2005, Criteria for flame-spray synthesis of hollow, shell-like, or inhomogeneous oxides: Journal of the American Ceramic Society, v. 88, no. 6, p. 1388-1393.

Knijnenburg J. T. N., Hilty F. M., Krumeich F., Zimmermann M. B., and Pratsinis S. E., 2013, Multimineral nutritional supplements in a nano-cao matrix: Journal of Materials Research, v. 28, no. 8, p. 1129-1138.

Knijnenburg J. T. N., Seristatidou E., Hilty F. M., Krumeich F., and Deligiannakis Y., 2014, Proton-promoted iron dissolution from nanoparticles and the influence by the local iron environment: Journal of Physical Chemistry C, v. 118, no. 41, p. 24072-24080.

Loher S., Stark W. J., Maciejewski M., Baiker A., Pratsinis S. E., Reichardt D., Maspero F., Krumeich F., and Gunther D., 2005, Fluoro-apatite and calcium phosphate nanoparticles by flame synthesis: Chemistry of Materials, v. 17, no. 1, p. 36-42.

Loste E., Wilson R. M., Seshadri R., and Meldrum F. C., 2003, The role of magnesium in stabilising amorphous calcium carbonate and controlling calcite morphologies: Journal of Crystal Growth, v. 254, no. 1-2, p. 206-218.

Lu H., Smirniotis P. G., Ernst F. O., and Pratsinis S. E., 2009, Nanostructured ca-based sorbents with high co2 uptake efficiency: Chemical Engineering Science, v. 64, no. 9, p. 1936-1943.

Madler L., Kammler H. K., Mueller R., and Pratsinis S. E., 2002, Controlled synthesis of nanostructured particles by flame spray pyrolysis: Journal of Aerosol Science, v. 33, no. 2, p. 369-389.

Mao Z. Q., Maeno Y., and Fukazawa H., 2000, Crystal growth of sr2ruo4: Materials Research Bulletin, v. 35, no. 11, p. 1813-1824.

Margolis H. C., and Moreno E. C., 1992, Kinetics of hydroxyapatite dissolution in acetic, lactic, and phosphoric acid solutions: Calcified Tissue International, v. 50, no. 2, p. 137-143.

Marie P. J., Ammann P., Boivin G., and Rey C., 2001, Mechanisms of action and therapeutic potential of strontium in bone: Calcified Tissue International, v. 69, no. 3, p. 121-129.

Meiron O. E., Bar-David E., Aflalo E. D., Shechter A., Stepensky D., Berman A., and Sagi A., 2011, Solubility and bioavailability of stabilized amorphous calcium carbonate: Journal of Bone and Mineral Research, v. 26, no. 2, p. 364-372.

Meyer K., 1998, Characterisation of the structure of binary calcium ultraphosphate glasses by infrared and raman spectroscopy: Physics and Chemistry of Glasses, v. 39, no. 2, p. 108-117.

Morse J. W., Arvidson R. S., and Luttge A., 2007, Calcium carbonate formation and dissolution: Chemical Reviews, v. 107, no. 2, p. 342-381.

Mueller R., Madler L., and Pratsinis S. E., 2003, Nanoparticle synthesis at high production rates by flame spray pyrolysis: Chemical Engineering Science, v. 58, no. 10, p. 1969-1976.

Nordin B. E. C., 1997, Calcium and osteoporosis: Nutrition, v. 13, no. 7-8, p. 664-686.

Orchard T. S., Larson J. C., Alghothani N., Bout-Tabaku S., Cauley J. A., Chen Z., LaCroix A. Z., Wactawski-Wende J., and Jackson R. D., 2014, Magnesium intake, bone mineral density, and fractures: Results from the women's health initiative observational study: American Journal of Clinical Nutrition, v. 99, no. 4, p. 926-933.

Pak C. Y. C., and Avioli L. V., 1988, Factors affecting absorbability of calcium from calcium salts and food: Calcified Tissue International, v. 43, no. 2, p. 55-60.

Pak C. Y. C., Poindexter J., and Finlayson B., 1989, A model system for assessing physicochemical factors affecting calcium absorbability from the intestinal tract: Journal of Bone and Mineral Research, v. 4, no. 1, p. 119-127.

Pemberton J. E., Latifzadeh L., Fletcher J. P., and Risbud S. H., 1991, Raman-spectroscopy of calcium-phosphate glasses with varying cao modifier concentrations: Chemistry of Materials, v. 3, no. 1, p. 195-200.

Puech J., Heughebaert J. C., and Montel G., 1982, A new mode of growing apatite crystallites: Journal of Crystal Growth, v. 56, no. 1, p. 20-24.

Recker R. R., 1985, Calcium absorption and achlorhydria: New England Journal of Medicine, v. 313, no. 2, p. 70-73.

Rohner F., Ernst F. O., Arnold M., Hilbe M., Biebinger R., Ehrensperger F., Pratsinis S. E., Langhans W., Hurrell R. F., and Zimmermann M. B., 2007, Synthesis, characterization, and bioavailability in rats of ferric phosphate nanoparticles: Journal of Nutrition, v. 137, no. 3, p. 614-619.

Rudin T., and Pratsinis S. E., 2012, Homogeneous iron phosphate nanoparticles by combustion of sprays: Industrial & Engineering Chemistry Research, v. 51, no. 23, p. 7891-7900.

Rudin T., Wegner K., and Pratsinis S. E., 2011, Uniform nanoparticles by flame-assisted spray pyrolysis (fasp) of low cost precursors: Journal of Nanoparticle Research, v. 13, no. 7, p. 2715-2725.

Shih S. M., Ho C. S., Song Y. S., and Lin J. P., 1999, Kinetics of the reaction of ca(oh)2 with co2 at low temperature: Industrial & Engineering Chemistry Research, v. 38, no. 4, p. 1316-1322.

Silaban A., and Harrison D. P., 1995, High temperature capture of carbon dioxide: Characteristics of the reversible reaction between cao(s) and co2(g): Chemical Engineering Communications, v. 137, p. 177-190.

Sipponen P., and Harkonen M., 2010, Hypochlorhydric stomach: A risk condition for calcium malabsorption and osteoporosis?: Scandinavian Journal of Gastroenterology, v. 45, no. 2, p. 133-138.

Strobel R., and Pratsinis S. E., 2007, Flame aerosol synthesis of smart nanostructured materials: Journal of Materials Chemistry, v. 17, p. 4743-4756.

Stumm W., and Morgan J. J., 1996, Aquatic chemistry: Chemical equilibria and rates in natural waters, New York, Wiley.

Sun L. M., Chow L. C., Frukhtbeyn S. A., and Bonevich J. E., 2010, Preparation and properties of nanoparticles of calcium phosphates with various ca/p ratios: Journal of Research of the National Institute of Standards and Technology, v. 115, no. 4, p. 243-255.

Tsugawa N., Yamabe T., Takeuchi A., Kamao M., Nakagawa K., Nishijima K., and Okano T., 1999, Intestinal absorption of calcium from calcium ascorbate in rats: Journal of Bone and Mineral Metabolism, v. 17, no. 1, p. 30-36.

Vaisman N., Shaltiel G., Daniely M., Meiron O. E., Shechter A., Abrams S. A., Niv E., Shapira Y., and Sagi A., 2014, Increased calcium absorption from synthetic stable amorphous calcium carbonate: Double-blind randomized crossover clinical trial in postmenopausal women: Journal of Bone and Mineral Research, v. 29, no. 10, p. 2203-2209.

Weaver C. M., and Gallant K. M. H., 2014, Chapter 14 - nutrition, *in* Burr, D. B., and Allen, M. R., eds., Basic and applied bone biology: San Diego, Academic Press, p. 283-297.

Willis R. B., and Allen P. R., 1999, Measurement of amorphous ferric phosphate to assess iron bioavailability in diets and diet ingredients: Analyst, v. 124, no. 3, p. 425-430.

Wopenka B., and Pasteris J. D., 2005, A mineralogical perspective on the apatite in bone: Materials Science & Engineering C-Biomimetic and Supramolecular Systems, v. 25, no. 2, p. 131-143.

Yang L. C., Kim P., Meyer H. M., and Agnihotri S., 2009, Aging of nanocarbons in ambient conditions: Probable metastability of carbon nanotubes: Journal of Colloid and Interface Science, v. 338, no. 1, p. 128-134.

Supporting Information

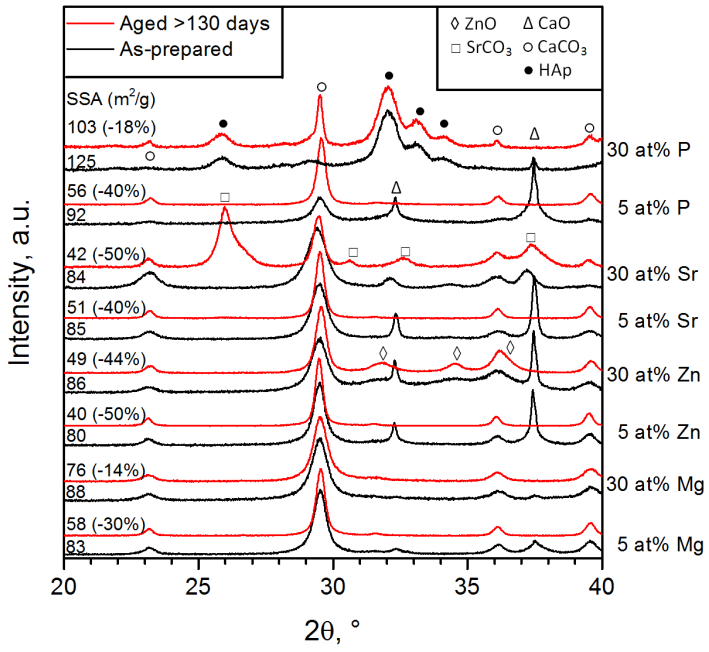

Figure S1: XRD patterns of as-prepared (black) and aged for more than 130 days (red) $CaCO_3$ doped with 5 and 30 at% of Mg, Zn, Sr, and P, produced with a 3/6 flame. The SSA values for each sample are given in the figure, with the relative decrease after aging in parenthesis. The patterns were normalized by the highest peak intensity.

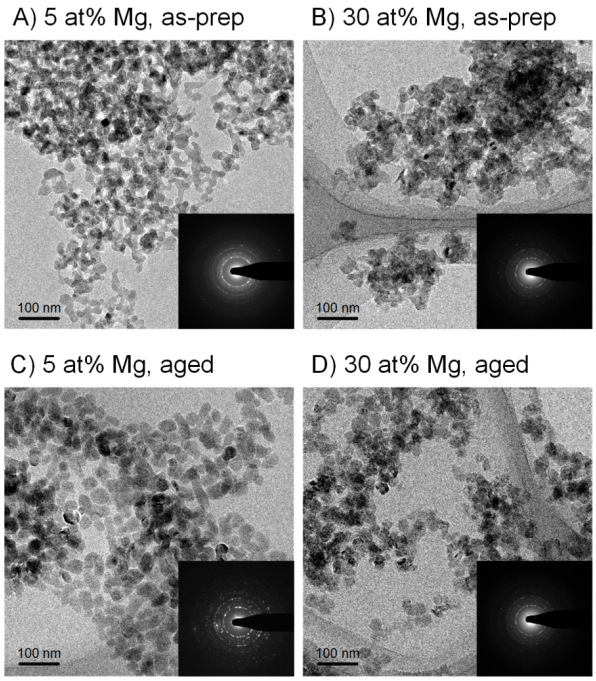

Figure S2: Typical TEM images of $CaCO_3$ doped with 5 at% (**a,c**) and 30 at% Mg (**b,d**), both as-prepared (**a,b**) and aged over 130 days (**c,d**). The powders were produced with a 3/6 flame.

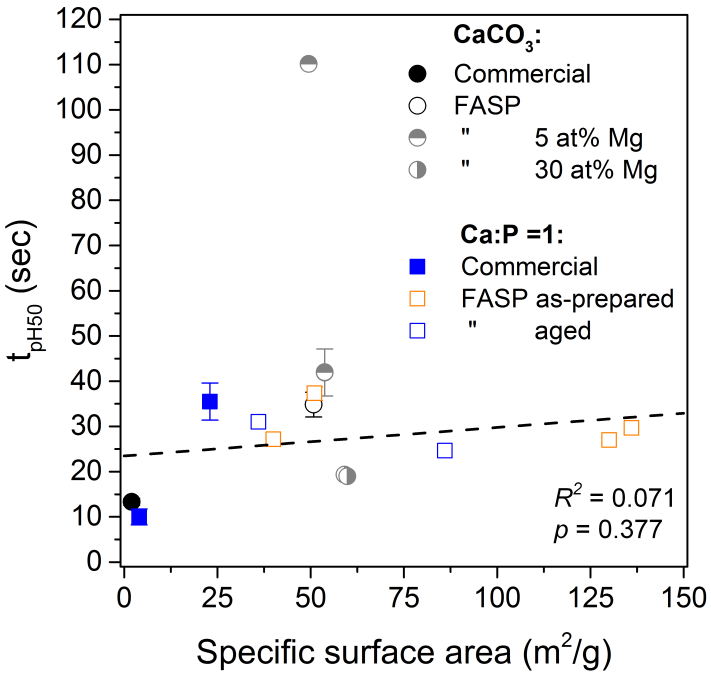

Figure S3: Time to reach 50% of final pH (t_{pH50}) as function of particle SSA after dissolution in 0.01 M H_3PO_4. Error bars are not shown for values with standard deviations smaller than the symbol.

Table S1: Ca content of different powders and pH increase after dissolution in 0.01 M H3PO4. Ca:P = 1 high and low SSA was produced in two different batches but only one was aged.

Powder	Flame	SSA (m^2/g)		Ca content (wt%)		Δ pH (-)	
		As-prep	Aged	As-prep	Aged	As-prep	Aged
Ca:P = 1	3/6	136	86	28 ± 1	26 ± 0	2.26 ± 0.02	2.25 ± 0.04
	3/6	130		28 ± 0		2.39 ± 0.06	
Ca:P = 1	9/3	51	36	29 ± 0	26 ± 0	2.22 ± 0.01	2.24 ± 0.06
	9/3	40		28 ± 1		2.39 ±0.03	
$CaCO_3$	3/6		51		38 ± 1		3.76 ± 0.02
$CaCO_3$ 5at%Mg	3/6		49		36 ± 0		3.71 ± 0.01
$CaCO_3$ 5at%Mg	7/6		54		36 ± 0		3.78 ± 0.01
$CaCO_3$ 30at%Mg	3/6		59		25 ± 0		4.31 ± 0.02
$CaCO_3$ 30at%Mg	7/6		60		26 ± 0		4.45 ± 0.02
Ca pyrophosphate cryst.			4		29 ± 0		0.08 ± 0.02
Ca phosphate amorphous nano			23		28 ± 1		2.26 ± 0.06
$CaCO_3$ commercial			2		38 ± 0		3.64 ± 0.03

MANUSCRIPT 2

The effect of size and chemical composition of nanostructured calcium compounds on calcium retention in growing rats

Lidija Posavec[1], Florentine M. Hilty[1], Hylton Buntting[2], Jeannine Baumgartner[3], Monika Hilbe[4], Frank Krumeich[5], Anne F. Grobler[2], Marlena Kruger[6], Michael B. Zimmermann[1]*

[1] Laboratory of Human Nutrition, Department of Health Sciences and Technology, ETH Zurich, Switzerland

[2] Preclinical Drug Development Platform, North-West University Potchefstroom, South Africa

[3] Centre of Excellence for Nutrition, North-West University Potchefstroom, South Africa

[4] Institute of Veterinary Pathology, Vetsuisse Faculty, University of Zurich, Switzerland

[5] Laboratory of Inorganic Chemistry, Department of Chemistry and Applied Biosciences, Switzerland

[6] Human Nutrition and Dietetics, Institute of Food, Nutrition and Human Health, Massey University, New Zealand

Manuscript in preparation

This work was supported by the Swiss South African Joint Research Program (project number IZLSZ3_149090).

Abstract

Low calcium (Ca) intake or bioavailability can adversely affect bone health. Reducing the size of Ca compounds used in nutritional supplementation and fortification increases their specific surface area (SSA) and this may increase solubility and Ca absorption from the gastrointestinal tract. We investigated the influence of SSA and chemical composition of nanostructured Ca compounds on *in vitro* dissolution and on Ca retention in growing rats. We tested: a) calcium carbonate ($CaCO_3$) with 3 different SSAs (3, 36 and 64 m^2/g); and b) 2 compounds with high SSA: $CaCO_3$ (64 m^2/g), mixed $CaCO_3$/hydroxyapatite (HAp) 50:50 wt% (94 m^2/g) and pure HAp (100 m^2/g). We characterized the compounds, assessed stability during 4 months storage, measured Ca solubility *in vitro*, and sensory performance in foods and drinks. Then, in a 5-days metabolic balance study in growing male Sprague-Dawley rats, we measured Ca-retention, femoral and vertebral bone mineral density (BMD) and performed extensive tissue histology. HAp 100 m^2/g showed higher Ca dissolution among the 5 compounds and significantly greater Ca-fractional retention compared to $CaCO_3$ (64 m^2/g) ($P = 0.044$). For pure $CaCO_3$ increasing SSA did not improve Ca-retention. No significant differences in BMD were shown by SSA or by composition and no abnormal Ca deposition in tissues or histologic changes. Ca dissolution *in vitro* did not correlate with SSA or Ca absorbed *in vivo*. Our findings suggest that size reduction *per se* does not improve Ca-absorption or retention from $CaCO_3$. However, based on its superior sensory, *in vivo* and *in vitro* performance, HAp 100 m^2/g is a promising alternative to $CaCO_3$ as a food fortificant or supplement.

KEYWORDS: calcium, calcium carbonate, hydroxyapatite, nanomaterial, balance, rats, histology, dissolution, food fortification, organoleptic changes

Abbreviations: **AAS**, atomic absorption spectroscopy; **BMD**, bone mineral density; **FASP**, flame-assisted spray pyrolysis; **FSP**, flame spray pyrolysis; **HAp**, hydroxyapatite; **ICDD**, International Centre for Diffraction Data; **PTH**, para thyroid hormone; **SAED**, selected area electron diffraction; **SSA**, specific surface area; **TEM**, transmission electron microscopy; **XRD**, X-ray diffraction.

1. Introduction

Suboptimal calcium (Ca) intake is a major public health problem, not only in industrialized countries like Europe and the US (Ervin and Kennedy-Stephenson, 2002), but also in low-income countries (Abrams and Atkinson, 2003) where the intake of Ca-rich food remains low. During childhood, adequate Ca intake is important for skeletal development (Flynn, 2003) and may decrease the risk of developing osteoporosis in later life (Rafferty *et al.*, 2007). Ca requirements in adults are high (1-1.2 g/day) (Institute of Medicine, 2011) and often cannot be met by dietary sources; many individuals consume Ca supplements to try and cover their daily requirement (Kressel, 2010; Rafferty *et al.*, 2007). Ca absorption from foods and supplements may depend on gastric dissolution at low pH (Shangraw, 1989). The choice of a Ca supplement should also consider the amount of elemental Ca present; in this respect, calcium carbonate ($CaCO_3$) and mixtures of calcium and phosphate, such as tricalcium phosphate ($Ca_3(PO_4)_2$), hydroxyapatite (HAp, $Ca_5(PO_4)_3OH$) and calcium hydrogen phosphate ($HCaPO_4$) usually contain more Ca than comparable amounts of calcium citrate or lactate and may be preferable if their absorption is high (Shangraw, 1989).

Recently, we have shown that nanosized $CaCO_3$ and amorphous calcium phosphate (Ca:P = 1) produced by flame assisted spray pyrolysis (Maedler *et al.*, 2002; Posavec *et al.*, 2016) showed greater dissolution than their respective commercial micron-sized compounds. If nanosized calcium compounds deliver equal or higher amounts of calcium than the micronsized ones, smaller or fewer tablets can be ingested to reach a comparable amount of absorbable calcium. In addition, less bulk in fortification mixes would be needed. For instance, nanosizing was shown to be advantageous for food fortification since micron sized $CaCO_3$ and HAp give a chalky feel if added to certain foods (Tobelmann, 2001) and size reduction may decreases grittiness. For example, an increase in particle size increased grittiness for microcrystalline cellulose (Imai *et al.*, 1995). The reason why nanomaterials are so attractive is that a reduction in particle size increases the surface-to-volume ratio, and a smaller particle size increases the percentage of material that is on the surface (Nel *et al.*, 2006) which can be quantified as specific surface area (SSA). This results in an increased instability of the material and therefore reactivity (Hornyak *et al.*, 2009b), faster dissolution and increased dissolution rate (Hilty and Zimmermann, 2014).

It has been previously shown in animal (Erfanian *et al.*, 2014; Gao *et al.*, 2008; Hilty *et al.*, 2010; Huang *et al.*, 2009; Meiron *et al.*, 2011; Rohner *et al.*, 2007; Shahnazari *et al.*, 2009; Wegmuller *et al.*, 2004) and human (Chen *et al.*, 2008) studies that size reduction of minerals from micron- to nanosize can improve mineral absorption and bioavailability. Nanosizing of poorly bioavailable ferric phosphate, for example, increased its absorption to a level equivalent to ferrous sulfate, the gold standard for absorption (Hilty *et al.*, 2010; Rohner *et al.*, 2007; Wegmuller *et al.*, 2004). Ca absorption from $CaCO_3$ was increased in ovariectomized (OVX) mice – a model for postmenopausal-osteoporosis – if particle size was reduced from 3.7 µm to 151 nm (Huang *et al.*, 2009). Nanosized pearl powder increased Ca bioavailability in growing rats when compared to the Ca source commonly used in rat diets (Gao *et al.*, 2008) and a reduction of mean particle size (29.4 µm to 84 nm) of $CaCO_3$ from fresh water pearls increased Ca bioavailability (Chen *et al.*, 2008). However, a decrease in particle diameter of $CaCO_3$ from 18.5 to 13.0 µm did not improve Ca balance, bone density or strength in OVX rats (Shahnazari *et al.*, 2009), but the size difference was small.

Along with particle size, crystallinity may also be an important determinant of mineral bioavailability. Amorphous structuring has been used to improve bioavailability of drugs *in vivo* (Hancock and Parks, 2000). For ferric phosphate, amorphous compared to crystalline structuring showed higher bioavailability in rats (32 against 195 m^2/g) (Rohner *et al.*, 2007). However, in both these studies the specific surface area (SSA) or particle size was either not kept constant or was not reported. Meiron *et al.* (2011) combined nanosizing and amorphous structuring and compared the bioavailability of amorphous (40-100 nm) and crystalline (~5 µm) $CaCO_3$ using a dissolution and an *in vivo* absorption study in rats. The amorphous compound showed faster dissolution and higher absorption compared to the crystalline compound, but particle size was also different for the two compounds, limiting their conclusions. Although decreasing particle size has been shown to increase bioavailability of minerals (Chen *et al.*, 2008; Erfanian *et al.*, 2014; Gao *et al.*, 2008; Hilty *et al.*, 2010; Huang *et al.*, 2009; Meiron *et al.*, 2011; Shahnazari *et al.*, 2009), to our knowledge no study has systematically investigated the effect of SSA greater than 40 m^2/g on Ca bioavailability.

Our study aims were to investigate the effect of varying size and chemical composition of nanostructured calcium compounds on Ca-retention and bone formation/resorption using

the growing rat model (Kruger *et al.*, 2003b). We hypothesized that both greater SSA and a change in chemical composition would increase Ca bioavailability. Bioavailability was evaluated using Ca-absorption, -retention and -fractional retention as primary outcomes. As secondary outcomes, bone mineral density (BMD) of femur and spine and parathyroid hormone (PTH) were measured. In addition, histology of selected organs was performed to look for abnormal calcium deposition or tissue calcification.

2. Materials and methods

2.1 Compound characterization

Five calcium compounds (**Table 1**) were tested *in vivo* and *in vitro*. A large HAp 1 m^2/g (Sigma Aldrich) was only used in the sensory experiment as comparison to the HAp 100 m^2/g.

Compounds were characterized for their SSA by nitrogen adsorption at 77 K in the relative pressure range p/p_0 = 0.05 – 0.25 (Micromeritics Tristar 3000 or Tristar II plus, Micrometritics Instruments Corp, USA) after degasing with dry N_2 for at least 1 hour at 150°C. The equivalent particle diameter (d_{BET}) was calculated using Sear's Method (Hornyak *et al.*, 2009a) using $\rho_{calcite}$ = 2.710 g/cm^3 and $\rho_{hydroxyapatite}$ = 3.16 g/cm^3 (Haynes, 2015-2016). Even though HAp containing powders were not spherical (as shown in the TEM images), d_{BET} was still calculated and used as estimation. For that reason, the density of $CaCO_3$:HAp 50:50 was estimated to be 2.94 g/cm^3, corresponding to a mean between $\rho_{calcite}$ and $\rho_{hydroxyapatite}$.

X-ray diffraction patterns (XRD) were measured (Bruker AXS D8 Advance diffractometer, Bruker Instruments, USA) and the diffraction peaks were identified by EVA software (version 10.0 rev 1, Bruker AXS). The International Centre for Diffraction Data (ICDD) card numbers were the following: calcite ($CaCO_3$, 81-2027), calcium hydrogen phosphate hydroxide (CaHy, $Ca_9HPO_4(PO_4)_5(OH)$, 46-0905) and HAp ($Ca_{10}(PO_4)_6(OH)_2$, 03-0747). For (scanning) transmission electron microscopy ((S)TEM) analysis the particles were deposited on a carbon foil supported on a copper grid and analyzed on a Tecnai F30 microscope (FEI, The Netherlands; field emission gun, 300 kV) (Knijnenburg *et al.*, 2013). The respective selected area (electron) diffraction (SAED) images were recorded with a high angle annular dark field (HAADF) detector.

All wet chemical analyses and dilutions were carried out using nanopure water (Millipore, USA). Ca content was measured in triplicate by flame atomic absorption spectroscopy (AAS,

SpectrAA-240FS, Agilent Technologies, USA) after dissolving 0.05 g powder in 5 M hydrochloric acid (HCl, puriss. p.a. ≥ 32%, Sigma-Aldrich, USA) (Hilty *et al.*, 2010). Total inorganic phosphate (P) content was determined in triplicate using an adapted method by Vanveldhoven and Mannaerts (1987). In short, 50 mg powder was dissolved in 5 M HCl solution and further diluted in 0.5 M H_2SO_4 (Sulfuric Acid, puriss. p.a., 95.0-97.0%, Sigma Aldrich, USA). 150 µL of sample and P standard (10 µg/mL, P standard for AAS, Fluka, USA) were transferred to a 96 well plate and serially diluted with 150 µL 0.5 M H_2SO_4. After the addition of 30 µL molybdate solution 1.75 w/v (puriss p.a., Fluka, USA), the plate was shaken for 10 min at room temperature. Afterwards, 30 µL malachite green solution 0.035 w/v (for microscopy, crystalline, Sigma, USA) were added and the plate shaken for 45 min. The color change, which is proportional to the content of inorganic phosphate, was measured at 630 nm with a microplate reader (PowerWave, Biotek, USA).

Ca compounds used in the experiments were stored at ambient condition over a period of 4 months and characterized before and after storage in order to control for possible changes in crystallinity and SSA.

2.2 In vitro assay

2.2.1 Dissolution

In order to link *in vitro* dissolution to *in vivo* absorption, dissolution experiments were performed following Meiron *et al.* (2011). For each powder, 40 mg Ca were dissolved into 50 ml H_3PO_4 0.01 M (ortho-phosphoric acid, puriss. p.a. > 85%, Sigma-Aldrich). The solution was stirred at 625 rpm with a magnetic stirrer and pH was recorded every 1 s for 500 seconds using a continuous pH meter (Seven excellence, Mettler Toledo, Switzerland). Time to reach final pH (t_{pHend}) corresponded to the pH value on which the pH stayed constant for 10 seconds. The time to reach half of final pH ($t_{pH50\%}$) was interpolated, averaged between three replicates, and used to measure powder dissolution rate (Meiron *et al.*, 2011). At the end of the dissolution experiment, dissolved Ca was measured by filtering 2 mL aliquot through a 0.1 µm filter (nylon membrane, Infochroma, Switzerland) and the filtrate was further diluted in 0.1 M HCl. Each final sample (Ca dissolved) contained 0.1 mL HCl 32% and 5000 ppm La (lanthanum nitrate hexahydrate III, puriss. p.a. ≥ 99.0%, Sigma-Aldrich, USA) to eliminate P interference during flame AAS measurements.

2.2.2 Sensory performance

Color and pH change as a surrogate for sensory evaluation were measured after adding the powders to 100 mL of food matrix at a fortification level of 120 mg Ca / 100 mL (Russell *et al.*, 2010) for liquid and of 200 mg Ca / 100 g for solid matrices (Heaney *et al.*, 2000). The following foods were purchased at Migros (Zurich, Switzerland) and used as food matrices: orange juice (brand M classic), apple juice (M classic), cranberry juice (Berry splash), soy mixed berry yogurt (Bio soya line) or soy chocolate milk (made by mixing 68 g chocolate powder [(Hot chocolate powder]) with 682 g soy milk [(drink nature, Bio soya line])). Color change was measured in duplicate after stirring the powder for 120 min at 350 rpm. The matrix was transferred to a Quartz cuvette (5.5 cm inner diameter) and placed on the light projection tube of a spectral photometer (Chroma-Meter CR-310, Minolta Schweiz AG, Dietlikon, Switzerland) and measured in triplicate after rotating the dish each time by 120°. Absolute color change (ΔE^*_{ab}) was calculated by:

$$\Delta E^*_{ab} = \sqrt[2]{(\Delta L^*)^2 + (\Delta a^*)^2 + (\Delta b^*)^2}$$

where $\Delta L*$ (lightness), $\Delta a*$ (chromaticity coordinate) and $\Delta b*$ (chromaticity coordinate) correspond to the difference between the sample (with added compound) and the non-fortified matrix at the same timepoint. At beginning and end of the experiment pH was measured and ΔpH was calculated by subtracting $pH_{blank\ 120\ min}$ from $pH_{sample\ 120\ min}$.

2.3 In vivo assay

2.3.1 Diets

The base diet was a Ca free AIN-93G (Reeves *et al.*, 1993) amino acid semi-synthetic diet (Research Diets, Inc., USA, Nr. A07092701). Before pelleting, the different Ca sources were added to the diets to reach a final fortification level of 5 g Ca / kg. For the diets containing $CaCO_3$, P content was adjusted using monopotassium phosphate (food grade, ICL Performance Products, USA) to reach a final P content of 3.16 g P / kg diet. The excess potassium given by the potassium phosphate was leveled using potassium chloride (KCl, ≥ 99.0%, Sigma Aldrich, USA) in the diets containing HAp to a final content of 3.6 g K / kg diet (Supporting **Table S1**).

2.3.2 Study design

All experimental procedures were approved by the AnimCare Ethics Committee of the Faculty of Health Science of the North-West University Potchefstroom ethics number NWU-00198-14-A5.

Male Sprague-Dawley rats (12 per test diet, 60 in total) were bred in the Vivarium of the North-West University Potchefstroom (South Africa) and weaned until their body weight reached 50 g (21 ± 2 days). Throughout the whole study, the animals were kept at a 12:12 h light-dark cycle (lights off at 18:00 h), 22 ± 1°C and relative humidity of 55 ± 15%. The animals had ad libitum access to demineralized (0.3 M Ohm, corresponding to 0.15 mg Ca / L) water and diet.

On day 1 of the study (**Figure 1**a), the rats were group housed and fed the control diet ($CaCO_3$ 3 m^2/g) for 7 days to adapt the rats to the new diet. At study day 8, the rats were single caged and randomly allocated to receive one of the other 4 test diets or the control diet until the end of the study (study days 8-36). Food intake, body weight and animal health were assessed every second day.

At study day 29, the rats were single caged in metabolic cages (3701M081, Tecniplast, Italy). The experiment was staggered in such a way that 12 rats at the time were single-housed in a metabolic cage and each diet group was included at each stagger. For two days (days 29-30) the animals were acclimatized to new environment. Urine and feces were collected and food intake was measured over the next consecutive 5 days (days 31-36). During the collection period urine was collected daily into a collection flask containing 0.5 ml 0.1 M HCl (32% for analysis, Merck, Germany). Daily, collected urine was transferred to a storage flask by rinsing it with nanopure water, pooled together for each animal over 5 days of collection and stored at -20°C. Feces were collected daily into a collection flask, carefully cleaned from residual diet, pooled together for each animal over 5 days of collection and stored at -20°C. Food intake was measured over a total of 26 days: 21 days of feeding (study days 8-29) and 5 days of balance (study days 31-36).

At the end of the study, the rats were deeply anesthetized with an IP injection of sodium pentobarbitone (Euthapent(r), Kyron Laboratories Ltd, South Africa) and blood was collected by cardiac puncture. One aliquot of blood was transferred to a 2 mL K_3EDTA blood collection

tube (Lavender top, Greiner Bio-One, Vacuette North America) for whole blood count (BC-5300 Vet, Auto Hematology Analyzer, Mindray, China). The remaining blood was transferred to a 9 ml z-serum separator clot activator tubes (Gold top, Greiner Bio-One, Vacuette North America). After at least 1 h clotting period at room temperature the serum separator tubes were centrifuged (EBA 20, type 2002, Hettich Zentrifugen, Germany) at 2000 g for 20 min. Serum was transferred to 2 mL Eppendorf tubes and stored at -20°C until analysis. The following organs were excised and stored in 10% formalin prepared by mixing 1:10 v/v PBS (Sodium chloride for analysis, Merck; di-Sodium hydrogen phosphate dodecahydrate, for analysis, Merck; sodium di-hydrogen phosphate monohydrate, for analysis, Merck) and formaldehyde solution (formaldehyde solution 38% v/v, Medicolab cc., Amalgam, South Africa) for histopathology: heart, liver median lobe, stomach, duodenum, ileum, jejunum, caecum, colon, spleen, kidneys, heart, lungs and thyroid. The veterinary pathologist performing the histological examination observed 6 animals of each feeding group and was unaware of the group assignment. Right femur and spine were excised and stored in PBS at -20°C. Left femur was excised, scraped of flesh and stored at -20°C.

2.3.3 Sample processing and analyses

At the day of analysis, pooled urine samples (-20°C) were defrosted for at least 1 hour at ambient conditions and well shaken and mixed. Two aliquots from each rat were centrifuged for 5 min at 2000 rpm (Heraeus Multifuge X3R, Thermo Fisher Scientific, USA). Three ml of the supernatant were removed, weighed and diluted to 10 ml using nanopure water (18.2 MΩ, Thermo Scientific, USA). The samples were further diluted to approximately 0.5 ppm Ca and measured by flame AAS using external calibration to obtain a first estimate of the concentration and then measured using standard addition to obtain the final value. Standard curve and Ca solution were both prepared using a Ca stock solution (Titrisol 2000 mg Ca/L, Merck, Germany).

Pooled feces were freeze-dried (Freeze dryer alpha LDplus, Christ, Germany) for 24 hours, equalized to ambient humidity for 24 h and ground using porcelain mortar while diets were finely milled (0.25 µm mesh size, titan, Retsch ZM1, Germany). Left femurs were cleaned of remaining flesh and dried in an oven (SalvisLAB, Switzerland) for 12 h at 105°C (Kruger *et al.*, 2003a). Ca content in feces, diets and femurs was determined using flame atomic absorption spectrophotometry (AA240FS Varian) after mineralization with nitric acid 65% (in house

purified) by microwave digestion (MLS TurboWave; MLS GmbH). Analyses were performed in triplicates except for femurs. Quality controls (wheat flour standard reference material (1567b, National Institute of Standards & Technology, USA)) were digested in duplicate together with the samples and one blank sample for every 3rd digestion run. Ca intake and excretion were measured from the pooled amount collected over 5 days of balance.

Ca-absorption, -retention and -fractional retention over 5 days collection were calculated as follows:

$$Ca_{absorption} = Ca_{intake} - Ca_{excretion}\ (faecal)$$

$$Ca_{retention} = Ca_{intake} - Ca_{excretion}(faecal + urine)$$

$$Ca_{fractional\ retention} = \frac{Ca_{retention}}{Ca_{intake}} \times 100$$

Bone mineral density was measured *ex vivo* in the spine (L1-4) and right femur after defrosting (room temperature, 24 hours). Spine and femur were scanned in a plastic container covered with 3 cm PBS (Kruger *et al.*, 2003b), using fan beam unit (Hologic Discovery, USA and high-resolution software (Discovery W (S/N 84106)). Quality control scans were performed daily using small animal step phantom (Fan beam movement at 152.4 mm/30 sec, 8 lines/mm, 0.2 mm line spacing, 16 bit A/D conversion, Aperture size of 61 mm x 1 mm). PTH in serum was measured using the Rat intact PTH ELISA KIT (Immutopics, USA) following producer's instructions and results were accepted for CV ≤ 10%.

2.4 Statistical analyses

Statistical analyses were done using SPSS 20 (IBM, USA). We compared the $CaCO_3$ 3, 36 and 64 m^2/g groups by SSA and the $CaCO_3$ 64, $CaCO_3$:HAp 50:50 94 and HAp 100 m^2/g groups by composition (**Figure 1**b) using the parametric analysis of covariance (ANCOVA) followed by pairwise comparison using Bonferroni correction at a significance level of 0.05. For the ANCOVA, body weight at day 36 was added as a covariant, while Ca intake over 5 or 26 days was only introduced as covariate when it was not used to calculate the outcome variable. Simple linear regression analysis was carried out to test correlation between two variables. Values are expressed and shown as mean ± standard error of mean (SEM).

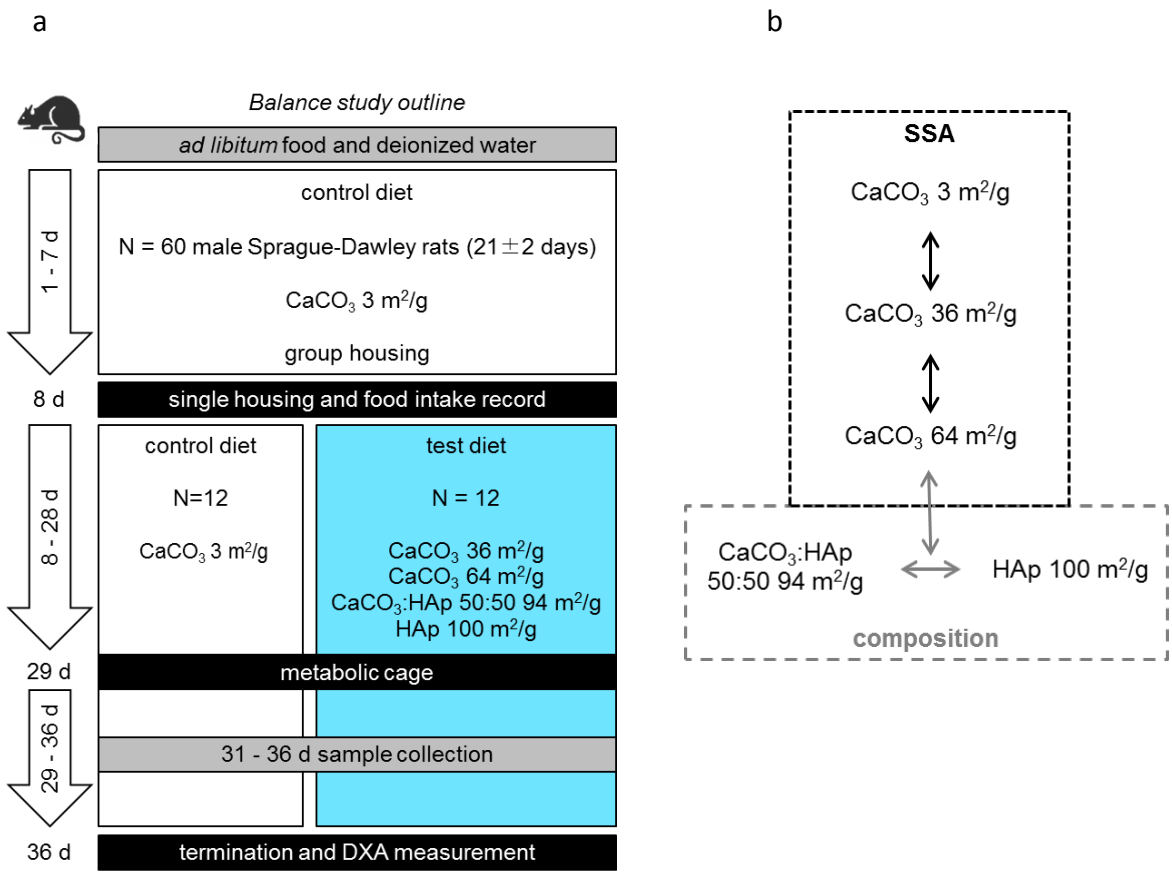

Figure 1: Animal study outline. **a**. Outline of the balance study using growing Sprague-Dawley rats and **b**. compound comparison design investigating differences in Ca bioavailability by SSA ($CaCO_3$ only, black arrows) and by chemical composition (similar SSA, gray arrows). $CaCO_3$, calcium carbonate; HAp, hydroxyapatite; SSA, specific surface area.

3. Results

3.1 Compounds and diet characterization

Compound SSA, d_{BET}, method of production, XRD phase, Ca and P content are summarized in **Table 1**. XRD patterns (Supporting **Figure S1**) clearly identified the presence of crystalline calcite (all 3 $CaCO_3$ and $CaCO_3$:HAp 50:50), crystalline calcium hydrogen phosphate hydroxide (CaHy) ($CaCO_3$:HAp 50:50) and crystalline HAp ($CaCO_3$:HAp 50:50 and pure HAp). During four months of storage at ambient conditions, no changes in SSA or crystallinity were observed for the five tested compounds (data not shown).

For $CaCO_3$, smaller SSA resulted in smaller primary particle size (**Figure 2**a-c). A clear difference in shape between $CaCO_3$ 3 m^2/g (cubic-like) and 36 m^2/g (round-like) can be observed. This difference in shape can probably be explained by the difference in production methods (grinding vs. precipitation). The difference in shape did not notably change between $CaCO_3$ 36 and 64 m^2/g, but the size of the primary particles became smaller.

Table 1: Compound characterization. All compounds with SSA ≥ 36 m^2/g were produced by precipitation, while $CaCO_3$ 3 m^2/g was produced by grinding. XRD, X-ray diffraction; HAp, hydroxyapatite; SSA, specific surface area.

	Ca compound					
	$CaCO_3$	$CaCO_3$	$CaCO_3$	$CaCO_3$:HAp 50:50	HAp	HAp*
SSA, m^2/g	3	36	64	94	100	1
d_{BET}, nm	783	62	35	22	19	1899
Ca, g/100g	39	37	35	36	35	37
P, g/100g	-	-	-	8	16	-
XRD phase	calcite	calcite	calcite	calcite, calcium hydrogen phosphate, HAp	HAp	HAp

* only used in the sensory experiment

SAED patterns show a transition from a microcrystalline state indicated by well separated diffraction spots to polynano crystallinity with continuous rings with increasing SSA (**Figure 2**a-c Insets). **Figure 2**d shows the $CaCO_3$ and HAp mixture with single crystals and powders' crystallinity is confirmed by the corresponding SAED. Needle-shaped HAp (Puech *et al.*, 1982) is clearly visible in **Figure 2**e. Broader humps (XRD, Supporting **Figure S1**) and presence of mainly diffuse rings with small bright spots (SAED, **Figure 2**e) suggest HAp to be polynano-crystalline.

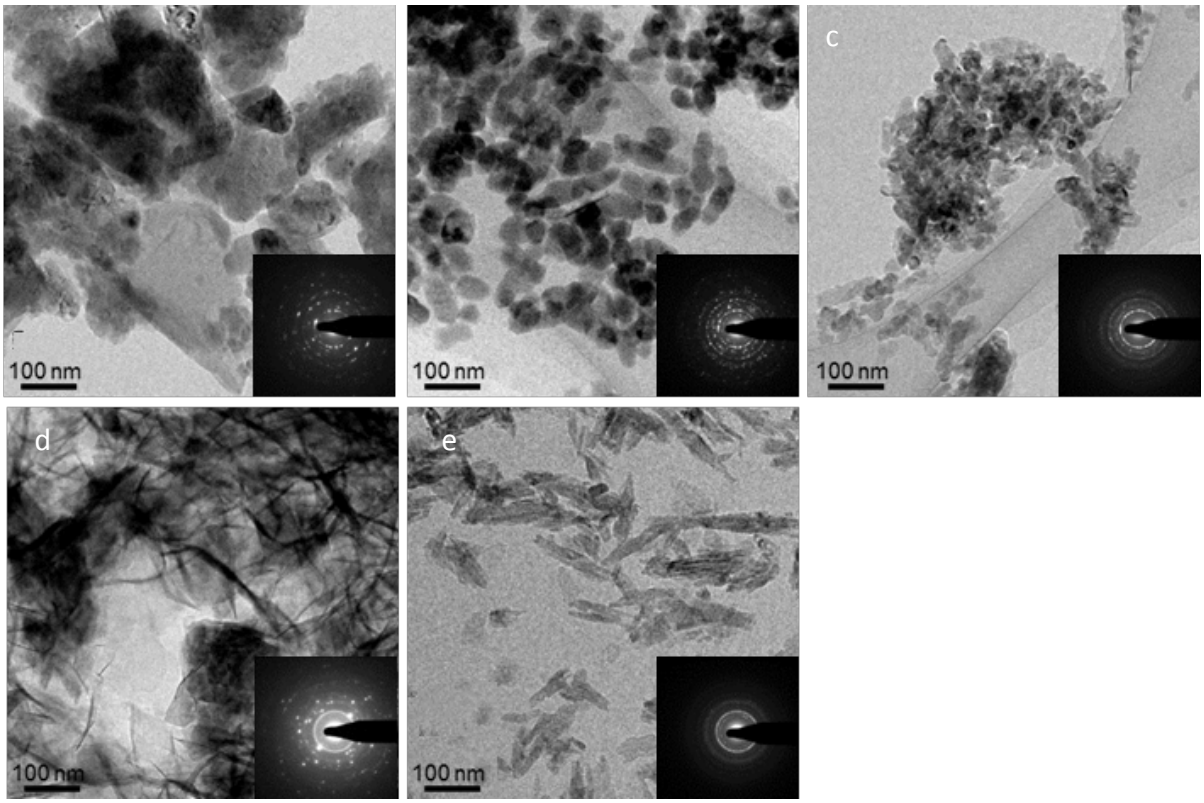

Figure 2: Transmission electron microscopy images with respective selected area (electron) diffraction patterns for the 5 Ca compounds at study end. **a**. $CaCO_3$ 3 m^2/g, **b**. $CaCO_3$ 36 m^2/g, **c**. $CaCO_3$ 64 m^2/g, **d**. $CaCO_3$:HAp 50:50 94 m^2/g and **e**. HAp 100 m^2/g. $CaCO_3$, calcium carbonate; HAp, hydroxyapatite.

3.1 In vitro assay

3.1.1 Compound dissolution

The amount of Ca delivered after dissolving 40 mg Ca in diluted H_3PO_4 was measured according to Meiron *et al.* (2011). Dissolution was measured after aging of the powders at room temperature. The dissolution results show a trend of higher amount of dissolved Ca with increasing SSA, however there was no significant correlation between the amount of dissolved Ca and compounds SSA (β = 0.705, R^2 Linear = 0.496, *P* = 0.184) (**Figure 3a**). Among all compounds, HAp delivered quantitatively the highest amount of Ca (243 ± 1 mg Ca/L) (**Figure 3**a). T_{pH50} of $CaCO_3$ decreased with increasing SSA (Supporting **Table 2**), but increased again with changing composition. $CaCO_3$ 3 m^2/g took the longest time to reach pH_{50}, but t_{pH50} and Ca-absorption were not correlated (β = -0.257, R^2 Linear = 0.066, *P* = 0.676) (data not shown).

3.1.2 Sensory performance

Measurement of color change in the three juices and in soy chocolate milk showed color changes below the detection limit (ΔE^*_{ab} = 5) for all compounds (**Figure 4**), except for HAp 1 m^2/g, which was mostly dispersed. Even though the color change was barely detectable, the end pH always increased by almost a unit for all compounds except HAp 100 and 1 m^2/g (Supporting **Table S3**). Soy berry yogurt showed the highest color change among all food matrices tested, with HAp 100 m^2/g showing the lowest color change (**Figure 4**) and pH increase (Supporting **Table S3**) among all tested compounds.

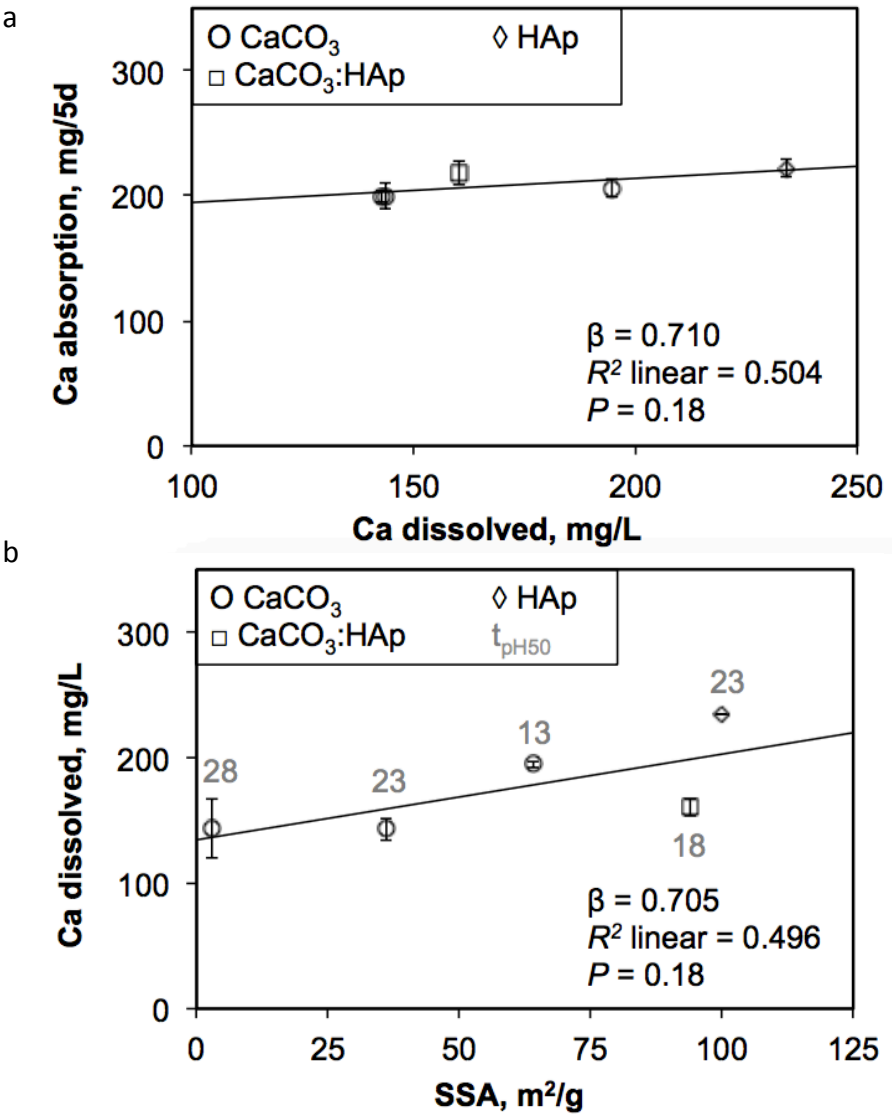

Figure 3: Ca dissolved in 0.01 M H_3PO_4 and t_{pH50} against SSA (a) and Ca absorption as a function of Ca dissolved (b). $CaCO_3$, calcium carbonate; $CaCO_3$:HAp, 50:50 wt% mixture of $CaCO_3$ and HAp; HAp, hydroxyapatite; SSA, specific surface area; t_{pH50}, time to reach half of final pH.

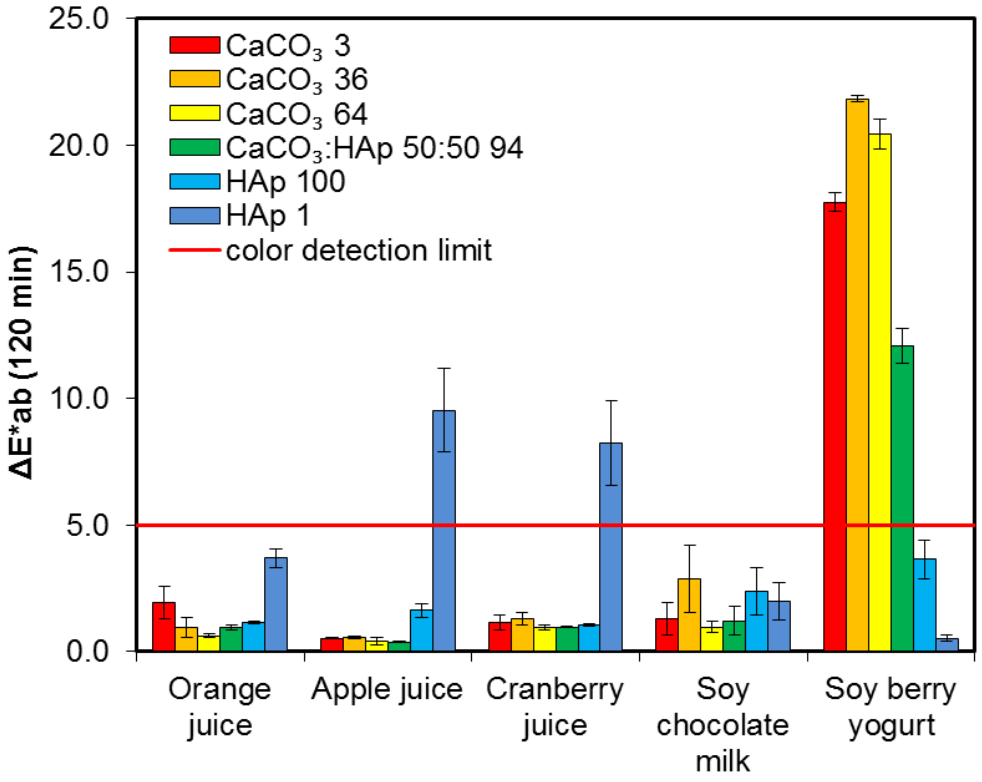

Figure 4: Sensory performance of 6 Ca containing compounds (including the large HAp_1) in selected food matrices. $CaCO_3$, calcium carbonate; $CaCO_3$:HAp, 50:50 wt% mixture of $CaCO_3$ and Hap. HAp, hydroxyapatite; SSA, specific surface area.

3.2 In vivo assay

3.2.1 Ca absorption, retention and balance

The final Ca content in the diet was similar among the 5 groups (Supporting **Table S1**). Results of the balance study are summarized in **Table 2**. The final Ca concentration in the diet was similar among the 5 groups. Rat body weight at day 36 did not differ significantly between the 5 diet groups. Body weight at day 36 correlate with Ca intake over 26 days (β = 0.803, R^2 linear = 0.65, $P < 0.001$), supporting the use of body weight at day 36 and Ca intake as cofactors for the ANCOVA analyses. Ca intake over 26 days of the total food intake record (study days 8-29 and 31-36) differed significantly between $CaCO_3$ 36 and $CaCO_3$ 64 m^2/g (P = 0.004) when compared by SSA and between $CaCO_3$ 64 and HAp 100 m^2/g (P = 0.029) when compared by chemical composition.

Table 2: Balance study results summary

	Ca compound				
	$CaCO_3$ 3 m^2/g	$CaCO_3$ 36 m^2/g	$CaCO_3$ 64 m^2/g	$CaCO_3$:HAp 94 m^2/g	HAp 100 m^2/g
5 day metabolic balance					
Ca intake[3], mg/5d	371 ± 16	385 ± 8	410 ± 10	405 ± 10	398 ± 10
Ca fecal excretion[2], mg/5d	170.7 ± 11.1	185.5 ± 8.2	204.3 ± 6.1 [A]	186.3 ± 8.5 [A,B]	175.5 ± 5.6 [B]
Ca absorption[3], mg/5d	199.8 ± 10.1	199.5 ± 4.4	206.1 ± 7.5	218.3 ± 9.3	222.4 ± 6.8
Ca urinary excretion[2], mg/5d	4.1 ± 0.8	3.8 ± 0.5	2.1 ± 0.2 [A]	4.5 ± 0.4 [B]	4.1 ± 0.4 [B]
Ca retention[3], mg/5d	195.7 ± 9.8	195.6 ± 4.5	204.0 ± 7.4	213.8 ± 9.3	218.3 ± 6.8
Ca fractional retention[3], %/5d	53.08 ± 1.91	50.98 ± 1.32	49.66 ± 1.15 [A]	52.83 ± 1.77 [A,B]	54.86 ± 0.95 [B]
End of study					
Bw at study day 36, g	230 ± 5	231 ± 6	237 ± 5	232 ± 5	234 ± 4
Ca intake[3], mg/26d	1758 ± 34 [a,b]	1726 ± 27 [b]	1840 ± 35 [a,A]	1777 ± 31 [A,B]	1757 ± 17 [B]
BMD femur[4], g/cm^2	0.161 ± 0.003	0.161 ± 0.002	0.160 ± 0.003	0.162 ± 0.002	0.159 ± 0.002
BMD L1-4 vertebra[4], g/cm^2	0.152 ± 0.004	0.153 ± 0.003	0.152 ± 0.003	0.150 ± 0.003	0.148 ± 0.003
PTH[+], pg/mL	161.8 ± 30.2	134.2 ± 25.4	174.0 ± 36.2 [5]	147.5 ± 18.7	178.5 ± 26.1
Femur[+], mg Ca/g dw	148.2 ± 6.8	156.7 ± 4.8	151.9 ± 4.7	145.2 ± 4.2	148.7 ± 4.5

[1]Values expressed as mean ± SEM, *n* = 12 / group. Mean values were statistically compared using ANCOVA with *post hoc* Bonferroni. Groups compared by SSA (non capital letters) and by chemical composition (capital letters). Labeled means in a column without a common letter differ, $P < 0.05$.

[2] Statistical analysis adjusted for Ca intake over 5 day metabolic balance and body weight at study day 36;

[3] Statistical analysis adjusted for body weight at study day 36

[4] Statistical analysis adjusted for Ca intake mg/26 d of test feeding (including balance period) and body weight at study day 36

[5] N = 11

BMD, bone mineral density; Bw, body weight; Ca, calcium; $CaCO_3$, calcium carbonate; dw, dry weight; .HAp, hydroxyapatite; PTH, parathyroid hormone; SSA, specific surface area.

For the 5 days of balance period, the following variables differed significantly by chemical composition (**Table 2**): Ca fractional retention between $CaCO_3$ 64 and HAp 100 m^2/g (P = 0.034); Ca urinary excretion between $CaCO_3$ 64 and $CaCO_3$:HAp 94 m^2/g (P < 0.001) and between $CaCO_3$ 64 and Hap 100 m^2/g (P < 0.001); and Ca fecal excretion between $CaCO_3$ 64 and HAp 100 m^2/g (P = 0.016). No significant differences were observed by SSA.

Ca dissolved did not correlate with Ca absorbed over 5 days of balance study (**Figure 3**b), or t_{pH50} (data not shown).

3.2.2 BMD, Ca femur content and PTH

Ca intake over 26 days correlated with BMD of femur (β = 0.576, R^2 Linear = 0.331, P < 0.001) and BMD of L1-4 (β = 0.352, R^2 Linear = 0.124, P = 0.006) (Supporting **Figure S2**). Also body weight at day 36 correlated with BMD of femur (β = 0.693, R^2 Linear = 0.480, P < 0.0001) or BMD of L1-4 (β = 0.461, R^2 Linear = 0.212, P < 0.001) (data not shown). These findings support the decision to use both body weight and Ca intake as cofactors in the analyses. BMD of femur, BMD of L1-4, Ca content of femur or PTH did not differ by SSA or composition.

3.2.3 Histological analysis

The histological examinations revealed light to mild BALT-hyperplasia in the lungs in all animals investigated (Supporting **Table S4**) likely caused by pulmonary mycoplasma infection, a common infection in animals housed in non-air filtered cages (Jacoby and Lindsey, 1998). Light to mild extramedullary blood formation in the spleen and light to mild infiltration of neutrophils in the submucosa of the stomach between the glandular and squamous area was also seen. These findings were observed for all the 5 compounds and categorized as incidental (Gopinath *et al.*, 1987; Martin, 1989). One animal (diet containing $CaCO_3$:HAp 50:50 94 m^2/g) presented with granulomatous hepatitis with calcification and fibrosis. Light calcification was found in the Peyer's patches of the ileum in one animal fed $CaCO_3$ 36 m^2/g but there were no other abnormalities in the GI tract and this was interpreted as an incidental finding. In summary, no significant Ca depositions or structural changes in stomach, pancreas, duodenum, ileum, jejunum, liver, spleen, kidney, lung and heart were observed in the five groups.

4. Discussion

In this study we used the growing rat model to investigate whether nanosizing and/or varying chemical composition at the nano scale affects Ca bioavailability. This model was chosen because growing rats respond rapidly to changes in Ca bioavailability from different food sources (Kruger *et al.*, 2003b; Peterson *et al.*, 1995). Our results of the calcium balance period (intake – excretion [feces + urine]) suggest how high calcium excretion in feces – which correspond to lower absorption (Ca intake – excretion [feces]) – is counter-balanced by lower calcium excretion in urine (**Table 2**). Therefore, the final retention remains similar among the groups, as expected for normal Ca homeostasis (Gueguen and Pointillart, 2000; Heller *et al.*, 2000) and no difference in Ca-fractional retention by SSA were seen. Other studies have investigated whether decreasing Ca particle size increases Ca bioavailability. Specifically, two studies focused on the uptake from micronized (size not given) and nanosized pearl powder (average diameter of 40–80 nm) in rats (Gao *et al.*, 2008) or humans (Chen *et al.*, 2008) and both studies showed a favorable effect of size reduction on Ca absorption or retention. Huang *et al.* (2009) (Huang *et al.*, 2009) compared $CaCO_3$ with 151 nm vs 3.7 µm hydrodynamic particle diameters in an OVX mice model and found a significantly higher whole body BMD for the 'nano compounds', while Chen *et al.* (2008) (Chen *et al.*, 2008) compared 84 nm vs 29.4 µm particle size by volume and reported faster and higher Ca appearance in serum after single dose administration for the smallest size. However, although in our study we compared $CaCO_3$ with SSAs of 3, 36 and 64 m^2/g, corresponding to an equivalent estimated d_{BET} of 738, 62 and 35 nm respectively, we did not see improved higher Ca-retention or Ca-fractional retention with increasing SSA. Similar to our results, Elble *et al.* (2011) and Shahnazari *et al.* (2009) did not see an increase in Ca retention. They compared particle sizes of 13.5 ± 10.4 µm vs.18 ± 13.56 µm and 13.0 vs. 18.5 µm respectively; in these studies the size difference of the compounds was likely too small to detect a difference in retention. The size difference between our smallest and largest compound was bigger than for Shahnazari *et al.* (2009) and Elble *et al.* (2011) but smaller than for Chen *et al.* (2008). Thus, it is possible that the size difference in our study was too small to observe a size effect. In addition, further size reduction below a threshold value may no longer result in greater Ca retention, as seen with our results for the SSA.

A significant difference in Ca-fractional retention was observed between $CaCO_3$ 64 m^2/g and HAp 100 m^2/g when comparing the compound composition at high SSA. A partial contribution of SSA cannot be ruled out for this comparison, since HAp 100 m^2/g (d_{BET} = 19 nm) had greater SSA compared to $CaCO_3$ 64 m^2/g (d_{BET} = 35 nm) and $CaCO_3$:HAp 50:50 (d_{BET} = 22 nm). Ca absorption from $CaCO_3$ and HAp was compared by Kruger *et al.* (2003b) in the same animal model; however, the compounds were not fully characterized and no size, SSA, or morphology was reported. They found no differences in BMD, bone Ca content and bone breaking strength and concluded that the type of Ca salt used for fortification did not play an important role in absorption or retention of Ca. However, of note in this study was the finding that the nanosized HAp (100 m^2/g) delivered more Ca and showed an overall Ca fractional retention higher than the micornsized $CaCO_3$ (3 m^2/g). This result is quite surprising because the nano HAp, with higher lattice energy of 10'602 kJ/mol (Zhang and Tamilselvan, 2007) and thus poor solubility (Tung, 1998), was as bioavailable as $CaCO_3$ which has a lattice energy of 2'804 kJ/mol only (Haynes, 2015-2016) and a higher solubility in water.

Bioavailability of different Ca sources can be also compared by measuring long term bone mineralization (Bagi *et al.*, 2006). This is usually observed in long term feeding experiments such as OVX models with feeding periods of 2-6 months (Shahnazari *et al.*, 2009). For example Huang *et al.* (2009) showed an improved BMD when feeding nano-sized $CaCO_3$ (hydrodynamic diameter of 151 nm vs 3.7 µm) and Ca-citrate (398 nm vs 1.8 µm) to OVX mice. We did not observe any differences in BMD or Ca content of femur for any of the SSA and the composition comparisons; this limitation may have been due to a shorter feeding period or a different animal model.

Previous studies on nanosized Ca have reported mean particle size, but characterization methods have varied, making it difficult to compare between the different studies. Moreover, in previous studies, the Ca compound's SSA, crystallinity, phase composition and images were generally not reported. An additional strength of this study is that we report SSA rather than particle size (d_{BET}) (Hilty *et al.*, 2009) which allows us to compare compounds with unknown densities (such as the mixture of $CaCO_3$ and HAp) with the ones containing pure $CaCO_3$ or HAp.

Safety evaluation of novel nanosized materials is needed when they are intended for applications in foods or supplements. While safety of insoluble nanomaterials used as food additive, such SiO_2 (Dekkers *et al.*, 2011) and TiO_2 (Powell *et al.*, 2010), has been extensively investigated, there are few data on the potential toxicity of nanosized Ca compounds. One previous study reported the safety of nano $CaCO_3$/Ca-citrate after acute toxicity exposure over 7 days and repeated dose sub-chronic toxicity over 28 days (Huang *et al.*, 2009). Nanosized minerals, once ingested, should dissolve quickly in the stomach and the ions join the common absorption pool independent of source. However, it is possible that intact nanoparticles translocate across the intestinal tract (Powell *et al.*, 2010). For instance, Hanes *et al.* (1999) discussed the possibility that low molecular weight complexes (such as Ca oxalate) could translocate across the gut mucosa without dissociation of Ca. Compound safety and potential toxicity was screened by extensive histologic evaluation to look for abnormal tissue calcification or other organ damage. The absence of microscopic calcification or calcium deposition in any tissue suggests these nanosized Ca compounds are safe. However, our animals were exposed for only 36 days and longer exposure periods with higher doses are still required in order to define their safety profile.

Whether Ca bioavailability can be predicted by *in vitro* dissolution or solubility remains unclear (Brennan *et al.*, 1991; Meiron *et al.*, 2011). Several papers report *in vitro* dissolution to be a good indicator of bioavailability (Gueguen and Pointillart, 2000; Hansen *et al.*, 1996) while others have criticized this approach (Heaney *et al.*, 1990). Recently, Meiron *et al.* (2011) have proposed a new approach to predict *in vivo* absorption by measuring the time to reach half of final pH (t_{pH50}) when dissolving 40 mg Ca in 0.01 M H_3PO_4. A synthetic amorphous $CaCO_3$ tested in human subjects was better absorbed than the crystalline form (Vaisman *et al.*, 2014). However, both size and crystallinity were changed at the same time (amorphous 40-100 nm vs. crystalline ~5 µm $CaCO_3$ (Meiron *et al.*, 2011)). We have criticized the use of (t_{pH50}) as a single indicator (Posavec *et al.*, 2016) and proposed that the amount of delivered Ca at the end of the dissolution experiment is also important. However, neither Ca delivered or t_{pH50} from our nanocompounds correlated significantly with *in vivo* absorbed Ca, suggesting this *in vitro* method is a poor predictor of *in vivo* Ca bioavailability.

In conclusion, increasing the SSA of CaCO3 from 3 to 64 m^2/g did not improve Ca-retention in growing rats. Varying composition at nanoscale significantly increased Ca-fractional

retention (HAp 100 m^2/g versus $CaCO_3$ 64 m^2/g), suggesting that once nanoscale is achieved, chemical composition is an important determinant of Ca bioavailability. Overall, the HAp 100 m^2/g performed well: it delivered the highest amount of Ca *in vitro*, caused minimal color changes and pH increases when added to food and drink matrices, and had greatest Ca-fractional retention *in vivo*. Thus, it may be a promising new compound for food fortification and/or supplementation.

Acknowledgements

The authors gratefully thank Céline Heri and Juwela Lam for the laboratory analyses, Anne Broomfield for her support in planning sample collection, Antoniette Fick and Jaco Vermeulen for their help with animal work and Magda Uys for the DXA measurements. Electron microscopy was performed at Scientific Center for Optical and Electron Microscopy (ScopeM, ETH Zurich). LP, FHV, JB, AG, MK, MZ designed the animal study; LP conducted the animal study, *in vitro* dissolution experiments and the sensory changes experiments; MK and JB advised on study design, sample collection and DXA measurements; HB collected animal tissues and MH performed histological analysis. LP, FHV, JB and MZ performed statistical analyses. LP, FHV and MZ drafted the manuscript. All authors read and approved the final manuscript. This study was funded by the Swiss South African Research Program, grant number IZLSZ3_149090.

References

Abrams S. A., and Atkinson S. A., 2003, Calcium, magnesium, phosphorus and vitamin d fortification of complementary foods: The Journal of Nutrition, v. 133, no. 9, p. 2994-2999.

Bagi C. M., Hanson N., Andresen C., Pero R., Lariviere R., Turner C. H., and Laib A., 2006, The use of micro-ct to evaluate cortical bone geometry and strength in nude rats: Correlation with mechanical testing, pqct and dxa: Bone, v. 38, no. 1, p. 136-144.

Brennan M. J., Duncan W. E., Wartofsky L., Butler V. M., and Wray H. L., 1991, In vitro dissolution of calcium carbonate preparations: Calcified Tissue International, v. 49, no. 5, p. 308-312.

Chen H. S., Chang J. H., and Wu J. S. B., 2008, Calcium bioavailability of nanonized pearl powder for adults: Journal of Food Science, v. 73, no. 9, p. 246-251.

Dekkers S., Krystek P., Peters R. J., Lankveld D. P., Bokkers B. G., van Hoeven-Arentzen P. H., Bouwmeester H., and Oomen A. G., 2011, Presence and risks of nanosilica in food products: Nanotoxicology, v. 5, no. 3, p. 393-405.

Elble A. E., Hill K. M., Park C. Y., Martin B. R., Peacock M., and Weaver C. M., 2011, Effect of calcium carbonate particle size on calcium absorption and retention in adolescent girls: Journal of the American College of Nutrition, v. 30, no. 3, p. 171-177.

Erfanian A., Mirhosseini H., Abd Manap M. Y., Rasti B., and Bejo M. H., 2014, Influence of nano-size reduction on absorption and bioavailability of calcium from fortified milk powder in rats: Food Research International, v. 66, p. 1-11.

Ervin R. B., and Kennedy-Stephenson J., 2002, Mineral intakes of elderly adult supplement and non-supplement users in the third national health and nutrition examination survey: The Journal of Nutrition, v. 132, no. 11, p. 3422-3427.

Flynn A., 2003, The role of dietary calcium in bone health: P Nutr Soc, v. 62, no. 4, p. 851-858.

Gao H. Y., Chen H. I., Chen W. X., Tao F., Zheng Y. H., Jiang Y. M., and Ruan H. J., 2008, Effect of nanometer pearl powder on calcium absorption and utilization in rats: Food Chemistry, v. 109, no. 3, p. 493-498.

Gopinath C., Prentice D. E., and Lewis D. J., 1987, Atlas of experimental toxicological pathology, MTP Press Limited.

Gueguen L., and Pointillart A., 2000, The bioavailability of dietary calcium: Journal of the American College of Nutrition, v. 19, no. 2, p. 119-136.

Hancock B. C., and Parks M., 2000, What is the true solubility advantage for amorphous pharmaceuticals?: Pharmaceutical Research, v. 17, no. 4, p. 397-404.

Hanes D. A., Weaver C. M., Heaney R. P., and Wastney M., 1999, Absorption of calcium oxalate does not require dissociation in rats: The Journal of Nutrition, no. 129, p. 170–173.

Hansen C., Werner E., Erbes H. J., Larrat V., and Kaltwasser J. P., 1996, Intestinal calcium absorption from different calcium preparations: Influence of anion and solubility: Osteoporosis International, v. 6, no. 5, p. 386-393.

Haynes W. M., 2015-2016, Properties of solids, Crc handbook of chemistry and physics, p. 12-21/12-33.

Heaney R. P., Dowell M. S., Rafferty K., and Bierman J., 2000, Bioavailability of the calcium in fortified soy imitation milk, with some observations on method: American Journal of Clinical Nutrition, v. 71, no. 5, p. 1166-1169.

Heaney R. P., Recker R. R., and Weaver C. M., 1990, Absorbability of calcium sources - the limited role of solubility: Calcified Tissue International, v. 46, no. 5, p. 300-304.

Heller H. J., Greer L. G., Haynes S. D., Poindexter J. R., and Pak C. Y. C., 2000, Pharmacokinetic and pharmacodynamic comparison of two calcium supplements in postmenopausal women: Journal of Clinical Pharmacology, v. 40, no. 11, p. 1237-1244.

Hilty F. M., Arnold M., Hilbe M., Teleki A., Knijnenburg J. T. N., Ehrensperger F., Hurrell R. F., Pratsinis S. E., Langhans W., and Zimmermann M. B., 2010, Iron from nanocompounds containing iron and zinc is highly bioavailable in rats without tissue accumulation: Nature Nanotechnology, v. 5, no. 5, p. 374-380.

Hilty F. M., Teleki A., Krumeich F., Buchel R., Hurrell R. F., Pratsinis S. E., and Zimmermann M. B., 2009, Development and optimization of iron- and zinc-containing nanostructured powders for nutritional applications: Nanotechnology, v. 20, no. 47.

Hilty F. M., and Zimmermann M. B., 2014, Nano- structured minerals and trace elements for food and nutrition applications: Nano- and Microencapsulation for Foods, p. 199-222.

Hornyak G. L., Tibbals H. F., Dutta J., and Moore J. J., 2009a, Characterization metods, Introduction to nanoscience and nanotechnology, CRC Press, p. 167-171.

Hornyak G. L., Tibbals H. F., Dutta J., and Moore J. J., 2009b, Chemical interactions at the nanoscale, Introduction to nanoscience and nanotechnology, CRC Press, p. 488-542.

Huang S., Chen J. C., Hsu C. W., and Chang W. H., 2009, Effects of nano calcium carbonate and nano calcium citrate on toxicity in icr mice and on bone mineral density in an ovariectomized mice model: Nanotechnology, v. 20, no. 37, p. 1-7.

Imai E., Hatae K., and Shimada A., 1995, Oral perception of grittiness: Effect of particle size and concentration of the dispersed particles and the dispersion medium: Journal of Texture Studies, v. 26, no. 5, p. 561-576.

Institute of Medicine, 2011, Dietary reference intakes: Calcium, vitamin d, Washington, D.C., The National Academies Press, Choice: Current reviews for academic libraries, p. 1115.

Jacoby R. O., and Lindsey J. R., 1998, Risks of infection among laboratory rats and mice at major biomedical research institutions: ILAR Journal, v. 39, no. 4, p. 266-271.

Knijnenburg J. T. N., Hilty F. M., Krumeich F., Zimmermann M. B., and Pratsinis S. E., 2013, Multimineral nutritional supplements in a nano-cao matrix: Journal of Materials Research, v. 28, no. 8, p. 1129-1138.

Kressel G., 2010, Bioavailability and solubility of different calcium-salts as a basis for calcium enrichment of beverages: Food and Nutrition Sciences, v. 1, no. 2, p. 53-58.

Kruger M. C., Brown K. E., Collett G., Layton L., and Schollum L. M., 2003a, The effect of fructooligosaccharides with various degrees of polymerization on calcium bioavailability in the growing rat: Experimental Biology and Medicine, v. 228, no. 6, p. 683-688.

Kruger M. C., Gallaher B. W., and Schollum L. M., 2003b, Bioavailability of calcium is equivalent from milk fortified with either calcium carbonate or milk calcium in growing male rats: Nutrition Research, v. 23, no. 9, p. 1229-1237.

Maedler L., Kammler H. K., Mueller R., and Pratsinis S. E., 2002, Controlled synthesis of nanostructured particles by flame spray pyrolysis: Journal of Aerosol Science, no. 33, p. 369–389.

Martin R. J., 1989, Atlas of experimental toxicological pathology: Veterinary Research Communications, v. 13, no. 6, p. 434-434.

Meiron O. E., Bar-David E., Aflalo E. D., Shechter A., Stepensky D., Berman A., and Sagi A., 2011, Solubility and bioavailability of stabilized amorphous calcium carbonate: Journal of Bone and Mineral Research, v. 26, no. 2, p. 364-372.

Nel A., Xia T., Madler L., and Li N., 2006, Toxic potential of materials at the nanolevel: Science, v. 311, no. 5761, p. 622-627.

Peterson C. A., Eurell J. A. C., and Erdman J. W., 1995, Alterations in calcium intake on peak bone mass in the female rat: Journal of Bone and Mineral Research, v. 10, no. 1, p. 81-95.

Posavec L., Knijnenburg J. T. N., Hilty F. M., Krumeich F., Pratsinis S. E., and Zimmermann M. B., 2016, Dissolution and storage stability of nano calcium carbonates and phosphates for nutrition: J Nanopart Res - In press, no. In press.

Powell J. J., Faria N., Thomas-McKay E., and Pele L. C., 2010, Origin and fate of dietary nanoparticles and microparticles in the gastrointestinal tract: Journal of Autoimmunity, v. 34, no. 3, p. J226-J233.

Puech J., Heughebaert J. C., and Montel G., 1982, A new mode of growing apatite crystallites: Journal of Crystal Growth, v. 56, no. 1, p. 20-24.

Rafferty K., Walters G., and Heaney R. P., 2007, Calcium fortificants: Overview and strategies for improving calcium nutriture of the us population: Journal of Food Science, v. 72, no. 9, p. 152-158.

Reeves P. G., Nielsen F. H., and Fahey G. C., Jr., 1993, Ain-93 purified diets for laboratory rodents: Final report of the american institute of nutrition ad hoc writing committee on the reformulation of the ain-76a rodent diet: The Journal of Nutrition, v. 123, no. 11, p. 1939-1951.

Rohner F., Ernst F. O., Arnold M., Hibe M., Biebinger R., Ehrensperger F., Pratsinis S. E., Langhans W., Hurrell R. F., and Zimmermann M. B., 2007, Synthesis, characterization, and bioavailability in rats of ferric phosphate nanoparticles: The Journal of Nutrition, v. 137, no. 3, p. 614-619.

Russell L. F., Sanford K. A., Gaul S. O., Haskett J., Johnston E. M., McRae K. B., and Stark R., 2010, Effect of calcium salts on fortified apple juice: British Food Journal, v. 112, no. 6-7, p. 751-762.

Shahnazari M., Martin B. R., Legette L. L., Lachcik P. J., Welch J., and Weaver C. M., 2009, Diet calcium level but not calcium supplement particle size affects bone density and mechanical properties in ovariectomized rats.: The Journal of Nutrition, v. 139, no. 10, p. 1308-1315.

Shangraw R. F., 1989, Factors to consider in the selection of a calcium supplement: Public Health Reports, v. 104, no. Suppl, p. 46-50.

Tobelmann R., 2001, Implementing calcium fortification: An industry case study: Journal of Food Composition and Analysis, v. 14, no. 3, p. 241-244.

Tung M. S., 1998, Calcium phosphates: Structure, composition, solubility and stability, *in* Anjad, Z., ed., Calcium phospahtes in biological and industrial systems, Springer Science & Business Media, LCC.

Vaisman N., Shaltiel G., Daniely M., Meiron O. E., Shechter A., Abrams S. A., Niv E., Shapira Y., and Sagi A., 2014, Increased calcium absorption from synthetic stable amorphous calcium carbonate: Double-blind randomized crossover clinical trial in postmenopausal women: Journal of Bone and Mineral Research, v. 29, no. 10, p. 2203-2209.

Vanveldhoven P. P., and Mannaerts G. P., 1987, Inorganic and organic phosphate measurements in the nanomolar range: Analytical Biochemistry, v. 161, no. 1, p. 45-48.

Wegmuller R., Zimmermann M. B., Moretti D., Arnold M., Langhans W., and Hurrell R. F., 2004, Particle size reduction and encapsulation affect the bioavailability of ferric pyrophosphate in rats: The Journal of Nutrition, v. 134, no. 12, p. 3301-3304.

Zhang D. J., and Tamilselvan A., 2007, Lattice energy and mechanical stiffness of hydroxyapatite: Journal of Materials Science - Materials in Medicine, v. 18, no. 1, p. 79-87.

Supporting Information

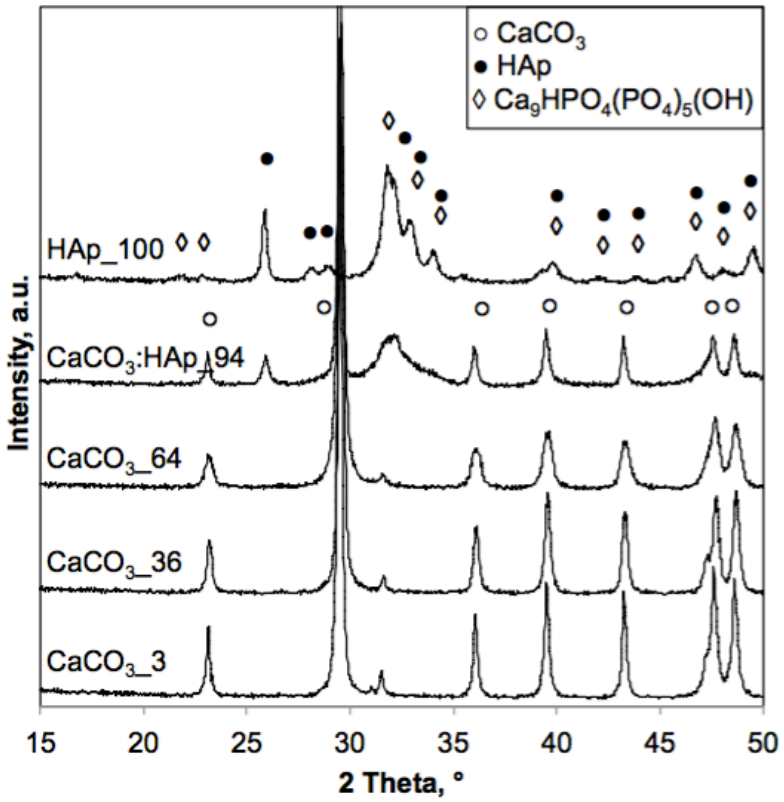

Figure S 1: X-ray diffraction patterns (not normalized) for the 5 compounds after aging. International Centre for Diffraction Data: $CaCO_3$ (calcite) 81-2027, $Ca_9HPO_4(PO_4)_5(OH)$ (CaHy) 46-0905, $Ca_{10}(PO_4)_6(OH)_2$ (HAp) 03-0747. CaHy, calcium hydrogen phosphate; HAp, hydroxyapatite.

Table S1: Dietary composition (g/kg) according to diet (Formulated by Research Diets Inc., USA, according to the National Research Council (1995) nutrient requirements for laboratory animals (AIN 93G)). $CaCO_3$, calcium carbonate; HAp, hydroxyapatite.

Dietary composition, g/kg	Ca compound				
	$CaCO_3$, 3 m^2/g	$CaCO_3$, 36 m^2/g	$CaCO_3$, 64 m^2/g	$CaCO_3$:HAp 50:50, 94 m^2/g	HAp, 100 m^2/g
Total L-Amino Acids			178.9		
Corn Starch			397.486		
Maltodextrin 10			132		
Sucrose			107.0777		
Cellulose			50		
Soybean Oil			70		
t-butylhydroquinone			0.014		
Mineral Mix S10022C (Ca/P Free)			3.5		
Potassium Chloride	0	0	0	2.62	5.35
Potassium Phosphate, Monobasic	9.8	9.8	9.8	5	0
Sodium Chloride			2.59		
Sodium Bicarbonate			5.12		
Sodium Phosphate			3.9		
Ca compound added	12.65	13.35	14.10	13.70	13.30
Vitamin Mix V10037			10		
Choline Bitrartrate			2.5		
Measured Ca content	4.73 ± 0.06	4.74 ± 0.11	4.80 ± 0.05	4.86 ± 0.04	4.71 ± 0.11

Table S2: Time to reach final pH and half of final pH together with corresponding pH values of the dissolution assay.

	Ca compound				
	$CaCO_3$, 3 m^2/g	$CaCO_3$, 36 m^2/g	$CaCO_3$, 64 m^2/g	$CaCO_3$:HAp 50:50, 94 m^2/g	HAp, 100 m^2/g
t_{pH50}, sec	28 ± 4	23 ± 2	13 ± 2	18 ± 4	23 ± 3
pH_{end}, -	5.8[1]	5.6 ± 0.1	5.4[1]	5.6 ± 0.1	4.7[1]
$t_{pH\ end}$, sec	192 ± 43	241 ± 54	146 ± 15	119 ± 15	135 ± 11
pH_{50}, -	4.0[1]	3.8[1]	3.8[1]	3.8[1]	3.4[1]
ΔpH, -	3.6[1]	3.7 ± 0.1	3.2[1]	3.6[1]	2.6[1]

[1] SD smaller than 0.05, therefore not indicated
All values are indicated as mean ± SD of 3 replicates.
$CaCO_3$, calcium carbonate; HAp, hydroxyapatite.

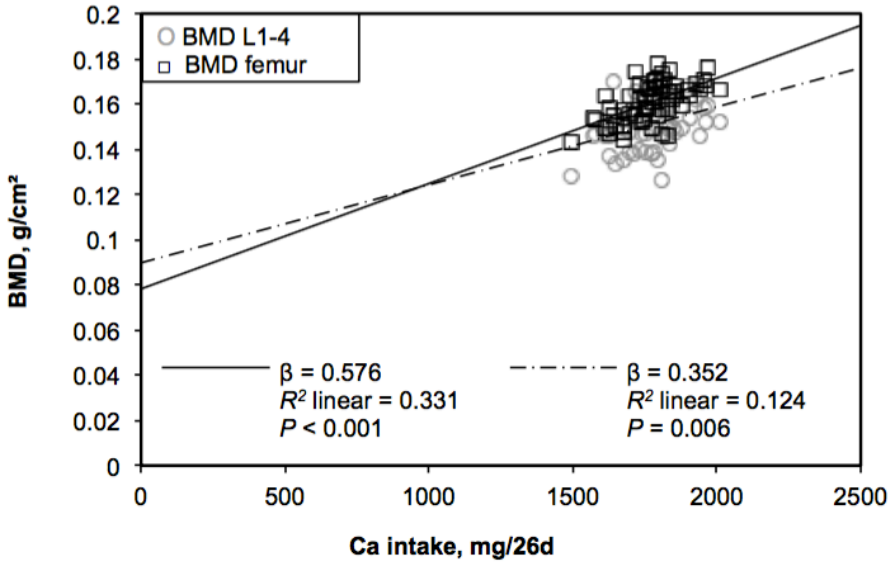

Figure S2: Simple linear regression analysis between Ca intake over 26 d of total food intake measurement and BMD L1-4 vertebra and BMD femur, respectively. BMD, bone mineral density.

Table S3: ΔpH values of the sensory performance experiment.

	Food matrix				
	Orange juice[1]	Apple juice[1]	Cranberry juice[1]	Soy chocolate milk[1]	Soy yogurt[2]
pH blank					
at 0 min[3], -	3.84 ± 0.02	3.42 ± 0.03	2.66 ± 0.02	6.57 ± 0.02	4.24 ± 0.02
at 120 min[3], -	3.84 ± 0.02	3.44 ± 0.01	2.67 ± 0.02	6.49 ± 0.01	4.27 ± 0.03
ΔpH[4]					
$CaCO_3$ 3 m^2/g, -	0.84[5]	1.38 ± 0.02	1.34 ± 0.01	0.37 ± 0.02	1.89 ± 0.04
$CaCO_3$ 36 m^2/g, -	0.86 ± 0.01	1.45 ± 0.05	1.41 ± 0.02	0.58[5]	1.87 ± 0.04
$CaCO_3$ 64 m^2/g, -	0.87 ± 0.01	1.42 ± 0.02	1.42 ± 0.06	0.74 ± 0.02	2.38 ± 0.16
$CaCO_3$:HAp 94 m^2/g, -	0.63 ± 0.01	1.05 ± 0.01	1.12 ± 0.01	0.31 ± 0.01	1.51 ± 0.13
HAp 100 m^2/g, -	0.39[5]	0.77 ± 0.01	0.98 ± 0.01	0.12[5]	0.31 ± 0.03
HAp 1 m^2/g, -	0.05[5]	0.31 ± 0.01	0.64[5]	0.08[5]	0.04[5]

[1] Fortification: 120 mg Ca / 100 g food
[2] Fortification: 200 mg Ca / 100 g food
[3] Values are displayed as mean ± SD of 5 replicates for the blank.
[4] Values are displayed as mean ± SD of 2 replicates for the samples.
[5] SD < 0.005, therefore not indicated
$CaCO_3$, calcium carbonate; HAp, hydroxyapatite.

Table S4: Summary of the histology report showing only the observed adverse effects.

Organ and type of observed change	*n* changes[1]				
	$CaCO_3$ 3 m^2/g	$CaCO_3$ 36 m^2/g	$CaCO_3$ 64 m^2/g	$CaCO_3$:HAp 94 m^2/g	HAp 100 m^2/g
Lungs					
atelectasis / light BALT hyperplasia / light leucocytosis	0	2	3	2	2
atelectasis / light leucocytosis	0	0	2	3	2
atelectasis / light leucocytosis / formalin deposition	0	0	0	1	1
atelectasis / moderate BALT hyperplasia / moderate leucocytosis	0	0	0	0	1
light atelectasis	0	2	0	0	0
light atelectasis / formalin deposition	2	0	0	0	0
light atelectasis / light BALT hyperplasia / formalin deposition	0	2	0	0	0
light atelectasis / light BALT hyperplasia	1	0	0	0	0
light atelectasis / light BALT hyperplasia / formalin deposition	0	0	1	0	0
multifocal atelectasis / light BALT hyperplasia	2	0	0	0	0
multifocal atelectasis / moderate BALT hyperplasia	1	0	0	0	0
Heart					
small foci of fibrosis in the myocardium	0	0	1	0	0
connective tissue in the endocardium	0	1	0	0	0
Liver					
calcification with fibrosis	0	0	0	1	0
rough surface but no changes	0	0	0	1	0
pale color / euthanasia artifact	0	0	0	0	1
Kidney					
slight proteinuria (incidental finding)	1	0	0	0	0
Spleen					
active white pulp / formalin deposition in the red pulp	0	2	0	0	0
active white pulp / light extramedullary blood formation in red pulp	1	0	0	0	0
light extramedullary blood formation in red pulp	0	4	4	5	5
light extramedullary blood formation in red pulp / formalin precipitation	0	0	1	1	1
light hemosiderosis / light extramedullary blood formation in red pulp	1	0	0	0	0
light hemosiderosis / light extramedullary blood formation in red pulp	1	1	0	0	0
light hemosiderosis / light extramedullary blood formation in red pulp	1	0	0	0	0
light hemosiderosis at hilum / macrophages with formalin in red pulp	1	0	0	0	0

[1] 6 out of 12 rats were randomly selected for histological examination for each group

Table S4: Summary of the histology report showing only the observed adverse effects.

Organ and type of observed change	*n* changes[1]				
	$CaCO_3$ 3 m^2/g	$CaCO_3$ 36 m^2/g	$CaCO_3$ 64 m^2/g	$CaCO_3$:HAp 94 m^2/g	HAp 100 m^2/g
Stomach					
submucosa with several neutrophils between glandular and squamous area	3	3	3	2	6
submucosa with several neutrophils / hyperkeratosis of the mucosa between glandular and squamous area	0	1	0	0	0
submucosa with some neutrophils between glandular and squamous area	0	0	0	2	0
Pancreas	0	0	0	0	0
Duodenum	0	0	0	0	0
Jejunum	0	0	0	0	0
Ileum	0	0	0	0	0
calcification in the Peyers patches	0	1	0	0	0
Colon	0	0	0	0	0

[1] 6 out of 12 rats were randomly selected for histological examination for each group

MANUSCRIPT 3

Amyloid fibrils reduce, stabilize and deliver bioavailable iron

Yi Shen[1§], Lidija Posavec[2§], Sreenath Bolisetty[1], Florentine M. Hilty[2], Gustav Nyström[1], Joachim Kohlbrecher[3], Monika Hilbe[4], Antonella Rossi[5,6], Jeannine Baumgartner[7], Michael B. Zimmermann[2], Raffaele Mezzenga[1*]*

[1]Laboratory of food and Soft Materials, Department of Health Sciences and Technology, ETH Zurich, Schmelzbergstrasse 9, Zurich 8092, Switzerland

[2]Human Nutrition Laboratory, Department of Health Sciences and Technology, ETH Zurich, Schmelzbergstrasse 7, Zurich 8092, Switzerland

[3]Laboratory for Neutron Scattering and Imaging, PSI Paul Scherrer Institute, Villigen 5232, Switzerland

[4]Institute of Veterinary Pathology, Vetsuisse Faculty, University of Zurich, Switzerland

[5]Laboratory for Surface Science and Technology, Department of Materials, ETH Zurich, Wolfgang-Pauli-Strasse 10, Zurich 8093, Switzerland

[6]Dipartimento di Chimica Inorganica ed Analitica, Università degli Studi di Cagliari, INSTM Unit, Cittadella Universitaria di Monserrato, I-09100 Cagliari, Italy

[7]Centre of Excellence for Nutrition, North-West University Potchefstroom, South Africa

[§] these authors contributed equally to this work

* these authors share corresponding authorship

Manuscript in preparation (format for Nature Letters)

This work was supported by Swiss National Science Foundation, National research Program 69, Grant number 406940-144166-1.

Abstract

Iron deficiency anemia (IDA) is a major global public health problem (Kassebaum *et al.*, 2014). A sustainable and cost-effective strategy to reduce IDA is iron fortification of foods (Zimmermann and Hurrell, 2007). However, fortification with iron is difficult because the most bioavailable fortificants cause adverse organoleptic changes in foods (Allen *et al.*, 2006; Hurrell, 2002). Iron nanoparticles have been proposed as novel iron fortificants with high bioavailability and low reactivity in food matrices (Acosta, 2009; Hilty *et al.*, 2010; Rohner *et al.*, 2007). Nevertheless, iron nanoparticles are easily oxidized as dry powder because of their large surface area and undergo rapid aggregation in solution due to their limited colloidal stability. This severely limits their use in fortification (Huber, 2005). Amyloid fibrils are self-assembled β-sheet protein aggregates known for their association with neurodegenerative disorders, such as Alzheimer's and Parkinson's diseases. However, they were recently described in the context of biological, chemical and physical functions in living organisms (Barnhart and Chapman, 2006; Fowler *et al.*, 2006; Iconomidou *et al.*, 2000; Maddelein *et al.*, 2002; Maji *et al.*, 2009) and are emerging as unique bio-material building blocks (Bolisetty and Mezzenga, 2016; Knowles and Mezzenga, 2016; Li *et al.*, 2012) due to their remarkable physico-chemical properties. Here we show an original application for these protein fibrils as efficient carriers for iron fortification. We use biodegradable amyloid fibrils made from β-lactoglobulin (BLG), an inexpensive milk protein with natural reducing effects (Bolisetty *et al.*, 2011), as anti-oxidizing nanocarriers and colloidal stabilizers for iron nanoparticles. The resulting new hybrid material, in which iron nanoparticles decorate the amyloid fibrils, forms a stable protein-iron colloidal dispersion and undergoes rapid dissolution and release of iron during acidic and enzymatic *in-vitro* digestion. Most importantly, this hybrid shows high *in-vivo* iron bioavailability, equivalent to ferrous sulfate in hemoglobin repletion and stable isotope studies in rats, but with reduced organoleptic changes in foods compared to ferrous sulfate. Feeding the rats with these hybrids did not result in abnormal iron accumulation in any organs, or changes in whole blood glutathione concentrations, inferring their primary safety. Therefore, these iron-amyloid fibril hybrids emerge as novel, highly effective delivery systems for iron in both solid and liquid matrices.

KEYWORDS: fibrils, iron, reducing effect, relative bioavailability, depletion-repletion, stable isotopes, organoleptic changes

Abbreviations: **AA**, amino acid; **AAS**, atomic absorption spectroscopy; **EDX**, Energy Dispersive X-ray spectroscopy; **RBV**, relative bioavailability; **SANS**, small angle neutron scattering; **TEM**, Transmission electron microscopy; **XPS**, X-ray photoelectron spectroscopy

1. Results and discussion

Despite iron deficiency anemia is a severe, global health risk estimated in 2010 to threat 2.2 billion people worldwide (Kassebaum *et al.*, 2014), iron (Fe) fortification of foods still remains a challenging field. Among commonly used iron fortificants, Fe(II) compounds tend to be more bioavailable than Fe(III) compounds but cause more adverse sensory changes in reactive food and liquid matrices (Allen *et al.*, 2006). Nanosized iron particles have been suggested as effective new fortificants (Acosta, 2009; Hilty *et al.*, 2010; Rohner *et al.*, 2007). However, Fe(II) salts and iron nanoparticles in form of dry powder oxidize to Fe(III) when exposed to air, becoming less bioavailable. BLG amyloid fibrils made from milk protein were recently described for their natural reducing effect and used as a green reducing agent to produce gold crystals (Bolisetty *et al.*, 2011). Can this reducing ability of BLG fibrils apply to iron and help maintain iron into its more bioavailable Fe(II) state? To answer this question, we tested the reducing effect of BLG fibrils on Fe(III). After mixing $FeCl_3$ solution with BLG fibrils, we found that Fe(III) ions were converted into Fe(II) as indicated by Fe(II)-phenanthroline complex formation (Rohner *et al.*, 2007). The more fibrils added to $FeCl_3$ the more Fe(II) ions were detected (**Figure 1**a). In order to investigate which amino acids (AAs) are responsible for this reducing effect, all the water-soluble AAs from the primary structure of BLG (Extended data **Figure 1**a) were tested. The non-water soluble AAs were considered to form the inner core of the protein and thus not reactive in the bulk. Cysteine was found to be the only AA allowing the conversion of Fe(III) to Fe(II) ions (Extended data **Figure 1**a). The sulfhydryl group of cysteine, which can be easily oxidized and form disulfide bonds, normally contributes to protein structures (Brosnan and Brosnan, 2006). Fibrillization of BLG reorganized the structure of the protein and made cysteine residues and sulfhydryl groups more accessible in the bulk (Bolisetty and Mezzenga, 2016), thus enhancing the reducing effect. This was demonstrated by the fact that production of Fe(II) ions (**Figure 1**b red dots) increased when a constant amount of FeCl3 was mixed with BLG fibrils with undergoing fibrillization level. BLG fibrils with longer fibrillization time were more effective to convert Fe(III) to Fe(II) ions. This trend stayed and enhanced over 20 h (Extended Data **Figure 1**b). BLG protein progressively grows into mature fibrils with increasing incubation time, as revealed by thiazole orange staining, a fibril-specific fluorescent dye working at low pH (**Figure 1**b blue bars) (Gao and Xu, 2013). These results indicate that BLG fibrils are ideal candidates for iron fortification because they can maintain the iron in the more bioavailable

Fe(II) state. This may also protect iron against dietary inhibitors such as phytate (Hallberg *et al.*, 1989), polyphenols (Hurrell *et al.*, 1999) and calcium (Hallberg *et al.*, 1991).

Iron nanoparticles generally show good bioavailability and sensory performance but cannot be used in aqueous drinks and foods because of strong colloidal aggregation (Hilty *et al.*, 2010). We tackled this problem by compositing iron nanoparticles directly onto the surface of BLG fibrils. This provided the twofold benefit of preventing colloidal aggregation while preserving the iron in Fe(II) state from oxidation. These hybrids were prepared in-situ in two steps (**Figure 1**c-e). First, we created BLG amyloid fibrils by self-assembly at pH 2 and 90 °C for 5 hours (**Figure 1**c-d) (Adamcik *et al.*, 2010). Second, Fe (III) ions were added in solution with the fibrils in the form of iron chloride, $FeCl_3$. Fe (III) ions strongly bind onto fibrils due to their high affinity to proteins (Leal *et al.*, 2012). Nanosized iron nanoparticles were thus nucleated on the surface of fibrils by adding sodium borohydride (**Figure 1**e) (Sun *et al.*, 2006). This strong reducing agent generated iron nanoparticles immediately after mixing and the reducing ability decayed quickly with time. Similarly to the pure BLG fibrils solution (**Figure 1**f), the iron-BLG fibrils (Fe-FibBLG) dispersion is transparent, with slightly darker color, and stable against sedimentation (**Figure 1**g). In contrast, dispersions with iron nanoparticles (Fe-Nano) directly reduced from $FeCl_3$ without BLG fibrils were not stable, and rapidly precipitated into black iron clusters (Extended data **Figure 2**). Transmission electron microscopy (TEM) gives insight into the morphology of these hybrids before and after nanoparticle composition. Compared to the typical morphology of BLG fibrils (**Figure 1**f), small (5-20 nm in diameter), spherical, nanoparticles were found to decorate the surface of the fibrils (**Figure 1**g). These particles are stable in solution at pH > 3 but dissolve very quickly at pH < 1.5. Furthermore, Fe-FibBLG solution can be converted into a gel with the addition of NaCl and freeze-dried into powders (Extended Data **Figure 3**a and **3**b), simplifying transportation and mixing with food products. After re-dispersing the dried material, the iron nanoparticles were found intact by TEM analysis (Extended Data **Figure 3**c). These results show that a stable iron-BLG fibril hybrid material can be produced by a simple chemical reaction and process in liquid, gel or powder forms.

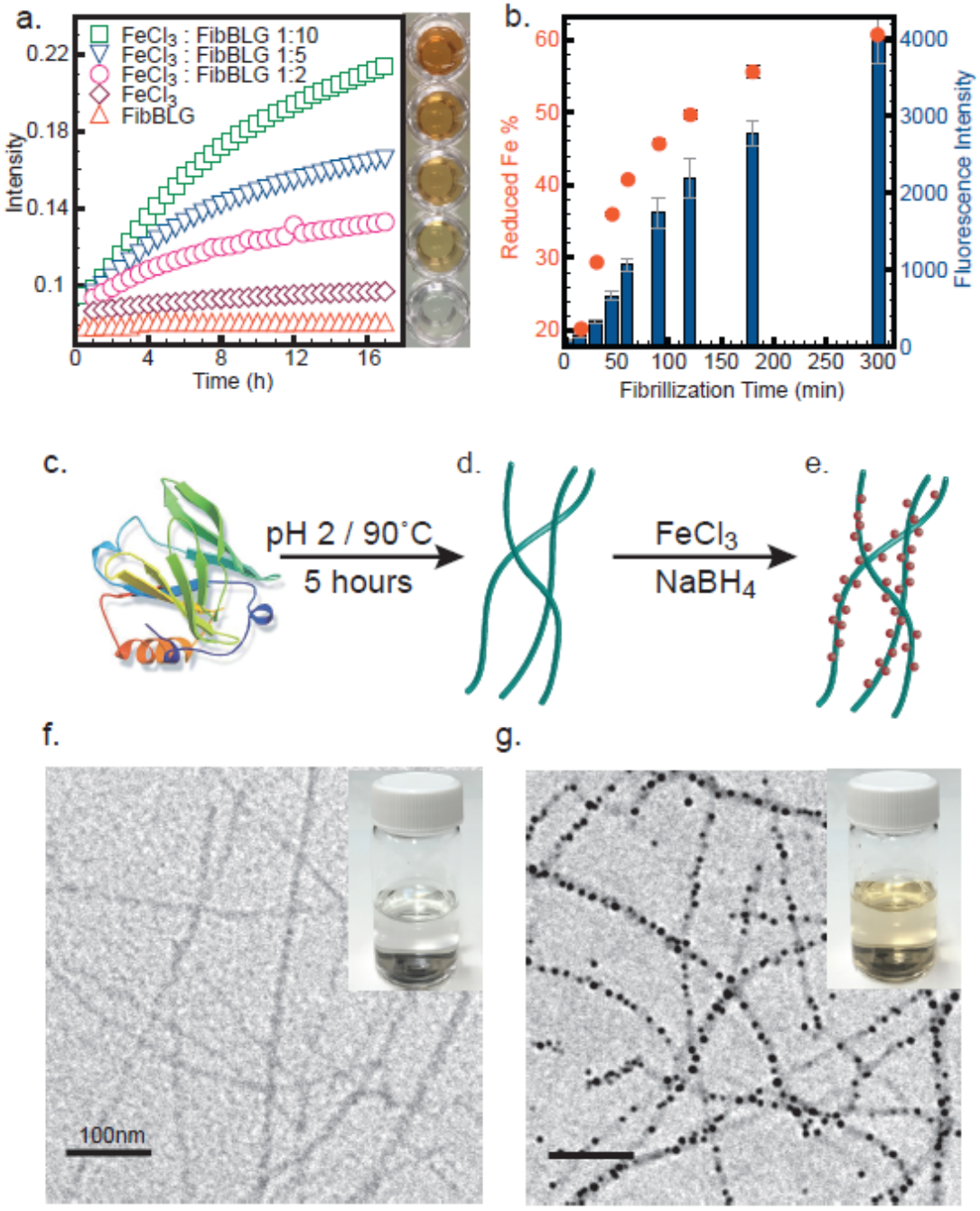

Figure 1: Reducing effect of BLG fibrils to iron. a. Fe(II) concentration rises with time and on increasing BLG fibrils/$FeCl_3$ weight ratio, indicated by the Fe(II)-phenanthroline complex with absorbance at wavelength 512 nm. $FeCl_3$ and BLG fibrils were tested individually as controls. Error bars from three experiments are too small to be shown. **b**. Amount of reduced iron (red dots) increases when mixing with BLG fibrils with increasing fibrillization level at different fibrillization time points, as indicated by the fluorescence intensity of the staining agent thiazole orange (blue bars) (error bars are standard deviations from three experiments). **Schematic of BLG fibrils and iron-BLG fibril nanocomposites production c**. Native β-lactoglobulin proteins (BLG) were incubated at pH 2 and 90°C for 5 hours to form amyloid fibrils **d**. By mixing amyloids with iron chloride and sodium borohydride reducing agent, iron nanoparticles were nucleated onto the fibrils, **e**. Panels **f**. and **g**.: Transmission electron microscopy (TEM) images of pure BLG fibrils and iron-BLG fibril nanocomposites, with inserts showing their respective suspensions. The scale bars are 100 nm.

X-ray photoelectron spectroscopy (XPS) measurements were carried out on freshly made Fe-FibBLG and Fe-Nano powder samples to investigate the composition of these hybrids. Due to its surface sensitivity, XPS can identify the iron composition as a function of the depth, differentiating between the iron core of the nanoparticles and its outer layer. XPS analysis detected the presence of Fe(II) oxide, Fe(III) oxi-hydroxide formed around the cores, and the residual Fe(II)-Cl_2 and Fe(III)-Cl_3 on the surface (Extended Data **Table 1**). The presence of iron chlorides on the surface is due to the sample preparation, the samples being freeze-dried without washing (Extended Data **Figure 4**b). The peak area ratio of Fe(0):Fe(II):Fe(III) is 0.9:74.8:24.3 for Fe-FibBLG and 29.5:33.2:37.3 for Fe-Nano (Extended Data Table 1). This indicates that Fe-FibBLG powder contains high concentration of Fe(II).

Contrast-matching small angle neutron scattering (SANS) was performed to measure the overall distribution of BLG fibrils and iron nanoparticles in solution (**Figure 2**). We matched the scattering length density of iron nanoparticles by using a mixture of deuterium oxide (D_2O) and H_2O in a ratio 100:0 (**Figure 2**a) as solvent. Under this condition only BLG fibrils can scatter neutrons (**Figure 2**b) and the resulting scattering pattern follows the typical slope of -1 revealing the rod-like nature of the fibrils (**Figure 2**c). On the other hand, when matching the scattering length density of BLG fibrils with a 50:50 D_2O:H_2O ratio (**Figure 2**d), only iron particles are visible (**Figure 2**e). If all the iron particles would be attached along the fibrils as nanoparticles one would expect to see a structure factor following the same q-dependency than the fibrils (Paris *et al.*, 2006) at the match-point of the iron particles. However, we find a much steeper decay slope, which can be roughly described by a sum of two potential laws of q^{-4} and $q^{-9.3}$, where the transition from one to the other scattering law happens at q=0.041nm^{-1}. The fact, that we see only these large potential laws means that also large iron clusters need to be present. As the scattering intensity scales with the square of the volume of the clusters, a few of them might be already enough to dominate the SANS signal. More details about the modelling of the SANS data at the match point of the fibrils are given in the SI, The presence of a few large cluster can also be seen in TEM images which show that such clusters are formed preferable where several fibrils are crossing each other.

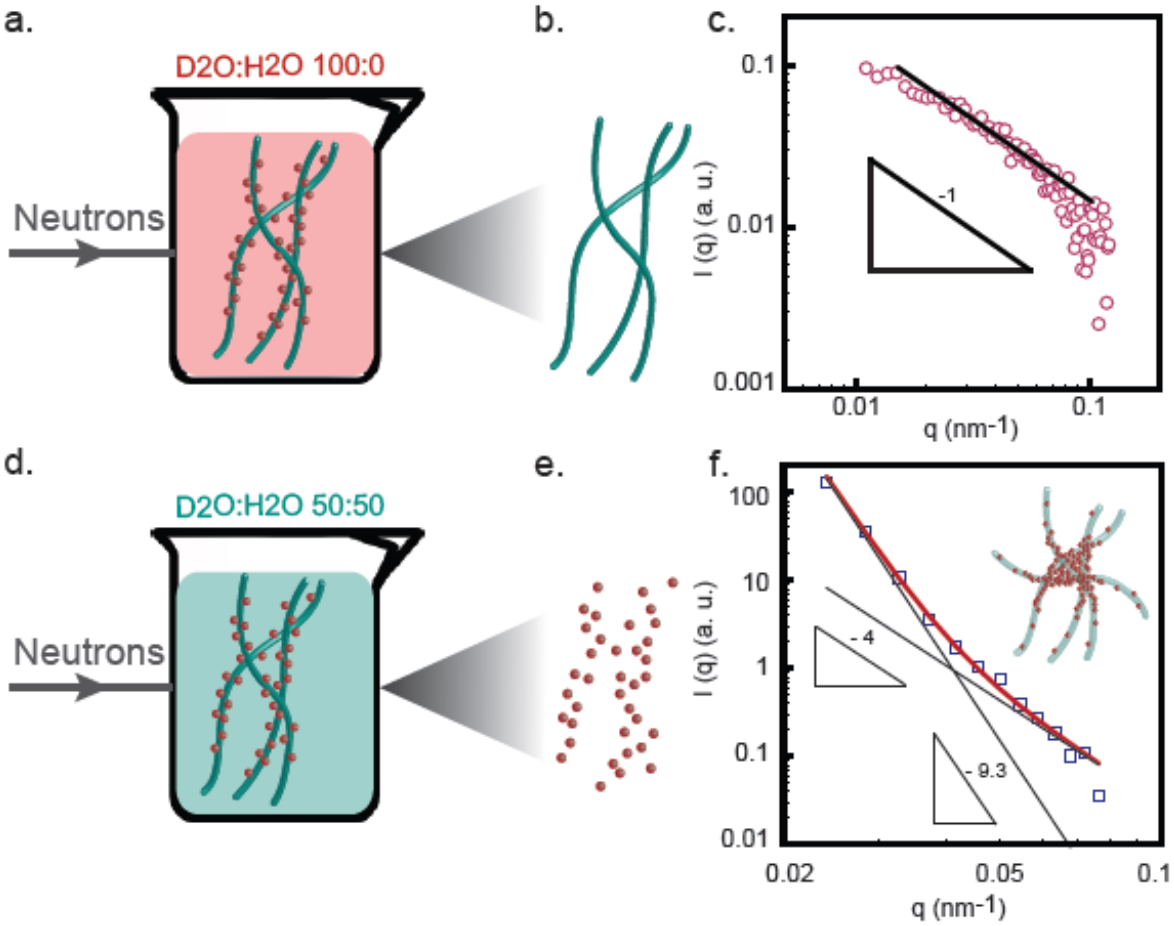

Figure 2: Schematic illustration and experimental results of contrast-matching small angle neutron scattering (SANS) on iron-BLG fibril hybrid suspensions. **a**. The D_2O:H_2O=100:0 ratio is used to contrast-match the scattering length density of the iron. **b**. Only BLG fibrils scatter and are detected. **c**. Pink circles represent the intensity scattered by BLG fibrils, decaying as q^{-1}, in agreement with the fractal dimension of 1 expected for rod-shaped objects. **d**. The D_2O:H_2O=50:50 ratio is used to contrast-match the scattering length density of BLG fibrils. **e**. Only iron nanoparticles scatter and are detected. **f**. Deep purple squares show the signal from scattering iron nanoparticles, fitted using the mass fractal model.

Having established the morphology of the hybrids after iron nanoparticle composition, we then investigated their *in-vitro* digestion in order to evaluate the suitability of this new hybrid material for iron supplementation via oral administration. We first performed acidic dissolution of iron nanoparticles at stomach physiological condition. Comparing the TEM images taken before (**Figure 3**a) and after (**Figure 3**b) digestion we observed that the iron particles are no longer observed but only the fibrils. Additionally, SANS was performed before and after the acidic digestion with a 50:50 D_2O:H_2O ratio to contrast-match BLG fibrils. Raw scattering data were compared to the background signal before and after acidic digestion (**Figure 3**d). The results clearly show that after acidic digestion, the curve meant to detect iron nanoparticles overlaps with the background curve, revealing a complete dissolution of the nanoparticles (**Figure 3**b).

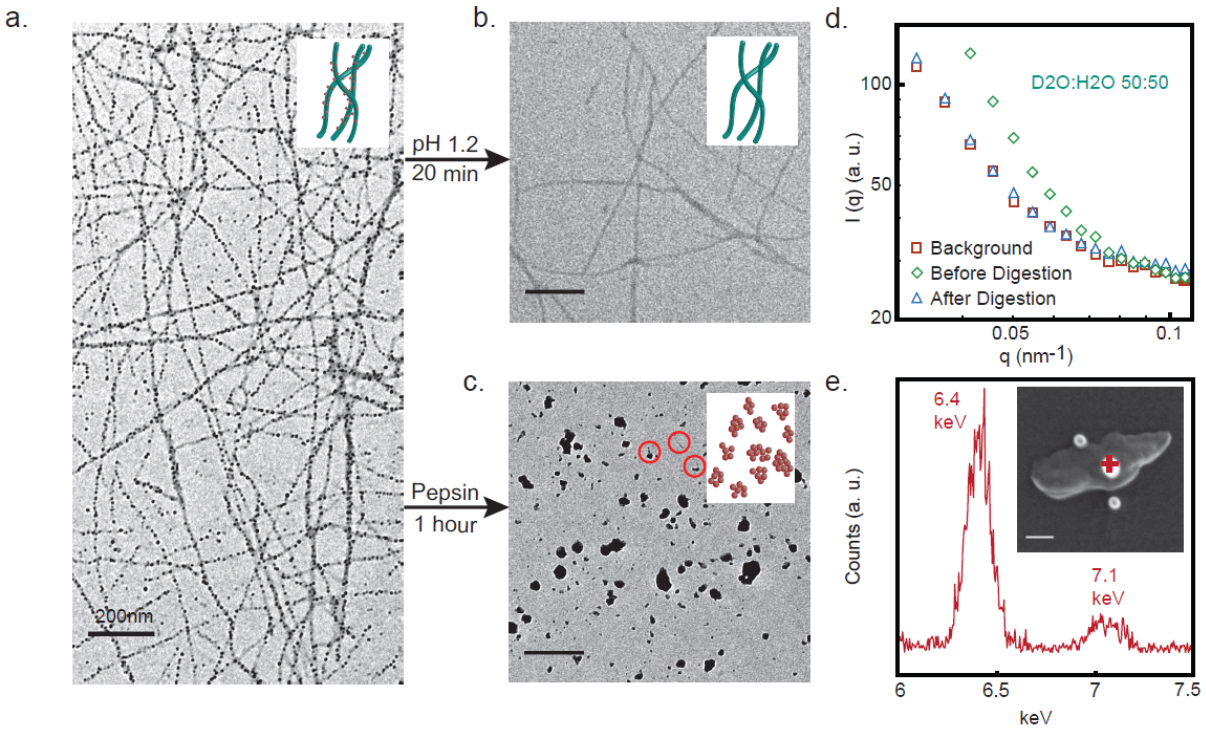

Figure 3: ***In-vitro*** **acidic/enzymatic digestion of iron-BLG fibrils characterized by TEM (a-c), SANS (d) and Energy dispersive X-ray spectroscopy (EDX) (e)**. **a**. TEM image of BLG fibrils fully decorated by iron nanoparticles. **b**. By decreasing the pH value to 1.2 and shaking at 50 rpm 37°C for 20 min, the iron particles are readily dissolved and only fibrils are detected by TEM. **c**. Fibrils are digested by pepsin at 50 rpm and 37°C for 1 hour resulting in iron nanoparticles aggregation. Red circles indicate the occasional presence of shortened, partially digested fibrils. Scale bars are 200 nm. **d**. In SANS data, D_2O:H_2O=50:50 ratio is used to contrast-match BLG fibrils, green diamonds represent the iron-BLG fibril sample, with only iron nanoparticles detectable. After acidic digestion, all the particles are dissolved and the detected signal, in blue triangles, drops and overlaps with the background scattering signal, in red squares. **e**. EDX was performed on the resulting iron nanoparticle aggregates. The peaks at 6.4 and 7.11 keV are characteristic for iron. The insert shows the scanning transmission electron microscopic image of the clump. The scale bar is 20 nm.

Similarly, enzymatic hydrolysis was also performed on the hybrid material. During the digestion, BLG fibrils were hydrolyzed by pepsin into short peptides (Bateman *et al.*, 2010; Li *et al.*, 2012) and the iron nanoparticles, no longer spatially distributed homogeneously along the amyloid fibrils, agglomerated together with protein residues forming large clumps as shown in **Figure 3**c. The composition of these aggregates was confirmed by Energy Dispersive X-ray spectroscopy (EDX) performed on the same sample used for TEM imaging (**Figure 3**c). Clear iron signal from these aggregates was found by the peaks at 6.4 and 7.1 keV (**Figure 3**e). Interestingly, a few short BLG fibrils could still be occasionally detected (**Figure 3**c red circled) after one-hour digestion, indicating a slow enzymatic hydrolysis of fibrils compared to the fast acidic dissolution of iron nanoparticles. This difference in digestion kinetics is crucial as it allows the delivery of iron ions prior to the digestion of fibrils, hence avoiding iron-particle clusters, yet allowing the dissolution of both the organic and inorganic phases via a synergistic acidic-enzymatic digestion.

Water soluble $FeSO_4$ is well absorbed in both rats and humans and its high bioavailability is the reference standard (Hurrell, 2002), although this compound has negative organoleptic impact on many food matrices. The relative bioavailability (RBV) to $FeSO_4$ and potential toxicity of novel nanostructured Fe-FibBLG in solid form were investigated *in-vivo* (outline in **Figure 4**a) using the hemoglobin repletion bioassay in rats (Cunniff, 1997; Forbes *et al.*, 1989). Iron nanoparticles (Fe-Nano) synthesized without BLG fibrils were used for comparison. Animal number, diet fortification, hemoglobin (Hb) change, iron and food intake per day and body weight gain are summarized in Extended Data **Table 3**. Daily iron intake and Hb change over 14 days of repletion were used to plot dose-response regression lines and the respective slopes were used to calculate RBV (**Figure 4**c). Fe-FibBLG and Fe-Nano in powder form showed RBVs of 90% and 95%, respectively, compared to $FeSO_4$ (**Figure 4**d). Acidic *in-vitro* digestion coupled with colorimetry were used to determine Fe(II) percentage in Fe-FibBLG, FeSO4 and Fe-Nano fortified animal diets with identical total iron fortification level. Specifically, diet with Fe-FibBLG contained similar amounts of Fe(II) (35±4%) as $FeSO_4$ (37±2%) but much more than Fe-Nano (14±3%). The high Fe(II) content in Fe-FibBLG compared to Fe-Nano may be explained by the reducing effect of BLG fibrils that partially protect the iron nanoparticles from oxidation. Although we do not know how much Fe(II) is needed to reach a 100% RBV, the Fe(II) data show that BLG fibrils have an advantage in keeping iron nanoparticles in the reduced form and protect it against oxidation. Extensive histological examination (Extended Data **Table 5**) and measurement of glutathione (GSH) in whole blood as a marker for oxidation were performed to assess potential toxicity. No abnormal iron accumulation or histological changes were observed, and there were no significant differences in blood GSH (Extended Data **Table 4**). These initial results infer absence of cytotoxicity, although specifically designed long-term toxicity studies still remain necessary to complement these findings.

High bioavailability of the compounds in liquid form was confirmed by a stable isotope study (**Figure 4**b), where erythrocyte incorporation of stable isotopes after gavage administration of ^{57}Fe-FibBLG (RBV 99%) and ^{58}Fe-Nano (RBV 96%) was not significantly different from $^{54}FeSO_4$ (**Figure 4**e). The percentage of Fe(II) against total iron of Fe-Nano (84.9±0.2%) and Fe-FibBLG (83.1±0.4%) after acidic digestion was comparable to $FeSO_4$ (92.2±0.3%) (Extended Data **Table 2**), possibly explaining their high RBV. Although there was no significant difference in RBV among Fe-Nano, Fe-FibBLG and $FeSO_4$, it should be noted that

Fe-Nano cannot be used in liquid applications because it does not form a stable colloidal dispersion but agglomerates and precipitates at pH 3 as clearly shown in Extended Data **Figure 5**. Additionally, colloidal stability of Fe-FibBLG and Fe-Nano in powder form was tested by re-dispersing the compounds at pH 7 (Extended Data **Figure 5**). Fe-FibBLG formed a stable transparent dispersion, similar to that freshly made at pH 3, while Fe-Nano powder at pH 7 formed a dark yellow turbid solution with flocculated precipitates. The high RBV of Fe-FibBLG combined with excellent colloidal stability suggest that this new hybrid material is a versatile and easy to implement approach to fortify iron in liquid matrices.

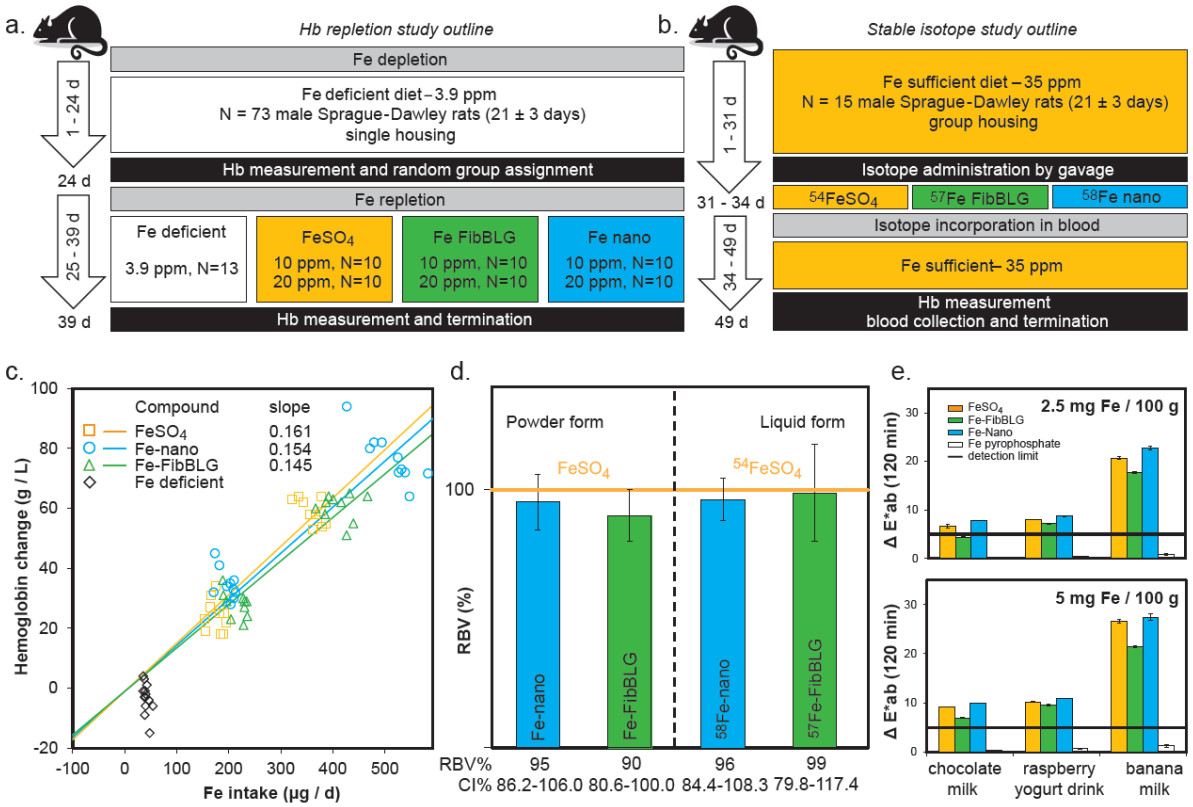

Figure 4: Animal Study design, Hb changes given by Fe-FibBLG and Fe Nano and color changes after fortification. a. Outline of the Hb-repletion study. For 24-25 days 73 rats were made iron deficient (depletion). Over 15 days, 60 rats were fed 3 iron sources incorporated in the pellet diets with 10 or 20 ppm iron (repletion). Over the entire study, 13 and 3 rats received iron deficient (3.9 ppm) and sufficient (35 ppm) diets, respectively. **b**. Outline of the stable isotope randomized crossover study. Stable isotopes ^{54}Fe, ^{58}Fe and ^{57}Fe were gavaged in liquid form at study days 32, 33, and 34. **c**. Dose-response curves with slopes calculated between iron intake and change in Hb. **d**. RBV% with confidence intervals (CI) for powder and liquid compounds against $FeSO_4$ (100%). No statistical difference in RBV was detected between compounds or when compared to $FeSO_4$ in both powder and liquid form ($p>0.05$). **e**. Sensory performance of iron-containing compounds in powder form, compared to $FeSO_4$ and FePP in selected food matrices at 2.5 and 5 mg iron / 100 g food matrix. Absolute color change, ΔE^*_{ab}±sd, of 2 replicates is given at 120 min against the non-fortified matrix.

Having established the potential of Fe-FibBLG in the liquid form, sensory performance of the hybrid in the powder form was further analyzed at 2.5 and 5 mg iron / 100 g food in

chocolate milk, fruit yogurt drink and banana milk (**Figure 4**e), using $FeSO_4$ and iron pyrophosphate (FePP) as positive and negative standards, respectively. ΔE, the value for color change, was determined by colorimetry. FePP shows the least organoleptic changes, however, it is poorly soluble and tends to precipitate in liquid matrices (Extended Data **Figure 5**). Both Fe-FibBLG and Fe-Nano caused color changes due to reaction with polyphenols (Hilty *et al.*, 2010; Hurrell, 2007), however, Fe-FibBLG showed significantly less color changes than $FeSO_4$ and for chocolate milk this change was lower than the detection limit of 5 ΔE*ab. Additionally, it should be noted that further washing steps could be applied to lower the content of reactive iron salts in the hybrid material thus reducing color changes, shall this become a critical determinant. These results taken together demonstrate that Fe-FibBLG is an ideal carrier and delivery system for nanosized iron, as bioavailable as FeSO4 but with improved sensory performance, and colloidally more stable than standard forms of nanosized iron.

To summarize, we synergistically combined organic and inorganic materials to produce highly bioavailable and cost-effective iron amyloid fibril hybrids. BLG fibrils with reducing effect properties were used to carry iron nanoparticles for food fortification for the first time. The resulting hybrid material, available in both powder and liquid forms, was shown to have excellent physical stability, chemical properties and undergo fast acid dissolution and enzymatic digestion demonstrated *in-vitro*. This material has a bioavailability equivalent to ferrous sulfate in Hb repletion and stable isotope studies in rats, without any tissue accumulation, and demonstrates less organoleptic changes in foods. Its reducing-antioxidant effects, stability in aqueous dispersion, improved sensory performance and high bioavailability demonstrate that iron-amyloid fibril hybrids are promising novel iron fortificants in both solid and liquid foods.

Acknowledgements

The authors gratefully thank for their support during the animal study: Erna Kemp, Hylton Bunnting, Christophe Zeder and Antoniette Fick. We thank Christophe Zeder, Adam Krzystek and Timo Christ for the isotope analyses. We thank Luciano Molinari for performing the statistical analyses.

References

Acosta E., 2009, Bioavailability of nanoparticles in nutrient and nutraceutical delivery: Current Opinion in Colloid & Interface Science, v. 14, no. 1, p. 3-15.

Adamcik J., Jung J. M., Flakowski J., De Los Rios P., Dietler G., and Mezzenga R., 2010, Understanding amyloid aggregation by statistical analysis of atomic force microscopy images: Nature Nanotechnology, v. 5, no. 6, p. 423-428.

Allen L., de Benoist B., Dary O., and Hurrell R., 2006, Guidelines on food fortification with micronutrients, Geneva: World Health Organization.

Barnhart M. M., and Chapman M. R., 2006, Curli biogenesis and function: Annual Review of Microbiology, v. 60, p. 131-147.

Bateman L., Ye A. Q., and Singh H., 2010, In vitro digestion of beta-lactoglobulin fibrils formed by heat treatment at low ph: Journal of Agricultural and Food Chemistry, v. 58, no. 17, p. 9800-9808.

Bolisetty S., and Mezzenga R., 2016, Amyloid-carbon hybrid membranes for universal water purification: Nature Nanotechnology, v. 11, no. 4, p. 365-+.

Bolisetty S., Vallooran J. J., Adamcik J., Handschin S., Gramm F., and Mezzenga R., 2011, Amyloid-mediated synthesis of giant, fluorescent, gold single crystals and their hybrid sandwiched composites driven by liquid crystalline interactions: Journal of Colloid and Interface Science, v. 361, no. 1, p. 90-96.

Brosnan J. T., and Brosnan M. E., 2006, The sulfur-containing amino acids: An overview: The Journal of Nutrition, v. 136, no. 6, p. 1636s-1640s.

Cunniff P., 1997, Aoac official method 9743.1: Bioavailability of iron: Rat hemoglobin repletion bioassay., Official methods of analysis of aoac international: Gaitherburg, AOAC International, p. 62-63.

Forbes A. L., Arnaud M. J., Chichester C. O., Cook J. D., Harrison B. N., Hurrell R. F., Kahn S. G., Morris E. R., Tanner J. T., and Whittaker P., 1989, Comparison of in vitro, animal, and clinical determinations of iron bioavailability: International nutritional anemia consultative group task force report on iron bioavailability: American Journal of Clinical Nutrition, v. 49, no. 2, p. 225-238.

Fowler D. M., Koulov A. V., Alory-Jost C., Marks M. S., Balch W. E., and Kelly J. W., 2006, Functional amyloid formation within mammalian tissue: Plos Biology, v. 4, no. 1, p. 100-107.

Gao G. Q., and Xu A. W., 2013, A new fluorescent probe for monitoring amyloid fibrillation with high sensitivity and reliability: Rsc Advances, v. 3, no. 43, p. 21092-21098.

Hallberg L., Brune M., Erlandsson M., Sandberg A. S., and Rossanderhulten L., 1991, Calcium - effect of different amounts on nonheme-iron and heme-iron absorption in humans: American Journal of Clinical Nutrition, v. 53, no. 1, p. 112-119.

Hallberg L., Brune M., and Rossander L., 1989, Iron-absorption in man - ascorbic-acid and dose-dependent inhibition by phytate: American Journal of Clinical Nutrition, v. 49, no. 1, p. 140-144.

Hilty F. M., Arnold M., Hilbe M., Teleki A., Knijnenburg J. T. N., Ehrensperger F., Hurrell R. F., Pratsinis S. E., Langhans W., and Zimmermann M. B., 2010, Iron from nanocompounds containing iron and zinc is highly bioavailable in rats without tissue accumulation: Nature Nanotechnology, v. 5, no. 5, p. 374-380.

Huber D. L., 2005, Synthesis, properties, and applications of iron nanoparticles: Small, v. 1, no. 5, p. 482-501.

Hurrell R., 2007, Linking the bioavailability of iron compounds to the efficacy of iron-fortified foods: International Journal for Vitamin and Nutrition Research, v. 77, no. 3, p. 166-173.

Hurrell R. F., 2002, Fortification: Overcoming technical and practical barriers: The Journal of Nutrition, v. 132, no. 4, p. 806-812.

Hurrell R. F., Reddy M., and Cook J. D., 1999, Inhibition of non-haem iron absorption in man by polyphenolic-containing beverages: British Journal of Nutrition, v. 81, no. 4, p. 289-295.

Iconomidou V. A., Vriend G., and Hamodrakas S. J., 2000, Amyloids protect the silkmoth oocyte and embryo: Febs Letters, v. 479, no. 3, p. 141-145.

Kassebaum N. J., Jasrasaria R., Naghavi M., Wulf S. K., Johns N., Lozano R., Regan M., Weatherall D., Chou D. P., Eisele T. P., Flaxman S. R., Pullan R. L., Brooker S. J., and Murray C. J. L., 2014, A systematic analysis of global anemia burden from 1990 to 2010: Blood, v. 123, no. 5, p. 615-624.

Knowles T. P. J., and Mezzenga R., 2016, Amyloid fibrils as building blocks for natural and artificial functional materials: Advanced Materials, p. n/a-n/a.

Leal S. S., Botelho H. M., and Gomes C. M., 2012, Metal ions as modulators of protein conformation and misfolding in neurodegeneration: Coordination Chemistry Reviews, v. 256, no. 19-20, p. 2253-2270.

Li C. X., Adamcik J., and Mezzenga R., 2012, Biodegradable nanocomposites of amyloid fibrils and graphene with shape-memory and enzyme-sensing properties: Nature Nanotechnology, v. 7, no. 7, p. 421-427.

Maddelein M. L., Dos Reis S., Duvezin-Caubet S., Coulary-Salin B., and Saupe S. J., 2002, Amyloid aggregates of the het-s prion protein are infectious: Proceedings of the National Academy of Sciences of the United States of America, v. 99, no. 11, p. 7402-7407.

Maji S. K., Perrin M. H., Sawaya M. R., Jessberger S., Vadodaria K., Rissman R. A., Singru P. S., Nilsson K. P. R., Simon R., Schubert D., Eisenberg D., Rivier J., Sawchenko P., Vale W., and Riek R., 2009, Functional amyloids as natural storage of peptide hormones in pituitary secretory granules: Science, v. 325, no. 5938, p. 328-332.

Paris O., Aichmayer B., and Fratzl P., 2006, Small-angle scattering from spherical particles on randomly oriented interfaces: Zeitschrift Fur Metallkunde, v. 97, no. 3, p. 290-294.

Rohner F., Ernst F. O., Arnold M., Hibe M., Biebinger R., Ehrensperger F., Pratsinis S. E., Langhans W., Hurrell R. F., and Zimmermann M. B., 2007, Synthesis, characterization, and bioavailability in rats of ferric phosphate nanoparticles: The Journal of Nutrition, v. 137, no. 3, p. 614-619.

Sun Y. P., Li X. Q., Cao J. S., Zhang W. X., and Wang H. P., 2006, Characterization of zero-valent iron nanoparticles: Advances in Colloid and Interface Science, v. 120, no. 1-3, p. 47-56.

Zimmermann M. B., and Hurrell R. F., 2007, Nutritional iron deficiency: Lancet, v. 370, no. 9586, p. 511-520.

Extended data: Figures and tables

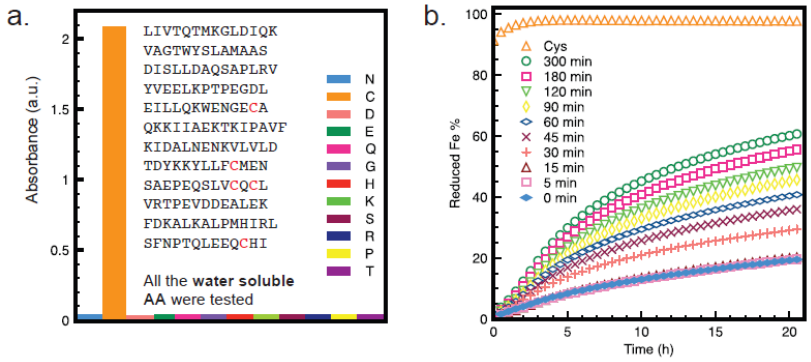

Extended Data Figure 1: a. The reducing effect of 12 water-soluble amino acids present among the 162 residues of BLG (listed in the middle of the plot) was tested using a colorimetric method. Cysteine showed the highest absorption. **b.** The reducing effect of BLG fibrils increases with increasing fibrillization level at different incubation time points. Cysteine was used with the same concentration ratio as comparison.

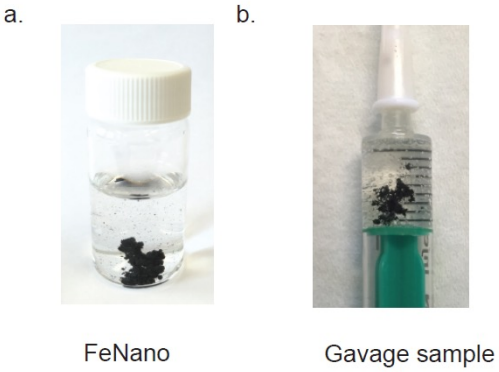

Extended Data Figure 2: **a**. Photograph of a freshly made Fe-Nano dispersion. Black iron clusters sediment to the bottom of the glass bottle. **b.** Similar aggregation occurred when the Fe-Nano dispersion was prepared in a syringe for gavage animal study.

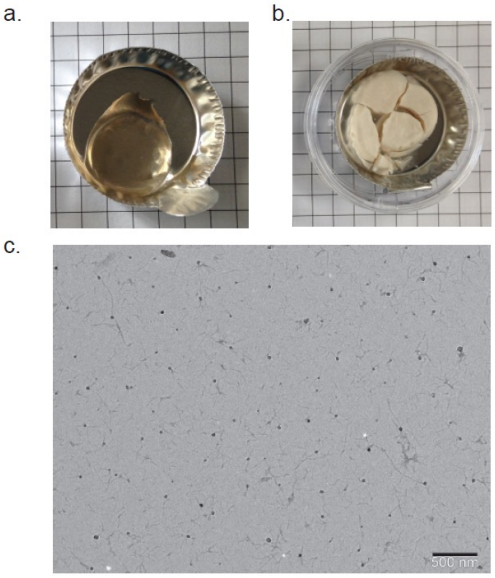

Extended Data Figure 3: a. Photographs of gel made out of Fe-FibBLG. and **b.** powder after freeze dry. **c.** TEM image of re-dispersed powder Fe-FibBLG.

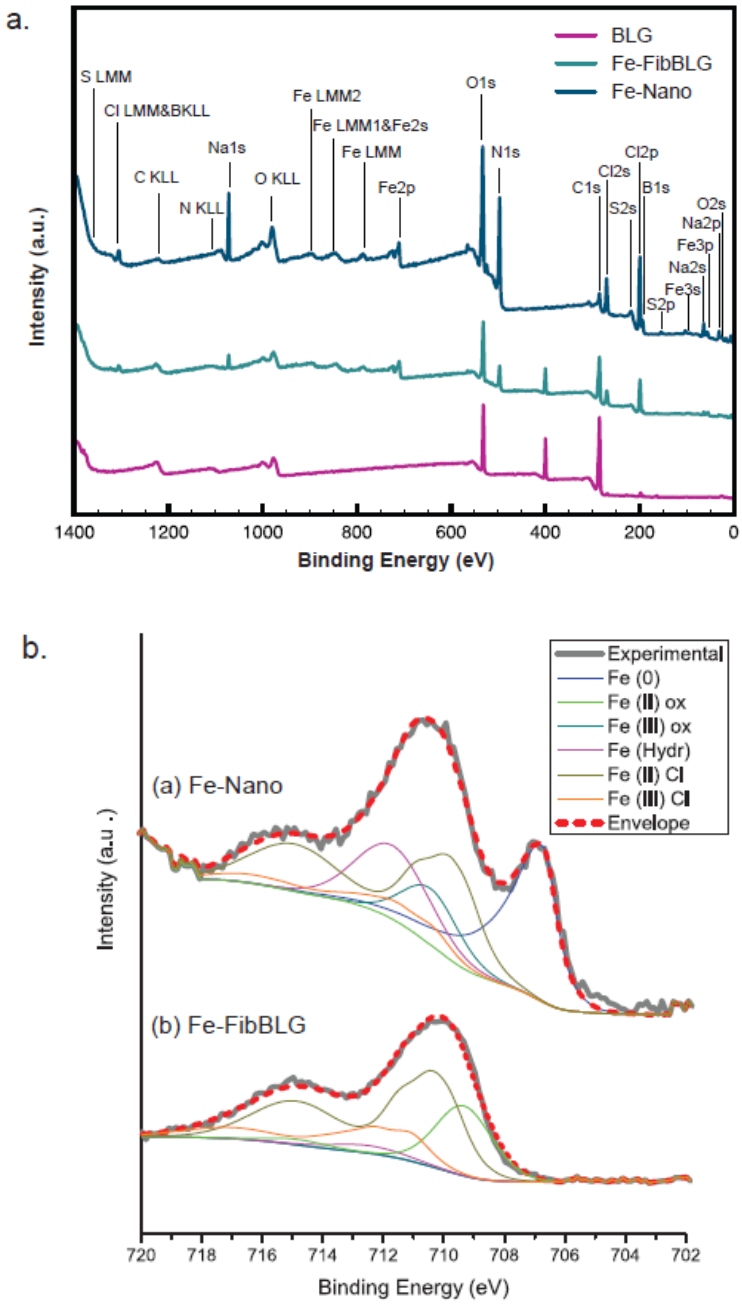

Extended Data Figure 4: a. XPS survey spectra of BLG, Fe-FibBLG and Fe-Nano. **b.** Fe $2p_{3/2}$ spectra of (a) Fe-Nano, (b) Fe-FibBLG. All samples were freeze-dried before XPS characterization.

Extended Data Table 1: Peak area % mean value of dried compounds from XPS measurements.

	Fe-Nano	Fe-FibBLG
Fe (0)	29.5 (0.8)	0.9 (1.4)
Fe (II) Ox	-	21.2 (0.6)
Fe (III) Ox	12 (1)	-
Fe (III) oxi-hyd	18 (4)	5 (2)
Fe (II) – Cl	33 (2)	53 (3)
Fe (III) – Cl	8 (2)	19.9 (0.9)

Extended Data Table 2: Iron content of dried compounds and Fe(II) percent in total iron after acidic *in-vitro* digestion.

	Fe content (g/100g)	Fe(II) % after acidic digestion	
	Powder form	Powder form mixed with diet	Liquid form for gavage
Fe-Nano	11.9	14 ± 3	84.9 ± 0.2
Fe-FibBLG	7.0	35 ± 4	83.1 ± 0.4
$FeSO_4$	32.0	37 ± 2	92.2 ± 0.3

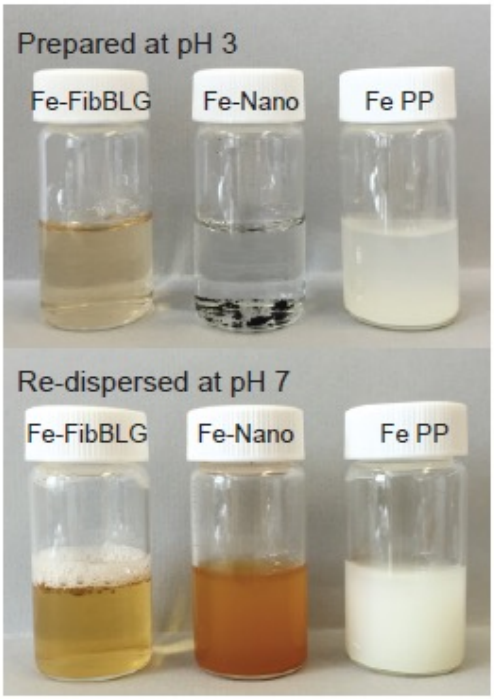

Extended Data Figure 5: Photographs of Fe-FibBLG, Fe-Nano and FePP dispersions at pH 3 and pH 7.

Extended Data Table 3: Depletion-repletion model. Fe fortification level, fortified Fe intake, body weight gain, change in Hb in Fe-depleted rats during 14 d repletion period, GSH level and histologically detected changes at the end of the repletion period.

Fe compound	n	**Fortification level**	**Fe intake**[+&]	**Body weight gain**[*]	**Hb change**[#]	**Food intake**[+]	n	**GSH/protein**[*]	**Histology**
		mg Fe/kg diet	**ug/d**	**g/14 d**	***baseline Hb*** **g/L**	**g/14 d**		**µmol/g protein**	**n investigated / n detected changes**
Fe deficient	13	3.9 ± 0.4	41 ± 5	24 ± 11 [a]	-3.2 ± 5.1 *48.6 ± 9.3*	149 ± 19 [a]	13	6.5 ± 1.3 [a]	8 / 0
$FeSO_4$	10	12.1 ± 0.5	175 ± 15 [a]	61 ± 8 [b]	24.2 ± 5.4 [a] *43.6 ± 5.1*	202 ± 17 [b]	10	7.8 ± 0.6 [a]	5 / 0
	10	21.1 ± 0.7	361 ± 22 [b]	84 ± 9 [cd]	59.0 ± 4.1 [α] *43.8 ± 5.5*	240 ± 14 [c]	7	7.4 ± 0.5 [a]	5 / 0
Fe-FibBLG	10	14.2 ± 1.6	217 ± 20 [c]	65 ± 10 [b]	27.9 ± 4.4 [a] *43.9 ± 3.5*	214 ± 19 [bd]	9	7.8 ± 0.7 [a]	5 / 0
	10	24.3 ± 0.9	411 ± 30 [d]	85 ± 7 [c]	60.4 ± 4.5 [α] *43.6 ± 4.2*	237 ± 18 [c]	9	7.0 ± 0.8 [a]	5 / 0
Fe-Nano	10	13.0 ± 1.1	197 ± 16 [c]	72 ± 9 [bd]	34.6 ± 5.1 [b] *44.0 ± 4.3*	211 ± 17 [bd]	10	7.4 ± 1.2 [a]	6 / 0
	10	29.1 ± 2.2	511 ± 43 [e]	91 ± 9 [c]	76.6 ± 8.4 [β] *43.5 ± 4.9*	246 ± 21 [c]	9	7.1 ± 1.4 [a]	5 / 0
Fe sufficient	3	34.0 ± 0.5	-	80 ± 4 [bc]	-	-	3	7.0 ± 1.1 [a]	3 / 0

NOTES: mean ± sd. Means in a column without a common superscript letter (a–n or Greek letters α, β and γ) differ significantly, $p < 0.05$ (ANOVA, Bonferroni).

+ Comparison was done between all the groups, excluding Fe-deficient and Fe-sufficient groups.

* Comparison was done between all the groups.

Comparison was done between for the low-Fe groups (superscript letters a-n) and the high-Fe groups (superscript Greek letters α and β) separately, excluding Fe-deficient and Fe-sufficient groups. No Differences in *baseline Hb* were detected.

& Data were Log10 transformed before ANOVA to ensure homogeneity of variance, not transformed data are shown.

Hb = hemoglobin. GSH = glutathione.

Extended Data Table 4: Diet composition of the Fe deficient AIN-93G purified rodent diet (#115072), with Fe content in ppm.

Ingredient	Diet					
	Fe deficient	$FeSO_4$ 10 ppm	$FeSO_4$ 20 ppm	$FeSO_4$ 35 ppm	Fe FibBLG/Fe-Nano 10 ppm	Fe FibBLG/Fe-Nano 20 ppm
Casein, g/kg	200	200	200	200	200	200
Sucrose, g/kg	100	98	96	93	90	80
Cornstarch, g/kg	397.486	397.486	397.486	397.486	397.486	397.486
Dyetrose, g/kg	132	132	132	132	132	132
L-Cysteine, g/kg	3	3	3	3	3	3
Cellulose (microcrystalline), g/kg	50	50	50	50	50	50
Soybean oil, g/kg	70	70	70	70	70	70
t-Buthylhydroquinone, g/kg	0.014	0.014	0.014	0.014	0.014	0.014
Mineral Mix #215009 (Rx, no Fe), g/kg	35	35	35	35	35	35
Vitamin mix #310025, g/kg	10	10	10	10	10	10
Choline bitartrate, g/kg	2.5	2.5	2.5	2.5	2.5	2.5
Fe premix 5 mg/g, g/kg	-	2	4	7	-	-
Fe premix 1 mg/g, g/kg	-	-	-	-	10	20

Extended Data Table 5: Results of the histological examination divided by compound and iron fortification level. Fe(II) or (III) positive results shown in bold.

		Group							
		Deficient	$FeSO_4$		Fe-FibBLG		Fe-Nano		$FeSO_4$
	Fe (mg/kg diet)	3.9	10	20	10	20	10	20	35
	N study	13	10	10	10	10	10	10	3
Organ									
Salivary gland	*n* changes / *n* investigated [a]	0 / 6	0 / 4	0 / 5	0 / 4	0 / 4	0 / 5	0 / 5	0 / 3
	Fe(III) positive	0	0	0	0	0	0	0	0
	Fe(II) positive	0	0	0	0	0	0	0	0
Lungs	*n* changes / *n* investigated	8 / 8	5 / 5	5 / 5	5 / 5	5 / 5	6 / 6	5 / 5	5 / 5
	light atelectasis (euthanasia artefact)	0	0	0	0	1	2	2	0
	light atelectasis / light BALT-hyperplasia	4	1	4	2	1	2	2	2
	light atelectasis / strong BALT- hyperplasia	0	1	1	0	1	0	1	1
	strong atelectasis	0	0	0	1	0	0	0	0
	strong atelectasis / light BALT- hyperplasia	0	0	0	1	0	1	0	0
	strong atelectasis / strong BALT- hyperplasia	4	3	0	1	2	1	0	0
	Fe(III) positive	0	0	0	0	0	0	0	0
	Fe(II) positive	0	0	0	0	0	0	0	0
Thymus	*n* changes / *n* investigated	0 / 8	0 / 5	0 / 5	0 / 5	0 / 5	0 / 6	0 / 5	0 / 3
	Fe(III) positive	0	0	0	0	0	0	0	**3**
	Fe(II) positive	0	0	0	0	0	0	0	0
Heart	*n* changes / *n* investigated	1 / 8	1 / 5	1 / 5	0 / 5	1 / 5	0 / 6	1 / 6	0 / 3
	lymphocytes and plasma-cells in myocardium	1	0	0	0	0	0	1	0
	light fibrosis	0	1	1	0	0	0	0	0
	light adventitial fibrosis	0	0	0	0	1	0	0	0
	Fe(III) positive	0	0	0	0	0	0	0	0
	Fe(II) positive	0	0	0	0	0	0	0	0
Kidney	*n* changes / *n* investigated	0 / 8	0 / 5	0 / 5	0 / 5	0 / 5	0 / 6	0 / 5	0 / 3
	Fe(III) positive	0	0	0	0	0	0	0	0
	Fe(II) positive	0	0	0	0	0	0	0	0
Stomach	*n* changes / *n* investigated	0 / 8	0 / 5	0 / 5	0 / 5	0 / 5	0 / 6	0 / 5	0 / 3
	Fe(III) positive	0	0	0	0	0	0	0	0
	Fe(II) positive	0	0	0	0	0	0	0	0

Extended Data Table 5: Results of the histological examination divided by compound and iron fortification level. Fe(II) or (III) positive results shown in bold.

		Group							
		Deficient	$FeSO_4$		Fe-FibBLG		Fe-Nano		$FeSO_4$
	Fe (mg/kg diet)	3.9	10	20	10	20	10	20	35
	N study	13	10	10	10	10	10	10	3
Organ									
Brain	*n* changes / *n* investigated	1 / 8	0 / 5	0 / 5	0 / 5	0 / 5	0 / 6	0 / 5	0 / 3
	vacuolation (euthanasia artefact)	1	0	0	0	0	0	0	0
	Fe(III) positive	0	0	0	0	0	0	0	0
	Fe(II) positive	0	0	0	0	0	0	0	0
Liver	*n* changes / *n* investigated	5 / 8	5 / 5	2 / 5	2 / 5	1 / 5	2 / 6	0 / 5	1 / 3
	artefact (euthanasia)	0	0	0	0	0	0	0	1
	light extramedullary formation	5	4	1	1	1	1	0	0
	light extramedullary formation / neutrophils and hepatocytes in cytoplasm	0	0	1	0	0	0	0	0
	light extramedullary formation / neutrophils, hepathocytes and plasmacells in portal region	0	0	0	0	0	1	0	0
	strong extramedullary formation	0	1	0	1	0	0	0	0
	Fe(III) positive	0	0	0	0	0	0	0	0
	Fe(II) positive	0	0	0	0	0	0	0	0
Spleen	*n* changes / *n* investigated	8 / 8	5 / 5	5 / 5	5 / 5	5 / 5	6 / 6	5 / 5	3 / 3
	active white pulp / extramedullary blood formation	8	5	5	5	5	5	5	3
	extramedullary blood formation	0	0	0	0	0	1	0	0
	Fe(III) positive	0	0	0	0	0	0	**1**	0
	Fe(II) positive	0	0	0	0	0	0	0	0
Testes	*n* changes / *n* investigated	2 / 8	2 / 5	2 / 5	3 / 5	1 / 5	2 / 6	3 / 5	0 / 3
	degenerated spermatogonia / round spermatids in epididymis	0	0	0	1	0	0	0	0
	round spermatids in epididymis	2	2	0	1	1	2	3	0
	Sertoli cell / no spermatids	0	0	1	0	0	0	0	0
	spermatogonia (degeneration)	0	0	1	1	0	0	0	0
	Fe(III) positive	0	0	0	0	0	0	0	0
	Fe(II) positive	0	0	0	0	0	0	0	0

Extended Data Table 5: Results of the histological examination divided by compound and iron fortification level. Fe(II) or (III) positive results shown in bold.

		Group Deficient	$FeSO_4$		Fe-FibBLG		Fe-Nano		$FeSO_4$
	Fe (mg/kg diet)	3.9	10	20	10	20	10	20	35
	N study	13	10	10	10	10	10	10	3
Organ									
Pancreas [b]	*n* changes / *n* investigated	0 / 3	0 / 2	0 / 3	0 / 3	0 / 3	0 / 4	0 / 2	0 / 1
	Fe(III) positive	0	0	**1**	0	0	**1**	0	0
	Fe(II) positive	0	0	0	0	0	0	0	0
Small intestine[1]	*n* changes / *n* investigated	0 / 8	0 / 5	0 / 5	0 / 5	0 / 5	0 / 6	0 / 5	0 / 3
	Fe^{3+} positive	**1**	0	**1**	**1**	**1**	**1**	**1**	**3**
	cytoplasm enterocytes	0	0	0	0	0	0	0	1
	duodenum	0	0	0	0	0	1	1	0
	duodenum/jejunum	0	0	0	0	0	0	0	2
	jejunum	1	0	0	0	0	0	0	0
	ileum	0	0	0	1	1	0	0	0
	duodenum/jejunum/ileum	0	0	1	0	0	0	0	0
	Fe^{2+} positive	**1**	0	0	0	0	**1**	0	**1**
	duodenum	0	0	0	0	0	1	0	0
	duodenum/jejunum	0	0	0	0	0	0	0	1
	jejunum	1	0	0	0	0	0	0	0
Large intestine[2]	*n* changes / *n* investigated	0 / 8	0 / 5	0 / 5	0 / 5	0 / 5	0 / 6	0 / 5	0 / 3
	Fe(III) positive	0	0	**1**	0	0	**1**	**1**	**1**
	Fe(II) positive	0	0	0	0	0	0	0	0
Mesenteric lymph nodes [b]	*n* changes / *n* investigated	0 / 1	0 / 3	0 / 1	0 / 2	0 / 2	0 / 1	0 / 0	0 / 0
	Fe(III) positive	0	0	0	0	0	0	-	-
	Fe(II) positive	0	0	0	0	0	0	-	-
Mediastinal lymph nodes [b]	*n* changes / *n* investigated	0 / 3	0 / 2	0 / 3	0 / 1	0 / 3	0 / 5	0 / 2	0 / 0
	Fe(III) positive	0	**1**	0	0	0	**1**	0	-
	Fe(II) positive	0	0	0	0	0	0	0	-

Extended data: Materials and methods

1. Hybrids production

β-lactoglobulin (BLG) was purchased from Technische Universität Munich, Department of Food Process Engineering and Dairy Technology, Munich, Germany (>98%). BLG was used after dialysis and BLG amyloid fibrils were prepared based on a previously reported protocol (Jung and Mezzenga, 2010). Purified H2O was used with varied pH values adjusted by HCl. For neutron scattering measurements, D_2O and DCl were used instead.

Iron (Fe) nanoparticles were composited onto BLG fibrils (Fe-FibBLG) by in-situ chemical reduction of $FeCl_3.6H_2O$ (97%, Sigma-Aldrich). First, 2 wt % of BLG fibrils at pH 2 were mixed with 0.1 M $FeCl_3.6H_2O$ solution. Fe(III) ions that bound to BLG fibrils were then chemically reduced by NaBH4 (≥99%, Sigma-Aldrich) (Amar-Yuli *et al.*, 2011; Li *et al.*, 2006). The final concentrations of BLG fibrils, $FeCl_3$ and $NaBH_4$ were 0.45 wt %, 0.015 M and 0.026 M. The iron/protein weight ratio was 1:5. By reducing the $FeCl_3.6H_2O$ solution alone with $NaBH_4$ at the same concentrations, iron nanoparticles were obtained (Fe-Nano).

2. Reducing effect colorimetric test

A 2 wt % BLG fibrils solution was mixed with 0.1 M $FeCl_3.6H_2O$ (97%, Sigma-Aldrich) to reach final iron/protein weight ratios of 1:2, 1:5, 1:10. The presence of Fe(II) ions was revealed by adding 5 mM 1,10-phenanthroline (≥99%, Sigma-Aldrich) to the solution and the distinctive orange color was measured at 512 nm wavelength (Tecan, 200 PRO multimode reader, Switzerland).

In order to measure the contribution of each amino acid (AA) residuum of BLG to the reducing effect, only the ones that are water soluble at experimental conditions were investigated. In short, asparagine, cysteine, aspartic acid, glutamic acid, glutamine, glycine, histidine, lysine, serine, arginine, proline and threonine were mixed with $FeCl_3$ to a final iron/AA weight ratio of 1:2 and measured for absorbance as described above.

The influence of fibrillization level of BLG on the reducing effect was tested by preparing the BLG amyloid fibrils and measuring the reducing effect at selected time points. A BLG solution (2 wt %, pH 2) was incubated at 90°C for 5 hours and samples were taken after 0, 5, 15, 30, 45, 60, 90, 120, 180 and 300 minutes. The fluorescent dye thiazole orange was used to

indicate the fibrillization level with excitation wavelength 421 nm and emission wavelength 455 nm by plate reader (Tecan, 200 PRO multimode reader) (Gao and Xu, 2013). These solutions were mixed with $FeCl_3$ with final concentration BLG fibrils 36.7 µM and $FeCl_3$ 166.7 µM aiming to have Fe(III) completely reduced (there are 5 cysteine residues in 1 BLG and equal amount of cysteine and FeCl3 are needed to have complete reduction reaction). The amount of Fe(II) produced over time was estimated from the calibration curve made from $FeSO_4.7H_2O$ (≥99%, Sigma-Aldrich) solutions with concentrations 0, 20, 50, 100, 200, 400 µM. To exclude the time effect a series of calibration curves were used at different time points. Cysteine was tested in the same experiment as a comparison.

3. Hybrids characterization methods

3.1 Transmission electron microscopy (TEM)

TEM imaging was performed on copper grids covered with a carbon layer (Electron Microscopy Sciences) without staining. A 4 µl dispersion was placed on the grids for 1 minute then drained and washed with purified water twice. The images were taken on dried grids by bright-field TEM (FEI, Morgagni 268, USA) operated at high voltage 100 kV.

3.2 Small angle neutron scattering (SANS)

SANS experiments were performed at the SANS I beamline of the Swiss Neutron source at the Paul Scherer Institute (PSI), Switzerland. For these experiments the samples were prepared in a series of D_2O and H_2O mixtures to obtain different scattering contrasts. The ratio 50:50 of D_2O:H_2O was used as solvent to match the contrast of BLG fibrils. Conversely, 100:0 of D_2O:H_2O was used to contrast match iron nanoparticles. The wavelength of the incident beam was λ=0.5269 nm, and the sample to detector distance was 18 m. The q range over which the data could be reliably collected was 0.01–0.1 nm^{-1}. The raw spectra were corrected for background from the solvents, electronic noise and detector efficiency according to standard SANS I procedure. The 2D scattering spectra at the primary Bragg peak was radially averaged by GRASP program. 1D contrast matching scattering data with the solvent ratio D_2O:H_2O=50:50 was fitted with the mass fractal model using SASFIT program (Bressler *et al.*, 2015).

3.3 Energy-dispersive X-ray spectroscopy (EDX)

The components of the material were detected by EDX. Samples were prepared with the same procedure as for TEM. Scanning-TEM Hitachi HD 2700 was used to image the samples and detect the elements in the samples.

3.4 X-ray photoelectron spectroscopy (XPS)

The surface chemistry of the hybrid material was investigated by XPS. Samples of BLG fibrils, Fe-Nano and Fe-FibBLG were first freeze-dried and then pressed into small cuvettes mounted on a standard PHI sample holder; this was immediately transferred in the spectrometer to minimize further oxidation. A PHI QuanteraSXM (ULVAC-PHI, USA) spectrometer was used for acquiring the survey and detailed spectra using a monochromatic AlK source (1486.6 eV at 24.3 W; beam size = 100 µm). All spectra were recorded in fixed analyzer transmission mode setting the pass energy at 280 eV and 69 eV when acquiring the survey and the high-resolution spectra respectively. The emission angle was 45°. The base pressure in the analysis chamber was 8.9.10-10 mbar and during analysis 5.0.10-9 mbar. The calibration of the spectrometer was performed following the ISO 15472 – 2010 (last reviewed in 2015); in the analysis conditions here applied the resolution was found to be equal to 0.83 eV (full-width at half height of the Ag $3d_{5/2}$ peak maximum). Charge compensation was achieved using a low-voltage argon ion gun combined with an electron neutralizer; the operating conditions were 1.0 V 20.0 µA. The spectra were further corrected with reference to C1s, at 285.0 eV.

The spectra were processed using CasaXPS software (version 2.3.15 dev.52, Casa Software Ltd, UK). The background subtraction was performed using the Shirley-Sherwood iterative method. After background subtraction, the peaks were fitted using the product of Gaussian and Lorentzian functions and following the approach reported previously (Fantauzzi *et al.*, 2010) as far as the Fe(III) and Fe(II) oxides. The peak fitting of the iron oxy-hydroxide contribution was carried out using the parameters given by (Frau *et al.*, 2010) while the fitting parameters of the Fe(II) and Fe(III) chlorides have been obtained from the spectra acquired using the operating conditions reported above for the fibrils and following Gupta and Grosvenor's approach (Grosvenor *et al.*, 2004; Gupta and Sen, 1974).

3.5 *In-vitro* digestion

In order to observe the digestion of iron nanoparticles and protein fibrils separately at physiological condition, *in-vitro* experiments were performed at two complementary conditions. For the acidic dissolution of iron nanoparticles, 1 mL Fe-FibBLG solution with 0.08 wt% iron content were adjusted to pH 1.2 and shaken at 50 rpm and 37°C for 20 min in a shaking water bath (GFL 1086, Germany) to simulate the physiological condition of stomach (Bateman *et al.*, 2010). For the enzymatic hydrolysis of BLG fibrils, 150 mM NaCl and 2 mg/mL pepsin (from porcine gastric mucosa with 3,200–4,500 units/mg protein, Sigma-Aldrich) were added to the Fe-FibBLG solution at pH 2.7. The samples were shaken at 50 rpm and 37°C for 1 hour.

4. *In-vivo studies*

4.1 Depletion-repletion study

4.1.1 Animals and diets

All experimental procedures were approved by the AnimCare Ethics Committee of the Faculty of Health Science of the North-West University Potchefstroom under ethics number NWU-00152-15-A5.

The bioavailability of the Fe compounds in powder form was determined by the hemoglobin (Hb) repletion method (Cunniff, 1997; Forbes *et al.*, 1989) using two levels of 10 and 20 mg Fe/kg (ppm) for each Fe source (FeSO4 (dried ferrous sulfate, micronized, Dr. Paul Lohmann GmbH, Germany) Fe-FibBLG and Fe-Nano). A schematic outline of the animal study is shown in **Figure 4**a. The base diet was an Fe deficient AIN-93G (Reeves *et al.*, 1993) purified rodent diet (Dyets, Inc., USA, Nr. 115072). Before pelleting, the different Fe sources were added to reach final fortification levels of 10, 20 or 35 ($FeSO_4$ only) ppm. Diet compositions are shown in **Table 6** (Extended data). The final Fe content of all diets was verified by AAS (SpecrAA-240Z with GTA-120 Graphite Tube Atomizer, Varian Techtron) at the Laboratory of Human Nutrition (ETH Zurich, Switzerland). Male Sprague-Dawley rats (n = 76) were bred in the Vivarium of the North West University Potchefstroom (South Africa). At 21 ± 3 days of age, the animals were housed individually in grid (stainless steel) floor cages (Tecniplast, Italy), having ad libitum access to demineralized (18 MΩ, Millipore) water and diet throughout the whole study. A 12:12 h light-dark cycle (lights off at 18:00 h), room temperature of 22 ± 1°C

and relative humidity of 55 ± 15% were ensured. Body weight measurement, health check and animal handling to reduce stress at blood collection and euthanasia were performed 3 times per week. The animals were trained to enter the restrainer 3 days before sampling. The animals were depleted in Hb for a period of 24 d during which they were fed the Fe deficient diet (3.9 ppm). At the end of the depletion period, the animals were weighed, restrained and blood was collected from the tail vein into EDTA coated capillary tubes (Microvette 200/300, Sarstedt, Germany) for the measurement of Hb (BC-5300 Vet, Auto Hematology Analyzer, Mindray, China). The rats were assigned to groups so that the average baseline Hb was not significantly different between groups. During the repletion period of 14 d, the rats received either one of the test compounds (10 or 20 ppm, n = 10) or the Fe deficient diet (n = 13). One additional Fe sufficient group (n = 3) was fed the diet containing 35 ppm $FeSO_4$ and served as a control with normal organ structure for the histological investigation. At the end for the repletion period, the animals were restrained and blood was collected from the tail vein and Hb measured. Individual food intake during the repletion period was recorded every second day by subtracting the amount of food refused and spilled on the collection tray (paper lined underneath the wired cage floor) from the amount that was offered.

At the end of the study, the animals were deeply anesthetized with an IP injection of Sodium pentobarbitone (Euthapent(r), Kyron Laboratories Ltd, South Africa) and blood was collected (DB Vacutainers, K_2E(EDTA), United Kingdom) from the beating heart. Two aliquots were transferred to a 2 mL Eppendorf tube and stored at -80°C for measurement of glutathione in whole blood (GSH whole blood / protein ratio).

4.1.2 Glutathione (GSH) measurement

Briefly, whole blood was unfrozen for 1 hour on ice and diluted (5% v/v) with extraction buffer. The suspension was sonicated in a cup horn sonicator (with 40% amplitude, 15 cycles of 10 sec on / 5 sec off, 2 min and 30 sec; Vibra-cell, Sonics and Materials, United States) and centrifuged (14’000 g, 14 min, +4°C; Centrifuge 5418R, Eppendorf, Germany). The supernatant was collected and diluted (0.6% v/v) with extraction buffer, incubated on ice for 30 min and centrifuged (14’000 g, 15 min, +4°C). The second supernatant was collected and GSH was measured in duplicate using the assay described by Rahman *et al.* Rahman *et al.* (2006). The extraction buffer used in the GSH assay was prepared daily by diluting 0.1%

triton-X 100 (Roche, Switzerland) and 0.6% sulfosalicylic acid (EDTA free, Roche) in 0.1 M potassium phosphate buffer with 5 mM EDTA disodium salt (Sigma, United States), pH 7.5. Protein content of the second supernatant was measured in duplicate using the Pierce™ BCA Protein Assay Kit (Thermo Fisher Scientific, United States) following kit's manual for microplate procedure. GSH and protein contents were measured at 412 and 562 nm wavelength, respectively at 20°C (Infinite 200 Pro microplate reader, Tecan, Switzerland) and the final values for GSH (µM) and protein (g/L) extrapolated from standard calibration curve and the GSH whole blood / protein ratio (µmol/g prot) calculated.

4.1.3 Histology

The following organs were excised and fixed in 10% formalin for histological analysis: brain, heart, liver median lobe, stomach, duodenum, ileum, jejunum, caecum, colon, spleen, kidneys, heart, lungs and thymus. Formalin solution was prepared by mixing 1:10 v/v PBS (Sodium chloride for analysis, Merck; di-Sodium hydrogen phosphate dodecahydrate, for analysis, Merck; sodium di-hydrogen phosphate monohydrate, for analysis, Merck) and formaldehyde solution (formaldehyde solution 38% v/v, Medicolab cc., Amalgam, South Africa). For light microscopy, tissues were dehydrated with xylene and a descending alcohol row (Tissue Tek VIP), paraffin embedded, and stained with haematoxylin/eosin (H&E), Prussian Blue for detection of Fe(III) ions and Turnbull Blue for detection of Fe(II) ions. The veterinary pathologist (University of Zurich, Switzerland) examined histologically 5-6 animals of each test group, 8 animals from the Fe deficient group and 3 animals for the Fe sufficient group and was unaware of the group assignment.

4.2 Stable isotopes study

4.2.1 Animals and diets

All experimental procedures were approved by the AnimCare Ethics Committee of the Faculty of Health Science of the North-West University Potchefstroom under ethics number NWU-00152-15-A5. A schematic outline of the animal study is shown in **Figure 4**b. Male Sprague-Dawley rats (n = 30) were bred in the Vivarium of the North-West University Potchefstroom (South Africa). At 21 ± 3 days of age, the animals were housed in groups of 3 in individually ventilated cages for 31 days, having ad libitum access to demineralized (18 MΩ, Millipore) water and diet (35 ppm) throughout the whole study with a 12:12 h light-

dark cycle (lights off at 18:00 h), room temperature of 22 ± 1°C and relative humidity of 55 ± 15%. After 31 days of adaptation, the animals were fasted for 10-12 h in order to ensure gastric emptiness and the food was given back daily 2 hours post administration. The animals were divided into 2 groups (n = 15 each) and the isotope-labelled compound in liquid form (0.5 mL total volume) was carefully administered by gavage (stainless steel needles, G16) over 3 consecutive days. The administration was done in a randomized way such that each animal received the same compound ($^{54}FeSO_4$, ^{57}Fe-FibBLG and ^{58}Fe-Nano) only once. For each administration, extra care was taken to ensure that the compound would reach the animal's stomach. For $^{54}FeSO_4$ and ^{57}Fe-FibBLG the exact amount administered to the animal was calculated by subtracting the empty syringe and gavage needle weight from the full one. To record the administered amount of 58Fe-Nano in the most precise way, the syringe and the gavage needle were rinsed with deionized water and the rinsing collected, water was evaporated (80°C, 24 h), dissolved in 2 mL HNO_3 65% acid (sub boiled, Human Nutrition Laboratory, Switzerland) and measured for Fe concentration by AAS (SpecrAA-240Z with flame Atomizer, Varian Techtron). The 0.5 mL gavage dose contained 200 µg ^{54}Fe, ^{57}Fe or ^{58}Fe therefore below the acute toxicity level where LD50($FeSO_4$) = 51 mg Fe (Toblli *et al.*, 2008) and bigger than the detection limit of 16 µg for ICP-MS measurements (Brown *et al.*, 1962; Lee and Blaufox, 1985; Walczyk, 1997). The stable isotope method is commonly used in human studies (Walczyk *et al.*, 1997) and here it was specifically applied to directly measure the fractional incorporation of iron from the compounds in liquid form using each subject as its own control.

4.2.2 Analyses

After isotope incorporation over 15 days (Lopes *et al.*, 2010), all animals were deeply anesthetized with an IP injection of Sodium pentobarbitone and blood was collected (DB Vacutainers, K_2E(EDTA), United Kingdom) from the beating heart. Three aliquots were stored at -20°C until Fe was extracted from the erythrocytes by microwave-assisted acid digestion in whole blood and analyzed by ICP-MS (Hotz *et al.*, 2012) at the Laboratory of Human Nutrition (ETH Zurich, Switzerland). One aliquot was stored at -80°C and measured for GSH / protein concentration at the Laboratory of Food Toxicology (ETH Zurich, Switzerland).

4.2.3 Isotope preparation

Stable iron isotopes (^{54}Fe, ^{57}Fe and ^{58}Fe, with isotopic enrichments of respectively 99.9%, 96.3%, and 99.9%) were purchased from Chemgas, Boulogne, France, as elemental metal powders (>99.9% Fe). The stable isotopes ^{57}Fe-FibBLG and ^{58}Fe-Nano were prepared daily before administration using $^{57}FeCl_3$ and $^{58}FeCl_3$ solutions as given in the 'hybrids production'. These solutions were prepared beforehand by dissolving ^{57}Fe and ^{58}Fe in excess concentrated HCl and by adding H_2O_2 to oxidize iron (II) to iron (III). This solution was then evaporated to near dryness, re-dissolved in 0.01 M HCl, and diluted with water to a final concentration of 0.1 M $FeCl_3$. On the other hand, ^{54}Fe was dissolved in 1.5 M H_2SO_4 under argon atmosphere, diluted with water to get a final concentration of 7.1 mM $FeSO_4$ and kept under argon atmosphere until use. Iron in form of ^{57}Fe-FibBLG, ^{58}Fe-Nano and $^{54}FeSO_4$ was gavaged to a final content of 200 µg iron.

4.3 Sensory performance

Sensory evaluation was performed by adding the different iron sources to 100 mL of either chocolate milk, banana milk (103 g banana mixed with 297 g whole milk (3.5% fat, homogenized UHT) and raspberry drink yogurt (all foods were purchased in Migros, Switzerland). Two different fortification levels of 2.5 and 5 mg iron / 100 g food were used. Both levels are higher than the typically applied (2 mg / 100 g) to identify any possible color changes (Hurrell *et al.*, 1991). Color change was measured in duplicate after stirring the powder for 120 min at 350 rpm. The matrix was transferred to the cuvette (5.5 cm inner diameter) and placed on the light projection tube of a spectral photometer (Chroma-Meter CR-310, Minolta Schweiz AG, Switzerland) and measured in triplicate after rotating the dish each time by 120°. Absolute color change (ΔE*ab) was measured using the Hunter Lab color system and calculated as follows:

$$\Delta E^*_{ab} = \sqrt[2]{(\Delta L^*)^2 + (\Delta a^*)^2 + (\Delta b^*)^2}$$

where ΔL∗ (lightness), Δa∗ (chromaticity coordinate) and Δb∗ (chromaticity coordinate) correspond to the difference between the sample (with added compound) and the not fortified matrix. FeSO4 and ferric pyrophosphate (FePP, 20% Fe, food quality micronized powder, Dr. Paul Lohmann GmbH, Germany) were used as positive and negative controls.

4.4 Statistical analyses

Data analysis was done using Excel and SPSS (version 20; SPSS, IBM software). For the Hb-repletion study only, relative bioavailability to FeSO4 (RBV) was calculated using the slope-ratio method after plotting the Fe intake (ug/d) against the change in Hb over 14 days (g/L) (Amine *et al.*, 1972; Finney, 1951). Common-intercept multiple linear regression model was used to calculate the dose-response slopes, using the Fe deficient group as common blank point (average ug/d, average change in Hb). The slopes were compared between each other and to $FeSO_4$ with Tukey's method while Fieller's method was applied to calculate the 95% CI for the RBV to $FeSO_4$. Means between the treatment groups were compared by one-way analysis of variance (ANOVA) followed by a post hoc Bonferroni test for multiple comparisons (significant at $p < 0.05$). Data for Fe intake were Log10 transformed to ensure homogeneity of variance. Values are expressed as mean ± 1 SD. In the isotopes study, iron RBV compared to FeSO4 was tested using repeated measures ANOVA followed by a post hoc Bonferroni test for multiple comparisons (significant at $p < 0.05$). For both *in vivo* studies, the hypothesis that the group means are equal has been tested statistically using an ANOVA model, followed by post-hoc testing (Bonferroni) with a significance level of 0.05 and homogeneity of the variance was tested by Levene's test. Sensory performance was evaluated with a non-parametric Kruskal-Wallis one-way ANOVA using $p = 0.05$ and 95% confidence interval (CI).

Extended data: Results and discussion

1. Hybrids characterization

1.1 XPS

The survey spectra are provided in Extended data **Figure 4**a: they show the presence of C, O, S and N signal in the case of BLG while the photoelectron signals and the X-ray Auger excited signals of iron are only detected on the spectra collected from Fe-FibBLG and Fe-Nano. The signals of sodium, boron and chlorine are also detected and they are due to the steps involved in the sample preparation procedure.

The high-resolution iron spectrum, Fe $2p_{3/2}$, was acquired on Fe-Nano and Fe-FibBLG (Extended data **Figure 4**b). The iron signal is always a complex convolution of peaks; each of them could be assigned to iron in a different chemical state. In the spectra of Fe-FibBLG it is possible to detect a very small contribution (it ranges between 0.5% and 3% of the total peak area) due to metallic iron (706.8 eV (0.2 eV)), the presence of the signals (21.2% of the total peak area) at 709.5 (0.2) eV with its shake-up satellite at 715.0 eV are assigned to the Fe(II) oxide (Biesinger *et al.*, 2011) and that at 712.4 (0.2) eV is assigned to iron oxi-hydroxide (5 %) (Frau *et al.*, 2010). Fe(II) and Fe(III) chloride are respectively about 53% and 20% of the total area (Extended data **Table 1**). The signal of the Fe(III) oxide (at about 711.0 eV) was not detected in Fe-FibBLG.

These data might be interpreted on the basis of the spectra collected on the Fe-Nano. The binding energies of the iron signals are the same within the experimental uncertainty (± 0.2 eV).

In all spectra $FeCl_2$ and $FeCl_3$ were detected and the $FeCl_2$ contribution to the peak was found always higher than that of $FeCl_3$.

The high-resolution spectra of carbon, C 1s, oxygen, O 1s, sulfur, S 2p and nitrogen, N 1s, due to the protein were also acquired and fitted with model Gaussian/Lorentzian functions. The aliphatic carbon was taken as internal reference at 285.0 eV. The C1s signal exhibited four signals in the pure BLG but in Fe-FibBLG the peak at 289.3 eV (not shown) was not detected. The only signal that shifted towards high binding energy values was the component of the

nitrogen, N 1s, which was found at 401.8 eV in the pure BLG and moved to 402.4 eV in Fe-FibBLG.

2. In-vivo study

2.1 GSH

The Fe deficient group showed the lowest GSH level (Extended data **Table 3**) among all feeding groups, as expected in case of iron deficiency (Moriarty *et al.*, 1995), however, no significant difference among the groups was detected.

2.2 Histology

Additionally, extensive histological investigation and organ staining for Fe(II)/Fe(III) ions deposition in the brain, salivary gland, heart, lungs, thymus, pancreas, liver median lobe, stomach, mesenteric and mediastinal lymph nodes, duodenum, ileum, jejunum, caecum, colon, spleen, kidneys, testis with epididymis as well as sternal bone marrow, did not detect compound-related histological changes (Extended data **Table 6**).

Specifically, light to strong atelectasis and light to strong BALT-hyperplasia in the lungs were observed in all examined animals. The BALT-hyperplasia is a normal finding in animals that are not kept specific-pathogen free and the atelectasis is euthanasia related. Few lymphocytes and plasma-cells were found in the myocardium of Fe deficient (1 animal, multifocal) and Fe-Nano 20 ppm (1 animal, focal). In addition, light fibrosis ($FeSO_4$ 10 (1, focal and epicardial in the right ventricle) and $FeSO_4$ 20 (1, multifocal around some vessels)) and light adventitial fibrosis (Fe-FibBLG (1, around some bigger arteries with active media-cells) were observed in the heart and interpreted as incidental findings. In the liver, light to strong extramedullary hematopoiesis were observed in 23 animals (Fe deficient (5), $FeSO_4$ 10 (5), $FeSO_4$ 20 (2), Fe-FibBLG 10 (2), Fe-FibBLG 20 (1), Fe-Nano 10 (2)). No relevant structural changes or Fe(II)/Fe(III) ions deposition were detected in the brain as well as in the thymus, kidney, stomach and the mesenteric lymph nodes. Although no histological changes were detected in the small / large intestine, some reacted positive to Fe(III) (7 diets / 4 diets) and to Fe(II) ions (3 diets / 0 diets). Fe(III) ions was detected within cells (enterocytes), while Fe(II) ions was only observed on top of the microvilli seam and justified with possible presence of food into the gastrointestinal tract, since the sample was not washed before formalin fixation. Contrary to Hilty *et al.* (2010), we detected histological changes in testis.

Specifically, degenerated multinucleate spermatogonia (Fe-FibBLG 10 (1)), round spermatids in the epididymis (Fe deficient (2), $FeSO_4$ 10 (2), Fe-FibBLG 10 (1), Fe-FibBLG 20 (1), Fe-Nano 10 (2), Fe-Nano 20 (3)), no spermatidis (FeSO4 20 (1)), and spermatogonia ($FeSO_4$ 20 (1), Fe-FibBLG 10 (1)) were observed. Even though iron deficiency might be direct cause for incorrect testicular (Hamdi *et al.*, 1997) and sexual development (Allen *et al.*, 2006), these has been usually linked to zinc rather than iron deficiency. However because the degeneration of the testis was always unilateral and is known to be age related these changes are interpreted as background lesions (Gopinath *et al.*, 1987; Sahota *et al.*, 2013). Interestingly, mediastinal lymph nodes for diets $FeSO_4$ 10 (1) and Fe-Nano 10 (1) reacted positive to the Fe(III) ions staining. This has been linked to the fact that lymph nodes are involved in the erythrocytes degradation process due to their drainage function.

Extended data: References

Allen L., de Benoist B., Dary O., and Hurrell R., 2006, Guidelines on food fortification with micronutrients, Geneva: World Health Organization.

Amar-Yuli I., Adamcik J., Lara C., Bolisetty S., Vallooran J. J., and Mezzenga R., 2011, Templating effects of lyotropic liquid crystals in the encapsulation of amyloid fibrils and their stimuli-responsive magnetic behavior: Soft Matter, v. 7, no. 7, p. 3348-3357.

Amine E. K., Neff R., and M. H., 1972, Biological estimation of available iron using chicks or rats Journal of agricoltural food chemistry, v. 20, no. 2.

Bateman L., Ye A. Q., and Singh H., 2010, In vitro digestion of beta-lactoglobulin fibrils formed by heat treatment at low ph: Journal of Agricultural and Food Chemistry, v. 58, no. 17, p. 9800-9808.

Biesinger M. C., Payne B. P., Grosvenor A. P., Lau L. W. M., Gerson A. R., and Smart R. S., 2011, Resolving surface chemical states in xps analysis of first row transition metals, oxides and hydroxides: Cr, mn, fe, co and ni: Applied Surface Science, v. 257, no. 7, p. 2717-2730.

Bressler I., Kohlbrecher J., and Thunemann A. F., 2015, Sasfit: A tool for small-angle scattering data analysis using a library of analytical expressions: Journal of Applied Crystallography, v. 48, p. 1587-1598.

Brown E., Hopper J., Jr., Hodges J. L., Jr., Bradley B., Wennesland R., and Yamauchi H., 1962, Red cell, plasma, and blood volume in the healthy women measured by radiochromium cell-labeling and hematocrit: J Clin Invest, v. 41, p. 2182-2190.

Cunniff P., 1997, Aoac official method 9743.1: Bioavailability of iron: Rat hemoglobin repletion bioassay., Official methods of analysis of aoac international: Gaitherburg, AOAC International, p. 62-63.

Fantauzzi M., Pacella A., Atzei D., Gianfagna A., Andreozzi G. B., and Rossi A., 2010, Combined use of x-ray photoelectron and mossbauer spectroscopic techniques in the analytical characterization of iron oxidation state in amphibole asbestos: Analytical and Bioanalytical Chemistry, v. 396, no. 8, p. 2889-2898.

Finney D. J., 1951, The statistical analysis of slope-ratio assays: J Gen Microbiol, v. 5, no. 2, p. 223-230.

Forbes A. L., Arnaud M. J., Chichester C. O., Cook J. D., Harrison B. N., Hurrell R. F., Kahn S. G., Morris E. R., Tanner J. T., and Whittaker P., 1989, Comparison of in vitro, animal, and clinical determinations of iron bioavailability: International nutritional anemia consultative group task force report on iron bioavailability: American Journal of Clinical Nutrition, v. 49, no. 2, p. 225-238.

Frau F., Addari D., Atzei D., Biddau R., Cidu R., and Rossi A., 2010, Influence of major anions on as(v) adsorption by synthetic 2-line ferrihydrite. Kinetic investigation and xps study of the competitive effect of bicarbonate: Water Air and Soil Pollution, v. 205, no. 1-4, p. 25-41.

Gao G. Q., and Xu A. W., 2013, A new fluorescent probe for monitoring amyloid fibrillation with high sensitivity and reliability: Rsc Advances, v. 3, no. 43, p. 21092-21098.

Gopinath C., Prentice D. E., and Lewis D. J., 1987, Atlas of experimental toxicological pathology, MTP Press Limited.

Grosvenor A. P., Kobe B. A., and McIntyre N. S., 2004, Studies of the oxidation of iron by air after being exposed to water vapour using angle-resolved x-ray photoelectron spectroscopy and quases: Surface and Interface Analysis, v. 36, no. 13, p. 1637-1641.

Gupta R. P., and Sen S. K., 1974, Calculation of multiplet structure of core p-vacancy levels: Physical Review B, v. 10, no. 1, p. 71-77.

Hamdi S. A., Nassif O. I., and Ardawi M. S. M., 1997, Effect of marginal or severe dietary zinc deficiency on testicular development and functions of the rat: Archives of Andrology, v. 38, no. 3, p. 243-253.

Hilty F. M., Arnold M., Hilbe M., Teleki A., Knijnenburg J. T. N., Ehrensperger F., Hurrell R. F., Pratsinis S. E., Langhans W., and Zimmermann M. B., 2010, Iron from nanocompounds containing iron and zinc is highly bioavailable in rats without tissue accumulation: Nature Nanotechnology, v. 5, no. 5, p. 374-380.

Hotz K., Krayenbuehl P. A., and Walczyk T., 2012, Mobilization of storage iron is reflected in the iron isotopic composition of blood in humans: Journal of Biological Inorganic Chemistry, v. 17, no. 2, p. 301-309.

Hurrell R. F., Reddy M. B., Dassenko S. A., Cook J. D., and Shepherd D., 1991, Ferrous fumarate fortification of a chocolate drink powder: British Journal of Nutrition, v. 65, no. 2, p. 271-283.

Jung J. M., and Mezzenga R., 2010, Liquid crystalline phase behavior of protein fibers in water: Experiments versus theory: Langmuir, v. 26, no. 1, p. 504-514.

Lee H. B., and Blaufox M. D., 1985, Blood volume in the rat: J Nucl Med, v. 26, no. 1, p. 72-76.

Li X. Q., Elliott D. W., and Zhang W. X., 2006, Zero-valent iron nanoparticles for abatement of environmental pollutants: Materials and engineering aspects: Critical Reviews in Solid State and Materials Sciences, v. 31, no. 4, p. 111-122.

Lopes T. J., Luganskaja T., Vujic Spasic M., Hentze M. W., Muckenthaler M. U., Schumann K., and Reich J. G., 2010, Systems analysis of iron metabolism: The network of iron pools and fluxes: BMC Syst Biol, v. 4, p. 112.

Moriarty P. M., Picciano M. F., Beard J. L., and Reddy C. C., 1995, Classical selenium-dependent glutathione-peroxidase expression is decreased secondary to iron-deficiency in rats: The Journal of Nutrition, v. 125, no. 2, p. 293-301.

Rahman I., Kode A., and Biswas S. K., 2006, Assay for quantitative determination of glutathione and glutathione disulfide levels using enzymatic recycling method: Nature Protocols, v. 1, no. 6, p. 3159-3165.

Reeves P. G., Nielsen F. H., and Fahey G. C., Jr., 1993, Ain-93 purified diets for laboratory rodents: Final report of the american institute of nutrition ad hoc writing committee on the reformulation of the ain-76a rodent diet: The Journal of Nutrition, v. 123, no. 11, p. 1939-1951.

Sahota P. S., Popp J. A., Hardisty J. F., and Gopinath C., 2013, Toxicologic pathology: Nonclinical safety assessment, CRC Press.

Toblli J. E., Cao G., Olivieri L., and Angerosa M., 2008, Comparative study of gastrointestinal tract and liver toxicity of ferrous sulfate, iron amino chelate and iron polymaltose complex in normal rats: Pharmacology, v. 82, no. 2, p. 127-137.

Walczyk T., 1997, Iron isotope ratio measurements by negative thermal ionisation mass spectrometry using fef4- molecular ions: International Journal of Mass Spectrometry and Ion Processes, v. 161, no. 1-3, p. 217-227.

Walczyk T., Davidsson L., Zavaleta N., and Hurrell R. F., 1997, Stable isotope labels as a tool to determine the iron absorption by peruvian school children from a breakfast meal: Fresenius Journal of Analytical Chemistry, v. 359, no. 4-5, p. 445-449.

GENERAL DISCUSSION

1. Thesis summary

It is generally accepted that mineral bioavailability is strongly dependent on the dissolution/solubility properties of the mineral source and the faster the release of the mineral from the source, the better the bioavailability. As shown in the Literature chapter, approaches like size reduction (and increase in SSA), amorphous structuring and changes in chemical composition could lead to a positive improvement in calcium or iron bioavailability. Additionally, physiological pH in the gut strongly affects mineral bioavailability. For instance, acid secretion in the stomach strongly influence mineral absorption and can be impaired in elderly or patients with hypochlorhydria. Because the pH in the gastrointestinal tract increases from stomach (pH 2) to colon (pH 7), it is crucial that the mineral remains in solution at higher pH. This characteristic may be particularly important for calcium, which can be absorbed through the entire length of the small and large intestine, while the main site of iron absorption is the duodenum. Therefore, smart material design could be an efficient approach to improve mineral absorption. For instance calcium carbonate, the most widely used as supplement or fortificant, can cause an undesired increase in pH upon dissolution. Calcium phosphate causes less of an increase in pH but still has a high calcium content and might thus be an alternative food fortificant. Therefore, the overall aim of this thesis was to evaluate the *in vivo* bioavailability of nanostructured calcium and iron nanomaterials materials synthesized using a materials design approach.

While producing nanostructured calcium compounds by FASP (*Manuscript 1*) we have observed that the flame parameters play a crucial role in determining the final CaO and $CaCO_3$ content in the powder. The as-prepared CaO naturally reacts with CO_2 and H_2O when exposed to air, and converts into $CaCO_3$ in a process known as carbonation, as already observed by Knijnenburg *et al.* (2013). During carbonation, crystal size increases while SSA decreases until a final (stable) SSA and crystal size are reached. This 'aging process' cannot be completely avoided, but in our case it could be inhibited by doping the powders with strontium, zinc, magnesium or phosphorous. The smallest increase in crystal size was obtained by magnesium and phosphorus. Powders containing phosphorus were produced and characterized with changing calcium to phosphorus molar ratio (Ca:P). We observed that crystallinity increased with increasing Ca:P ratio, while the SSA remained constant at around

130 m^2/g for Ca:P = 1-2.33. The most promising compound was Ca:P = 1 because it has high SSA and high calcium content but low presence of the stable HAp (confirmed by Raman spectroscopy) and it is XRD-amorphous. Even though this powder showed a decrease in SSA during storage, the decrease was less pronounced than with $CaCO_3$.

It is uncertain whether *in vitro* dissolution can be used to predict *in vivo* absorption for calcium, an approach that is commonly used for iron. We evaluated a dissolution method proposed by Meiron *et al*. (2011) as a possible predictor for *in vivo* absorption of our nanostructured calcium compounds. Specifically, time to reach half of the final pH (t_{pH50}) in 0.01 M H_3PO_4 was used to see how fast a powder would dissolve. In addition to the original method we also measured the amount of dissolved calcium after 500 seconds of dissolution. This was done because we observed how the powders with low SSA also needed the shortest time to reach pH_{50}, when t_{pH50} was extrapolated from pH versus time curves (the final pH was defined as 'when the pH change was less than 0.05% during a 10-second period' (Meiron *et al.*, 2011)). Poorly dissolving powders reached the final pH very soon because the release of calcium is so slow. For this reason we concluded that the use of t_{pH50} as an indicator for dissolution is limited and we therefore introduced the amount of dissolved calcium as an additional quantifying measure.

In the dissolution experiment, nanosized powders released more calcium than the micronized commercial compounds and Ca:P=1 dissolved more calcium than $CaCO_3$. Increasing the SSA above 23 m^2/g, did not further improve the amount of released Ca. This method standardizes the powder amount to 40 mg calcium, allowing for comparisons between powders with different composition. When dissolving $CaCO_3$, the resulting Ca^{2+} could potentially bind to PO_4^{2-} groups coming from the H_3PO_4, resulting in the formation of less soluble calcium-phosphate forms (such as stable HAp) that would then precipitate. At the same time, the pH would increase, resulting in a lower amount of dissolved $CaCO_3$. With pure HAp, this increase in pH is less strong since HAp itself releases PO_4^{2-} groups. In addition, we did not see an improvement in calcium dissolution by SSA. Possible reasons explaining this include the fast dissolution of phosphate nanopowders, the advantage of amorphous structuring over SSA, and also the reaching of their solubility limit that resulted in slow dissolution. Composition (Ca:P = 1 vs. $CaCO_3$) and structure (crystalline vs. amorphous), rather than SSA, appeared to be determinant for dissolution for the tested powders.

The bioavailability of nanostructured calcium compounds by SSA and chemical composition was evaluated in growing rats (*Manuscript 2*). Three $CaCO_3$ compounds with SSAs of 3, 36 and 64 m^2/g were compared to assess their bioavailability by SSA, and two additional compounds, a 50/50 wt% mixture of $CaCO_3$ and HAp ($CaCO_3$:HAp 50:50, 94 m^2/g) and pure HAp (100 m^2/g), were added to compare calcium bioavailability by chemical composition. In order to investigate calcium bioavailability by chemical composition, the SSA of the compounds containing HAp was kept as close as possible to the highest SSA of $CaCO_3$, considering the limitations given by the production method. The compounds were characterized for their SSA, phase composition (XRD), crystallinity (XRD and TEM), morphology (TEM) and Ca/P content (atomic absorption spectroscopy). We measured calcium absorption, retention and fractional retention over a 5-days sample collection period as primary outcomes. Additionally, we also evaluated BMD in femur and L1-4 vertebra, calcium content of femur and PTH hormone level in serum. For any of the outcomes, no difference by SSA were observed, while a significant difference in fractional retention between $CaCO_3$ 64 m^2/g and HAp 100 m^2/g was seen by chemical composition. Moreover, extensive histology on selected organs was used as primary indicator for safety of the tested nanocompounds and we did not observe any visual calcium accumulation in tissues. Delivered calcium or tpH50 obtained from the *in vitro* dissolution method (adapted from Meiron *et al.* (2011)) did not correlate with calcium absorbed *in vivo*; the highest amount of calcium was delivered *in vitro* by HAp 100 m^2/g. We showed how an increase in SSA of $CaCO_3$ from 3 to 64 m^2/g did not improve the retention of calcium, while changing the composition from $CaCO_3$ to HAp at nanoscale significantly increased fractional calcium retention. Our results suggest that chemical composition is an important determinant of calcium bioavailability when nanoscale is reached. Fortifying fruit juices and berry-flavored yogurt with HAp 100 m^2/g caused minimal color changes and pH increase and it thus may be a promising alternative to $CaCO_3$ for fortification.

Material properties play a crucial role also in the bioavailability of iron. We combined soft and hard material properties to synthesize iron-amyloid fibril hybrids as novel iron fortificants (*Manuscript 3*). For this purpose, beta-lactoglobulin was denaturated from its globular shape and converted to an elongated fibrilar structure (BLG fibrils or FibBLG) and iron nanoparticles then nucleated on the fibrilar base. These iron-amyloid fibril hybrids were extensively characterized using the reducing effect colorimetry (Fe(II)/Fe(III) of BLG fibrils),

transmission electron microscopy (structure), small angle neutron scattering (phase composition), energy dispersive X-ray analysis (material-elements detection), X-ray photoelectron spectroscopy (surface chemical composition) and *in vitro* digestion (human digestion simulation of fibrils and nanoparticles separately). The bioavailability of two types of iron compounds with fibrils (Fe-FibBLG) and without fibrils (Fe-Nano) were evaluated in a hemoglobin dose-response and stable isotope study in male rats. These two studies allowed the evaluation of the compounds in dry (dose-response) and liquid (isotope) form, respectively. For each study, each compound's performance was evaluated by comparing its relative bioavailability (RBV) to the 'golden standard' ferrous sulfate ($FeSO_4$). In both studies, the RBV values did not significantly differ from $FeSO_4$ or between the nanocompounds. This bioavailability was highly independent of source and could be explained by the high percentage of well-soluble Fe(II) in both powder and liquid form. However, only Fe-FibBLG form showed colloidal stability, and therefore is a possible candidate as a fortificant for liquid matrices. The primary safety of the compounds in powder form (in the Hb dose-response study) was confirmed by extensive histological examination. Additionally, the evaluation of color change after fortifying blueberry yogurt, chocolate milk and banana milk showed superior performance of Fe-FibBLG compared to FeSO4, however, the reduced color change is likely only relevant for chocolate milk.

2. Critical evaluation and future research

Challenges in the production of calcium nanomaterials for in vivo studies

Study length, animal number and mineral concentration in the animal chow are all variables that play a crucial role in planning a study that involves nanomaterials. For example, iron fortification level of 35 mg/kg in animal chow is very low compared to calcium which is 5 g/kg food (Reeves *et al.*, 1993). In order for the FASP-produced Ca:P = 1 to be used for an *in vivo* balance study, about 270 g powder is necessary (15 kg diet calculated on 20 g food intake per day over 36 days) and even more for a study involving OVX animals that could last up to several months (Kruger *et al.*, 2005; Shahnazari *et al.*, 2009). However, due to its constant manual re-filling of the precursor and low production rate, the laboratory-scale (batch) FASP production is not suitable to produce such large amounts of powders. Therefore, large-scale production was implemented to continuously synthesize the necessary amount in the shortest time possible. Unfortunately, long time synthesis with

acetylene resulted in a contamination of the powder with black carbon soot that could not be separated from the powder. The use of soot-containing powder in a feeding study, likely might have caused changes in animal eating behaviour. Therefore we opted to use commercially available nanocompounds, leaving the absorption performance of FASP-made calcium nanocompounds still an open question. In order to include the FASP made calcium compounds in an animal study, several approaches could be taken: optimization of the production method, different study design and different animal model.

Firstly, further optimization of the scale-up production method is necessary, for example by using H_2 instead of C_2H_2 as combustion gas as proposed by Rudin *et al.* (2013). The authors have observed how, during flame synthesis with C_2H_2, CO_2 is often a by-product resulting from precursors containing aqueous solutions of nitrate salts. H_2 is therefore a valid alternative to C_2H_2 for the synthesis of homogeneous, CO_2 free particles.

Secondly, the amount of powder needed for the study could be reduced by changing the study design. For instance, calcium absorption can be measured by the appearance of calcium in blood. For this purpose, radioactive calcium in form of calcium-45 (^{45}Ca) can be activated (made radioactive) by irradiation of $CaCO_3$ over 16 days in a nuclear reactor. The preparation of ^{45}Ca can be done at the Nuclear Energy Corporation South Africa facility under the experienced supervision of Prof. Zeevaart. The resulting ^{45}Ca has a half-life of 162.7 days and emits beta particles with a maximum energy of 0.257 MeV (Lide, 2015). However, only ^{45}Ca from $CaCO_3$ but not from calcium phosphates can be made radioactive with this method. When irradiating calcium phosphates, additionally to ^{45}Ca, also radionuclides phosphorus-32 (^{32}P) and -33 (^{33}P) are formed. Both ^{32}P (half-life of 14.28 days) and ^{33}P (half-life of 25.3 days) emit beta particles of 1.71 and 0.25 MeV maximum energy, respectively. Therefore, because all three radionuclides, ^{45}Ca, ^{32}P and ^{33}P, emit the same type of beta particles during decay, the P signal would interfere with the signal of calcium. One possibility of radiolabelling calcium phosphates would be to produce them by precipitation from aqueous solutions using a ^{45}Ca source. For instance, precursors such as $Ca(NO_3)_2$ (Narasaraju and Phebe, 1996) or $CaCl_2$ (Murugan and Ramakrishna, 2005) were used to produce HAp (Ca:P = 1.67). However, because of the difficulties given in producing well-defined and reproducible orthophosphates (Vallet-Regi and Gonzalez-Calbet, 2004), further method optimization is necessary to reach the desired compound composition (Ca:P

= 1), crystallinity, particle size and SSA. Another aspect to consider during the activation process is that calcium is exposed to a maximum temperature of 180°C. In order to ensure the expected compound performance after irradiation a stability test should be carried out. For instance, heating the powder at 200°C over a few days would give a first indication of whether heating can change the compounds by decreasing the SSA (caused by sintering) or changing the composition (caused by dissociation). Specifically for $CaCO_3$, changes in composition could be caused by dissociation of CO_2, however, this only occurs after reaching 600°C (Dollimore *et al.*, 1996), while any change below this temperature is usually associated with the evaporation of surface water.

Once ready, radioactive $CaCO_3$ and calcium phosphates can be dispersed into saline solution and administered to rats by gavage. Appearance of ^{45}Ca in blood can be measured at specific time intervals and be used to demonstrate how well the different calcium sources are absorbed.

Lastly, the change of animal model from rats to mice would allow a reduction in the amount of powder needed for the study. Assuming that an adult mouse eats about 5 g/day (Halaas *et al.*, 1995), about 50 g of powder Ca:P = 1 (28 wt% calcium) powder would be needed to feed 12 mice for 36 days. Lastly, stable isotopes could also be used to produce FASP-made Ca:P = 1 and $CaCO_3$, however, due to the quite elevated material costs (mainly consisting of the amount of isotopes and glass-fibre free Teflon filters), the study design would need to be carefully considered.

Ultimately, a study design involving stable isotopes would be particularly appropriate to evaluate the absorption of calcium from FASP-made compounds in human subjects. A study design given by Denk *et al.* (2005) (unpublished) can be used for the purpose and it was used to estimate the following study costs. For a stable isotope study, ^{42}Ca (natural abundances of 0.65% (Lide, 2015)) can be used. In order to be measured a single dose of 40 mg ^{42}Ca would be necessary for each subject, resulting in a total amount of 400 mg ^{42}Ca for 10 subjects and to about 1.5 and 1.2 g powder of Ca:P = 1 and $CaCO_3$ respectively. The price for 220 mg ^{42}Ca in form of $CaCO_3$ is Euro 2'300 (www.chemgas.com, quote request on 26.07.2016). However, because ^{42}Ca can be purchased in form of $CaCO_3$, and the FASP-nanopowders were produced using a nitrate precursor, further method optimization would be necessary in order to produce intrinsically labelled nanocompounds from $CaCO_3$ precursors.

Some considerations about the balance model

As reviewed in the Literature Chapter, balance studies are especially useful for comparing the bioavailability of different calcium sources. However, because of their short feeding period (around 4-5 weeks of study), balance studies usually focus on short term outcomes such as calcium absorption and retention and they only partially take into account long term effects, such as the biological use of calcium to form new bone material, leading to improved bone mineral density, structure and strength. For this reason, a long term study (up to 3 months) using OVX rats or mice (model for post-menopausal osteoporosis) would be complementary to clarify whether bone mineral density could be improved after a long term feeding with nanostructured calcium compounds compared to commercial compounds. Compared to a balance study this model needs longer feeding periods and thus higher quantities of the studied compounds. Again, the production method must be carefully considered. Additionally, trained staff is necessary to perform ovariectomy because if the ovaries are not completely removed, remnants can continue to produce hormones that influence bone metabolism. Micro-CT can be a valid alternative to DXA measurements and give information about bone architecture and geometry rather than density only (Day *et al.*, 2000). Major limitations of DXA are the absence of information about volume density (g/cm3), bone geometry, differentiation of bone type (cortical or cancellous) and that the measured areal density depends on bone size (Lentle and Prior, 2003). Live 3D imaging of time-lapsed changes in architecture was proposed as a novel and non-invasive monitoring of bone regeneration and tested after femoral implant insertion in sheep (Hildebrand *et al.*, 1999). For this purpose, time-lapsed micro-computed tomography (µCT) can be used to observe longitudinal changes in bone architecture, bone remodelling process and mineralization (Li *et al.*, 2015), possibly also reducing the number of experimental animals because such changes can be followed in the same animal.

A balance study gives information about the apparent absorption of calcium, measured as ‘intake - faecal excretion’, and retention, measured as ‘intake - (faecal + urinary excretion)’. It however does not take into consideration any endogenous losses (Gueguen and Pointillart, 2000). Therefore, when done in animals, it involves the use of metabolic cages, which seem an ideal setup for separate collection of faeces and urine. Yet, extreme care must be taken when choosing the feeder size, since many animals can use it as a sleeping place even

though a sleeping tube is provided. This unwanted behaviour can lead to contamination of refused food with urine and faeces and lead to inaccurate collection.

The importance of relevant material characterization

A decrease in primary particle size leads to an increase in SSA and therefore the amount of surface available to interact with the surroundings, so surface area and energy are relevant to the dissolution, aggregation and accumulation of nanomaterial (Lin *et al.*, 2014). Hilty *et al.* (2009) discussed the importance of using SSA as a measure of comparison between compounds that do not have a specific chemical composition and are therefore considered mixtures, possessing an unknown density. During production of calcium phosphates with FASP, we observed how the chemical phase changes according to Ca:P molar ratio (going from γ-$Ca_2P_2O_7$ to HAp with increasing P content) and how, independently of molar ratio, Raman spectroscopy revealed that these compounds were composed by mixtures of γ-$Ca_2P_2O_7$, $HCaPO_4$ and HAp. Consequently, because the FASP-made calcium phosphates contain several chemical phases, the use of one single phase density would not be representative for the calculation of d_{BET} of a mixed compound (formula given in the Literature chapter). Additionally, the estimation of d_{BET} assumes monodisperse, dense and spherical particles (Maedler *et al.*, 2002), and is especially inadequate for cubic-shaped crystals or for porous materials. Therefore, we used SSA rather than d_{BET} as a primary measure to compare compounds independently of composition. Other methods such as dynamic light scattering (DLS) or transmission electron microscopy (TEM) (covered in the Literature chapter) give additional information about the size. Yet, both techniques are complementary to each other and give different information: TEM gives information about the primary particle size of the particles, while DLS measurements are done in order to determine the true state of particles in media. Therefore, often several methods are combined to have a comprehensive idea about particle size.

As discussed in the Literature Chapter, nanomaterial's physical and chemical properties can be characterized by several methods. However, there is a discrepancy in characterization methods used and not all publications use the same characterization method. Usually, characterization methods are selected depending on the relevance of the outcome on the research question. Having a unified measure would also allow the comparison of compounds between studies, especially for the *in vivo* studies. But, since all characterization methods

are seen complementary to each other, there is no single standard method. Additionally to particle size, which is almost always reported *in vivo* experiments, phase composition (from e.g. XRD or Raman spectroscopy) is usually missing, especially in case of calcium phosphates. For instance, crystal structure of calcium phosphate changes with varying Ca:P ratios and consequently so does their lattice energy and solubility. Yet, many researchers and production companies generalize about the compound's chemical composition and name, and may label a certain Ca:P ratio with a misleading or incorrect name. Therefore, more care must be taken in carefully characterizing calcium phosphates.

Is nanosizing really necessary for calcium?

Size reduction is a well-known approach to improve bioavailability of poorly bioavailable compounds. Although this approach has shown positive results for micronutrients such as iron and zinc, no clear answer has yet been obtained for nano calcium. Our approach to answer this question was to compare $CaCO_3$ with different SSA, but we did not see improved calcium retention or fractional retention with increasing SSA. Instead, we hypothesize that not only size but also chemical composition matters, considering the best *in vitro* and *in vivo* performance was provided by a nanosized HAp of 100 m^2/g. In the *in vitro* dissolution experiments, FASP made Ca:P = 1 did not show improved dissolution for an SSA above 23 m^2/g, however, Ca:P = 1 always released more calcium than $CaCO_3$. For the dissolution experiment, Ca:P = 1 powders with SSA > 23 m^2/g, including the commercial one, were all amorphous, leaving open the question of whether amorphous structuring plays a role in enhancing calcium dissolution and therefore bioavailability. Because amorphous materials have a disorganized and therefore unstable lattice, this disorder might facilitate a nanopowder's dissolution (Blagden *et al.*, 2007). Specifically for $CaCO_3$, Meiron *et al.* (2011) and Vaisman *et al.* (2014) have shown improved performance of amorphous $CaCO_3$ in animals and humans. However, whether amorphous structuring is more relevant than nanosizing, especially for calcium phosphates, needs further investigation. Also, we showed how doping $CaCO_3$ with magnesium and P reduced the size for $CaCO_3$ crystals (Posavec *et al.*, 2016). Our results are similar to the multimineral calcium compounds containing iron, copper and manganese reported by Knijnenburg *et al.* (2013), and demonstrate that doping not only improves compound's value nutrition-wise, by delivering several micronutrients at the same time, but may also improve compound's performance. Understanding whether

nanosizing is really necessary for calcium absorption might give a first insight into future development of calcium compounds where production and efficacy testing should rather focus on material properties such as amorphous structuring, chemical composition and doping than smaller sizes.

Carriers for nanoiron to fortify liquid matrices

The production and characterization of the nanocarrier-bound-iron was part of another doctoral thesis by Ms. Yi Shen from the Laboratory of Soft Materials (Prof. Mezzenga, ETH Zurich) and are not part of this thesis. As a result of our research, we have shown that iron bound to FibBLG nanocarrier was as bioavailable as the gold standard $FeSO_4$, but it only showed slightly better sensory performance in chocolate milk, banana milk and berry yogurt. Iron amyloid fibrils has shown good stability as dispersion being therefore a valid option to fortify liquid matrices which may also be extended to juices. However, several experiments focusing on the characterization and absorption still must be carried out. For instance, it still remains unclear whether nano-iron or residuals of $FeCl_3$ are actually bound to the fibrilar structure as shown in the TEM images or simply adjacent to it as separate particle. Methods such as ultrafiltration and ultracentrifugation were tried to clarify this question, but resulted in inconclusive results. Therefore, further optimization of the characterization method and compound production needs to be carried out.

3. References

Blagden N., de Matas M., Gavan P. T., and York P., 2007, Crystal engineering of active pharmaceutical ingredients to improve solubility and dissolution rates: Advanced Drug Delivery Reviews, v. 59, no. 7, p. 617-630.

Day J. S., Ding M., Odgaard A., Sumner D. R., Hvid I., and Weinans H., 2000, Parallel plate model for trabecular bone exhibits volume fraction-dependent bias: Bone, v. 27, no. 5, p. 715-720.

Denk E., Walczyk T., and Hurrell R., 2005, Effect of calcium supplementaiton on dietary calcium absorption and bon emetabolism in healthy postmenopausal women: unpublished work.

Dollimore D., Tong P., and Alexander K. S., 1996, The kinetic interpretation of the decomposition of calcium carbonate by use of relationships other than the arrhenius equation: Thermochimica Acta, v. 283, p. 13-27.

Gueguen L., and Pointillart A., 2000, The bioavailability of dietary calcium: Journal of the American College of Nutrition, v. 19, no. 2, p. 119-136.

Halaas J. L., Gajiwala K. S., Maffei M., Cohen S. L., Chait B. T., Rabinowitz D., Lallone R. L., Burley S. K., and Friedman J. M., 1995, Weight-reducing effects of the plasma-protein encoded by the obese gene: Science, v. 269, no. 5223, p. 543-546.

Hildebrand T., Laib A., Muller R., Dequeker J., and Ruegsegger P., 1999, Direct three-dimensional morphometric analysis of human cancellous bone: Microstructural data from spine, femur, iliac crest, and calcaneus: Journal of Bone and Mineral Research, v. 14, no. 7, p. 1167-1174.

Hilty F. M., Teleki A., Krumeich F., Buchel R., Hurrell R. F., Pratsinis S. E., and Zimmermann M. B., 2009, Development and optimization of iron- and zinc-containing nanostructured powders for nutritional applications: Nanotechnology, v. 20, no. 47.

Knijnenburg J. T. N., Hilty F. M., Krumeich F., Zimmermann M. B., and Pratsinis S. E., 2013, Multimineral nutritional supplements in a nano-cao matrix: Journal of Materials Research, v. 28, no. 8, p. 1129-1138.

Kruger M. C., Plimmer G. G., Schollum L. M., Haggarty N., Ram S., and Palmano K., 2005, The effect of whey acidic protein fractions on bone loss in the ovariectomised rat: British Journal of Nutrition, v. 94, no. 2, p. 244-252.

Lentle B. C., and Prior J. C., 2003, Osteoporosis: What a clinician expects to learn from a patient's bone density examination: Radiology, v. 228, no. 3, p. 620-628.

Li Z. H., Kuhn G., von Salis-Soglio M., Cooke S. J., Schirmer M., Muller R., and Ruffoni D., 2015, In vivo monitoring of bone architecture and remodeling after implant insertion: The different responses of cortical and trabecular bone: Bone, v. 81, p. 468-477.

Lide D. R., 2015, Crc handbook of chemistry and physics, 96th edition, internet version 2015-2016, CRC Press.

Lin P. C., Lin S., Wang P. C., and Sridhar R., 2014, Techniques for physicochemical characterization of nanomaterials: Biotechnology Advances, v. 32, no. 4, p. 711-726.

Maedler L., Stark W. J., and Pratsinis S. E., 2002, Flame-made ceria nanoparticles: Journal of Materials Research, v. 17, no. 6, p. 1356-1362.

Meiron O. E., Bar-David E., Aflalo E. D., Shechter A., Stepensky D., Berman A., and Sagi A., 2011, Solubility and bioavailability of stabilized amorphous calcium carbonate: Journal of Bone and Mineral Research, v. 26, no. 2, p. 364-372.

Murugan R., and Ramakrishna S., 2005, Aqueous mediated synthesis of bioresorbable nanocrystalline hydroxyapatite: Journal of Crystal Growth, v. 274, no. 1-2, p. 209-213.

Narasaraju T. S. B., and Phebe D. E., 1996, Some physico-chemical aspects of hydroxylapatite: Journal of Materials Science, v. 31, no. 1, p. 1-21.

Posavec L., Knijnenburg J. T. N., Hilty F. M., Krumeich F., Pratsinis S. E., and Zimmermann M. B., 2016, Dissolution and storage stability of nanostructured calcium carbonates and phosphates for nutrition: Journal of Nanoparticle Research, v. 18, no. 310, p. 1-13.

Reeves P. G., Nielsen F. H., and Fahey G. C., Jr., 1993, Ain-93 purified diets for laboratory rodents: Final report of the american institute of nutrition ad hoc writing committee on the reformulation of the ain-76a rodent diet: The Journal of Nutrition, v. 123, no. 11, p. 1939-1951.

Rudin T., Wegner K., and Pratsinis S. E., 2013, Towards carbon-free flame spray synthesis of homogeneous oxide nanoparticles from aqueous solutions: Advanced Powder Technology, v. 24, no. 3, p. 632-642.

Shahnazari M., Martin B. R., Legette L. L., Lachcik P. J., Welch J., and Weaver C. M., 2009, Diet calcium level but not calcium supplement particle size affects bone density and mechanical properties in ovariectomized rats.: The Journal of Nutrition, v. 139, no. 10, p. 1308-1315.

Vaisman N., Shaltiel G., Daniely M., Meiron O. E., Shechter A., Abrams S. A., Niv E., Shapira Y., and Sagi A., 2014, Increased calcium absorption from synthetic stable amorphous calcium carbonate: Double-blind randomized crossover clinical trial in postmenopausal women: Journal of Bone and Mineral Research, v. 29, no. 10, p. 2203-2209.

Vallet-Regi M., and Gonzalez-Calbet J. M., 2004, Calcium phosphates as substitution of bone tissues: Progress in Solid State Chemistry, v. 32, no. 1-2, p. 1-31.

CONCLUSIONS

Novel calcium and iron nanocompounds produced and tested in this thesis were shown to be valid alternatives to the already existing food fortificants and supplements. However, before implementing these novel sources of minerals for human consumption, toxicity studies focusing on proving their safety still need to be performed. In this thesis we have demonstrated how smart material design might be a promising alternative to nanosizing, especially in case of calcium. Clearly avoiding the 'nano' labelling given by the food industry would definitively improve consumer's perception towards these novel compounds. Yet, studies focusing on refining material properties targeting higher absorption without decreasing the particle size still must be implemented.